AN EXPERIMENTAL STUDY OF WING TIP VORTEX IN THE NEAR WAKE OF A RECTANGULAR WING

By

Youxin Zheng and B.R. Ramaprian

Sponsored By

The U.S. Army Research Office

Grant No. DAAL03-91-G-0026

Report No. MME-TF-93-1

WASHINGTON STATE UNIVERSITY
Department of Mechanical and Materials Engineering

JUNE 1993

REPORT DOCUMENTATION PAGE

Form Approved
OMB No 0704-0188

1. AGENCY USE ONLY (Leave blank)	2. REPORT DATE	3. REPORT TYPE AND DATES COVERED
	June 1993	Interim technical 2/1/91-5/31/93

4. TITLE AND SUBTITLE
An Experimental Study of Wing Tip Vortex in the Near Wake of a Rectangular Wing

5. FUNDING NUMBERS
DAAL03-91-G-0026

6. AUTHOR(S)
Youxin Zheng and B.R. Ramaprian

7. PERFORMING ORGANIZATION NAME(S) AND ADDRESS(ES)
Washington State University
Pullman, WA 99164-2920

8. PERFORMING ORGANIZATION REPORT NUMBER

9. SPONSORING / MONITORING AGENCY NAME(S) AND ADDRESS(ES)
U.S. Army Research Office
P. O. Box 12211
Research Triangle Park, NC 27709-2211

10. SPONSORING / MONITORING AGENCY REPORT NUMBER
ARO 28159.6-EG

11. SUPPLEMENTARY NOTES
The view, opinions and/or findings contained in this report are those of the author(s) and should not be construed as an official Department of the Army position, policy, or decision, unless so designated by other documentation.

12a. DISTRIBUTION / AVAILABILITY STATEMENT
Approved for public release; distribution unlimited.

12b. DISTRIBUTION CODE

13. ABSTRACT *(Maximum 200 words)*

An experimental study of the tip vortex behind a NACA 0015 rectangular wing of aspect ratio 4 was carried out to understand the structure and evolution of the vortex in the near-wake region. The results of these experimental studies are presented in this report. These measurements were made nonintrusively using three-component laser-Doppler velocimetry (LDV). The experiments were carried out at a Reynolds number of about 180,000 in a low-speed wind tunnel. Two cases were studied, namely, (i) stationary wing and (ii) wing oscillating in pitch sinusoidally about its quarter-chord axis. The flow properties measured were the three components of the instantaneous velocity. These data were processed to obtain time-mean and phase-locked flow properties such as velocity, vorticity and turbulence. The data were obtained at several locations at 0.15 - 3.0 chord lengths downstream from the trailing edge. The typical distributions of mean velocity, vorticity, circulation and turbulent intensity in the near wake are presented and discussed for the stationary wing. In the case of the oscillating wing, the phase-locked velocity, vorticity and turbulence data show details of the evolution of the unsteady tip vortex downstream from the trailing edge. The results also show that the flow is strongly non-quasi-steady at the oscillation frequency studied. The results are fully archived on tape and are available to any interested reader. These can be used as database in the development of wake models for the finite wing, and in studies of three-dimensional wing aerodynamics.

14. SUBJECT TERMS	15. NUMBER OF PAGES
Wing Tip Vortex, Unsteady Aerodynamics, Dynamic Stall	206
	16. PRICE CODE

17. SECURITY CLASSIFICATION OF REPORT	18. SECURITY CLASSIFICATION OF THIS PAGE	19. SECURITY CLASSIFICATION OF ABSTRACT	20. LIMITATION OF ABSTRACT
UNCLASSIFIED	UNCLASSIFIED	UNCLASSIFIED	UL

GENERAL INSTRUCTIONS FOR COMPLETING SF 298

The Report Documentation Page (RDP) is used in announcing and cataloging reports. It is important that this information be consistent with the rest of the report, particularly the cover and title page. Instructions for filling in each block of the form follow. It is important to ***stay within the lines*** to meet ***optical scanning requirements***.

Block 1. Agency Use Only *(Leave blank)*.

Block 2. Report Date. Full publication date including day, month, and year, if available (e.g. 1 Jan 88). Must cite at least the year.

Block 3. Type of Report and Dates Covered. State whether report is interim, final, etc. If applicable, enter inclusive report dates (e.g. 10 Jun 87 - 30 Jun 88).

Block 4. Title and Subtitle. A title is taken from the part of the report that provides the most meaningful and complete information. When a report is prepared in more than one volume, repeat the primary title, add volume number, and include subtitle for the specific volume. On classified documents enter the title classification in parentheses.

Block 5. Funding Numbers. To include contract and grant numbers; may include program element number(s), project number(s), task number(s), and work unit number(s). Use the following labels:

C	- Contract	**PR**	- Project
G	- Grant	**TA**	- Task
PE	- Program Element	**WU**	- Work Unit Accession No.

Block 6. Author(s). Name(s) of person(s) responsible for writing the report, performing the research, or credited with the content of the report. If editor or compiler, this should follow the name(s).

Block 7. Performing Organization Name(s) and Address(es). Self-explanatory.

Block 8. Performing Organization Report Number. Enter the unique alphanumeric report number(s) assigned by the organization performing the report.

Block 9. Sponsoring/Monitoring Agency Name(s) and Address(es). Self-explanatory.

Block 10. Sponsoring/Monitoring Agency Report Number. *(If known)*

Block 11. Supplementary Notes. Enter information not included elsewhere such as: Prepared in cooperation with...; Trans. of...; To be published in.... When a report is revised, include a statement whether the new report supersedes or supplements the older report.

Block 12a. Distribution/Availability Statement. Denotes public availability or limitations. Cite any availability to the public. Enter additional limitations or special markings in all capitals (e.g. NOFORN, REL, ITAR).

- **DOD** - See DoDD 5230.24, "Distribution Statements on Technical Documents."
- **DOE** - See authorities.
- **NASA** - See Handbook NHB 2200.2.
- **NTIS** - Leave blank.

Block 12b. Distribution Code.

- **DOD** - Leave blank.
- **DOE** - Enter DOE distribution categories from the Standard Distribution for Unclassified Scientific and Technical Reports.
- **NASA** - Leave blank.
- **NTIS** - Leave blank.

Block 13. Abstract. Include a brief *(Maximum 200 words)* factual summary of the most significant information contained in the report.

Block 14. Subject Terms. Keywords or phrases identifying major subjects in the report.

Block 15. Number of Pages. Enter the total number of pages.

Block 16. Price Code. Enter appropriate price code *(NTIS only)*.

Blocks 17. - 19. Security Classifications. Self-explanatory. Enter U.S. Security Classification in accordance with U.S. Security Regulations (i.e., UNCLASSIFIED). If form contains classified information, stamp classification on the top and bottom of the page.

Block 20. Limitation of Abstract. This block must be completed to assign a limitation to the abstract. Enter either UL (unlimited) or SAR (same as report). An entry in this block is necessary if the abstract is to be limited. If blank, the abstract is assumed to be unlimited.

AN EXPERIMENTAL STUDY OF WING TIP VORTEX IN THE NEAR WAKE OF A RECTANGULAR WING

By

Youxin Zheng and B.R. Ramaprian

Sponsored By

The U.S. Army Research Office

Grant No. DAAL03-91-G-0026

Report No. MME-TF-93-1

WASHINGTON STATE UNIVERSITY
Department of Mechanical and Materials Engineering

JUNE 1993

ACKNOWLEDGMENTS

The authors wish to express their appreciation of the help rendered by the shop personnel, Messrs. Tommy Hellesto and Norman Martel in the design and fabrication of the wing model and its mounting. Special thanks are also due to Mr. Robert Lentz for his invaluable help in the area of instrumentation and data acquisition.

ABSTRACT

An experimental study of the tip vortex behind a NACA 0015 rectangular wing of aspect ratio 4 was carried out to understand the structure and evolution of the vortex in the near-wake region. The results of these experimental studies are presented in this report. These measurements were made nonintrusively using three-component laser-Doppler velocimetry (LDV). The experiments were carried out at a Reynolds number of about 180,000 in a low-speed wind tunnel. Two cases were studied, namely, (i) stationary wing and (ii) wing oscillating in pitch sinusoidally about its quarter-chord axis. The flow properties measured were the three components of the instantaneous velocity. These data were processed to obtain time-mean and phase-locked flow properties such as velocity, vorticity and turbulence. The data were obtained at several locations at 0.15 - 3.0 chord lengths downstream from the trailing edge. The typical distributions of mean velocity, vorticity, circulation and turbulent intensity in the near wake are presented and discussed for the stationary wing. In the case of the oscillating wing, the phase-locked velocity, vorticity and turbulence data show details of the evolution of the unsteady tip vortex downstream from the trailing edge. The results also show that the flow is strongly

non-quasi-steady at the oscillation frequency studied. The results are fully archived on tape and are available to any interested reader. These can be used as database in the development of wake models for the finite wing, and in studies of three-dimensional wing aerodynamics.

NOMENCLATURE

c	wing chord
f	frequency of oscillation
$\vec{i}, \vec{j}, \vec{k}$	unit vectors along x, y and z directions
k	$\equiv \pi f c / U_\infty$, reduced frequency
r	radial distance from the center of vortex
r_1	radial distance at the maximum tangential velocity in the vortex
s	wing chord
Re	$= \frac{cU_\infty}{\nu}$, Reynolds number

s	wing span
t	time
t_0	time lag
u, v, w	normalized instantaneous velocity components measured in x, y, z directions
u_1, v_1, w_1	instantaneous velocity components measured by LDV
U, V, W	normalized velocity components in x, y, z directions
$< U >$	phase-locked velocity component in x direction
$< V >$	phase-locked velocity component in y direction

$< W >$	phase-locked velocity component in z direction
U_∞	freestream velocity
u', v', w'	normalized mean rms turbulence intensities
$< u' >$	phase-locked rms turbulence intensity in the x direction, normalized
$< v' >$	phase-locked rms turbulence intensity in the y direction, normalized
$< w' >$	phase-locked rms turbulence intensity in the z direction, normalized
x, y, z	coordinates relative to the wind tunnel (also c/4 axis of the wing)
x_0, y_0, z_0	coordinates of the vortex center
$\bar{x}$	downstream distance from the trailing edge

α	angle of incidence
$\Delta\alpha$	amplitude of oscillation
α_0	mean angle of incidence
$\Delta\alpha$	amplitude of oscillation
Γ	circulation around a circle of radius r in the vortex
Γ_0	$\equiv (1/2)C_L U_\infty c$
Γ_1	circulation at $r = r_1$ in the vortex
$< \Gamma_1 >$	phase-locked circulation at $r = r_1$ in the vortex
θ	angle between the laser beams

θ_1	angle between the axis of the optical probes
$\omega_x, \omega_y, \omega_z$	normalized vorticity components in x, y, z directions
$< \omega_x >$	phase-locked vorticity components in x direction
$< \omega_y >$	phase-locked vorticity components in y direction
$< \omega_z >$	phase-locked vorticity components in z direction
ν	kinematic viscosity of the fluid

Table of Contents

ACKNOWLEDGEMENT iii

Abstract iv

1. INTRODUCTION 1

1.1 General 1

1.2 Previous Studies of the Wing-Tip Vortex 2

1.3 Objectives of the Experiments 11

1.4 Experimental Approach 12

2. EXPERIMENTAL SET-UP AND PROCEDURE FOR THE STEADY FLOW EXPERIMENTS 17

2.1 Experimental Facility 17

2.2 Control, Data Acquisition and Processing 22

2.3 Experimental Particulars 25

2.3 Uncertainty 26

3. RESULTS OF THE STEADY FLOW EXPERIMENTS 34

3.1 Velocity Distribution within the Vortex 34

3.2 Vorticity Distribution within the Vortex 38

3.3 Circulation Distribution within the Vortex 40

3.4 Turbulent Intensity Distribution within the Vortex 41

3.5 Effect of the Angle of Incidence on the Vortex 42

3.6 Approach of the Vortex towards Asymptotic Behavior 43

3.5 Conclusions from the Steady Flow Experiments 45

4. EXPERIMENTAL SET-UP AND PROCEDURE FOR THE UNSTEADY FLOW EXPERIMENTS 80

4.1 Experimental Set-Up 80

4.2 Data Acquisition and Processing 82

4.3 Uncertainty 85

5. RESULTS AND DISCUSSIONS OF THE STUDIES OF THE UNSTEADY TIP-VORTEX 90

5.1 Velocity Distribution within the Vortex 90

5.2 Vorticity Distributions within the Vortex 95

5.3 Circulation Distributions within the Vortex 96

5.4 Turbulent Intensity Distribution within the Vortex 99

5.4 Downstream Development of the Vortex 100

5.5 Conclusions for the Unsteady Flow Experiments 101

6. CONCLUSIONS AND RECOMMENDATIONS 181

Appendix A 169

List of Figures

Figure Page

1.1 Flow configuration in the tip vortex 14

1.2 The structure of the fully developed turbulent line vortex 15

1.3 Flow visualization of the tip vortex in the near wake 16

2.1 Schematic of the wing. The distance between two adjacent perforations is 1 cm.28

2.2 Schematic of the wing installation 29

2.3 Optical system set-up 30

2.4 Instrumentation for the signal processing of the steady flow experiments 31

2.5 Flow chart of the data acquisition program 32

2.6 Configuration of the laser beams in the probes 33

2.7 Measurement grid in the cross flow plane 33

3.1 Mean velocity contours at different x-locations for $\alpha = 10$ degrees. Outermost contour level of velocity plotted is 1.0 (maximum). Decrement interval of contours is 0.05. 46

3.2 Mean velocity contours in the vortex at (a) $x/c = 0.16$, (b) $x/c = 0.33$, (c) $x/c = 0.65$, (d) $x/c = 1.00$, (e) $x/c = 1.64$, (f) $x/c = 2.26$, (g) $x/c = 3.28$. $\alpha = 10$ degrees 47

3.3 Maximum velocity defect in the vortex during the downstream development . 51

3.4 Distribution of the mean velocity vector $(\vec{j}V + \vec{k}W)$ in the cross-stream plane at the same angle of incidence and downstream distance as Fig. 3.2. The magnitude of velocity is proportional to the length of the arrow. 52

3.5 Motions of the vortex center.(a) Vertical motion. (b) Horizontal motion. 56

3.6 Distribution of the circumferential velocity V_θ at a) $\alpha = 2$ degrees, b) $\alpha = 5$ degrees, c) $\alpha = 10$ degrees, d) $\alpha = 15$ degrees. 57

3.7 Changes of the radius r_1 *vs* x/c. 59

3.8 Plot of the maximum velocity V_1 *vs* x/c. 59

3.9 Axial-vorticity(ω_x) contours at different x-locations. The stations and incidence angle are the same as in Fig. 3.2. 60

3.10 Contours of ω_x in the vortex at the same angle of incidence and downstream distance as Fig. 3.2 61

3.11 Distribution of the cross-stream vorticity vector ($\vec{j}\omega_y + \vec{k}\omega_z$) across the vortex at the same angle of incidence and downstream distance as Fig. 3.2. The scale used in Figs. (a) to (c) is three times larger than that in Figs. (d) to (g). The magnitude of vorticity is proportional to the length of the arrow. 65

3.12 Variation of circulation Γ with distance r from the vortex center. α = 10 degrees. 69

3.13 Distribution of the longitudinal component of the turbulent intensity u' across the vortex at (a) $x/c = 0.33$, (b) $x/c = 1.16$, (c) $x/c = 2.26$, (d) $x/c = 3.28$. (i)three-dimensional carpet plot, (ii) contour plot. 70

3.14 Distribution of $v'^2 + w'^2$ across the vortex at (a) $x/c = 1.16$, (b) $x/c = 3.28$. 74

3.15 Distribution of the longitudinal component of the velocity and vorticity at (a) α = 2 degrees, (b) α = 5 degrees, (c) α =10 degrees, (i) Velocity, (ii) Vorticity. x/c = 3.28. 75

3.16 Semilogarithmic plot of Γ/Γ_1 vs r/r_1 for $x/c = 1.0$. 78

3.17 Semilogarithmic plot of Γ/Γ_1 vs r/r_1 for all the stations and angles of incidence listed in Table 2. 79

4.1 Schematic of the Scotch-Yoke Mechanism. 87

4.2 Instrumentation for the unsteady flow studies 88

4.3 Measurement grid in the cross flow plane 89

5.1 Mean velocity $< U >$ contours at x = 40 cm, α = 5 to 15 degrees by increments of 1 degree. a)Pitch-up. b)Pitch-down 103

5.2 Mean velocity $< U >$ contours at x = 10 cm, α = 6 to 14 degrees by increments of 2 degrees. a)Pitch-up. b)Pitch-down 114

5.3 Distribution of the mean velocity vector, ($\vec{j} < V > + \vec{k} < W >$) in the cross-stream plane at the same downstream distance and angles of incidence as Fig. 5.1. a)Pitch-up. b)Pitch-down. The magnitude of velocity is proportional to the length of the arrow. 119

5.4 Vertical movement of the vortex center during the oscillating cycle at a) $\bar{x}/c$ = 1.0, b) $\bar{x}/c = 1.33$, c) $\bar{x}/c = 2.0$, d) $\bar{x}/c = 2.62$. 130

5.5 Plot of the phase delay t_0 *vs* the downstream distance x. 132

5.6 Axial-vorticity $< \omega_x >$ contours at the same downstream distance and angles of incidence as Fig. 5.1. a)Pitch-up. b)Pitch-down. 133

5.7 Axial-vorticity $< \omega_x >$ contours at the same downstream distance and angles of incidence as Fig. 5.2. a)Pitch-up. b)Pitch-down. 144

5.8 Distribution of the cross-stream vorticity vector ($\vec{j} < \omega_y > + \vec{k} < \omega_z >$) across the vortex at the same downstream distance and angles of incidence as Fig. 5.1. a)Pitch-up. b)Pitch-down. The magnitude of vorticity is proportional to the length of the arrow. 149

5.9 Variation of circulation $< \Gamma >$ with distance r from the vortex center. a)Pitch-up. b)Pitch-down. 160

5.10 Semilogarithmic plot of Γ/Γ_1 vs r/r_1 for $\alpha = 5$, 10 and 15 degrees at $\bar{x}/c = 1.31$, '+' for pitch-up and '-' for pitch-down. 161

5.11 Semilogarithmic plot of Γ/Γ_1 vs r/r_1 for $\alpha = 10$ degrees at $\bar{x}/c = 0.66$, 1.31 and 2.62, '+' for pitch-up and '-' for pitch-down. 161

5.12 Changes of the length scale r_1 with time at $\bar{x}/c = 1.31$. 162

5.13 Changes of the circulation scale Γ_1 with time at $\bar{x}/c = 1.31$. 162

5.14 Distribution of the longitudinal component of the non-dimensional turbulent intensity u' across the vortex at (i) $\alpha = 5$, (ii) $\alpha = 7$, (iii) $\alpha = 9$, (iv) $\alpha = 11$, (v) $\alpha = 13$, (vi) $\alpha = 15$ degrees at $\bar{x}/c = 1.0$. (a) pitch-up, (b) pitch-down. . . . 163

5.15 Downstream development of the longitudinal component of the velocity U across the vortex. (a) pitch-up. (b) pitch-down. (i) $\alpha = 9$ degrees, $\bar{x}/c = 0.33$. (ii) $\alpha = 9$ degrees, $\bar{x}/c = 0.66$. (iii) $\alpha = 10$ degrees, $\bar{x}/c = 1.0$. (iv) $\alpha = 10$ degrees, $\bar{x}/c$ = 1.32. (v) $\alpha = 10$ degrees, $\bar{x}/c = 1.64$. (vii) $\alpha = 11$ degrees, $\bar{x}/c = 2.62$. 169

5.16 Downstream development of the longitudinal component of the vorticity ω_x across the vortex at the same angles of incidence and downstream locations as in Fig. 15. (a) pitch-up. (b) pitch-down. 175

List of Tables

Table Page

2.1 Main Components of the Measurement System. 21

2.2 Parameters and settings used in the Measurement System. 21

2.3 Measurement Locations 27

4.1 Main Components of the Measurement System 83

4.2 Parameters and settings used in the Measurement System in the Unsteady Flow Studies. 83

CHAPTER 1

INTRODUCTION

1.1 General

The study of the tip vortex behind a lifting wing of finite aspect ratio has been of interest to aerodynamicists for many years because of its many important applications in fixed and rotary aerodynamics. The knowledge of the tip vortex dynamics is essential to specify the detailed boundary conditions necessary for calculating the aerodynamic forces and moments on the wing, for understanding the interaction between the tip vortex and rotor blades in helicopter aerodynamics and, for understanding the three-dimensional dynamic stall characteristics of a pitching/oscillating wing, in general.

The generation of the tip vortex in steady flow over a wing is a result of the viscous boundary layers that develop on the lifting surfaces of the wing. A schematic view of the vortex generation is illustrated in Fig. 1.1. The pressure difference that exists between the lower and upper surfaces of the wing drives a portion of the vorticity-laden fluid in the boundary layer around the tip and toward the upper surface (suction side) of the wing. Streaklines on the upper surface and near the leading edge will therefore show the flow near the tip to be moving towards the inboard direction. The boundary-layer vorticity, which was initially oriented parallel to the span of the wing, is redirected and reorganized as the fluid undergoes a highly three-dimensional deformation and mixing at the tip. As the fluid near the tip reaches the trailing edge of the wing, it emerges from

the upper surface of the wing to form a vortex with its axis oriented in the downstream direction. This vortex is called the tip vortex. This tip vortex then leaves the surface and enters the wake, carrying about half of the circulation at the midspan of the wing (Francis *et al.*, 1979). Meanwhile, the shear layer, in the wake being drawn in to the tip vortex, continues to roll up into the vortex in a spiral-like pattern. The spiral becomes tighter and tighter as the fluid moves downstream. The flow in this region of the wake, known as the near-wake, is highly three-dimensional. The vortex undergoes viscous/turbulent diffusion and dissipation as it moves further downstream. The final, asymptotic stage of the vortex far downstream, is a well organized, axisymmetric pattern, usually referred as the fully developed trailing vortex. In the case of unsteady flow behind an oscillating wing, it has been reported that the structure of the tip vortex from a rotor is essentially the same as that from a fixed wing (Tung *et al.*, 1983), and centrifugal effect has little influence on the path of the tip vortex from a rotor (Spivey, 1986).

1.2 Previous Studies of the Wing-Tip Vortex

Most of the studies on wing-tip vortices in the past have been performed on stationary wings. These studies include experimental visualization of the flow field, quantitative measurements, and numerical simulation. Most of these refer to the dynamics of vortices at large downstream distances from the wing. As mentioned above, at these distances of the order of several tens of chord length, the mean flow in the vortex is almost axisymmetric and of asymptotically self-similar structure (fully developed trailing vortex). Figure 1.2 shows the typical structure and distribution of circulation in

a fully developed turbulent trailing vortex, as proposed originally by Hoffmann & Joubert (1963). The following conceptual picture of the trailing vortex is now well accepted:

The vortex can be divided into three subregions, analogous to the turbulent boundary layers over solid walls:

i) The viscous core region. In this region the circulation is proportional to the square of the vortex radius, analogous to the laminar sublayer;

ii) Semilogarithmic law region. The distribution of circulation is semilogarithmic with radial distance, analogous to the law of the wall;

iii) Defect law region. A 'defect law' can be applied to the outer part of the vortex, analogous to the outer region of a turbulent boundary layer.

The universal 'logarithmic region' of the fully developed turbulent vortex was first described by Hoffmann and Joubert (1963). It was predicted by theory and confirmed by experiment that circulation in the vortex is proportional to the logarithm of radius. In their theoretical analysis, analogous to that of the turbulent boundary layer, Prandtl's mixing-length theory was used to model Reynolds shear stress and all inertia force was neglected to derive the log distribution of circulation. In their experiment, the velocity distribution was obtained by a set of Pitot-type probes. A 'differential' wing, in which half of wing was mounted at an angle of incidence equal and opposite to the another half, was used to generate a steady tip vortex and avoid vortex wandering, which would be caused by the insertion of the measuring probe into the flow. And also, a length scale r_1,

the vortex radius of maximum tangential velocity, and a circulation scale Γ_1, circulation at r_1, were suggested to normalize the distribution of Γ with r in the logarithmic law region. The experiment led to the conclusion that when $U_\infty x/\Gamma_0 \geq 150$, the vortex is turbulent and fully developed, and the flow is independent of viscosity, where x is downstream distance and Γ_0 is circulation of the wing at midspan. Also, existence of the logarithmic region of circulation was confirmed as predicted by the theory. They also attempted to identify the existence of a 'defect law' region but failed to arrive at any definitive conclusion, due to the poor accuracy of the measurements.

An extensive experimental investigation of the vortex structure in the far downstream of a wing was also carried out by Gorsiglia (1973). His experimental results obtained from three-component hot-wire measurements confirmed the functional form as proposed by Hoffmann and Joubert (1963). Later, Bake *et al.* (1974) studied a similar vortex using a two-component laser-Doppler velocimetry in a water tunnel. The results also agreed with those in the previous studies after the error caused by the random motion of the vortex was corrected by an empirical method.

In addition to mean flow properties, details of the turbulent properties in the vortex have been measured in some experiments. These measurements are useful not only in the understanding the vortex structure, but also in developing a general understanding of the behavior of swirling turbulent flows. The turbulent properties of the tip vortex at three downstream locations (x/c = 45, 78, 109) were reported by Phillips (1984). The experimental set-up used was similar to that used by Saffmann and Joubert

(1963). A three-component hot-wire system was used to obtain the instantaneous velocity. The results included the time-mean velocities and all components of the Reynolds stresses. Phillips (1984) also studied the detailed effect of different coaxial axisymmetric jets and wakes on the turbulent intensities and Reynolds shear stresses in the vortex. The results indicated that the distributions of Reynolds stresses were non-axisymmetric even though the mean-velocity of the flow was locally axisymmetic. These results thus implied that the time scale of turbulent decay is much larger than that of velocity decay in the turbulent wake. This information is helpful to understand, and model the development of the turbulent line vortex in the far field.

In the downstream development of the trailing vortex, the maximum tangential velocity v_1, and corresponding radius r_1, are important parameters. The decay/growth rates of these parameters were reported by Saffman (1973) and Phillips (1981). Saffman predicted that $r_1 \sim (\mu\Gamma_1 t^2)^{\frac{1}{4}}$, where Γ_1 is circulation at r_1 and μ is viscosity of the fluid. Phillips' theory proposed his models with respect to the tip vortex behind a wing: i) $v_1 \propto t^{\frac{-1}{4}}$ for $r_1 << s$, and ii) $v_1 \propto t^{\frac{-1}{4}}$ for $r \sim s$, where s is wing span. The limited flying hot-wire measurements obtained by Ronold *et al.* (1980) confirmed that $v_1 \propto x^{\frac{-1}{2}}$ where $x = U_\infty t$. There have been no further experimental data available to assess these models in more detail.

Although the trailing vortex in the far downstream region has been studied for many years, and although its general characteristics are well known, there are considerable discrepancies among the available experimental results with respect to the details

of their downstream development, as well as diffusion or dissipation rate caused by viscosity and turbulence in the wake. Ronold *et al.* (1980) reported measurements made in a wing tip vortex behind an aircraft, obtained by using a hot-film anemometer. It was found that the tangential velocity was 2.5 times higher than in earlier measurements. And the turbulence level was found to be substantially smaller than observed in previous experiments. Therefore, the final similarity state may depend strongly upon the initial tip shape, initial turbulent levels of the vortex, and/or the ambient turbulent levels.

Recently Bandyopadhyay *et al.* (1991) measured the velocity distribution of the tip vortex by a two-component hot wire. However, their results exhibited that the vortex core is not a benign solid body of rotation if certain types of screen were used upstream to change the freestream turbulence level. It was found that the turbulent structure of the vortex is significantly affected by the type of screens. There is an intermittent exchange of momentum between the outer and core regions. The core receives a patch of turbulent fluid and the rotational motion partially relaminarizes it. This process in the tip vortex seems to be carried out by organized motions. These findings strongly suggested that in addition to Reynolds number, other physical conditions may also be an important aspect to affect the turbulent structure of the vortex.

There is some controversy with respect to the total circulation that is contained in the tip vortex from a wing. Earlier investigators (like Spreiter *et al.* 1951) claimed that the total circulation is equal to that associated with the spanwise bound vortex at the midspan of the wing. Others reported that the circulation is somewhat less than the theoretical value at the midspan because of dissipation or diffusion (Higuchi *et al.*

1986, and Ikohagi *et al.* 1986). There is also some difference of opinion with respect to the characteristic length on which the vortex core size scales. The length scale that is most often used in the literature is the wing span (Higuchi *et al.* 1986, Gorsiglia *et al.* 1973), but others disagree (Ikohagi *et al.* 1986). Another example of controversy that can be found in the literature is with reference to the length scale used to define vortex Reynolds number *etc.*. It is thus sufficiently evident that there is much more to learn about the fully developed trailing vortex.

In the study of the tip vortex, another important aspect is understanding the generation and evolution of the tip vortex in the near wake of the wing since the flow in this region influences the entire downstream development of the vortex. However, this near wake flow, within a distance of few chords from the trailing edge, has been less thoroughly investigated, mainly because of the existence of strong spatial velocity gradients and highly three dimensional flow with strong interaction of spanwise and longitudinal vorticities. Earlier studies, which consisted of smoke visualization were carried out by Patel *et al.* (1974), Francis (1988), Freymuth (1988, 1991) and Lian *et al.* (1991). The results showed that in the near wake region of the wing tip, the flow is characterized by tne rolling up of the shear layer coming out of the trailing edge, into a spiral (see Fig. 3). However, few quantitative results on the flow in this region have been reported in the past (Brooks *et al.* 1986, and Francis *et al.* 1979). Francis *et al.* (1979) examined the mean velocity distribution in the vicinity ($-1.0 \leq x/c \leq 0.0$) of a lifting rectangular finite wing with a two-component hot-wire measurement. The results exhibited that shed vorticity emanating from the lower aerodynamic surface near the

wing tip rolls up adjacent to the tip and then over onto the upper wing surface. Due to the restrictions of instrumentation, it was impossible to obtain in these experiments any data that would explain how the vorticity is transformed from spanwise direction to the main flow direction. Also no results were reported in the region downstream of the trailing edge in their experiments.

Recently McAlister *et al.* (1991) explored the distributions of mean velocity in the three-dimensional wake of a rectangular wing, by using two-component LDV, for various operating conditions. These conditions included different aspect ratios, lengths and the geometries of the wing. The angles of attack were set to be 4 - 12 degrees. The measurements were made in the trailing vortex at numerous downstream stations ranging from 0.1 to 13.0 chordlengths behind the wing. Downstream development of the mean flow (streamwise and cross-stream velocity), Reynolds number effects, the angle of incidence effects, and aspect ratio effects were discussed in detail. However, as in the other previous experiments, no distributions of vorticity were obtained in this region, due to the restriction of the measurement instrumentation.

In addition to the experimental studies of the tip vortex in the near wake, there have been a few attempts to numerically model the flow of the tip vortex from a rectangular wing. The numerical simulation of the vortex flow is quite complicated because of the three dimensionality of the flow and the difficulty of modeling turbulence. Discrete vortex methods (Yeh *et al.* 1986, Roberts *et al.* 1984, Yin *et al.* 1989 and Chen *et al.* 1989) represent the simplest approach and these have been used in the prediction of the vortex flow. However, these methods cannot yield the details of vortex development

since viscosity and turbulence are not taken into account. Furthermore, these methods can only be used when the distribution of vorticity on the surface of the wing is given by experimental data. A detailed review of these methods has been made by Sarpkaya (1988).

Quite recently Dagan *et al.* (1991) has looked at viscous flow around a slender delta wing using a fast plane-marching solution scheme. The governing equations are assumed to be parabolic (diffusion in the main flow direction is neglected because of slender wing assumption) to save the computer memory and CPU time. The results include aerodynamic coefficients, velocity field and vorticity in the crossflow planes. Accuracy of numerical prediction strongly depends on the wing model. Very good agreement is obtained between the calculated aerodynamic coefficients and experimental data for the delta wing. However, it seems that more experimental data are needed to check the accuracy of the numerical model if the method is to be extended to predict the development of the tip vortex from a rectangular wing.

The study of unsteady flow field over, and in the near wake of a pitching or oscillating airfoil has received considerable attention in recent years since such flow is associated with the phenomenon of dynamic stall. Much of the work done so far is limited to two-dimensional rectangular wings, and restricted to events occurring in the midspan plane of the airfoil (see Ahmed *et al.* 1991, Carr *et al.* 1989, 1991, Chandrasekhara *et al.* 1989, 1991, Huyer *et al.* 1991, Kim *et al.* 1991, Liou *et al.* 1990, Ohmi *et al.* 1990, and Park *et al.* 1990). There is very little comparable work performed on three-dimensional unsteady vortex dynamics in the near wake of the wing. Most of the recent

three-dimensional studies reported in this area are related to the leading edge vortices on the delta wing. Only qualitative flow visualization studies have been reported by Freymuth *et al.* (1986a, 1986b, 1989, 1991) and Atler *et al.* (1985) on the wing tip vortex system in starting flow for the rectangular wing, and some preliminary studies by Gad-el-Hak *et al.* (1986), and Zheng & Ramaprian (1991). on the three dimensional effects on a pitching liftir surface. These flow visualization studies have indicated that the flow in this region is dominated by the three-dimensional leading edge vortex and the wing tip vortex, with strong interaction between the two. It is impossible to model the unsteady flow around a finite-aspect-ratio wing just by using a two-dimensional model with some modification. There is a need for more detailed quantitative information on the flow structure in this three-dimensional unsteady near-wake flow, especially when associated with dynamic stall.

From the detailed survey of the literature presented above, the following important points can be summarized:

1. In steady flow, the structure of the asymptotic wing tip vortex far downstream from the wing, the so called trailing vortex, has been explored in some detail. A conceptual model of the trailing vortex is available. Existing Pitot and hot-wire data seem to support it. However, more extensive measurements, especially obtained using nonintrusive techniques are needed to improve the model and provide a better understanding of the flow physics.

2. In steady flow, the structure of the tip vortex in the near wake is not quite clear. More quantitative experimental studies are needed to obtain detailed information

about the three-dimensional vorticity distribution and the turbulent structure of the vortex, in this region.

3. In unsteady flow, no quantitative experimental data on the characteristics of the turbulent tip vortex, are available.

It can be concluded that there is a need for more detailed quantitative experimental information on the three-dimensional flow field associated with the turbulent wing tip vortex in the near wake.

1.3 Objectives of the Experiments

The present experimental study focuses on the understanding of the generic aspects of the vorticity dynamics, consisting of evolution and diffusion in three dimensional flow field in the near wake ($0.0 \leq x/c \leq 3.0$) of the wing tip vortex, under steady and unsteady conditions. Answering the following specific questions is the main objective of this research:

• What is the flow structures of the wing tip vortex in steady flow (including mean and turbulent properties)? How dose it develop and convect from the trailing edge of the wing, as it travels downstream? How far downstream from the trailing edge does the tip vortex become axisymmetric, and how closely is this axisymmetric tip vortex similar to the fully developed (asymptotic) trailing vortex?

• What is the strength and structure of the wing tip vortex when the wing is sinusoidally pitching? How is the unsteady vortex different from that in steady flow?

1.4 Experimental Approach

This report presents the experimental studies of the turbulent wing tip vortex in the near wake($0.0 \leq x/c \leq 3.0$). These studies were performed using three-component laser-Doppler velocimetry (LDV) technique. The current experiments have the following distinguishing features:

1. nonintrusive measurements, so as not to disturb the flow and to avoid vortex wandering

2. measurement of all the three instantaneous components of velocity to obtain all components of mean velocity as well as turbulent intensity

3. a very high spatial density of data points that allows the calculation of all the three components of vorticity in the flow field with acceptable accuracy.

The experiments were carried out in a wind tunnel at a Reynolds number of about 180,000. The test model used was a rectangular wing of NACA 0015 profile. Two cases were studied, viz., (i)stationary wing and (ii)wing sinusoidally oscillating in pitch about its $c/4$ axis. The flow properties obtained include velocities, vorticity and turbulence. Time averaged values of these properties were obtained in the case of the stationary wing. In the case of the oscillating wing, phase-locked values of the above properties were obtained.

The experimental data were obtained for several mean angles of incidence and at several downstream locations. Only some typical results are presented in this report.

The complete set of data have been recorded on tape for possible use by interested readers, and for possible future studies of the turbulent tip-vortex.

The contents of this report are arranged as follows: Chapter 2 presents the detailed description of the experimental set-up and procedure for the LDV measurements in steady flow (stationary wing). The results obtained in this study are given in Chapter 3, including the distributions of the velocity, vorticity, circulation and turbulent intensity at different angles of incidence in the near wake of the tip vortex. The experimental set-up and procedure for the studies of the wing-tip vortex behind an oscillating wing are provided in Chapter 4. Typical results and discussions of these unsteady flow studies are given in Chapter 5. Conclusions and some suggestions for further research on the tip-vortex are summarized in Chapter 6.

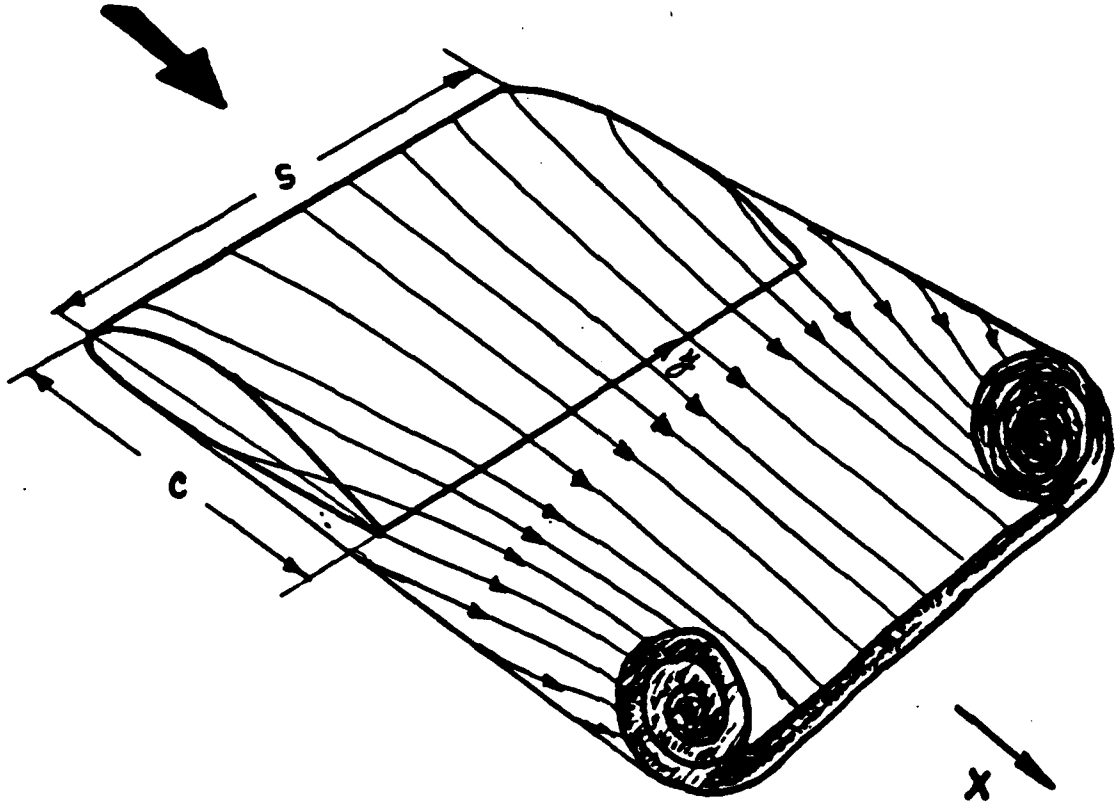

Figure 1.1 Flow configuration in the tip vortex

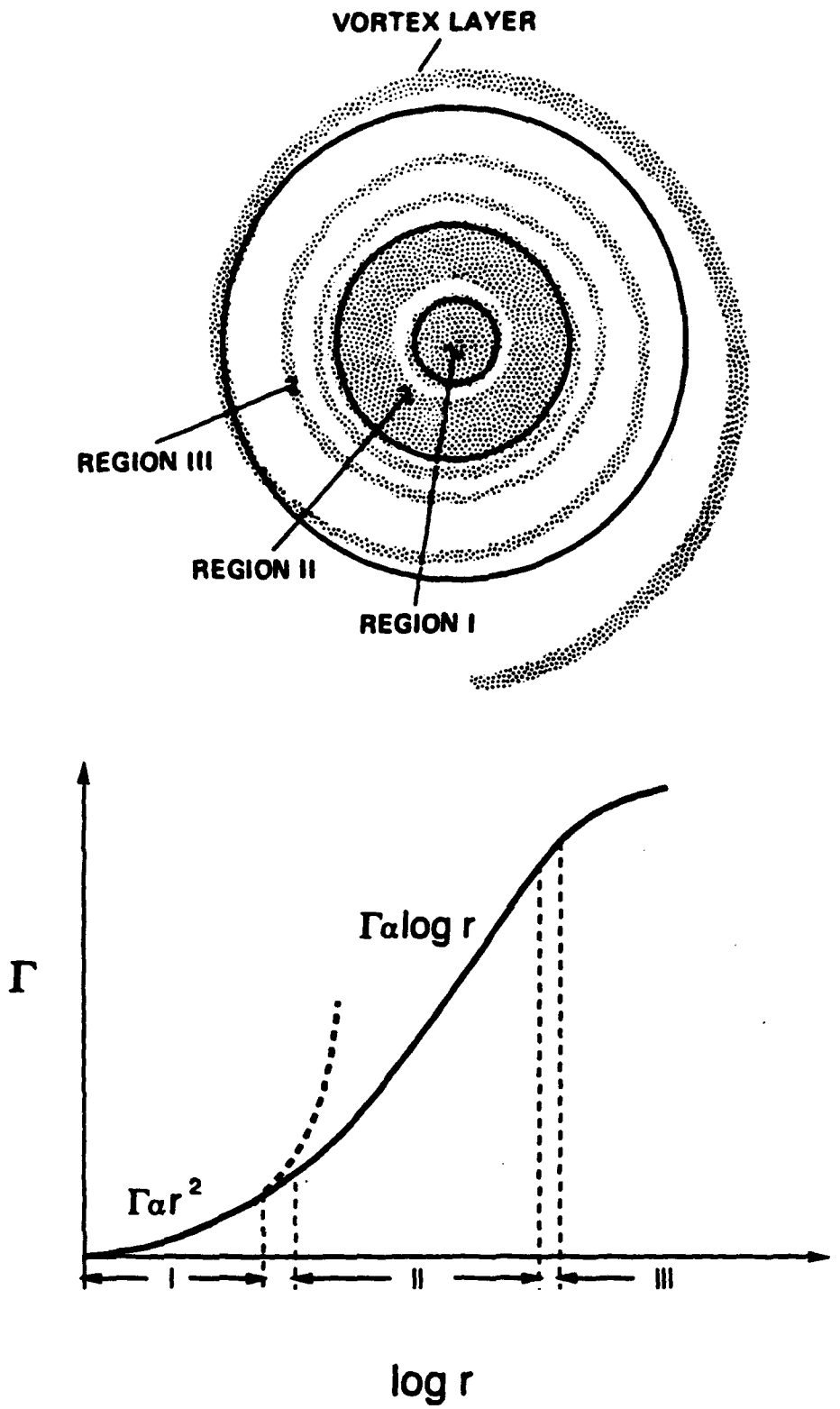

Figure 1.2 The structure of the fully developed turbulent line vortex

Figure 1.3 Flow visualization of the tip vortex in the near wake

CHAPTER 2

EXPERIMENTAL SET-UP AND PROCEDURE FOR THE STEADY FLOW EXPERIMENTS

2.1 Experimental Facility

The experiments were performed in an open-return blower-type wind tunnel with $1m \times 1m \times 5m$ test section. One of the side walls of the test section is made of glass to allow optical access to the inside of the tunnel, needed for the use of LDV. The free stream velocity can be adjusted continuously from 2 m/s to 20 m/s in the test section. The freestream turbulence intensity in the wing tunnel is about 0.7%.

A rectangular wing of NACA 0015 profile and with a chord of $30cm$, semispan of $60cm$ was used as the test model. The wing consists of four identical pieces of aluminum frames of $3cm$ thickness with NACA 0015 profile, a steel axis of $1.6cm$ diameter, and an aluminum skin of $0.1cm$ thickness. The frames were fixed on the axis at an equal interval, and covered by the skin. A schematic of the wing is shown in Fig. 2.1. A set of perforations, represented by the dots, was made to seed the flow for the LDV measurements (described in detail later). The wing was mounted with its span horizontal on a Scotch-Yoke mechanism driven by a speed-controlled D.C. motor at the middle of the test section. Using this mechanism, the wing can be set at any angle of incidence for

the steady-flow experiments, or can be oscillated sinusoidally in pitch about its quarter-chord (c/4) axis for the unsteady-flow studies. A schematic of the wing installation in the wind tunnel is shown in Fig.2.2.

A three-color, six-beam, fiber-optics based backscatter LDV system was used to measure the three components of instantaneous velocity in this study. The optical system of the LDV was manufactured by Dantec Inc.. A detailed schematic of the optical set-up is illustrated in Fig. 2.3. A coherent laser beam from a six-watt argon-ion laser is split into two beams by a dichroic separator, one is purple and another is a mixture of blue and green beams. The purple beam is first split by a natural beam splitter, into two beams with an equal ratio of energy distribution between them. Next, one of these purple beams passes through a Bragg cell. Each of these two purple beams is then transmitted by a single-mode, 10 m long optical fiber, to a cylindrical probe of 50 mm diameter and 400 mm length, as shown in Fig. 2.3. Finally, these beams coming out of the probe are then focused at the measuring volume by a lens of 600 mm focal length. Similary, the green and blue mixed beam, coming out of the dichroic separator, is split into two identical beams by a natural beam splitter. One of those then passes through a Bragg cell. After that each of these two beams is split into a pair of blue and green beams by a color beam splitter. The four beams are then transmitted into another optical probe by four $10m$-long single-mode optical fibers. These four beams are focused on the measuring volume by a similar lens as used for the purple beams.

In the receiving optics, the back scattered light from the seed particles in the measuring volume is collected by the same lenses in the two probes, and then transmitted

by two multi-mode receiving optical fibers to the potomultiplier tubes (via color filters to separate blue and green light), where the collected light is converted to electrical signals. The electrical signals from PM are mixed with shift frequency by the frequency down shifters, in order to remove the ambiguity of velocity direction, then are processed independently by the three LDV counters to get the Doppler frequencies. These Doppler frequencies along with time information, coming from the LDV counters, are transferred to a personal computer, and then stored in the disk for further data processing. A schematic of the signal processing system is shown in Fig. 2.4. The main components and parameters of the measurement system used in the experiments are listed in Table 2.1 and 2.2 respectively. The positioning of the measuring volume is performed by a computer controlled three-dimensional traverse, on which the two optical probes are mounted horizontally, as shown in Fig. 2.2.

In the experiments, the seeds for the LDV measurements were provided by fine water particles from an ultrasonic humidifier. These water particles were introduced from a set of 5 mm diameter perforations located on the pressure side of the wing surface, close to the leading edge, and along the tip. The detailed positions and numbers of the perforations, represented by the dots, are shown in Fig. 2.1. No major difficulties were experienced with regard to the seeding of the flow by this method. The accuracy of the seeds following the flow was verified by carrying out a test measurement in the tip vortex, in which the flow was seeded by introducing smoke particles generated by a ROSCO 6300 smoke/fog machine from the entrance of the wind tunnel(about 10 meters upstream from the wing). There was no significant difference between the two results

obtained by two different kinds of particles and locations introduced. Also, the velocity in the wake, obtained by a single-sensor of hot-wire probe, was compared with that obtained by the LDV. The difference between these mean velocities was found to be less than 3%.

Table 2.1 Main Components of the Measurement System.

Description	Specification
Argon-ion laser	Coherent Innova 90 Series(6 Watt)
Beam Splitters	DANTEC 55X Series
Bragg Cells	DANTEC 55X29
Optical fibers	DANTEC 60X Series
Counter Processors	DANTEC 55L96
Frequency Shifters	DANTEC 55N12
Traverse	Velmex 8300 Series

Table 2.2 Parameters and settings used in the Measurement System.

Parameters	Green Channel	Blue Channel	Purple Channel
Wave length(nm)	514.5	488	476.5
Fiber length (m)	10	10	10
Focal length(mm)	600	600	600
Beam angle(degrees)	7.05	7.05	7.05
Size of Measuring volume (mm)	0.15 x 0.15 x 0.23	0.15 x 0.15 x 0.23	0.15 x 0.15 x 0.23
Number of fringes	35	35	35
Beam diameter(mm)	1.35	1.35	1.35
Power after fibers (watt)	0.31	0.18	0.05
Shift frequency	40 mega Hz	40 mega Hz	40 mega Hz
Downmix frequency	2 mega Hz	0.01 mega Hz	0.01 mega Hz
High-pass filter	1 mega Hz	1 mega Hz	1 mega Hz
Low-pass filter	4 mega Hz	2 mega Hz	2 mega Hz
Coincident windows (μs)	200	200	500
Typical data rate (Hz)	70	60	40
Typical validation(%)	70	50	40

2.2 Control, Data Acquisition and Processing

Experiments were conducted under the control of an IBM-PC/AT computer with Dantec 57G31 TBR processor. It was programmed to acquire data and perform control functions related to the operation of the experiments. The data acquisition software was also provided by Dantec Inc., and modified for use with the present motorized traverse. The modifications consisted of an interface with the 3-D traverse, and a program to drive the traverse. The flow chart of the data acquisition program is given in Fig. 2.5. The basic function of this program is to first position measuring volume of the LDV at a predetermined location in the wake, then to acquire velocity and time data from the three LDV counters simultaneously, and finally to pass them through a "coincidence filter". The function of the coincidence filter is to determine whether the velocity information obtained from the three channels are "coincident", i.e, pertain to the same scattering particle, or particles passing through the probe volume within an "acceptable" preset time interval, called the "coincidence window". If the time intervals between these velocities are less than the coincident window selected, these data, consisting of the three components of velocity and time, are written to the disk. The coincidence window was used to provide an 'acceptable' accuracy for the *rms* velocity measurements. This coincidence window was determined by running several tests in which it was reduced successively by half of that in previous test, until the difference in *rms* values between two measurements is less than 5%. The coincidence window used in the present experiments is listed in Table 2.2.

The three components of instantaneous velocity recorded in the disk were later transmitted over ETHENET to a MASSCOMP 5600 computer for further processing to obtain time-mean flow properties. The configuration of all six laser beams in the probes is shown in Fig. 2.6. The green beams were set to be in the vertical plane (z-direction) and other four beams were in the horizontal plane. The three instantaneous non-dimensional velocity components u, v and w with respect to the tunnel-fixed coordinate frame of reference x, y and z were obtained from the three components of the velocities measured, u_1, v_1 and w_1 using the relations

$$u = \frac{u_1 + v_1}{2U_\infty \cos\frac{\theta_1}{2}} \tag{2.1}$$

$$v = \frac{u_1 - v_1}{2U_\infty \sin\frac{\theta_1}{2}} \tag{2.2}$$

$$w = \frac{w_1}{U_\infty} \tag{2.3}$$

where θ_1 is the angle between the two probes, set to be 30 degrees in the present experiments, and u_1, v_1 and w_1 are instantaneous velocities obtained from Doppler frequencies from blue, purple and green beams respectively. These velocity components u_1, v_1 and w_1 can be obtained below, as typically illustrated for u_1

$$u_1 = \frac{\lambda(f_D - f_s)}{2\sin\frac{\theta}{2}} \tag{2.4}$$

where λ is wavelength of green color, f_D is Doppler frequency measured, f_s is down frequency shift, and θ is the beam angle, listed on Table 2.2.

Any component of velocity, e.g. u, can be decomposed to mean and fluctuating parts, as follows:

$$u(x, y, z, t) = U(x, y, z) + u'(x, y, z, t) \tag{2.5}$$

Consequently, the time-mean velocities and turbulent properties can be obtained as

$$U(x,y,z,) =< u(x,y,z,t) >$$

$$V(x,y,z) =< v(x,y,z,t) >$$

$$W(x,y,z) =< w(x,y,z,t) > \tag{2.6}$$

and

$$u'^2(x,y,z) =< (u(x,y,z,t) - U(x,y,z))^2 >$$

$$v'^2(x,y,z) =< (v(x,y,z,t) - V(x,y,z))^2 >$$

$$w'^2(x,y,z) =< (w(x,y,z,t) - W(x,y,z))^2 >$$

$$u'v'(x,y,z) =< (u(x,y,z,t) - U(x,y,z))(v(x,y,z,t) - V(x,y,z)) >$$

$$u'w'(x,y,z) =< (u(x,y,z,t) - U(x,y,z))(w(x,y,z,t) - W(x,y,z)) >$$

$$v'w'(x,y,z) =< (v(x,y,z,t) - V(x,y,z))(w(x,y,z,t) - W(x,y,z)) > \tag{2.7}$$

where $< \Phi >$ denotes the ensemble average of $\Phi_1, \Phi_2, \Phi_3, ..., \Phi_i, ..., \Phi_n$, over a large number of samples (N) collected over a long enough period time, and obtained as:

$$< \Phi >= \frac{1}{N}\sum_{i=1}^{N} \Phi_i \tag{2.8}$$

The velocity information was obtained in a fine spatial grid (see Fig. 2.7). This made it possible to compute the three vorticity components from the velocity data. This was done by using a first-order finite-difference approximation, as illustrated below, for the computation of ω_z

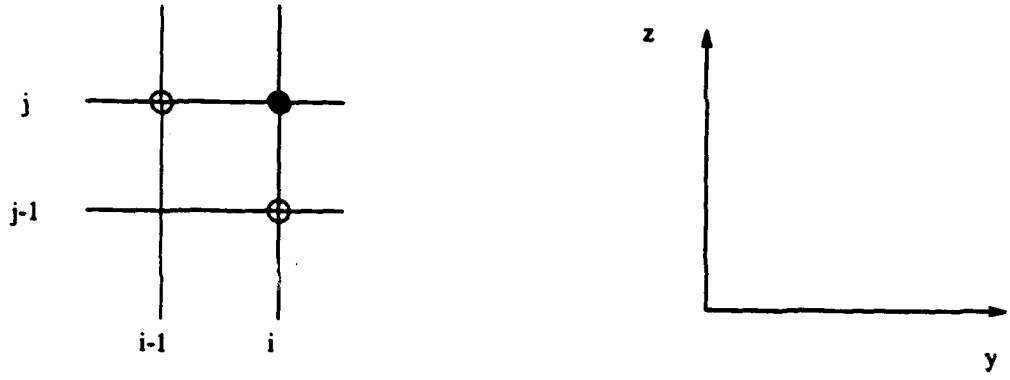

$$(\omega_x)_{i,j} = \frac{W_{i-1,j} - W_{i,j}}{y_{i-1,j} - y_{i,j}} - \frac{V_{i,j-1} - V_{i,j}}{z_{i,j-1} - z_{i,j}} \tag{2.9}$$

Similar formulas were used for ω_y and ω_z.

2.3 Experimental Particulars

The experiments were conducted at a free stream velocity of about 8.2 m/s, corresponding to a Reynolds number of about 180,000. Four incidences, namely 2, 5, 10 and 15 degrees, were studied. The data were obtained at several downstream locations in the region $0.15 \leq x/c \leq 3.3$ from the trailing edge ($x = \bar{x}$). The exact locations with respect to the different angle of incidences are listed in Table 2.3. Note that some pair of measurement stations were selected close to each other, so that derivatives of velocities in the main flow direction (x) could be obtained accurately for vorticity calculation. It was later found, however, that in most cases, the contribution to vorticity by the velocity gradient in the x direction was less than 3 percent of total vorticity, so it was reasonable to neglect velocity gradients in the x direction for the vorticity calculation.

At each location (x-station), data were obtained across the vortex (in $y - z$ plane) at an average of about 600 points which formed a fine grid as shown in Fig. 2.7. The grid size in the central part of the vortex was selected to be half of that in the outer part, since the spatial velocity gradients are larger near the center. At each grid, an average of about 1200 samples were collected over a period of about 30 - 200 seconds (depending on the location of the point in the vortex) to obtain the time-mean. The experiment at each longitudinal station lasted, on an average, for about 24 hours. The experimental procedure including probe positioning and data acquisition, was fully automated, it proceeded, nearly unattended during this period.

2.3 Uncertainty

For the experimental data obtained in this study, uncertainty estimates were performed taking into account the following parameters. The uncertainty in free stream velocity, which arose mainly due to the fluctuation of fan speed, and humidity in the room, was within 3% of U_∞, The temperature of the air was nearly constant inside the wind tunnel laboratory. Hence, for each test run, the Reynolds number was constant within an uncertainty of 3 %. No corrections were applied to the LDV velocity bias and fringe bias due to the high frequency shifts employed. The uncertainty in positioning of the measuring volume in the each direction (x, y and z) was 0.05 mm (0.002 c). The uncertainty in the absolute incident angle was $\pm$ 0.5 degree. Overall, the maximum uncertainties in the LDV measurements of the mean and *rms* velocities were estimated to be 5 and 3 percent of freestream velocity respectively. The accuracy of the vorticity

calculations can be verified by the distribution of circulation within the vortex. It was found that in the cross-stream stations the difference between the vorticity integral over the vortex area and the velocity integral around the same area (circulation) was about 3%. This means present LDV measurements have captured information on velocities as well as vorticities in the flow, with good accuracy.

Table 2.3 Measurement Locations

Downstream Distance x from the Trailing Edge(cm)	Angle of Incidence α (degrees)			
	2	5	10	15
4			x	
5		x	x	x
10		x	x	x
15		x	x	
20		x	x	x
30		x	x	
32			x	
40		x	x	
50		x	x	
60		x	x	
80	x	x	x	
100	x	x	x	

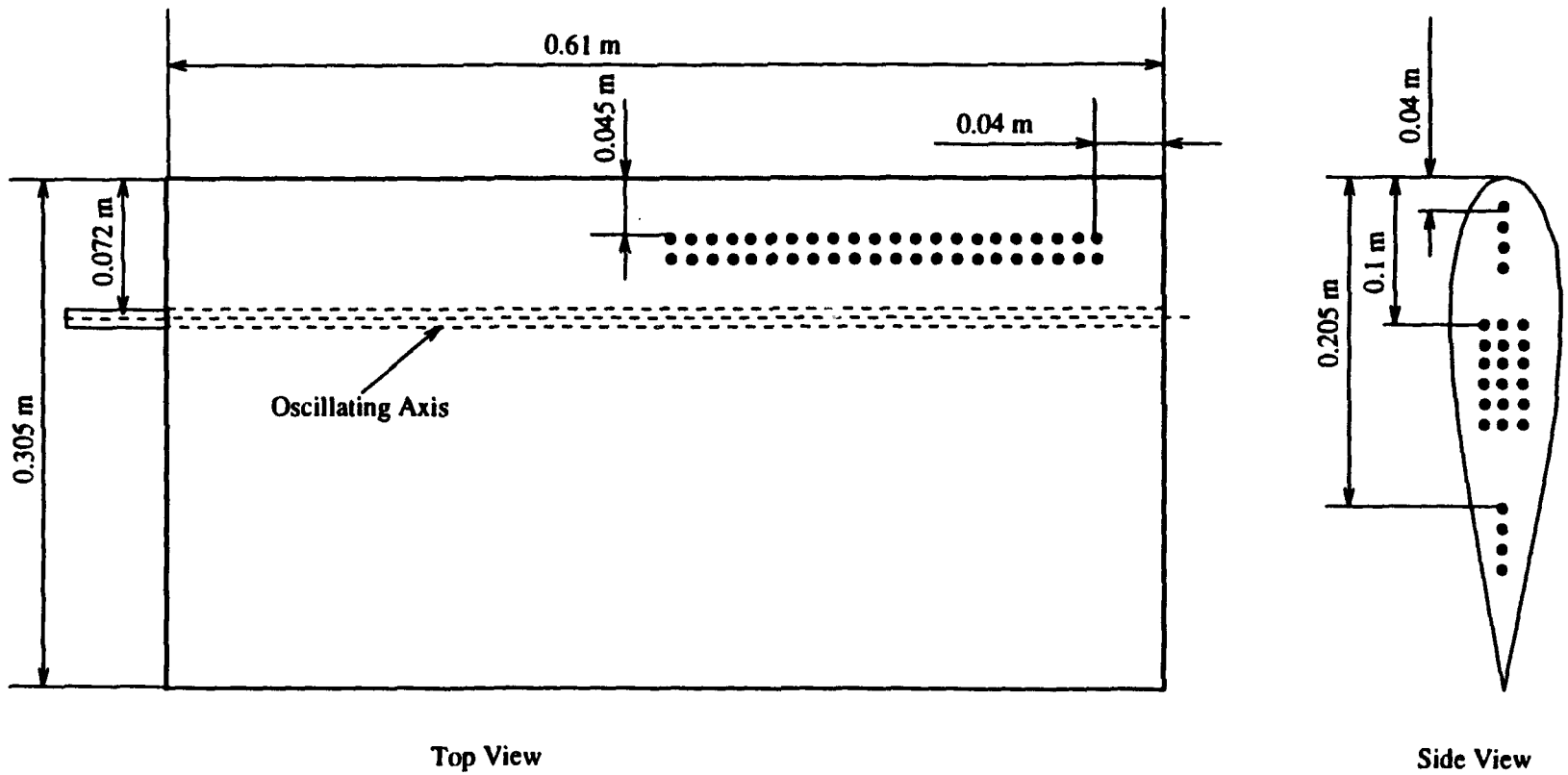

Figure 2.1 Schematic of the wing. The distance between two adjacent perforations is 1 cm.

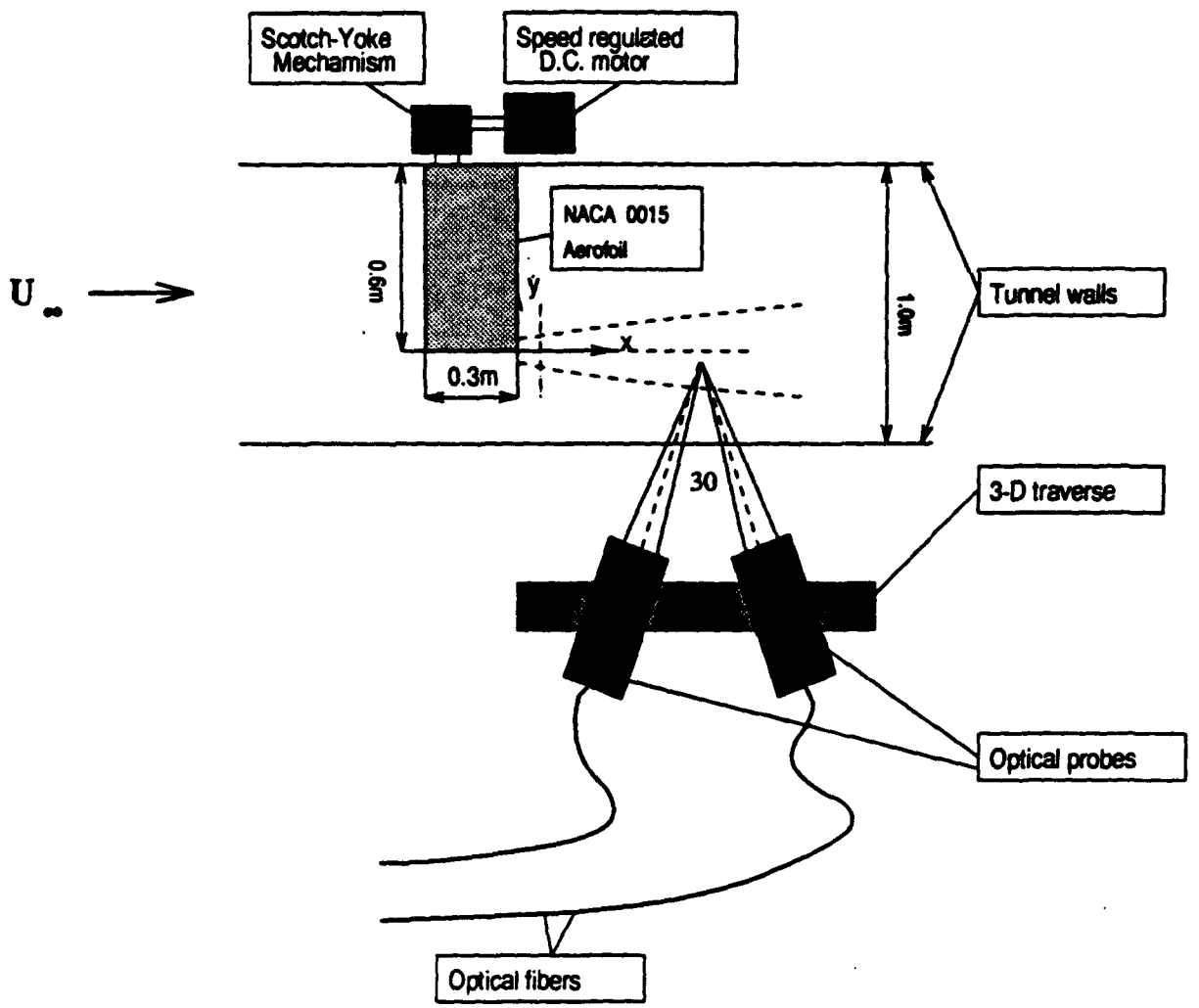

Figure 2.2 Schematic of the wing installation

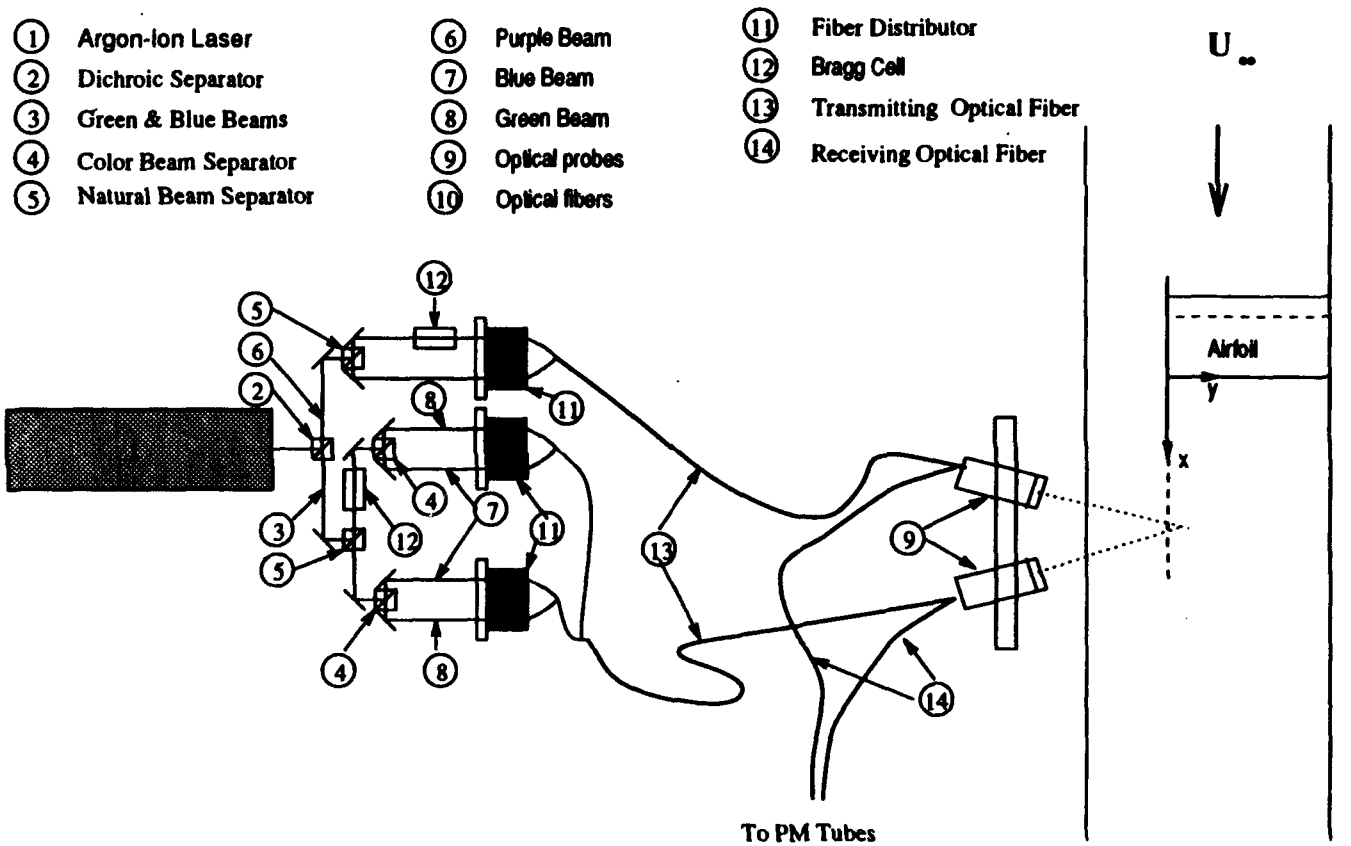

Figure 2.3 Optical system set-up

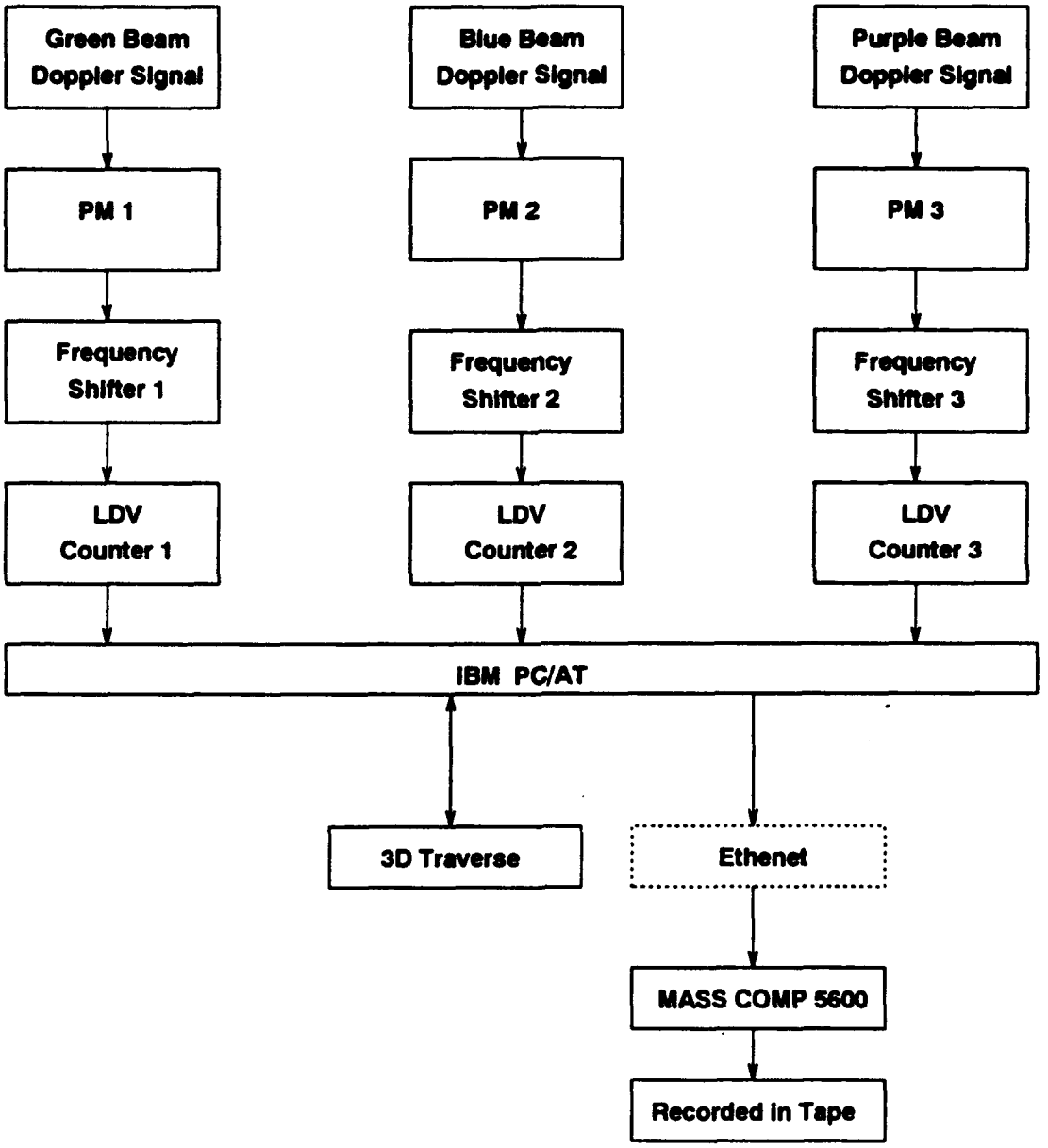

Figure 2.4 Instrumentation for the signal processing of the steady flow experiments

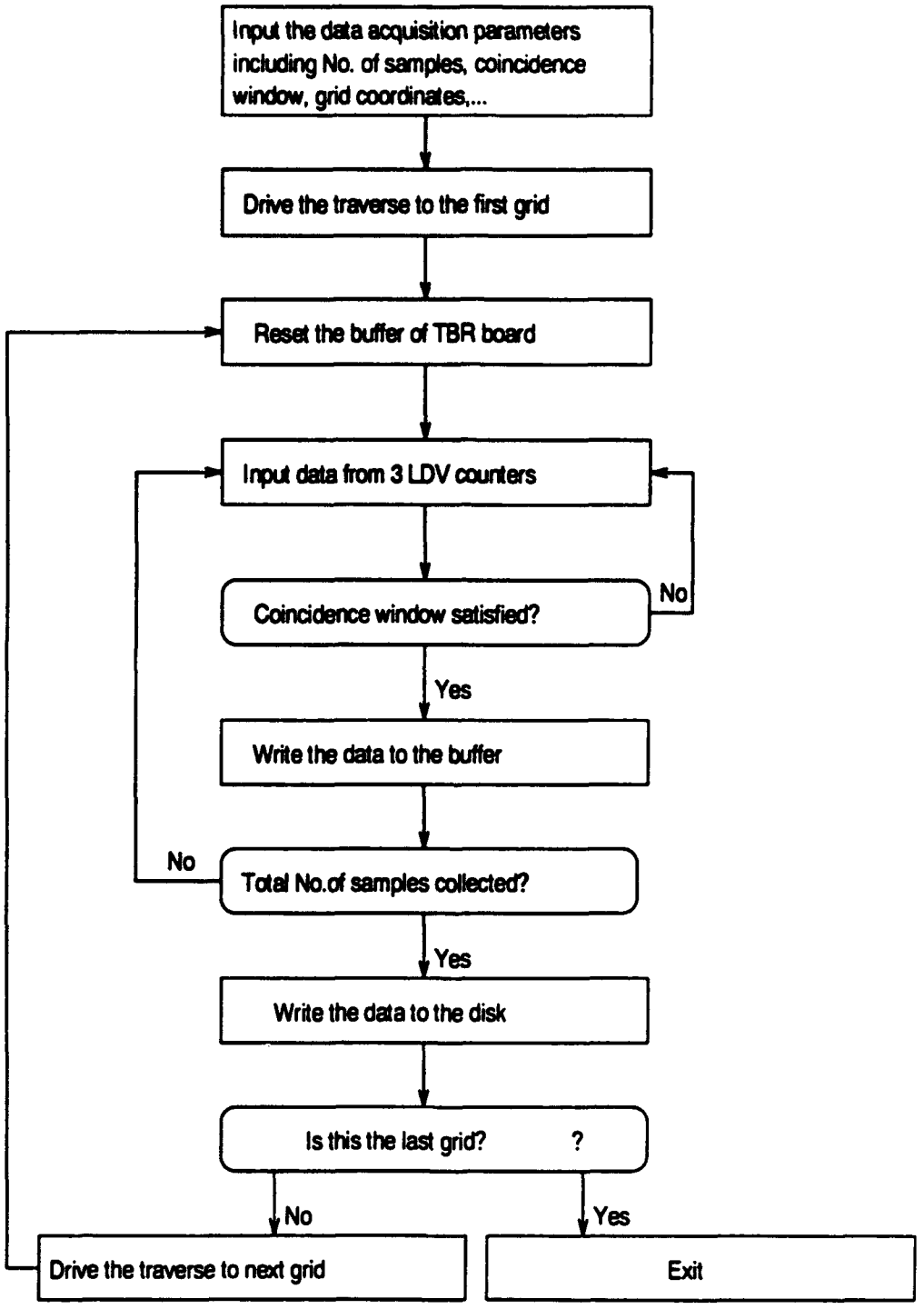

Figure 2.5 Flow chart of the data acquisition program

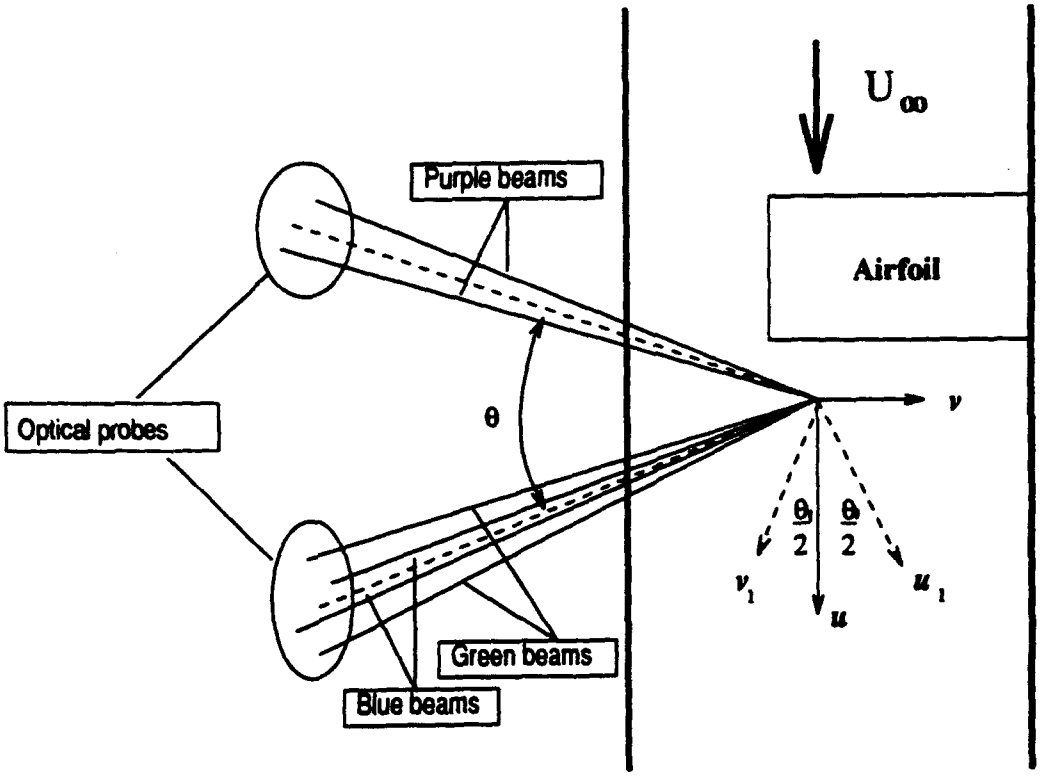

Figure 2.6 Configuration of the laser beams in the probes

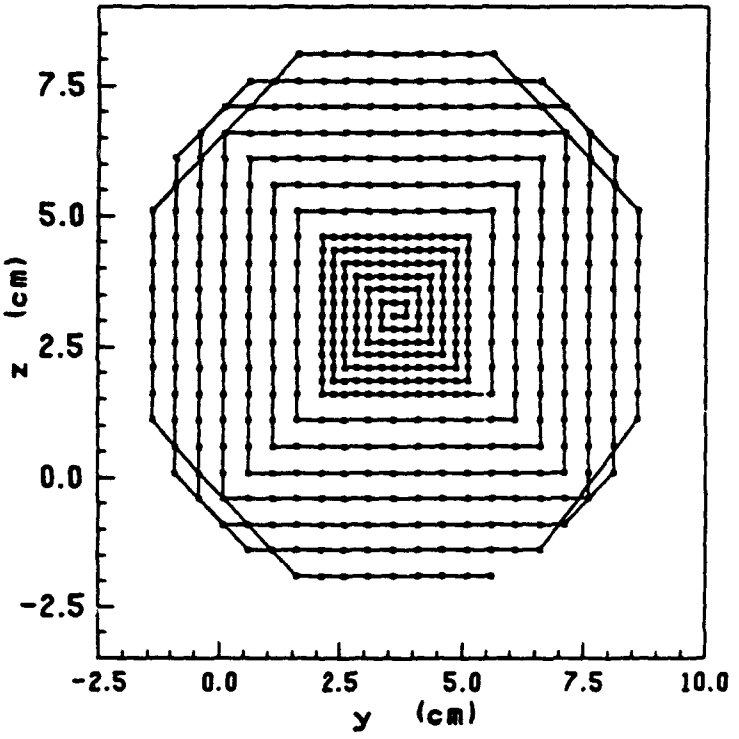

Figure 2.7 Measurement grid in the cross flow plane

CHAPTER 3

RESULTS OF THE STEADY FLOW EXPERIMENTS

All experimental results from the steady flow experiments, presented in this paper are normalized using the freestream velocity U_∞ and wing chord c as reference velocity and length scale respectively. Note that the origin of the coordinate system is located at the wing tip on the trailing edge (see Fig. 2.2) in all the figures presented. The extent of the cross-stream region scanned in the experiments was the maximum possible that could be measured with the LDV. It was impossible to obtain any data beyond that region either because of the lack of particles, or because of being outside the optical range of the LDV. Note, however, that in all cases, all the significantly vortical region of the tip vortex has been measured.

3.1 Velocity Distribution within the Vortex

Distribution of the normalized mean longitudinal velocity U across the vortex at x/c = 0.16, 0.33, 0.65, 1.00, 1.64, 2.26 and 3.28 for α=10 degrees are shown by the area-shaded grey-level contours in Fig. 3.1. It can be seen , by following any one grey-level band, that the shear layer from the wake of the wing rolls up into a spiral in the immediate near wake. This spiral is associated with the shear layer coming from the pressure side of the inboard regions of the wing. The spiral gets tighter as the flow moves downstream until the flow exhibits a well organized, near-axisymmetric vortex-like pattern beyond about one chord downstream from the trailing edge. And, it appears

that velocity deficit in the vortex is reduced quickly due to viscous diffusion/dissipation. A more detailed downstream development of velocity U, can be seen from the contours in Fig. 3.2. It can be noted that velocity U in the vortex is highly three dimensional in the initial region near the trailing edge (say, $x/c \leq 1.0$). Beyond that, the velocity is lower and very nearly axisymmetric near the central part of the vortex, while the velocity is higher and exhibits a spiral (non-axisymmetric) structure in the outer part. The velocity approaches the freestream velocity in the region beyond a distance of about 0.25c from the vortex center. The maximum velocity deficit in the center of the vortex is seen more clearly in Fig. 3.3. It is seen that the velocity deficit is reduced quickly in an initial region $x/c \leq 2.0$ due to strong viscous diffusion/dissipation in the vortex. Beyond that region, the decay rate of the velocity deficit is very small. Meanwhile, the velocity deficit is smaller at smaller angles of incidence than at larger angles of incidence, because of the weaker intensity of the vortex at small incidence. No velocity excess was found in all the cases studied. However, the velocity, obtained by McAlister *et al* (1991) in the similar experiments, exceeds the free stream velocity by up to 50% in the central regions of the vortex. Since the spiral, which rolls up into the tip vortex, comes from the wake associated with the shear layer from the pressure side of the wing, and the wake velocity is lower than the free stream velocity, the velocity observed in the vortex should not be more than the free stream velocity. Deviations from this in their experiments, are probably due to the seed particles not following the flow very well.

The mean velocity vectors ($\vec{j}\bar{V} + \vec{k}\bar{W}$) in the cross-stream plane for the same angles and distances as in Fig. 3.1 are shown in Figs. 3.4(a) to 3.4(g). A dashed line in

the figure represents the position of the trailing edge of the wing. It is seen that velocity vectors are quite smooth over the entire vortex. Also, unlike in some other studies, there was no particular difficulty in obtaining the measurements near the vortex center. In fact, data rates up to 100 samples/sec. were obtained in this region. This is presumably due to the seed injection scheme chosen and the small inertia of the water particles, at the low velocity studied. The tangential velocities are seen to increase rapidly from almost zero at the center of the vortex to a maximum at some distance r_1 from the center, beyond which they decrease gradually. Near the trailing edge, the velocities in the upper-left half of the vortex (outboard of the tip) are seen to be generally larger than those on the lower-right half(inboard of the tip). This tendency is reduced gradually and the distributions of velocities are more nearly axisymmetric after $x/c \geq 1.0$. Similar behavior was observed by McAlister *et al* (1991). The maximum cross-stream velocity was found to be about 45% of the freestream velocity, and is thus very significant. This velocity is of the same order as that obtained by McAlister *et al* (1991).

From plots like Figs. 3.4(a) to 3.4(g), one can locate the center (point of zero cross-stream velocity) of the tip vortex with very good accuracy by linear interpolation/extrapolation. It was found that the vertical coordinate of the vortex center essentially remained constant during the downstream development (at approximately 11 % of the wing chord above the trailing edge for $\alpha = 10$ degrees), as shown in Fig. 3.5(a) for $\alpha = 5$ and 10 degrees. The vortex center, however, keeps moving into the inboard direction during the downstream development, as shown in Fig. 3.5(b) for $\alpha = 5$ and 10

degrees. This inboard motion can be approximated as a straight line

$$\frac{y_0}{c} = 0.035\frac{x}{c} + 0.07 \tag{3.1}$$

where y_0 is the spanwise coordinate of the vortex center. This line is represented by a solid line in Fig. 3.5(b). The inboard motion of the vortex center is attributed to the continuing roll-up of the shear layer with some longitudinal vorticities. The vortex center, as well as the vortex, should approach an asymptotic state after all the shear layer rolls up into the vortex far downstream.

Since the vortex appears to approach eventually an axisymmetric configuration, it is useful to study the behavior of the flow properties in cylindrical coordinates. For example, one can study the evolution of the circumferentially averaged velocity components V_θ and V_r with distance downstream. Typical distributions of circumferential averaged velocity V_θ from the experiments at four different incidences, namely α = 2, 5, 10 and 15 degrees, are shown in Figs. 3.6 (a) to 3.6(d). It is seen clearly that as the vortex moves downstream, maximum circumferential velocity in the vortex decreases because of viscous/turbulent diffusion. If the radius r_1 at velocity peak is considered to be a measure of the size of the vortex core, the core size seems to approach a constant with downstream travel. This tendency can be seen more clearly in Fig. 3.7 (about 6%c for α = 5 degrees and 8 %c for α = 10 degrees). Similar results were obtained by Mason (1973) for a NACA 0012 airfoil with a square tip. Also, it is seen that the radius r_1 increases slightly with α. This is because the shear layer that rolls up into the vortex to enlarge the vortex size, is larger at larger angles of incidence. Similar tendencies can be observed in V_1, the maximum V_θ, as shown in Fig. 3.8. However, the magnitude of V_1 is

not determined by the thickness of the shear layer which rolls up into the vortex, but by the strength of the vortex, or circulation. These results obtained are not in agreement with the results predicted by Phillip's theory (1981) for the fully developed turbulent trailing vortex. The reason is that in this near-wake flow, the roll-up of the shear layer into the vortex with some longitudinal vorticity, tends to increase the strength of the vortex. On the other hand, the affect of viscous diffusion/dissipation tends to decrease it. The total affect of the above two aspects is balanced in the some regions of the near-wake so that the strength of the vortex is nearly unchanged. However, only viscous diffusion/dissipation affects the fully developed trailing vortex. Thus the strength of the vortex will decrease with the downstream development. Therefore, the magnitude of V_1 will decrease as the vortex moves to downstream, as predicted by Phillip's theory (1981).

3.2 Vorticity Distribution within the Vortex

The distributions of the normalized axial component of the mean vorticity ω_x across the vortex in the near wake, were obtained by numerical differentiation of the measured mean velocity field. Typical results are shown by the area-shaded grey-level contours in Fig. 3.9 at the same stations and incidence angle as in Fig. 3.2. Maximum (negative) contour level is -26., located in the center of the vortex, and contour increment is 6.0. It can be seen by studying the downstream evolution of any one grey-level band, that vorticity leaving the trailing edge rolls up and gradually accumulates at the center of the vortex. After a distance of about one chord from the tip, the vorticity distributions

become almost axisymmetric. These vorticity distributions exhibit a trend similar to the distributions of velocity components. However, as the rolling-up process continues, more and more vorticity from the shear layer is trapped by the vortex, so that the maximum vorticity increases with distance unlike the velocity deficit in the vortex. The vorticity ω_x distribution across the vortex is more clearly seen from the contour plots shown in Figs. 3.10(a) to 3.10(g). It is seen that the vorticity decreases gradually from a maximum at the vortex center to nearly zero in the outer part of the vortex. This shows that viscous/turbulent diffusion is significant in the inner part of the vortex. It is also noted that most of the vorticity is concentrated in a nearly circular area of a radius of about 0.15c. The outer part of the vortex carries very little axial vorticity. Compared with Figs. 3.1 and 3.2, it can be clearly seen that no appreciable longitudinal vorticity is carried into the vortex by the spiral shear layer from the trailing edge.

Figures 3.11(a) to 3.11(g) shows the distribution of the vorticity vector $(\vec{j}\omega_y + \vec{k}\omega_z)$ in the cross-stream plane for the same conditions as in Fig. 3.2. The dashed line represents the position of the trailing edge. The maximum magnitude of this vorticity vector is changed from 52% of the magnitude of $\vec{i}\omega_x$ at $x/c = 0.16$ to 10% at $x/c = 3.28$. It is seen that the shear layer coming from the trailing edge of the wing and carrying a significant amount of cross-stream vorticity rolls up into a spiral structure. As it rolls up into the core region of the vortex, the cross-stream vorticity components become small and virtually disappear at some distance (about 0.04c) from the center of the vortex. These figures, along with Fig. 3.9, clearly indicate that the resultant vorticity vectors in the shear layer gradually rotate from a cross-stream plane into the axial direction as

the roll-up process continues. As a result, the axial vorticity component is augmented near the vortex center. It is also seen that it is reasonable to consider ω_x as the only dominant vorticity in the vortex core region for x/c <3.5 and everywhere in the vortex for $x/c > 3.5$.

3.3 Circulation Distribution within the Vortex

The circulation Γ around any circle of radius r in the cross-stream plane can be calculated by evaluating the integral:

$$\Gamma = \oint (\vec{j}V + \vec{k}W) \cdot d\vec{s}$$

The distribution of circulation as a function of r across the vortex at $\alpha = 10$ degrees is shown in Fig. 3.12 for various x—locations. The vortex center ($r = 0$) at each station was assumed to coincide with the poin of minimum cross-stream velocity (the error for $r = 0$ caused by the grid size is less than 0.008c, see Figs. 2.9, 3.1 and 3.11). The dashed line represents the circulation $\frac{\Gamma_0}{cU_\infty}$, obtained from the theoretical relation:

$$\rho U_\infty \Gamma_0 = (1/2) C_L \rho {U_\infty}^2 c \qquad (3.2)$$

where the lift coefficient C_L for the present aspect ratio and angle of incidence was 0.66, obtained by interpolation from the experimental data of Gorsiglia *et al* (1973) for a similar wing. Γ_0 can be recognized as the span averaged value of circulation associated with the bound vortex. This should also be equal to the asymptotic value of Γ obtained in the tip vortex as $x \rightarrow \infty$. The results indicate that the distributions vary only slightly with downstream distance. On the other hand, the circulation increases rapidly with

radius in the core region and then more gradually approaches Γ_o towards the outer edge of the vortex. It is seen that 90% of Γ is contained within $r/c = 0.15$. However, there is still a slight increasing trend in Γ at the outer edge of the measured region. This is most likely due to the possibility that at all these stations, some shear layer is still rolling into the vortex center bringing with it additional vorticity. The data trend, however, suggests that Γ would eventually approach a value not too different from Γ_0. There is, however, a small nonmonotonic behavior observed in this approach. The reason for this is not clear. In any case, considering the uncertainties in the experimental data as well as in the value of Γ used, the present circulation measurements are reasonably consistent with earlier data obtained from lift measurements. Meanwhile, it is noted that the vortex already carries more than 85% of the midspan circulation at $x/c = 0.16$. It is thus suggested that most of spanwise vorticity has merged into the tip vortex within a very short distance from the trailing edge.

3.4 Turbulent Intensity Distribution within the Vortex

The rms turbulent intensities and turbulent shear stresses can be obtained from the instantaneous velocities. The downstream development of the rms of longitudinal velocity fluctuation u' for $\alpha = 10$ degrees is shown in Figs. 3.13 (a) to 3.11 (d) for $x/c = 0.65$, 1.31, 2.26 and 3.28. The maximum value is about 8% of the free stream velocity. It is seen that this intensity is associated mostly with the spiralled shear layer and is very small (about 3%) in the rest of the vortex. The shear layer coming from the wake carries with it the wake turbulence(see Fig. 3.13 a). Eventually as the spiral gets

tighter, the turbulence concentrates at the center of the vortex (Figs. 3.13 b - d). This accounts for the peak observed at the vortex center. Thus, for $x/c \geq 2.5$, the high level of turbulent intensity is limited to a small circular area of radius less than $0.08c$ with a nearly axisymmetric distribution around the vortex center. The presence of turbulence in the core region may appear to be somewhat of a contradiction. However, this is not so since this turbulence is not locally produced, but convected from the boundary layer of the wing in the flow. In fact, as the flow proceeds downstream towards full development, the turbulence near the center will dissipate and diffuse under the action of viscosity, so that the maximum turbulent intensity is reduced in the center of the vortex as seen in the figure. The very small level of turbulent intensity measured in most parts of the vortex (even in regions of significant velocity gradient) means also that there is very little jitter and hence no significant vortex wandering. In fact, this turbulence measured includes, in addition to any effect of vortex wandering, other factors like freestream turbulence (about 0.7%) and LDV noise. The distributions of other turbulent properties, say $v'^2 + w'^2$ in Fig. 3.14, are seen to be similar to u'. These data are recorded on the tape and are available to any interested reader.

3.5 Effect of the Angle of Incidence on the Vortex

It is known from invicid wing theory, that wing loading and hence the strength of the tip vortex is determined by the angle of incidence. The size of the vortex is determined by the thickness of the shear layer which rolls up into the vortex. Hence, the size is also determined by the angle of incidence. While there have been some recent

investigations about the effects on the angle of the incidence on the wing tip vortex and pressure distribution, it is still not clear how it affects the structure of the wing tip vortex with respect to details, such as distributions of velocity and vorticity. Some typical effects of the angle of incidence on the vortex structure are presented in Fig. 3.15, which shows the distribution of longitudinal velocity U as well as vorticity ω_z for α = 2, 5 and 10 degrees at $x/c = 3.28$. Basically, there are no significant differences among them. It is seen that the vortices are nearly axisymmetric in the center, but exhibit a spiral structure outside. However, there are some fine differences in their structure. First at small incidences, the size of the vortex is small due to the small pressure difference between the upper and lower surface of the wing. Second at large incidence, the rolling-up process is much faster and the vortex is better organized. No velocity excess was found in the main flow direction in all the cases studied.

3.6 Approach of the Vortex towards Asymptotic Behavior

Earlier studies (Hoffmann *et. al.* 1963, and Phillips 1981) on fully-developed, axisymmetric, turbulent, line vortices have resulted in the identification of several characteristic regions within the vortex. For example, within the rotational region of the vortex (i.e., where Γ varies), three subregions have been identified on the basis of phenomenological reasoning analogous to that used by Millikan for characterizing turbulent boundary layers. Thus, there exists a viscous core region where the circulation is proportional to r^2, analogous to the laminar sublayer; an intermediate region where the

circulation distribution is semi-logarithmic, analogous to the log layer; and an outer region where a 'defect law' applies, analogous to the outer region of a turbulent boundary layer. It is also known that in a *developing* turbulent boundary layer, both the viscous sublayer and the log layer with their small characteristic time scales become established much earlier than the outer defect layer which has a larger time scale. While the three-dimensional tip vortex is very different from a line vortex, when it is generated, it can be expected to approach asymptotically the state of a turbulent line vortex. The distance at which this occurs is of the order several tens of chords. Obviously, such an asymptotic state could not be reached in the present experiments. It is, however, interesting to examine how the behavior of the present wing tip vortex compares with the asymptotic behavior. For this purpose, we present its behavior in the framework of the asymptotic turbulent line vortex. Figure 3.16 shows a plot of Γ *vs* r in semilogarithmic coordinates, for $x/c = 1.0$, and Fig. 3.17 for all the stations and angles of incidence listed in Table 2.2. In order to remove any effect of a slight departure from axisymmetry, a mean length scale r_1 is obtained from the circumferential averaged value of r_1, which is the vortex radius of maximum tangential velocity. A circulation scale is defined by Γ_1, which is the circulation around a circle of radius r_1. These length and velocity scales are used to normalized the results in these figures. It is seen that there is a small region ($r/r_1 < 0.4$) near the vortex center where Γ can be described as:

$$\frac{\Gamma}{\Gamma_1} = 1.74(\frac{r}{r_1})^2 \tag{3.3}$$

Here the coefficient 1.74 is quite close to the value of 1.83 obtained by Hoffmann & Joubert (1963). Beyond the core region, there is an other region between $0.6 < r/r_1 <$

1.4, where Γ does seem to follow a semilogarithmic variation with r:

$$\frac{\Gamma}{\Gamma_1} = ln(\frac{r}{r_1}) + 1.05 \tag{3.4}$$

This is also in agreement with Hoffmann & Joubert's description for turbulent line vortex. Thus, the length and velocity scales used in the above circulation distribution seem suitable to describe the asymptotic behavior of the vortex in the near wake.

3.5 Conclusions from the Steady Flow Experiments

The present experiments have yielded very detailed information on the structure of the wing-tip vortex in the highly three-dimensional near-wake region. The data indicate that the shear layer from the trailing edge of the wing rolls up into a spiral in this region carrying with it the wake turbulence and cross-stream vorticity. During the roll-up process, the cross-stream vorticity vector associated with the shear layer is rotated into a streamwise direction augmenting the vorticity in that direction at the center of the tip vortex. The vortex becomes nearly axisymmetric within about one chord distance downstream. The vortex core is dominated by axial vorticity, which is maximum at the center and decreases nearly to zero (due to viscous/turbulent diffusion) in the outer part of the vortex. The circulation distribution across the inner part of the vortex is very similar to that observed i ..ly developed axisymmetric trailing vortices, namely, it varies as r^2 very near the center and follows a semilog law over a part of the region beyond. The extensive data obtained in this study can serve as a useful database in the development of wake models for finite wings.

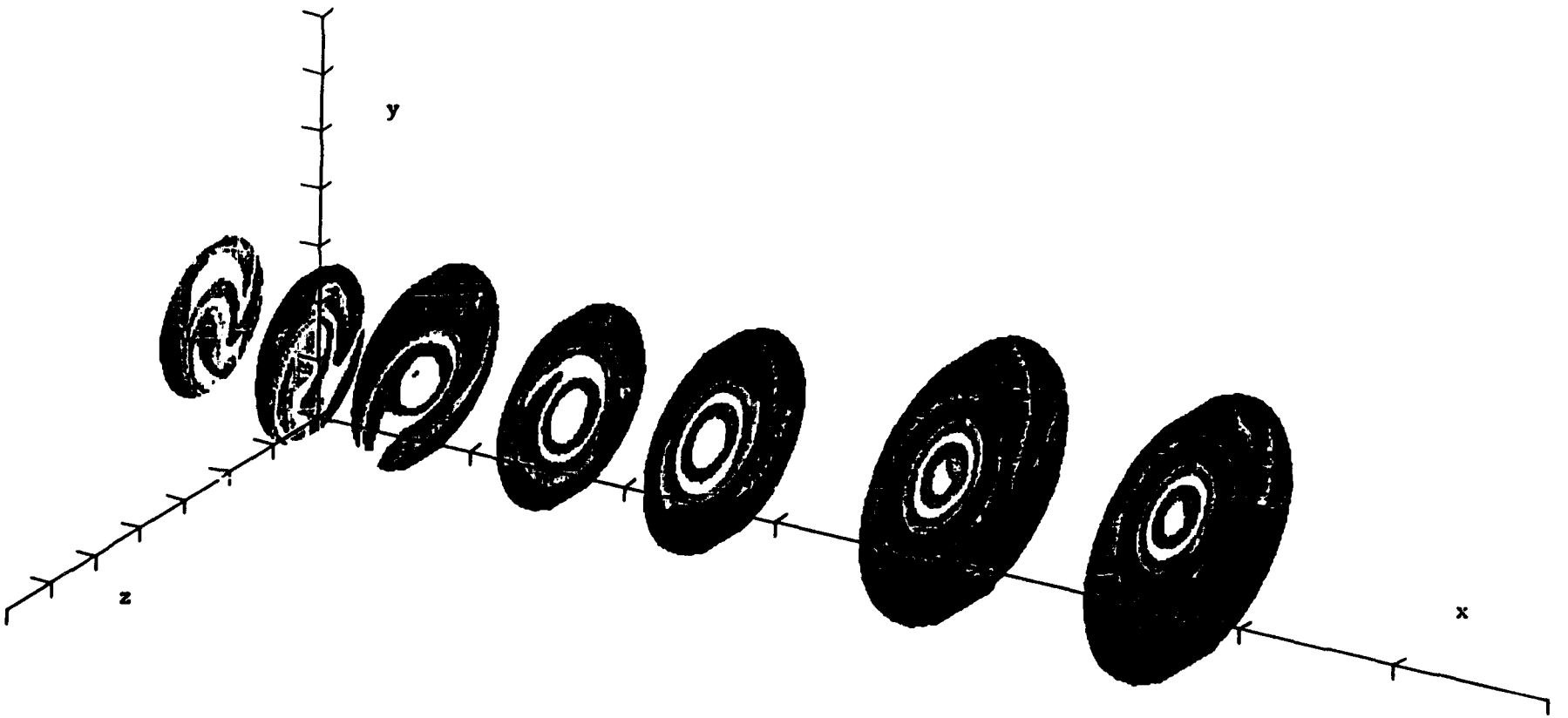

Figure 3.1 Mean velocity contours at different x-locations for $\alpha = 10$ degrees. Outermost contour level of velocity plotted is 1.0 (maximum). Decrement interval of contours is 0.05.

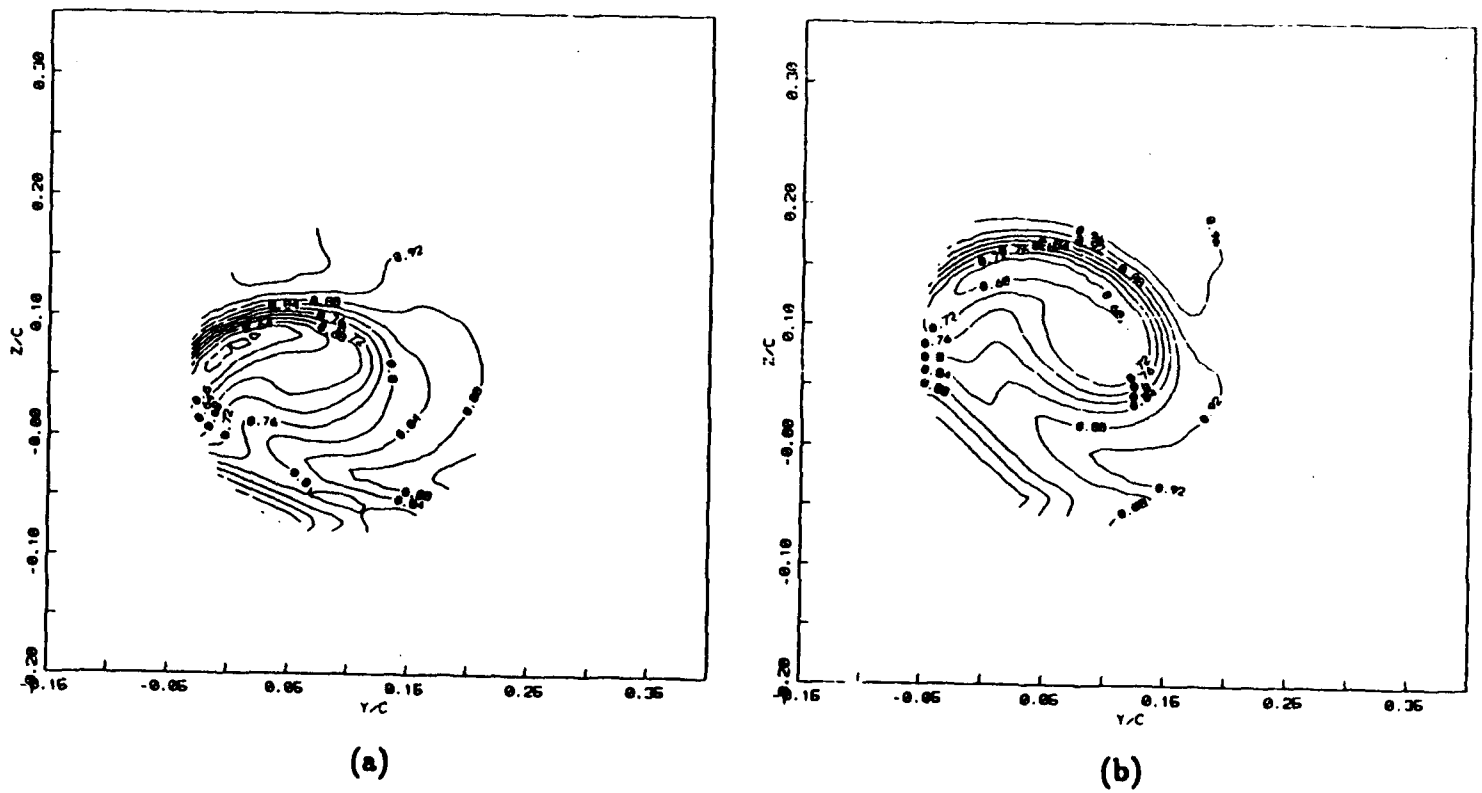

Figure 3.2 Mean velocity contours in the vortex at (a) $x/c = 0.16$, (b) $x/c = 0.33$, (c) $x/c = 0.65$, (d) $x/c = 1.00$, (e) $x/c = 1.64$, (f) $x/c = 2.26$, (g) $x/c = 3.28$. $\alpha = 10$ degrees

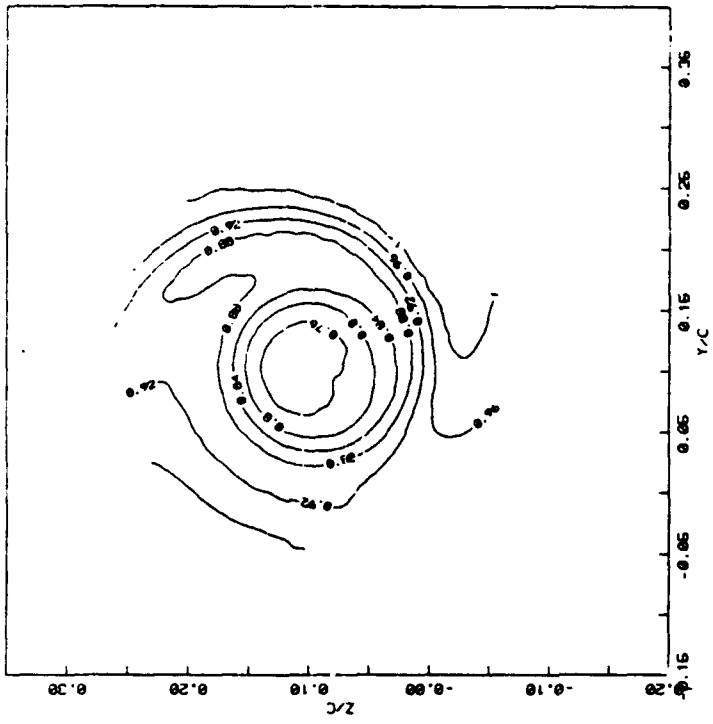

(d)

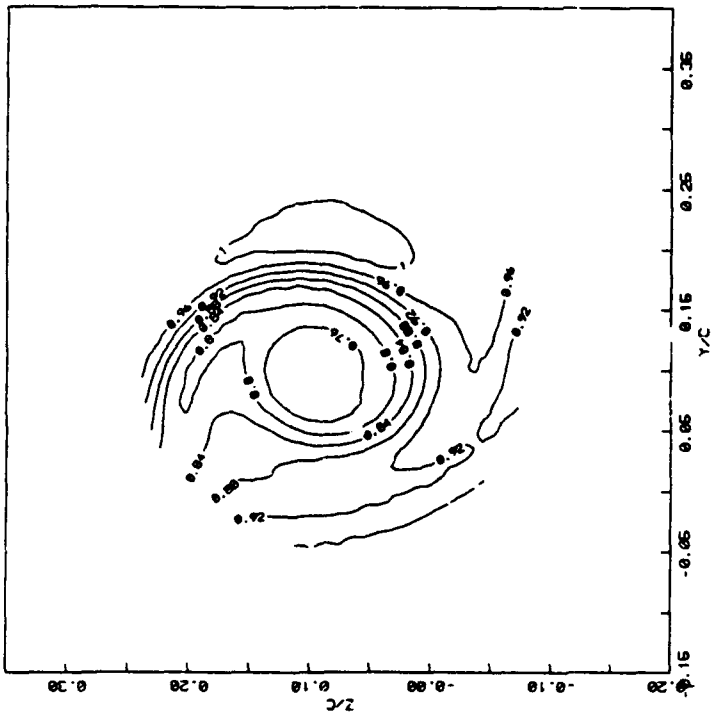

(c)

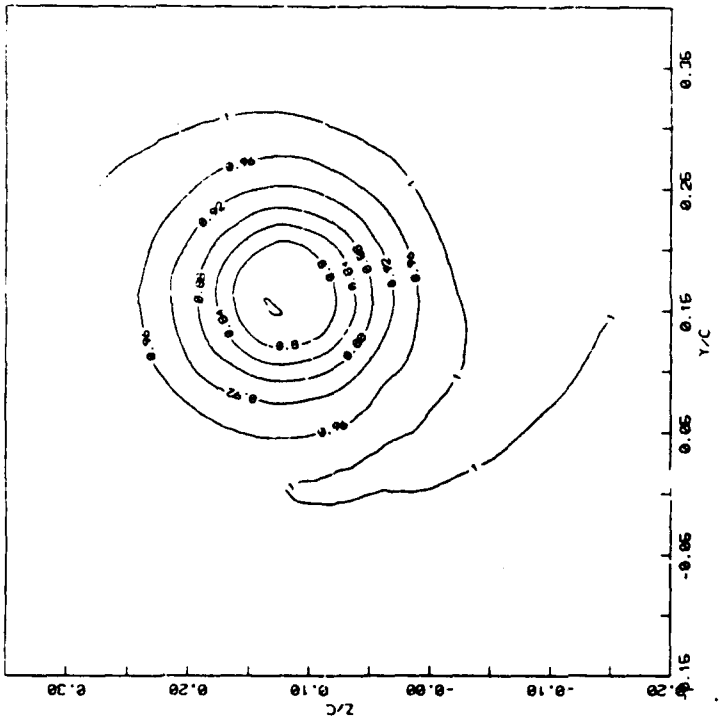
Z/C
Y/C
0.30
0.20
0.10
-0.00
-0.10
-0.20
0.35
0.25
0.15
0.05
-0.05
-0.15

(f)

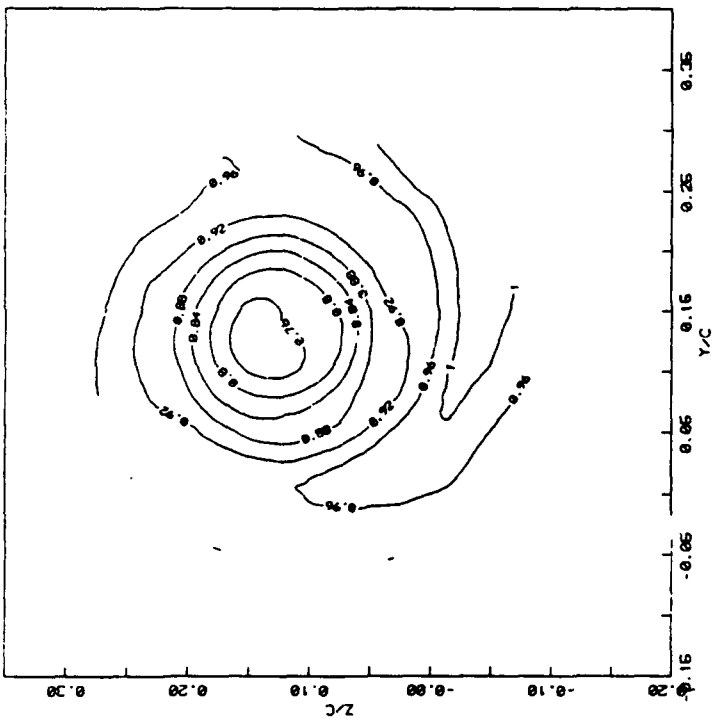
Z/C
Y/C
0.30
0.20
0.10
-0.00
-0.10
-0.20
0.35
0.25
0.15
0.05
-0.05
-0.15

(e)

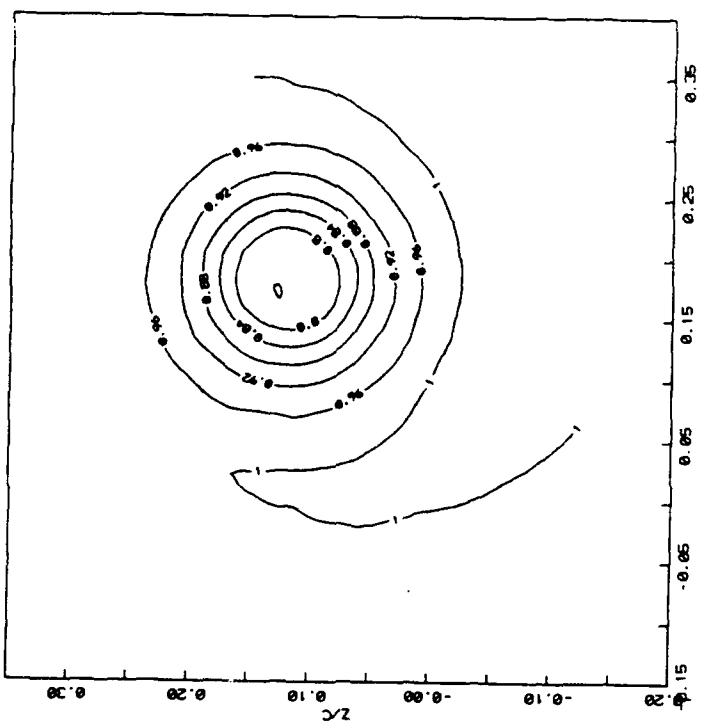

(g)

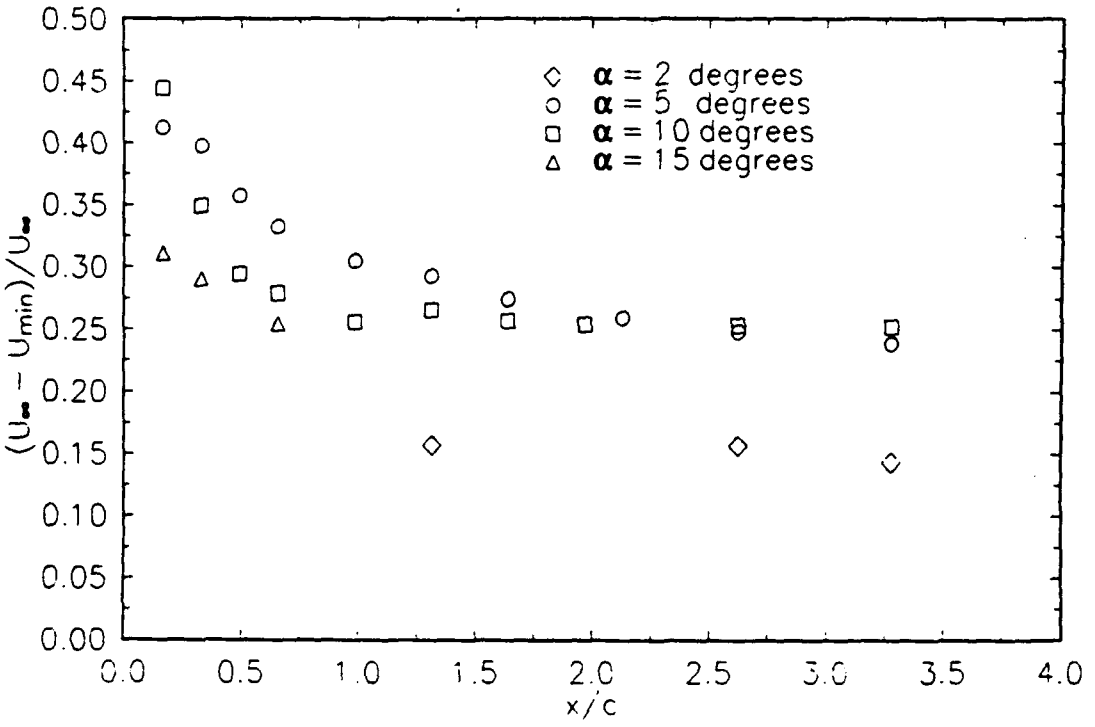

Figure 3.3 Maximum velocity U deficit in the vortex during the downstream development

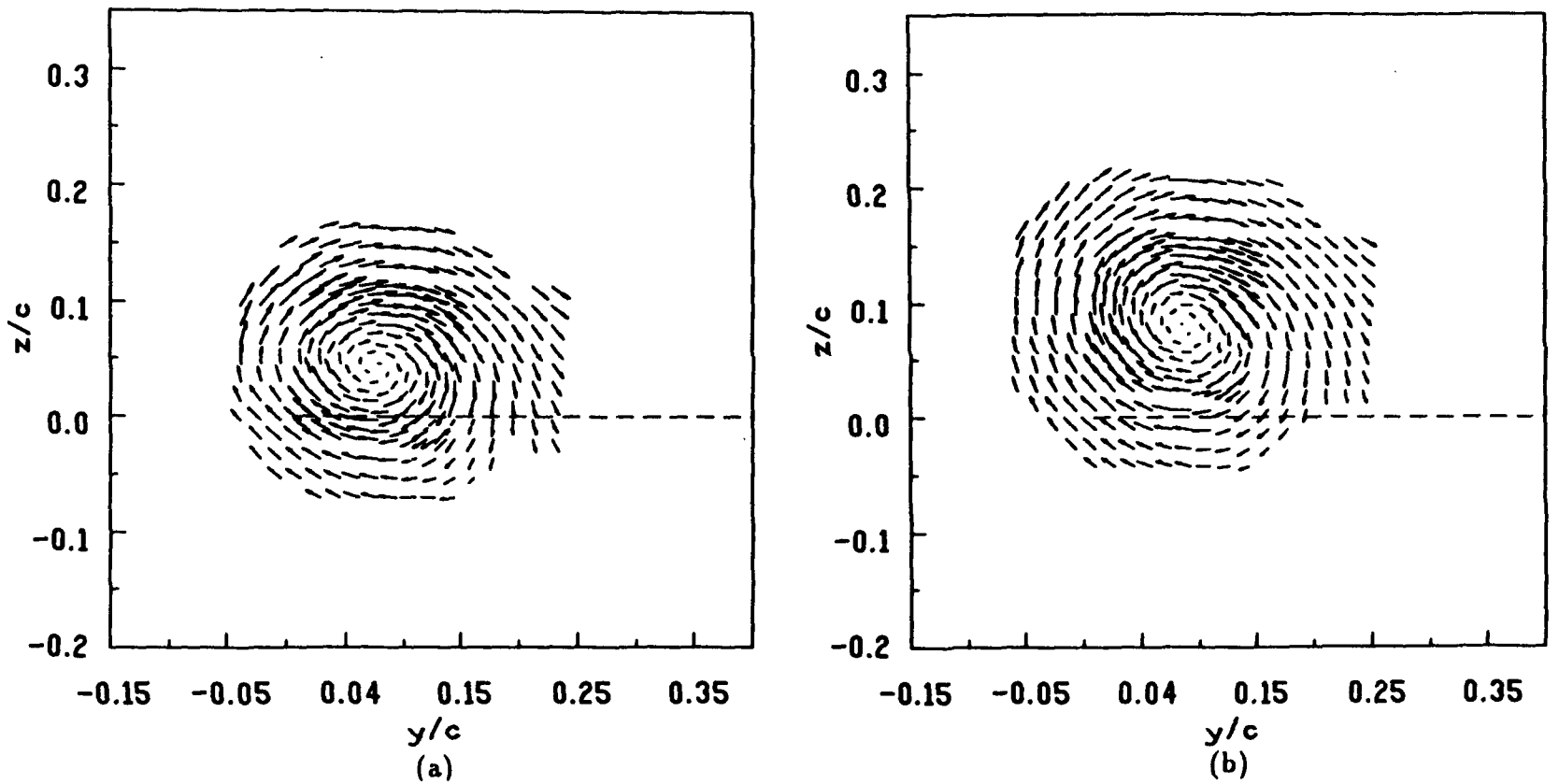

Figure 3.4 Distribution of the mean velocity vector ($\vec{j}V+\vec{k}W$) in the cross-stream plane at the same angle of incidence and downstream distance as Fig. 3.2. The magnitude of velocity is proportional to the length of the arrow.

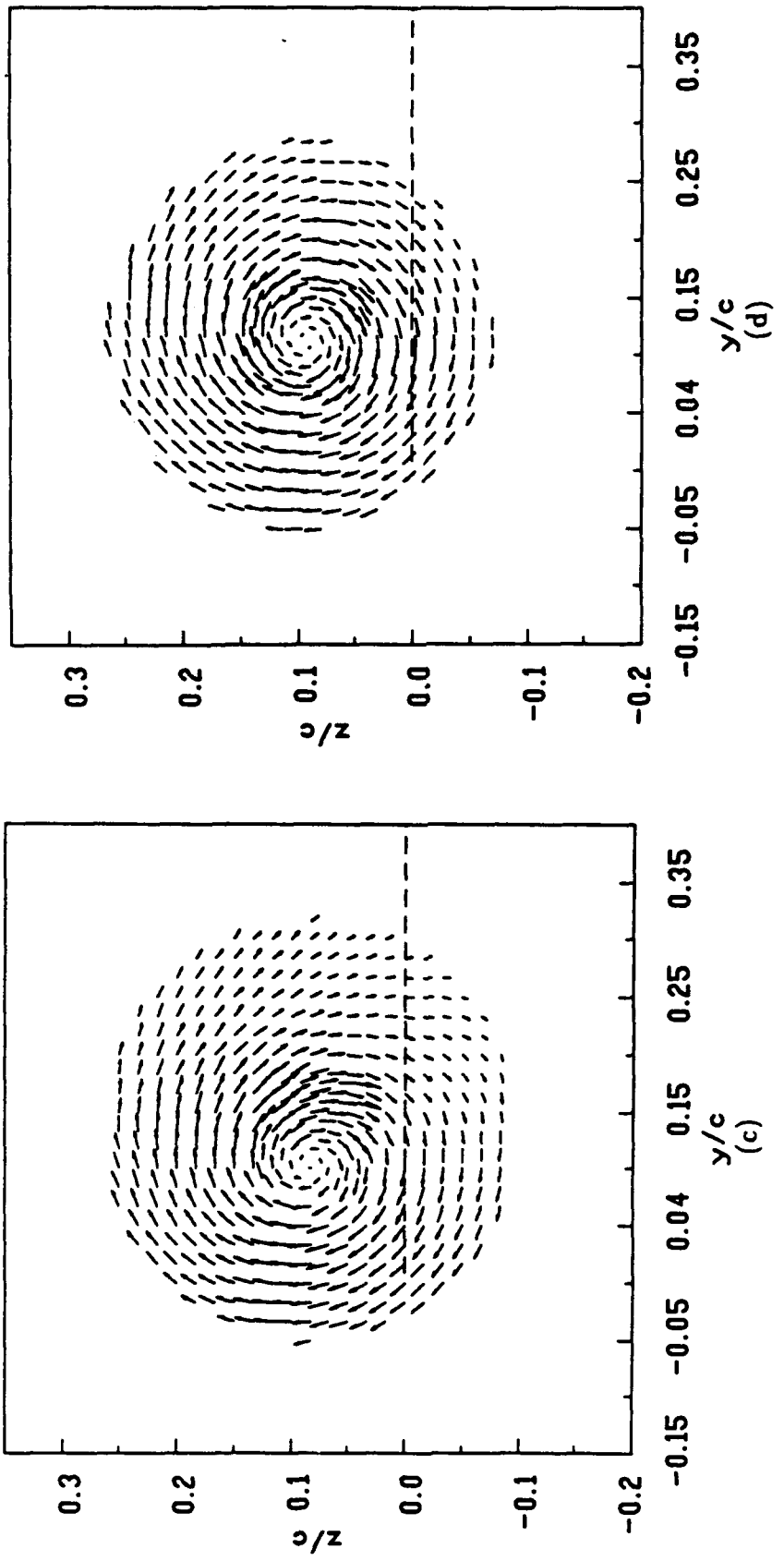
0.3
0.2
0.1
0.0
-0.1
-0.2
z/c
-0.15
-0.05
0.04
0.15
0.25
0.35
y/c
(d)
0.3
0.2
0.1
0.0
-0.1
-0.2
z/c
-0.15
-0.05
0.04
0.15
0.25
0.35
y/c
(c)

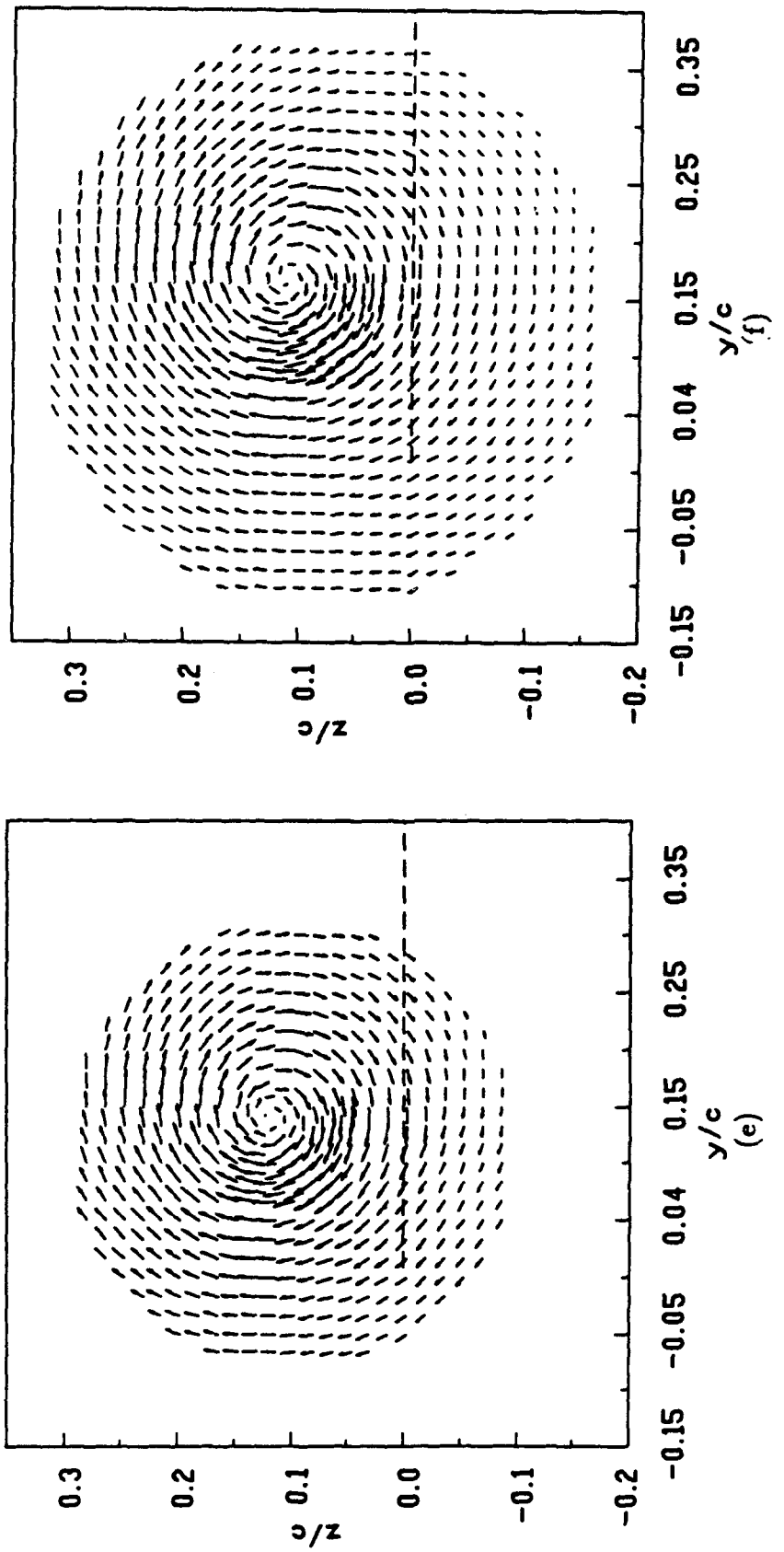
0.3
0.2
0.1
0.0
-0.1
-0.2
z/c
-0.15
-0.05
0.04
0.15
0.25
0.35
y/c
(f)
0.3
0.2
0.1
0.0
-0.1
-0.2
z/c
-0.15
-0.05
0.04
0.15
0.25
0.35
y/c
(e)

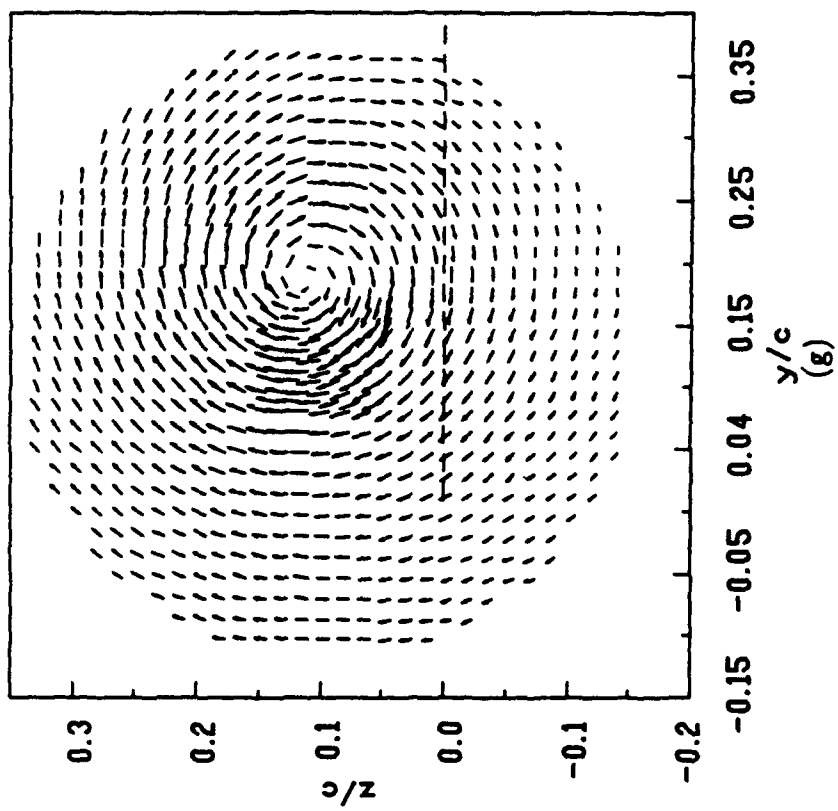
0.3
0.2
0.1
0.0
-0.1
-0.2
z/c
-0.15
-0.05
0.04
0.15
0.25
0.35
y/c
(g)

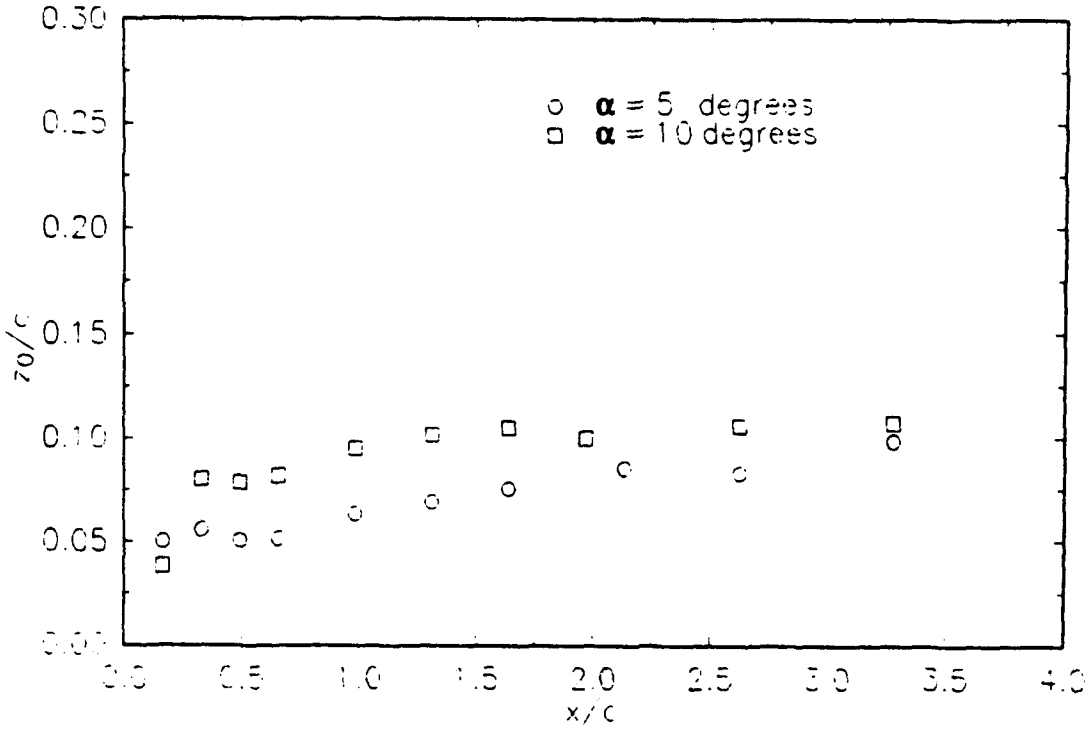

(a)

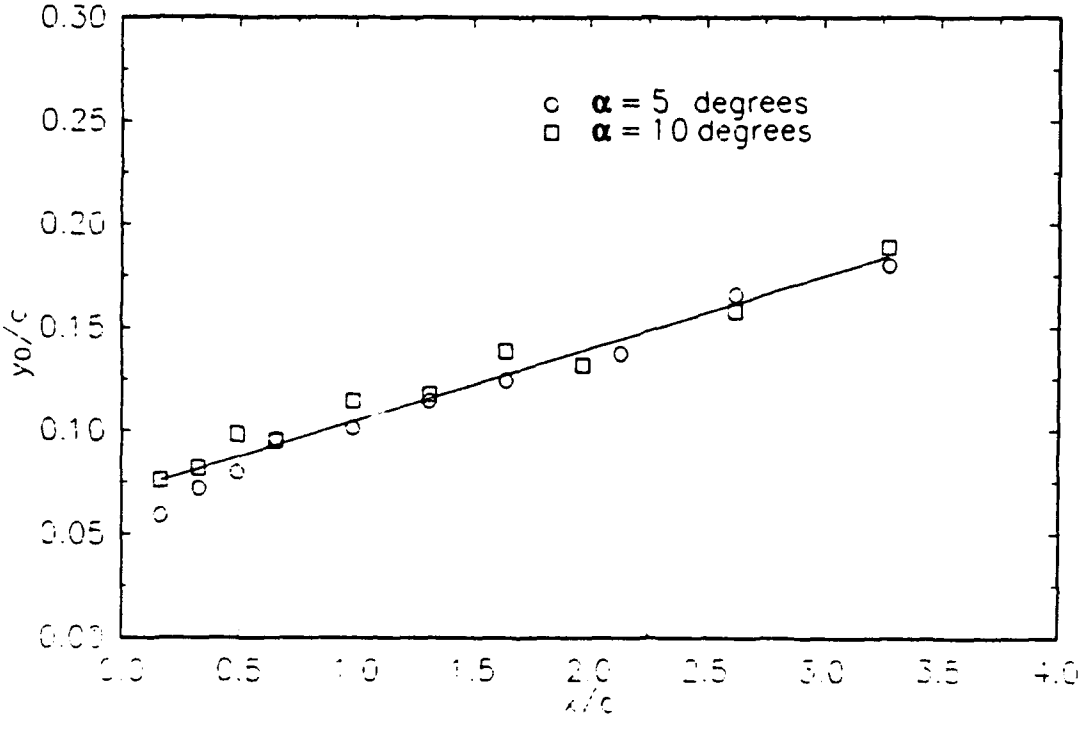

(b)

Figure 3.5 Motions of the vortex center.(a) Vertical motion. (b) Horizontal motion.

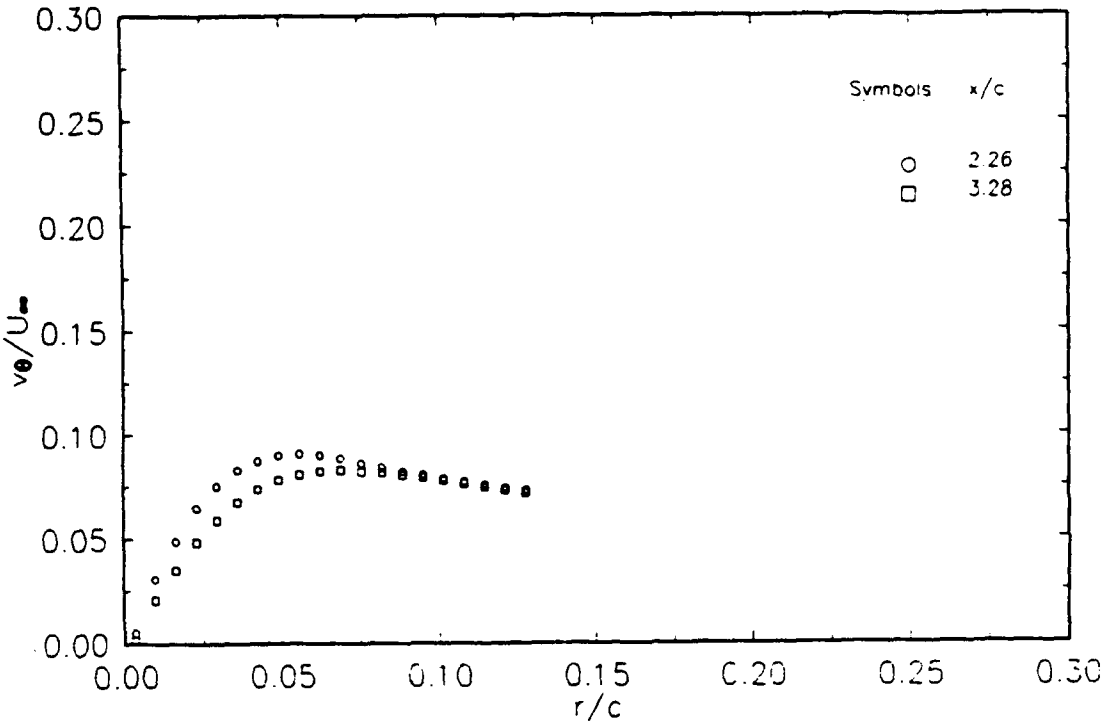

(a)

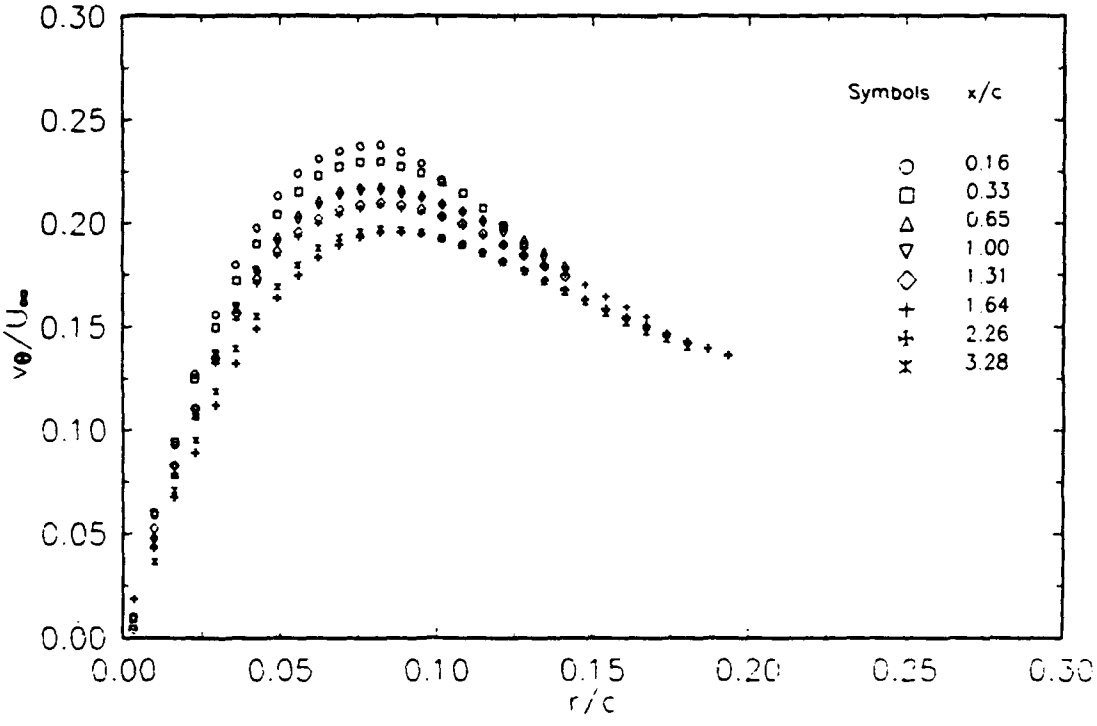

(b)

Figure 3.6 Distribution of the circumferential velocity V_θ at a) $\alpha = 2$ degrees, b) $\alpha = 5$ degrees, c) $\alpha = 10$ degrees, d) $\alpha = 15$ degrees.

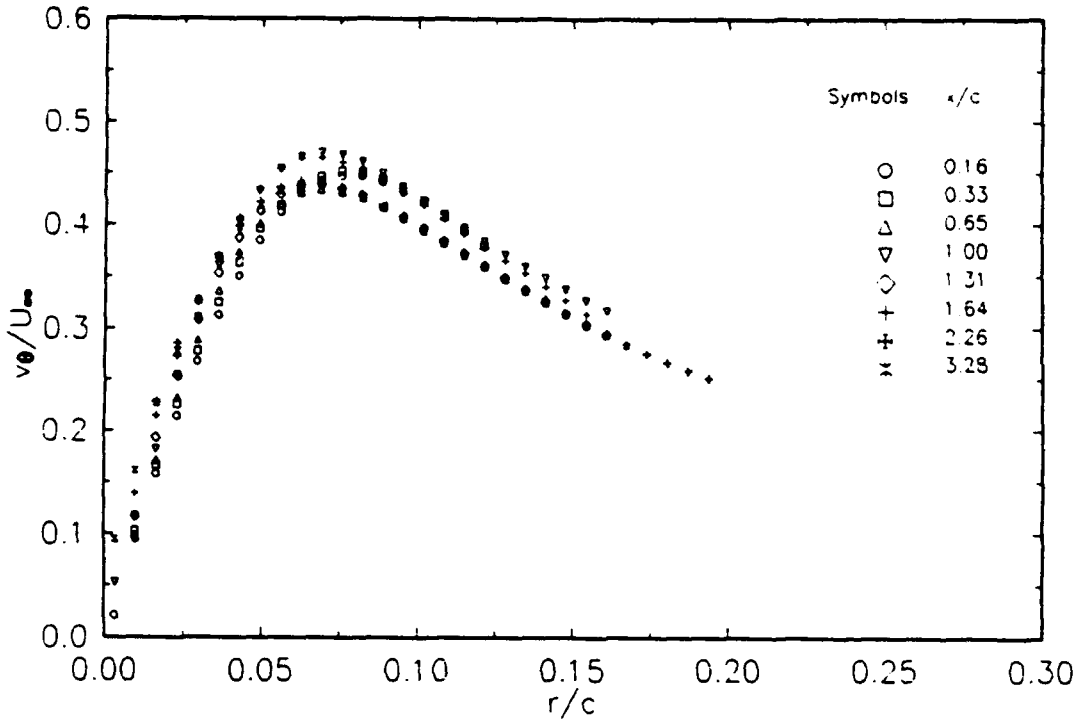
Symbols x/c
0.16
0.33
0.65
1.00
1.31
1.64
2.26
3.28
v_θ/U_∞
r/c
0.0
0.1
0.2
0.3
0.4
0.5
0.6
0.00
0.05
0.10
0.15
0.20
0.25
0.30

(c)

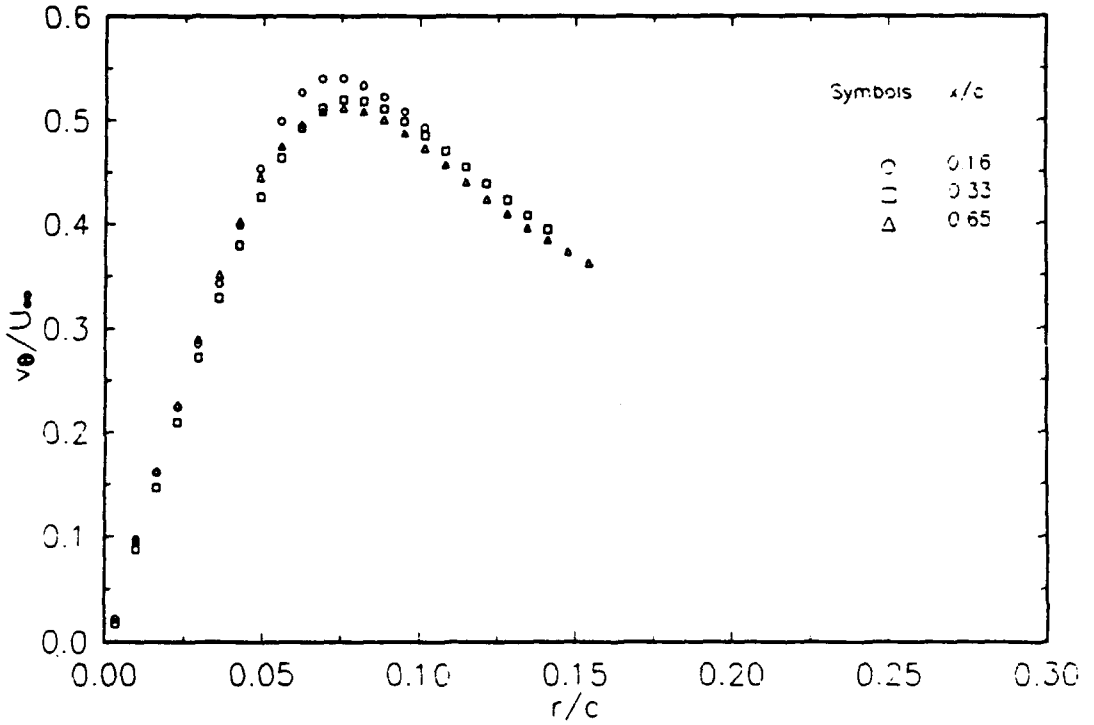
Symbols x/c
0.16
0.33
0.65
v_θ/U_∞
r/c
0.0
0.1
0.2
0.3
0.4
0.5
0.6
0.00
0.05
0.10
0.15
0.20
0.25
0.30

(d)

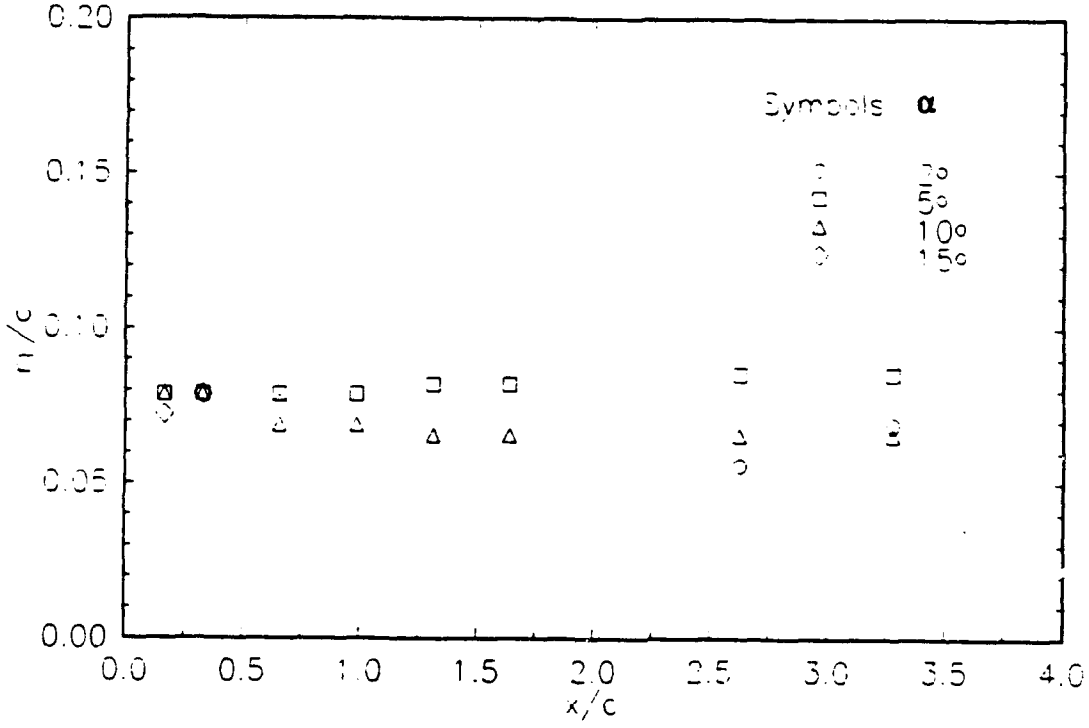

Figure 3.7 Changes of the radius r_1 *vs* x/c.

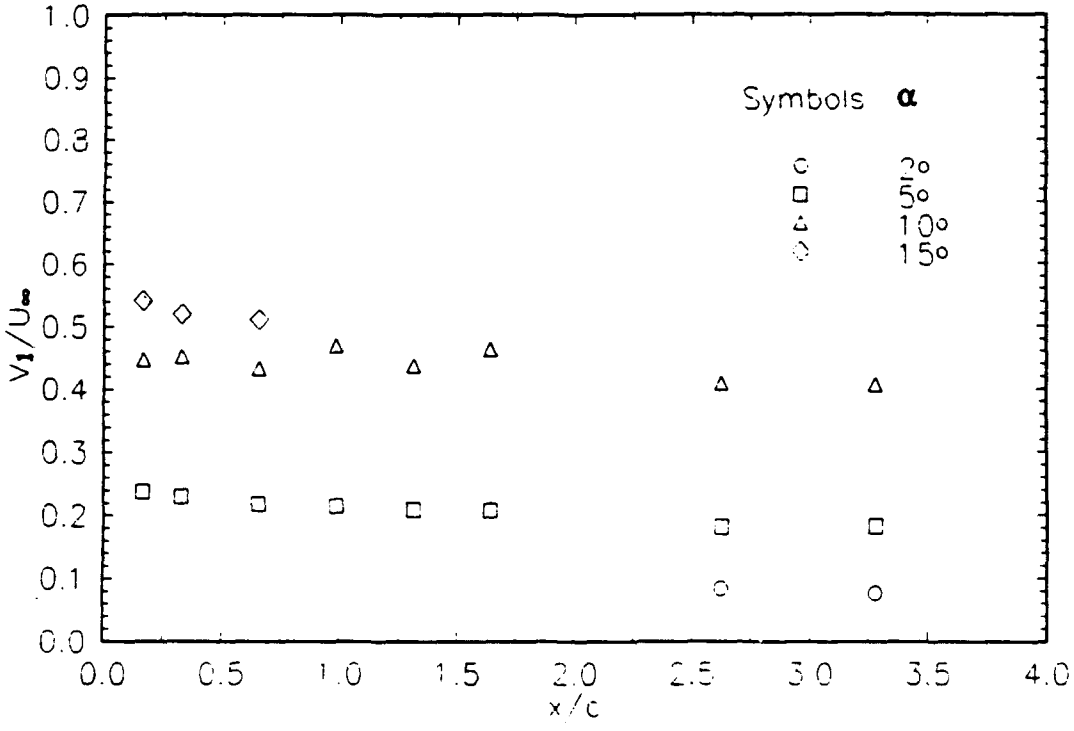

Figure 3.8 Plot of the maximum velocity V_1 *vs* x/c.

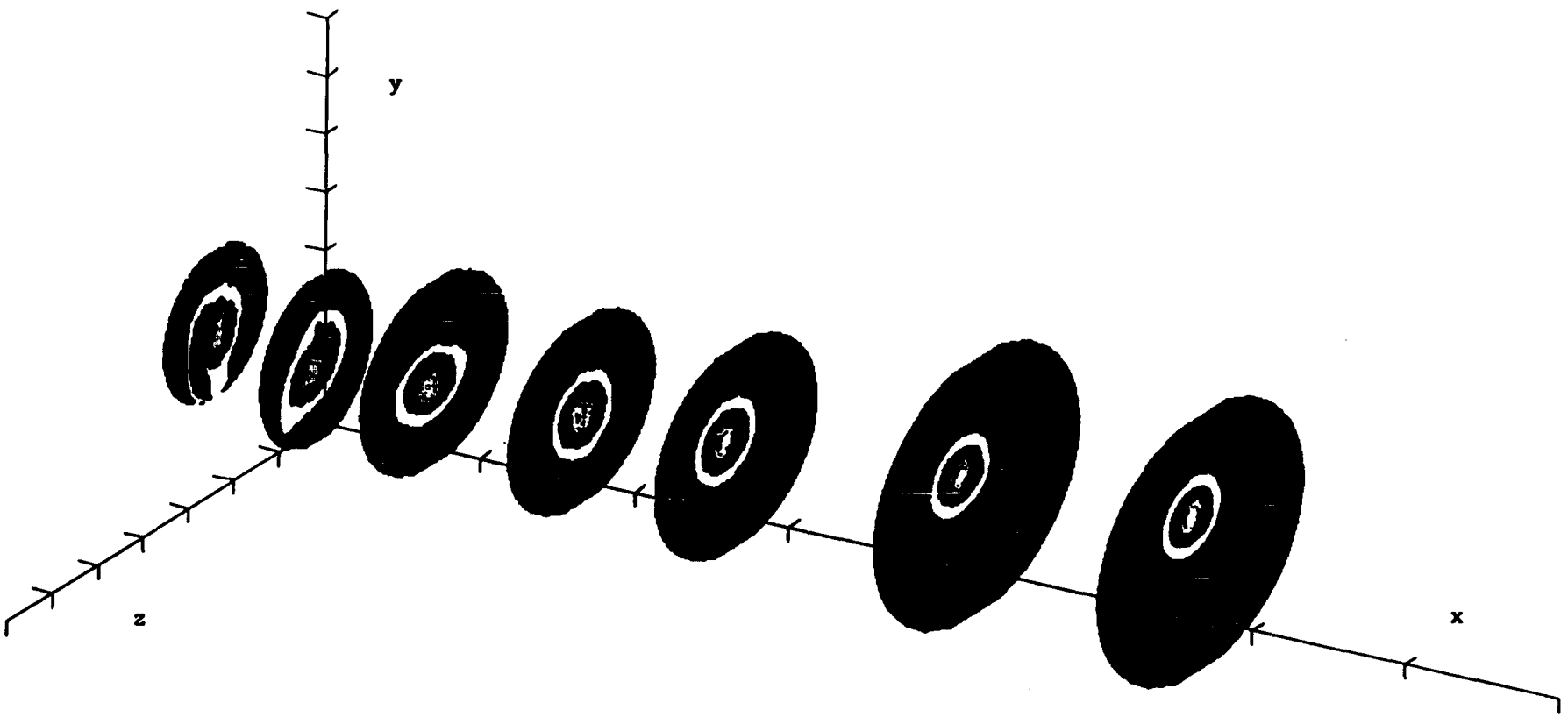

Figure 3.9 Axial-vorticity(ω_x) contours at different x-locations. The stations and incidence angle are the same as in Fig. 3.2.

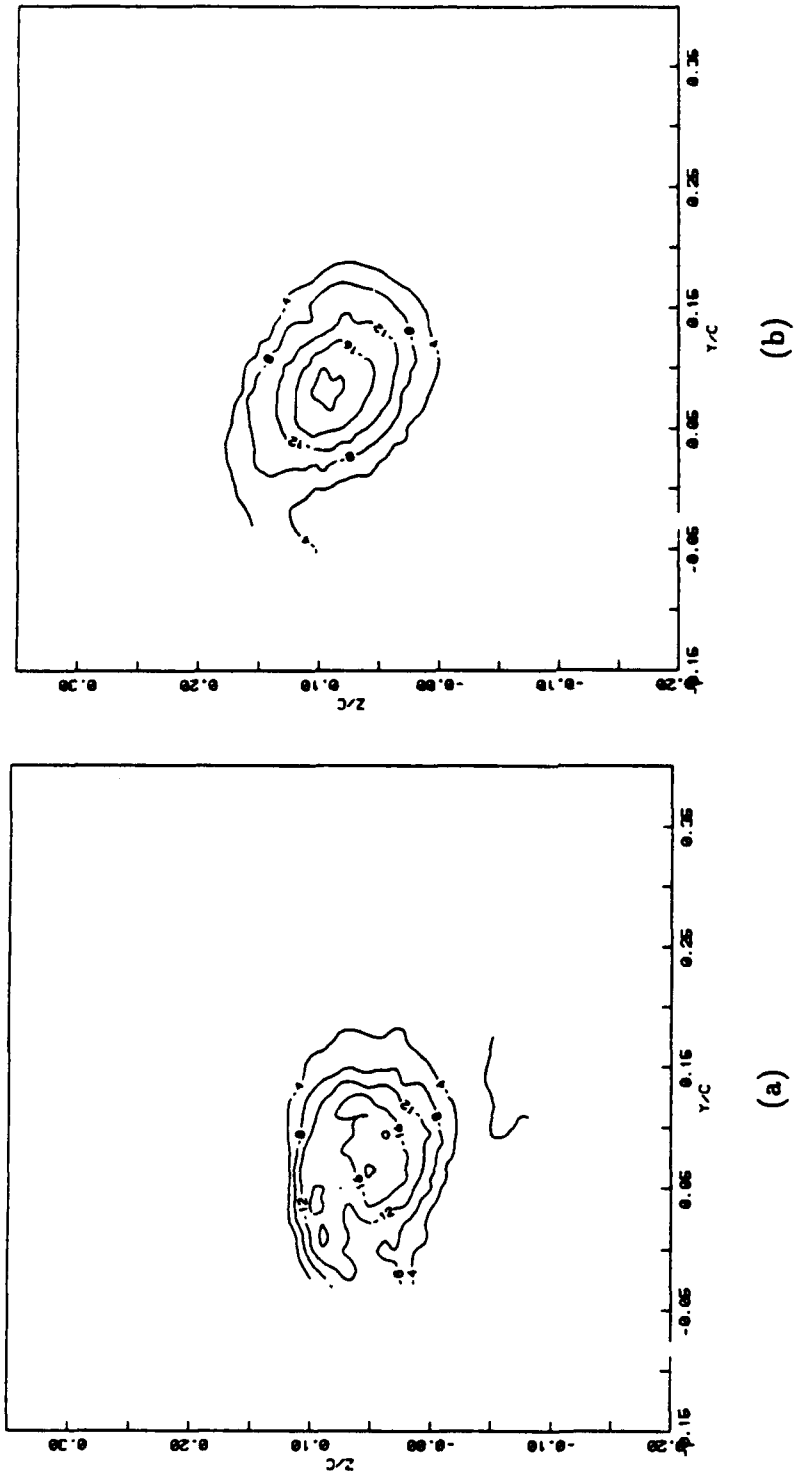

Figure 3.10 Contours of ω_z in the vortex at the same angle of incidence and downstream distance as Fig. 3.2

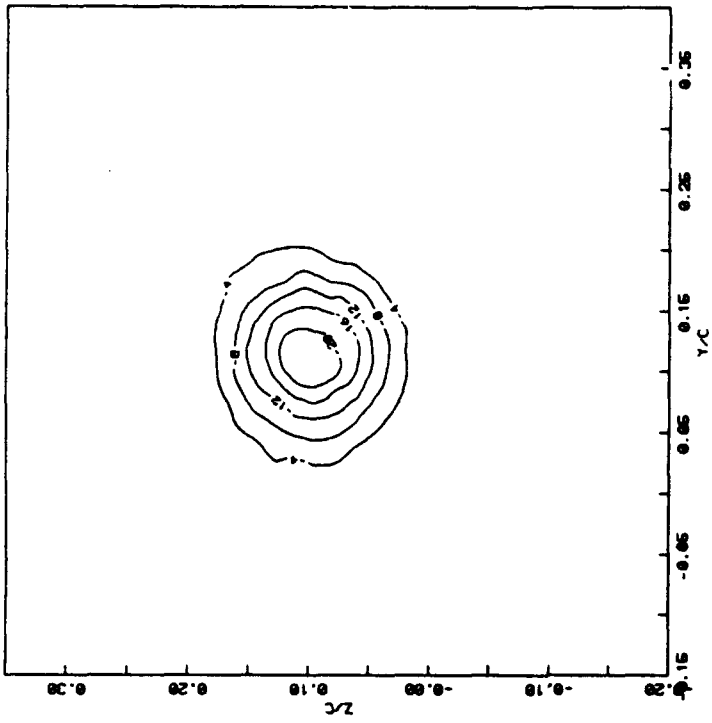
0.35
0.25
0.15
0.05
-0.05
-0.15
Y/C
-0.20
-0.10
0.00
0.10
0.20
0.30
Z/C

(d)

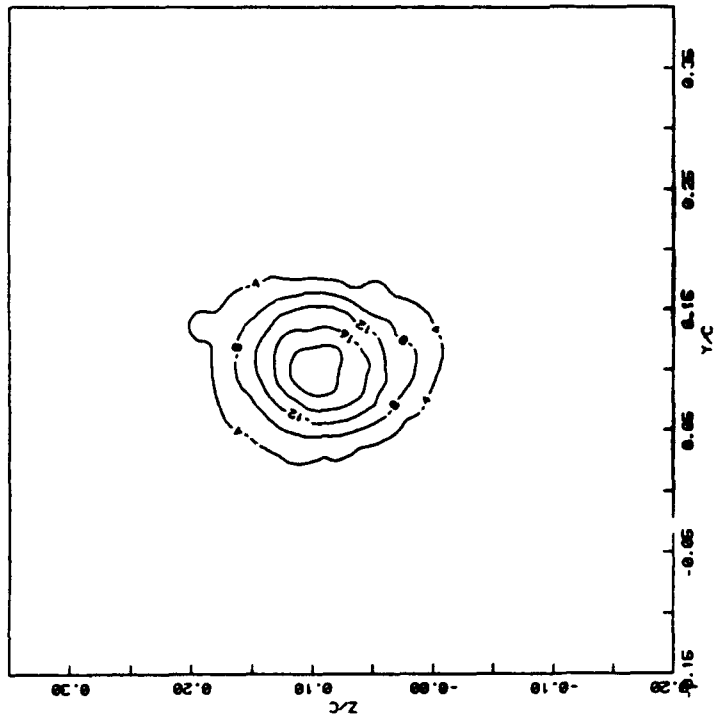
0.35
0.25
0.15
0.05
-0.05
-0.15
Y/C
-0.20
-0.10
0.00
0.10
0.20
0.30
Z/C

(c)

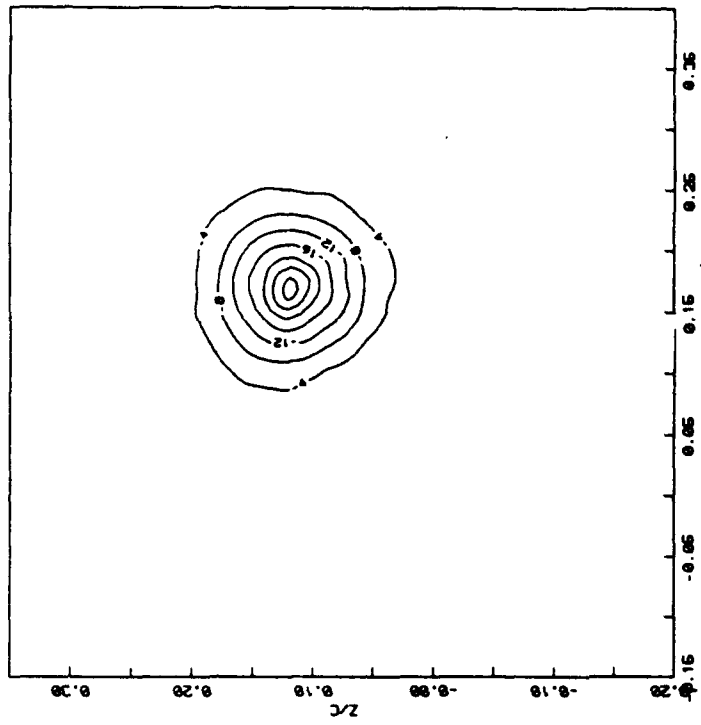
Z/C
0.30
0.20
0.10
-0.00
-0.10
-0.20
Y/C
0.35
0.25
0.15
0.05
-0.05
-0.15
4
8
12
16

(f)

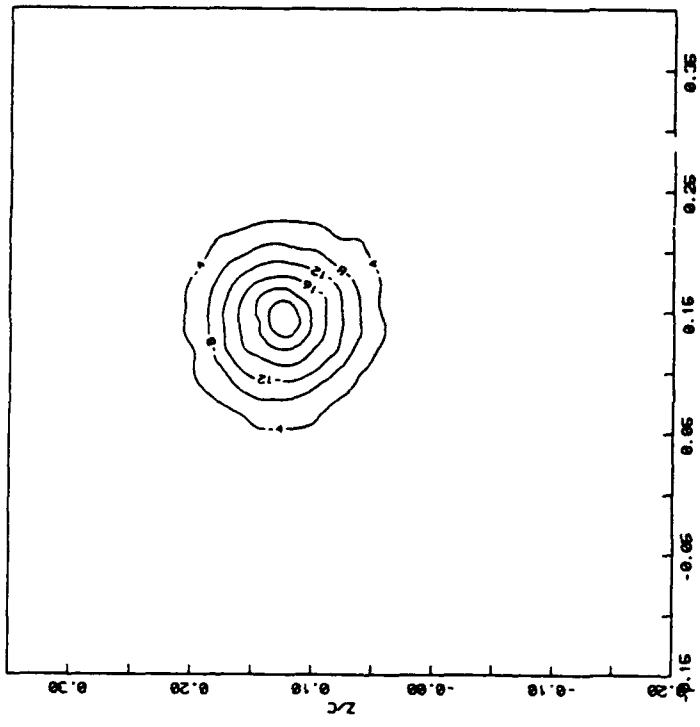
Z/C
0.30
0.20
0.10
-0.00
-0.10
-0.20
Y/C
0.35
0.25
0.15
0.05
-0.05
-0.15
4
8
12
16

(e)

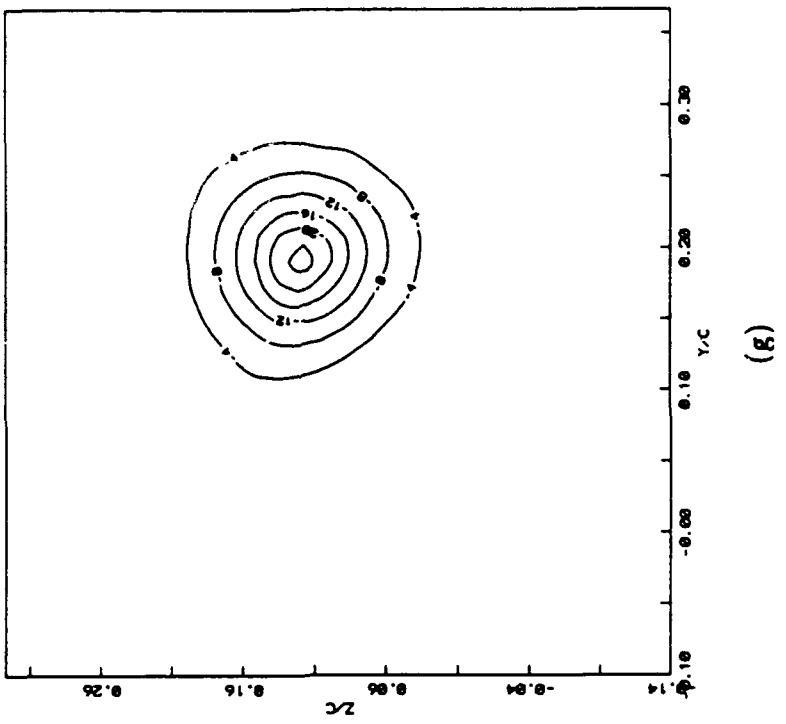

(g)

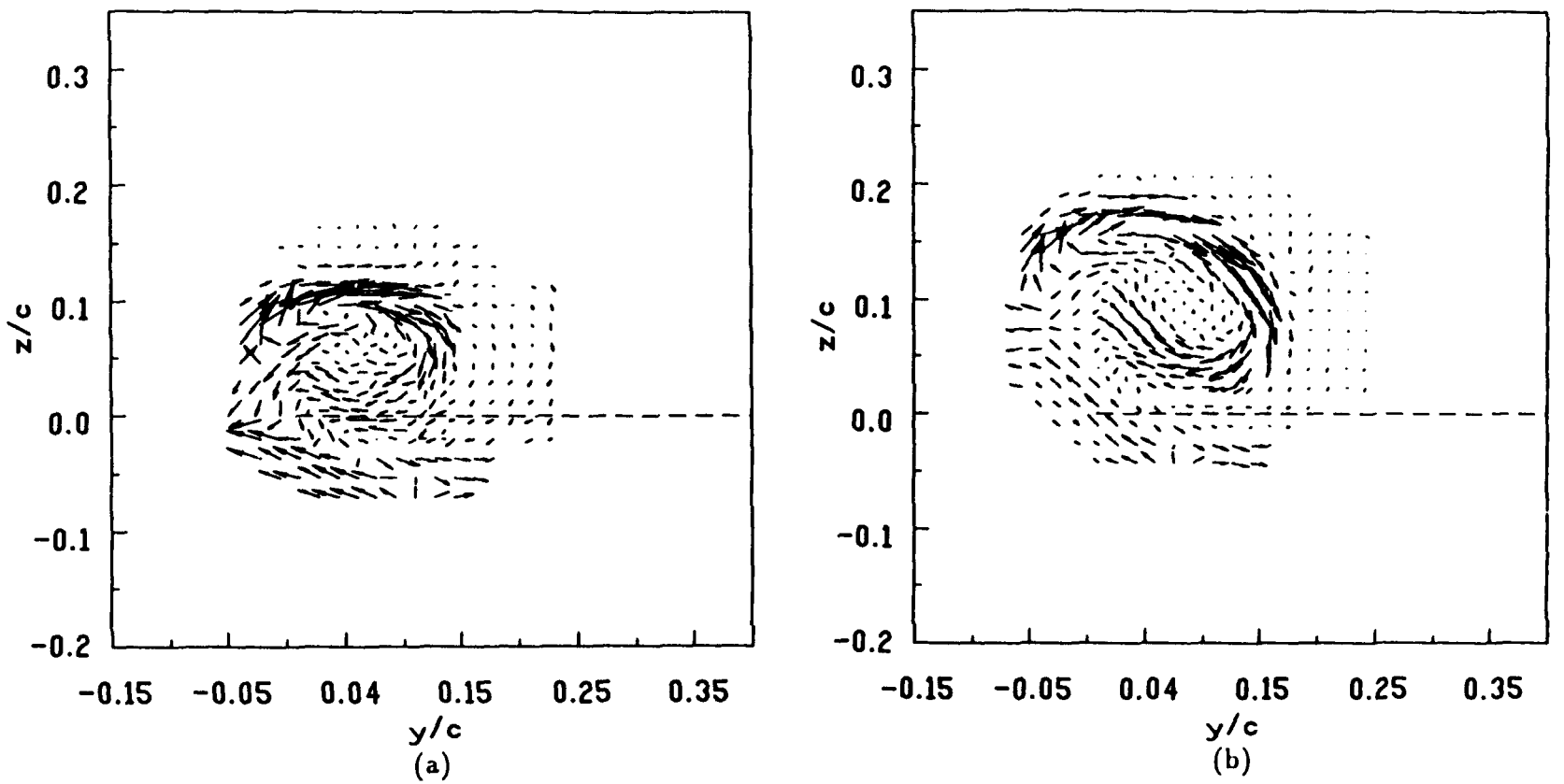

Figure 3.11 Distribution of the cross-stream vorticity vector ($\vec{j}\omega_y + \vec{k}\omega_z$) across the vortex at the same angle of incidence and downstream distance as Fig. 3.2. The scale used in Figs. (a) to (c) is three times larger than that in Figs. (d) to (g). The magnitude of vorticity is proportional to the length of the arrow.

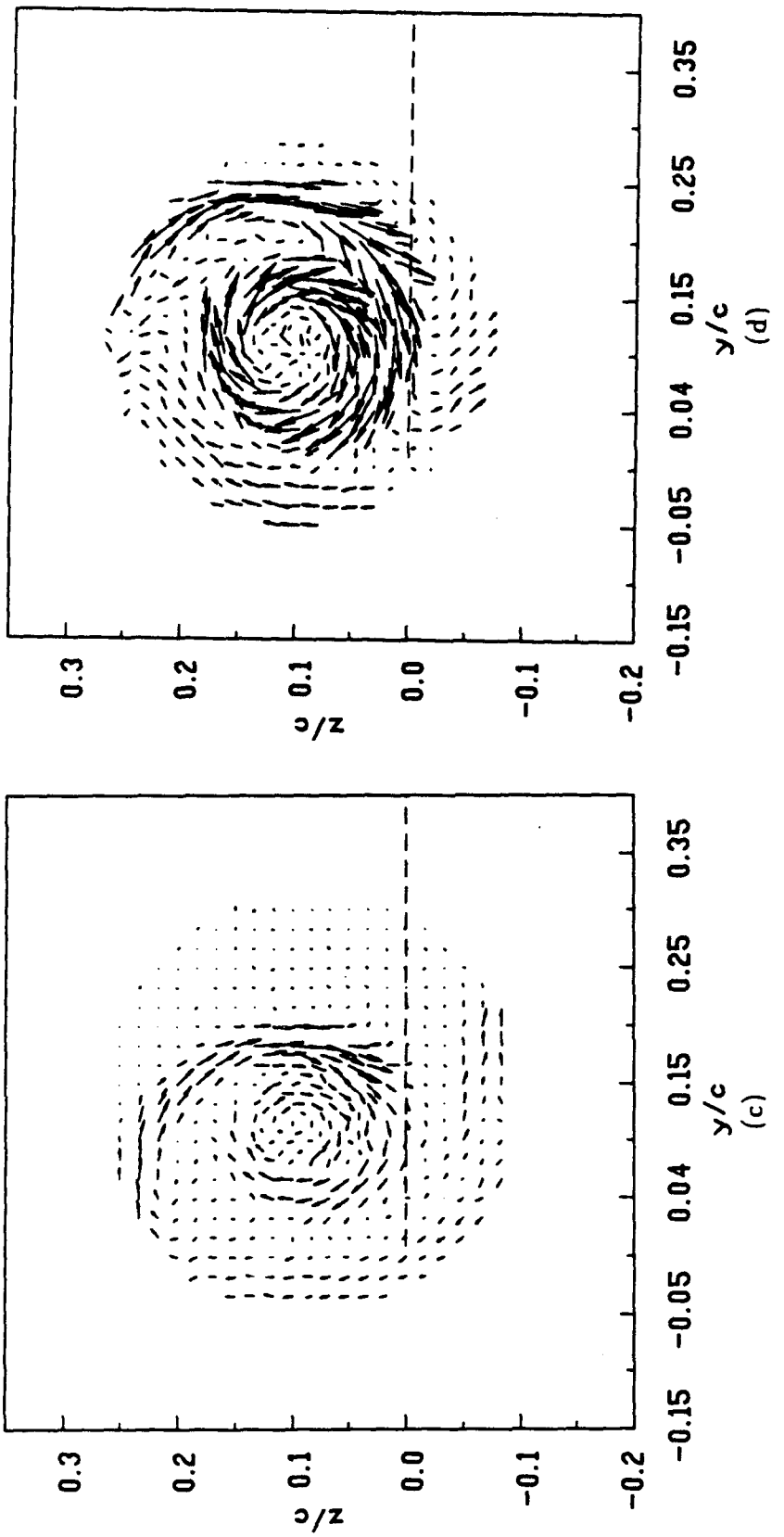
0.3
0.2
0.1
0.0
-0.1
-0.2
z/c
-0.15
-0.05
0.04
0.15
0.25
0.35
y/c
(d)
0.3
0.2
0.1
0.0
-0.1
-0.2
z/c
-0.15
-0.05
0.04
0.15
0.25
0.35
y/c
(c)

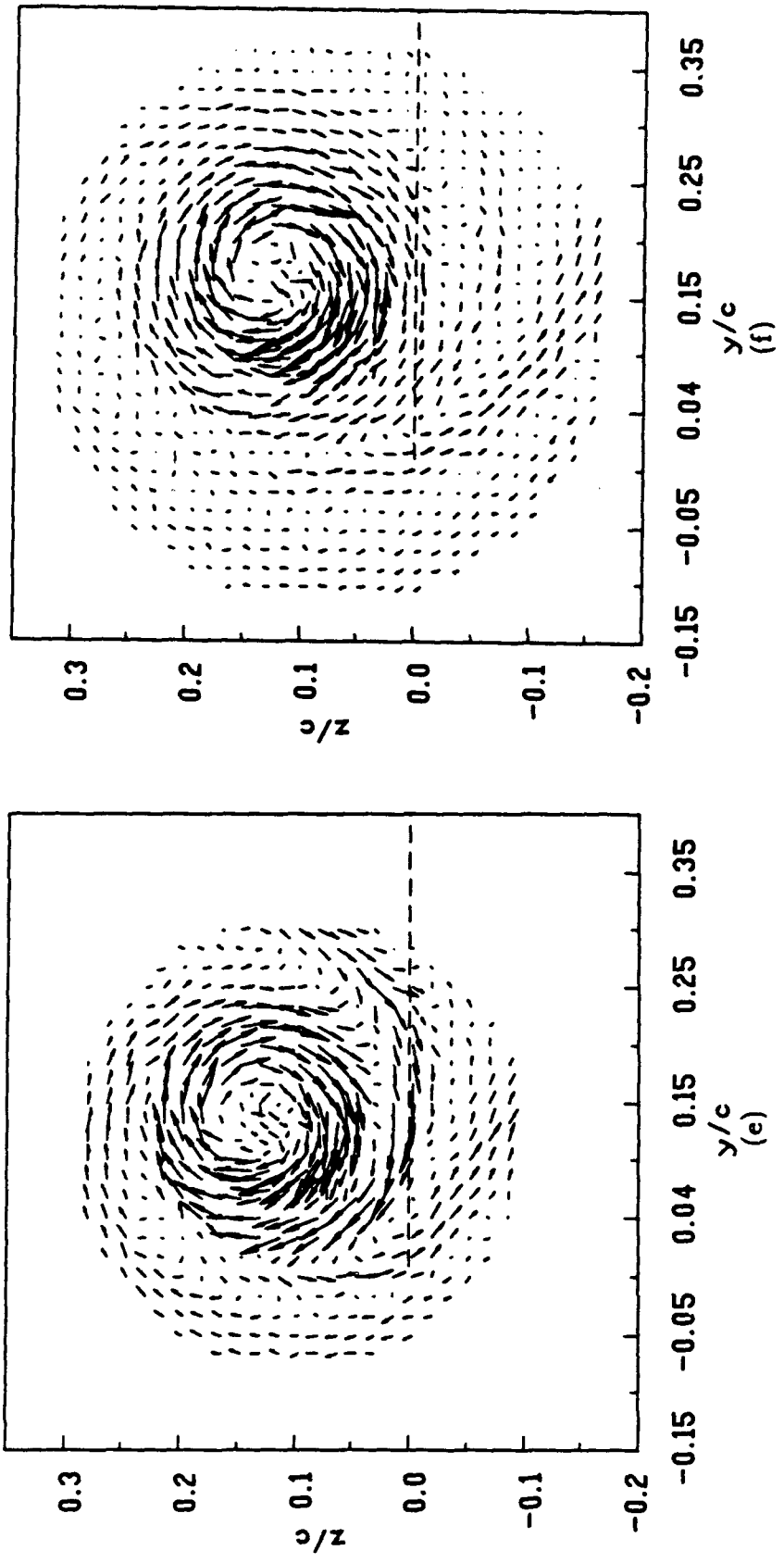
0.3
0.2
0.1
0.0
-0.1
-0.2
z/c
-0.15
-0.05
0.04
0.15
0.25
0.35
y/c
(f)
0.3
0.2
0.1
0.0
-0.1
-0.2
z/c
-0.15
-0.05
0.04
0.15
0.25
0.35
y/c
(e)

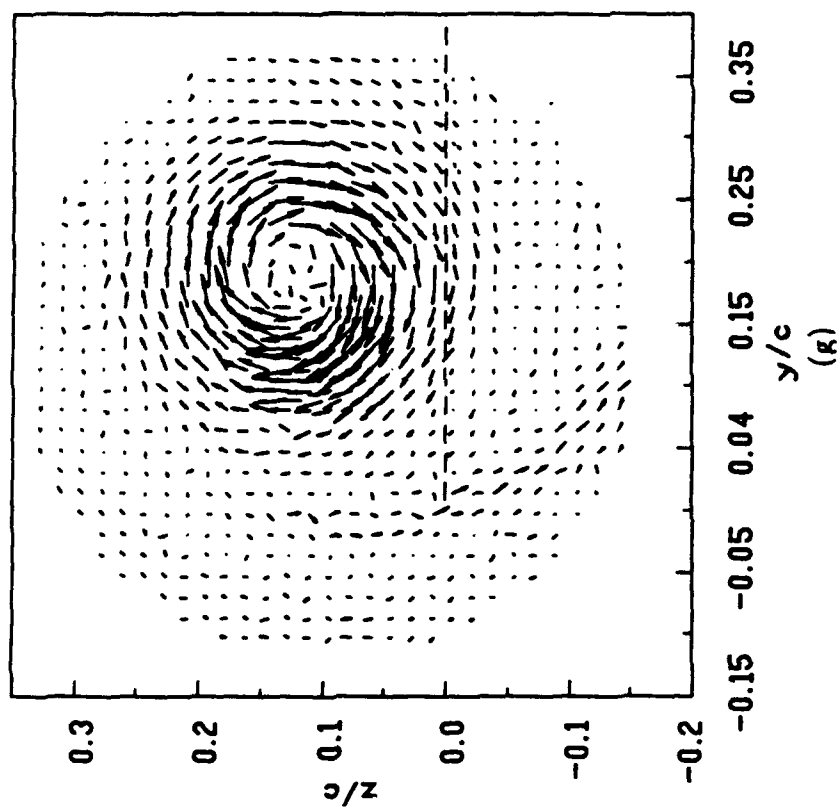
0.3
0.2
0.1
0.0
-0.1
-0.2
z/c
-0.15
-0.05
0.04
0.15
0.25
0.35
y/c
(R)

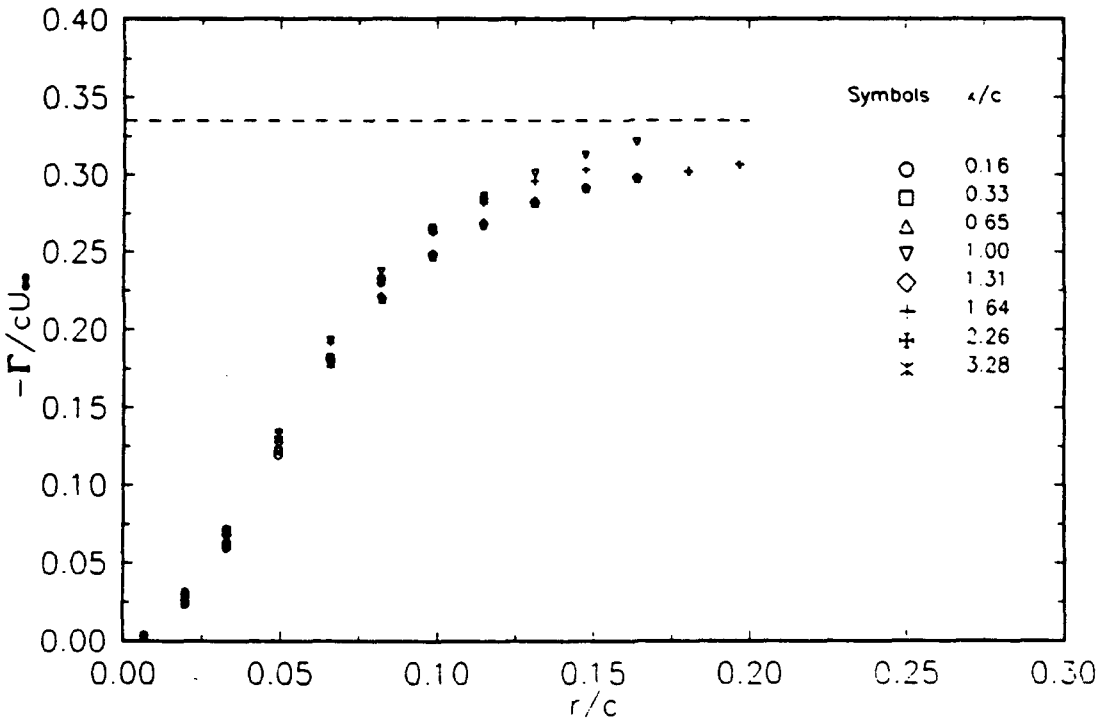

Figure 3.12 Variation of circulation Γ with distance r from the vortex center. α = 10 degrees.

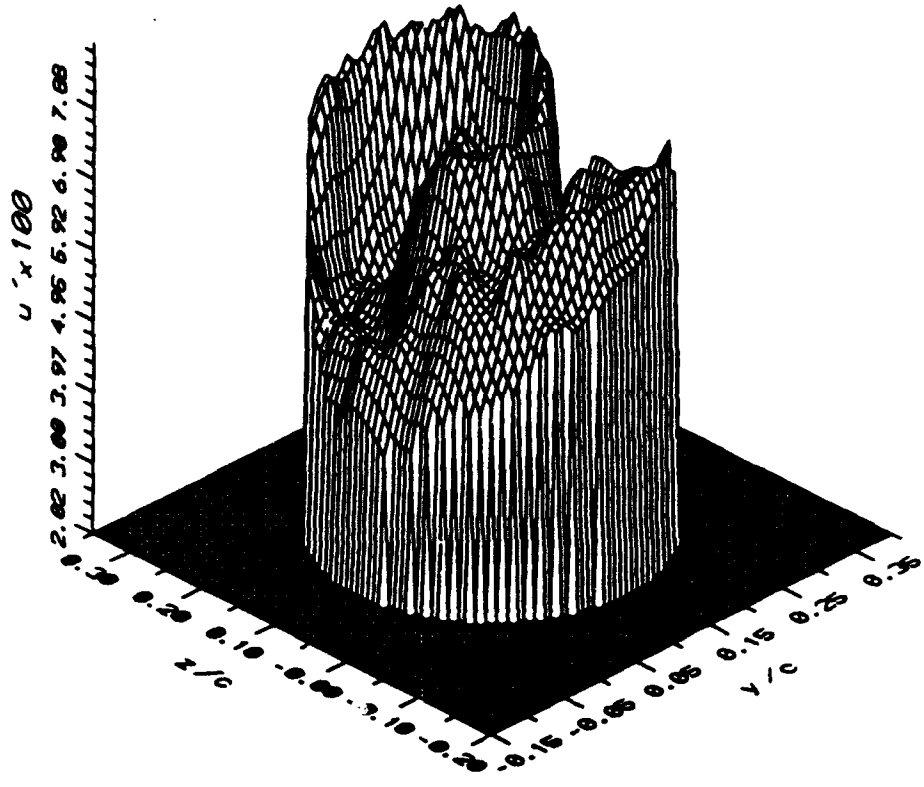

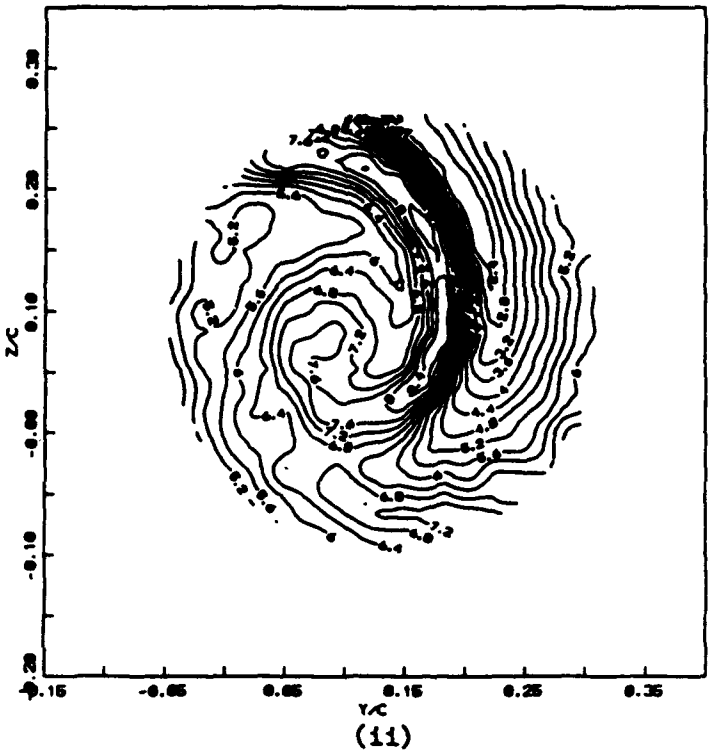

Figure 3.13 Distribution of the longitudinal component of the turbulent intensity u' across the vortex at (a) $x/c = 0.33$, (b) $x/c = 1.16$, (c) $x/c = 2.26$, (d) $x/c = 3.28$. (i)three-dimensional carpet plot, (ii) contour plot.

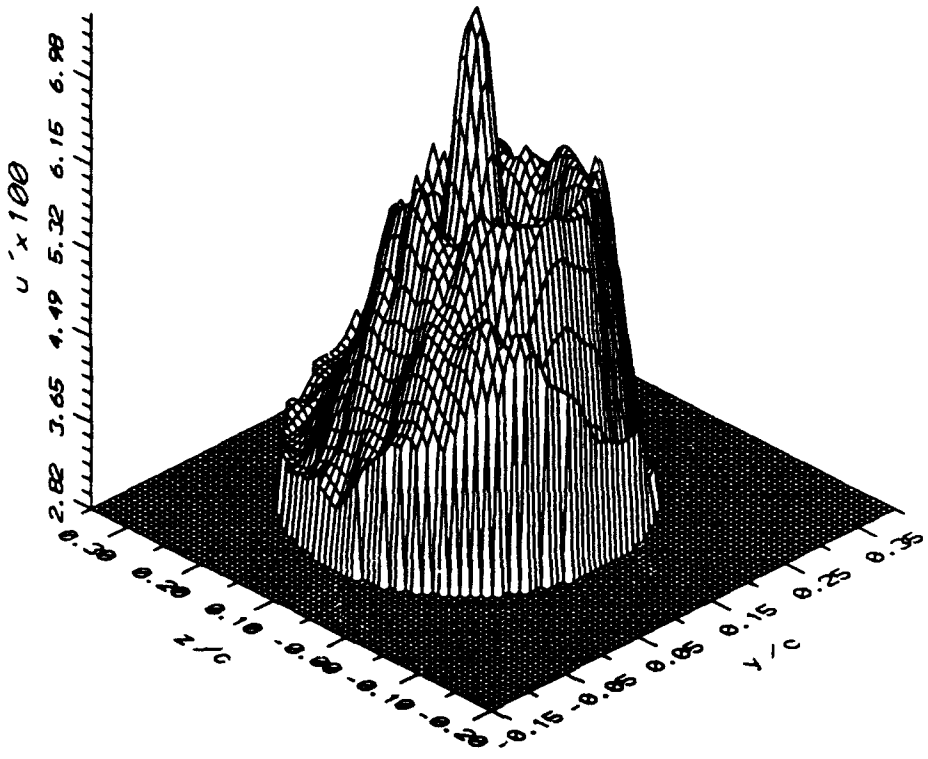

(i)

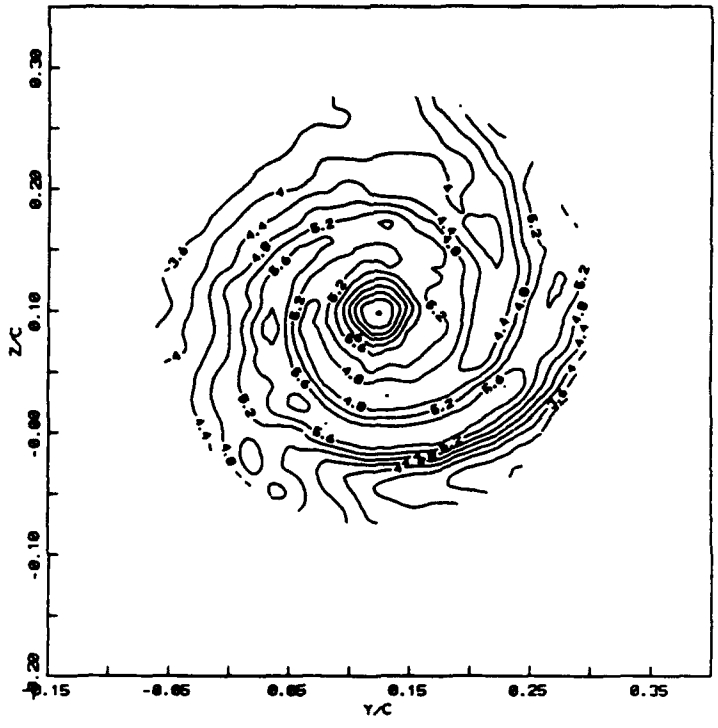

(ii)

(b)

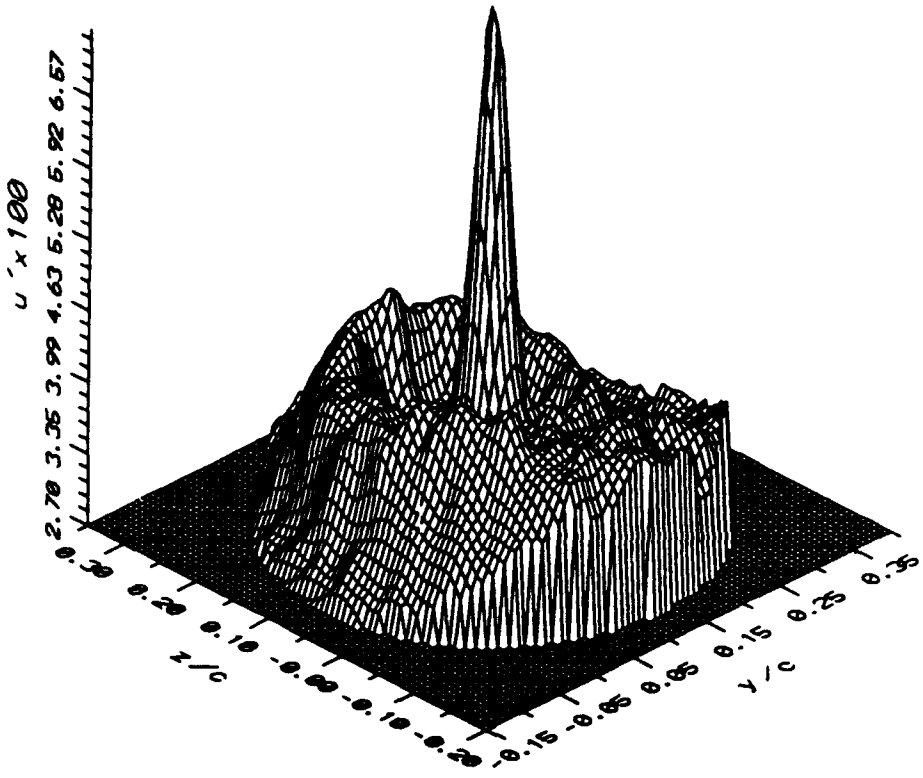

(i)

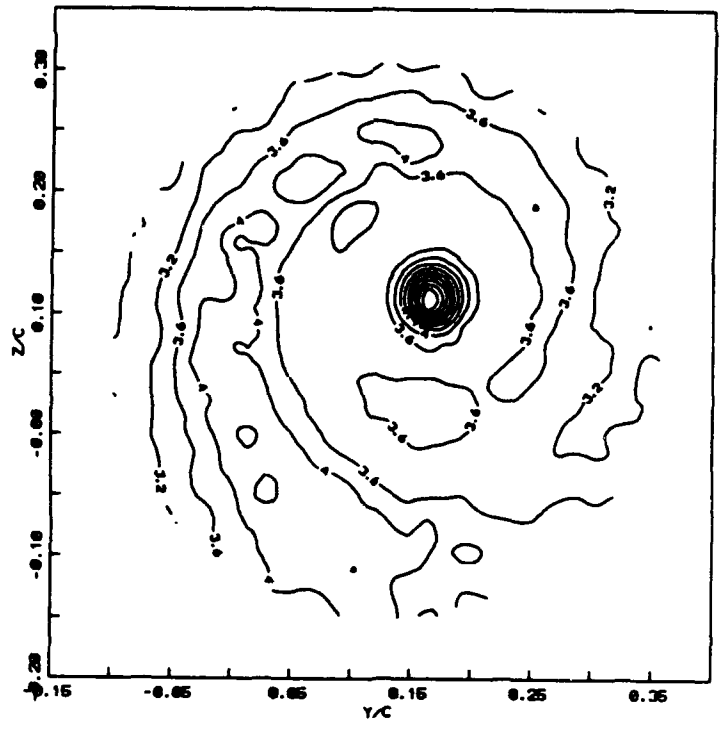

(ii)

(c)

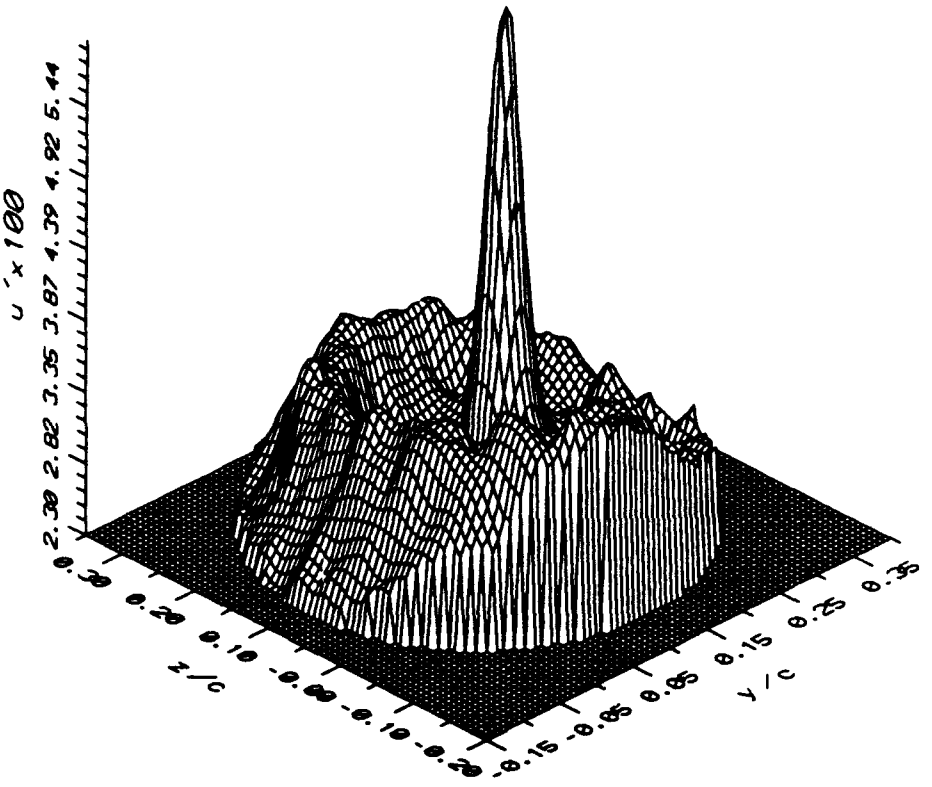

(i)

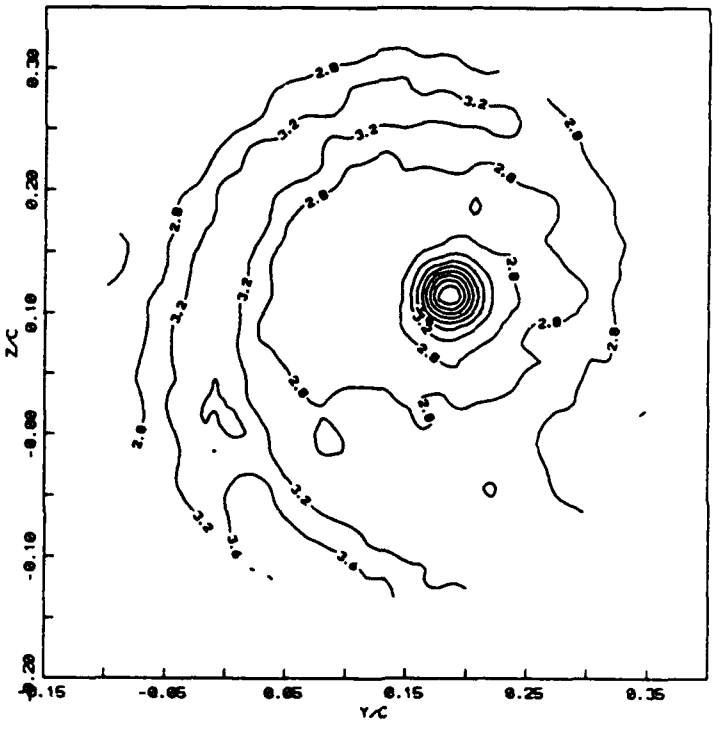

(ii)

(d)

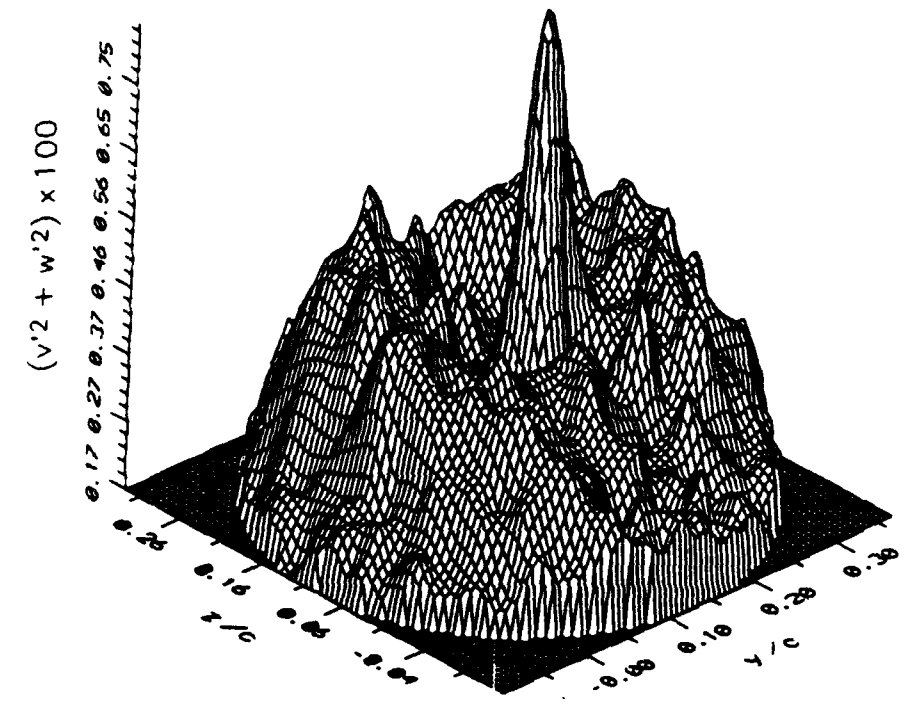

(b)

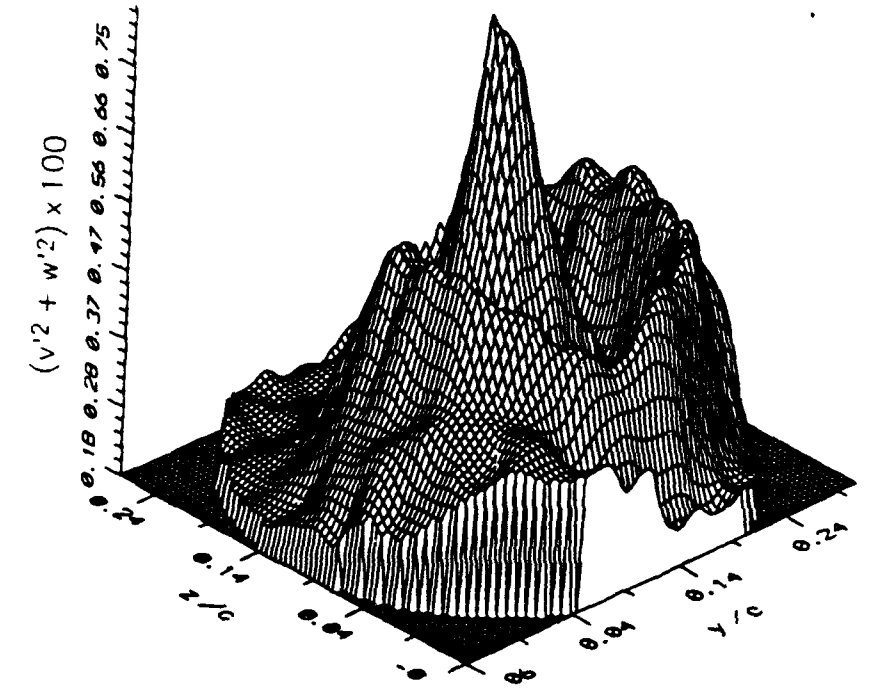

(a)

Figure 3.14 Distribution of $v'^2 + w'^2$ across the vortex at (a) $z/c = 1.16$, (b) $z/c = 3.28$.

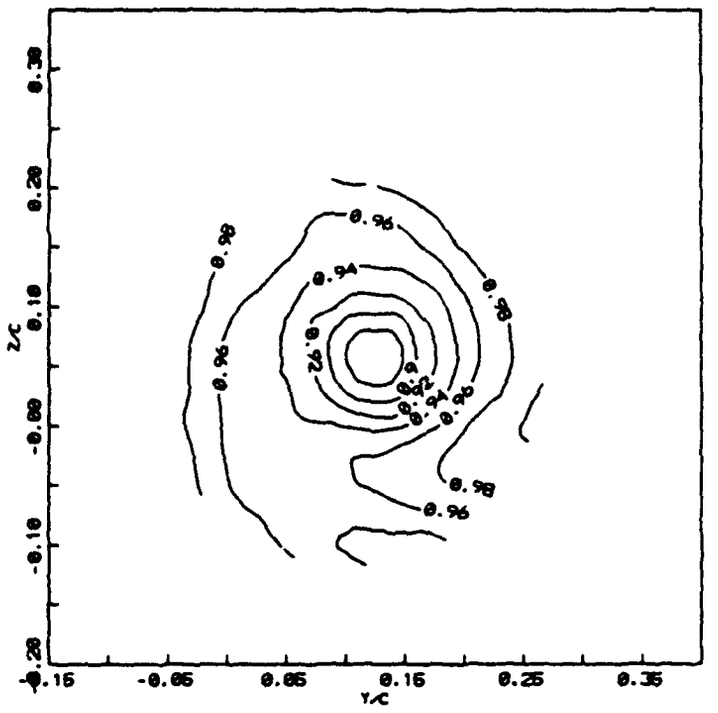

(i)

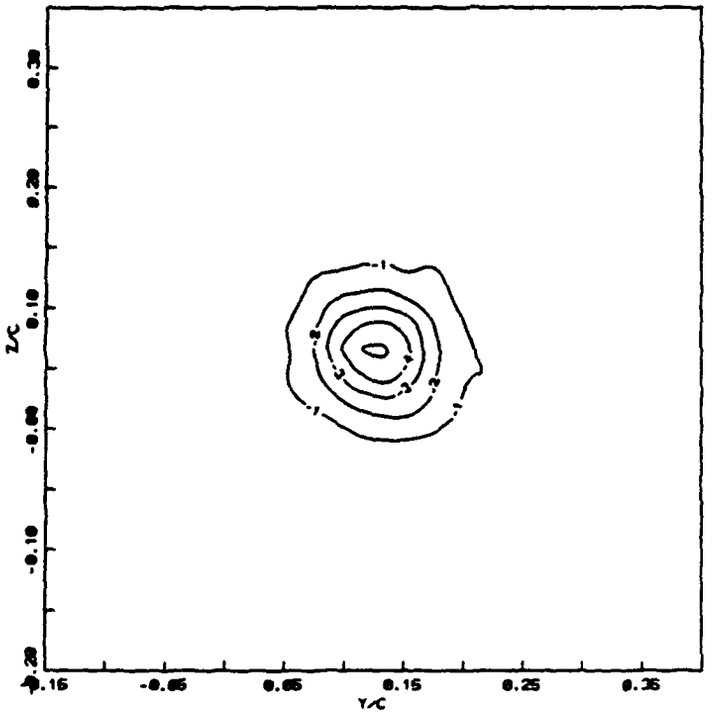

(ii)

(a)

Figure 3.15 Distribution of the longitudinal component of the velocity and vorticity at (a) α = 2 degrees, (b) α = 5 degrees, (c) α =10 degrees, (i) Velocity, (ii) Vorticity. x/c = 3.28.

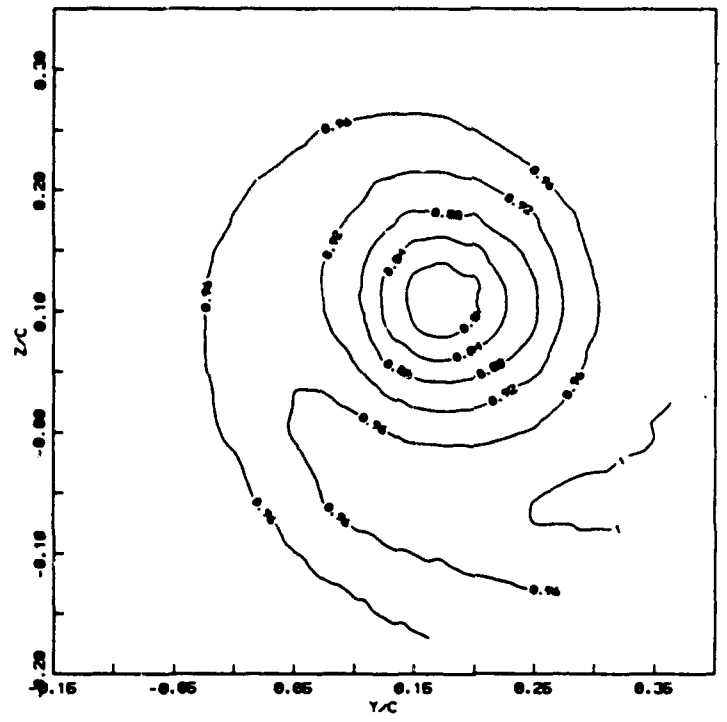
Z/C
0.30
0.20
0.10
-0.00
-0.10
-0.20
-0.15
-0.05
0.05
0.15
0.25
0.35
Y/C

(i)

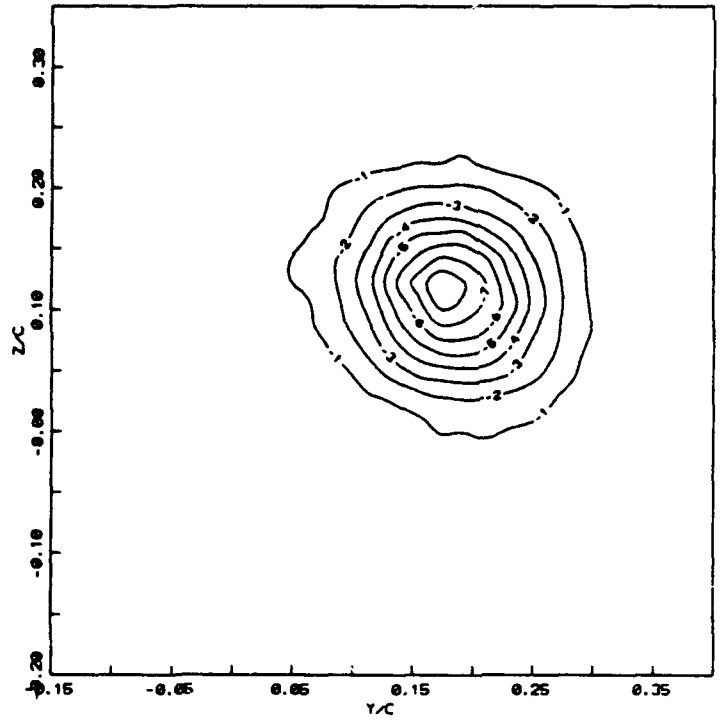
Z/C
0.30
0.20
0.10
-0.00
-0.10
-0.20
-0.15
-0.05
0.05
0.15
0.25
0.35
Y/C

(ii)

(b)

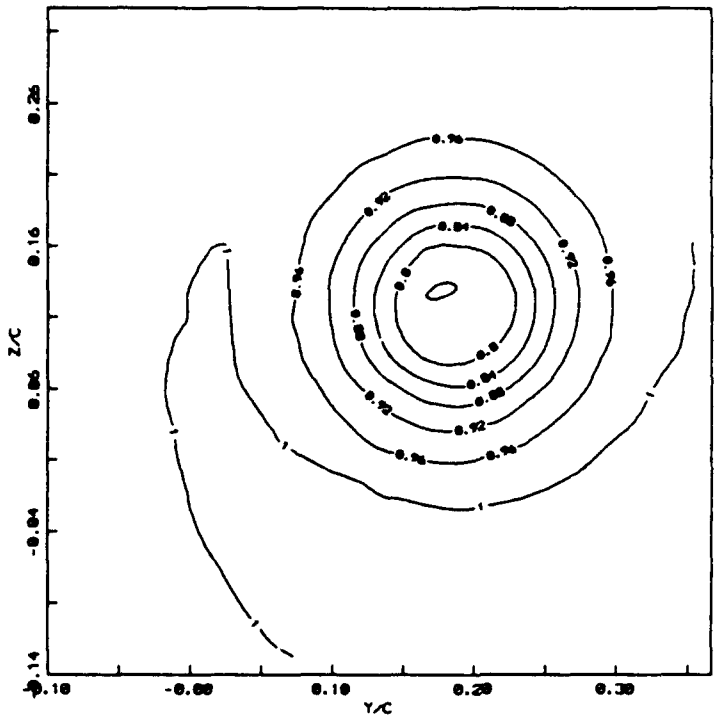
0.26
0.16
0.06
-0.04
-0.14
Z/C
-0.10
-0.00
0.10
0.20
0.30
Y/C

(i)

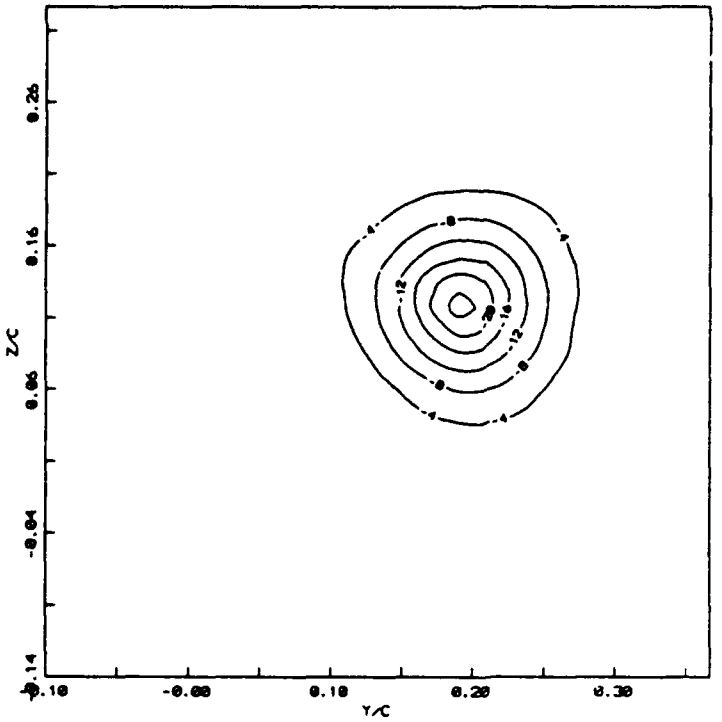
0.26
0.16
0.06
-0.04
-0.14
Z/C
-0.10
-0.00
0.10
0.20
0.30
Y/C

(ii)

(c)

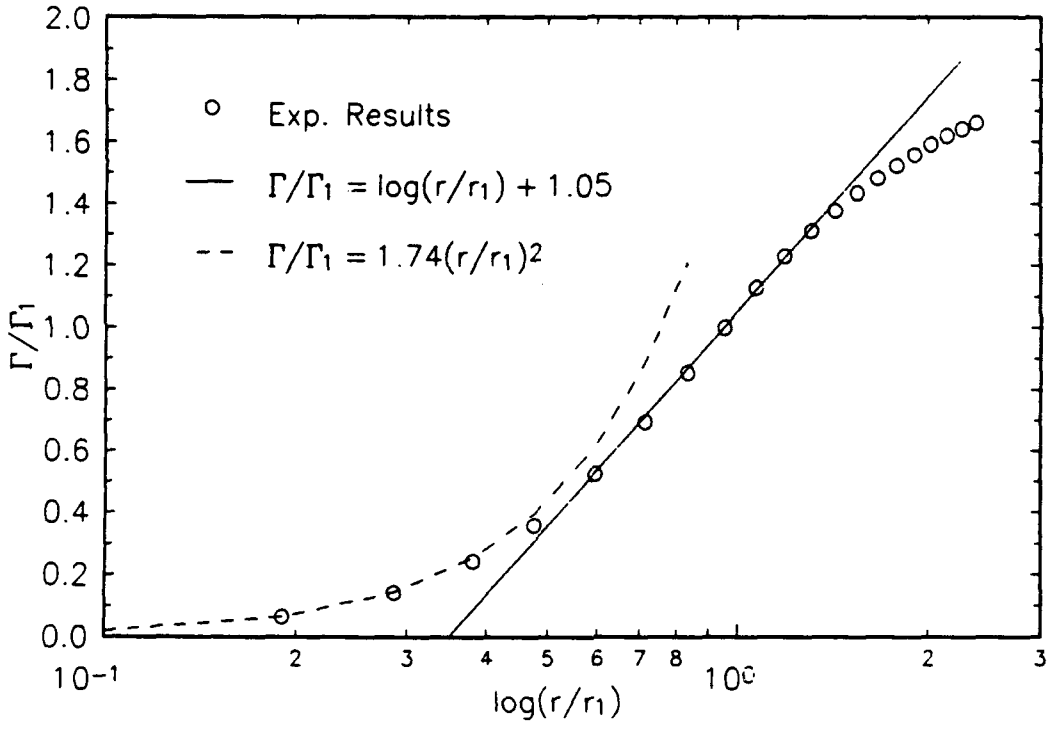

Figure 3.16 Semilogarithmic plot of Γ/Γ_1 vs r/r_1 for $x/c = 1.0$.

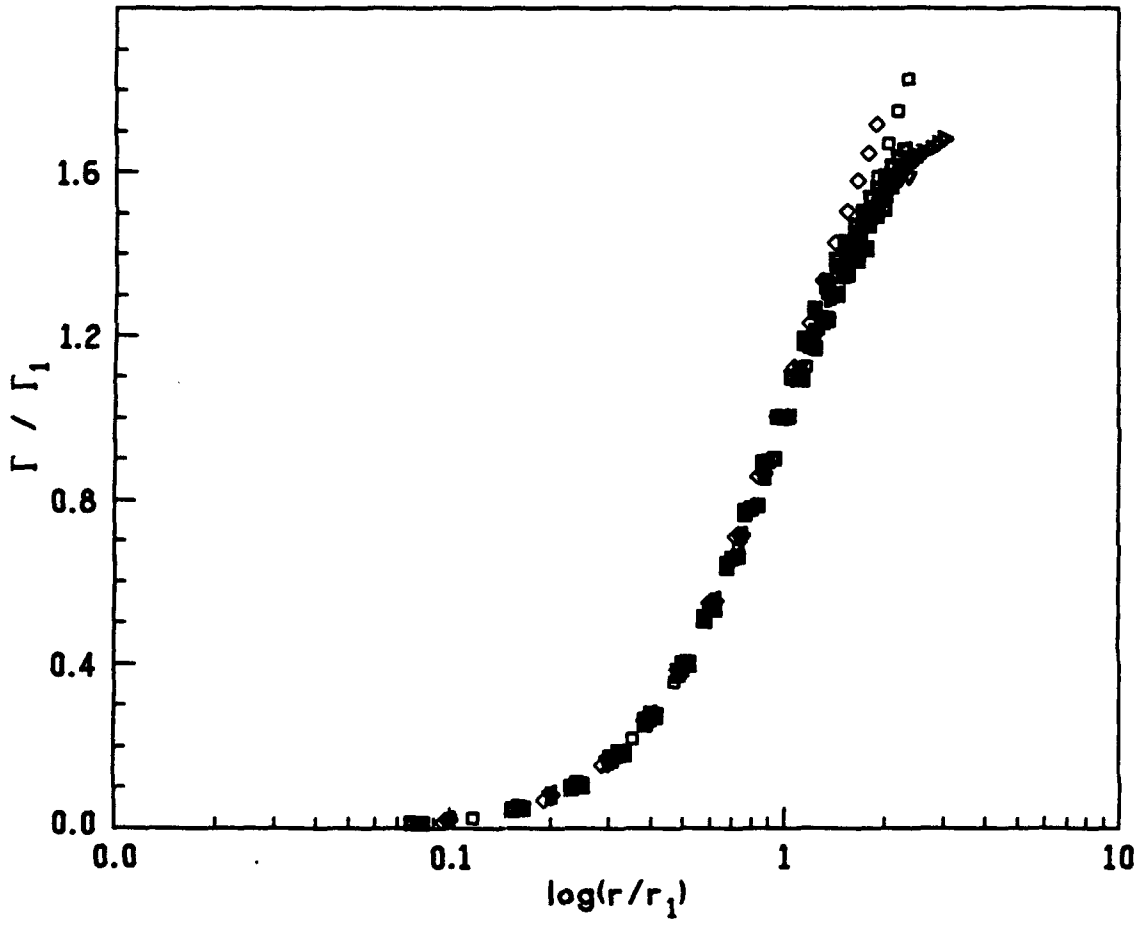

Figure 3.17 Semilogarithmic plot of Γ/Γ_1 vs r/r_1 for all the stations and angles of incidence listed in Table 2.

CHAPTER 4

EXPERIMENTAL SET-UP AND PROCEDURE FOR THE UNSTEADY FLOW EXPERIMENTS

In this chapter the experimental set-up and procedure for the studies of the tip-vortex behind an oscillating wing are described. Most of the instrumentation used in these studies was the same as that used in the stationary-wing studies described in Chapter 2. Only the main points of difference between the two experimental set-ups and procedures are described in this chapter. The results obtained from these studies will be presented and discussed in the next chapter.

4.1 Experimental Set-Up

The experiments were conducted in the same 1 m × 1 m low-speed wind tunnel, as described earlier. At the test section, the free stream velocity was set to about 8.2 m/s, corresponding to the mean Reynolds number of about 180,00. The wing tested was the same as used in the steady-flow experiments. The wing was mounted with its span horizontal and oscillated sinusoidally in pitch about its quarter-chord (0.25c) axis by a Scotch-Yoke Mechanism driven by a speed-regulated 0.75 hp D.C. motor. The wing installation relative to the wind tunnel was, again, as shown in Fig. 2.1. A schematic of the Scotch-Yoke mechanism is shown in Fig. 4.1. This Scotch-Yoke mechanism was designed such that when the motor rotates, a roller-cam mechanism transfers the circular motion of the roller to the periodically vertical motion of a rack. This periodic

vertical motion is converted again to a sinusoidal rotation of the wing via a rack and pinion mechanism. Thus, the instantaneous angle of incidence of the wing can be varied sinusoidally with time according to

$$\alpha = \alpha_0 + \Delta\alpha \sin(2\pi f t) \tag{4.1}$$

The frequency of oscillation can be adjusted in the ranges 0 - 2 Hz, by changing the rotational speed of the D.C motor; the amplitude can be varied from 0 to 45 degrees, by changing the distance between the roller and the axis of the D.C. motor, and the mean angle of incidence can be set to any value by changing the relative positions of the pinion and rack, to satisfy the requirements of these experimental studies. In the present experiments, the mean angle of incidence (α_0) was 10 degrees; the amplitude ($\Delta\alpha$) and frequency of oscillation (f) were 5 degrees and 1 Hz. respectively. This oscillation frequency corresponds to a 'reduced frequency' $k \equiv \pi f c/U_\infty \approx 0.1$, which is relevant to helicopter rotor-blade aerodynamics. An optical encoder (which has a resolution of 4096 parts per revolution) was mounted on the end of the pitching axis and rotated with it to provide information of the phase angle of motion of the wing during the oscillation cycle. The instantaneous direction (viz, clockwise or counterclockwise) of the wing motion was also provided as "0" or "1" by one bit on the encoder output. The encoder output was read by a counter whose output in turn was acquired by the data acquisition system.

A three-color, six-beam, fiber-optics based, backscatter laser-Doppler velocimetry system was used as in the steady-flow studies, to measure the three components of

instantaneous velocity in the flow field. The velocity data from the LDV measuring system were transferred to an IBM-PC, and recorded simultaneously with the phase information from the encoder, for further data processing. The main components of the measurement system in the experiments are listed in the Table 4.1. The parameters of the measuring system set-up in the experiments are listed in Table 4.2. A schematic of the signal processing system is shown in Fig. 4.2.

4.2 Data Acquisition and Processing

The data from the LDV and the encoder were acquired on an IBM PC based data acquisition system. The detailed description of this system has already been provided in Chapter 3. These data were later transmitted over ETHERNET to a MASSCOMP 5600 computer for processing and display.

The recorded data from these channels were resolved to obtain the velocity components in the x, y , z directions, just as in the case of the steady flow. The instantaneous velocity data were then analyzed using the well known principle of double decomposition (see Menendez, A.N. & B.R. Ramaprian 1989). Any instantaneous flow property $\Phi(x,y,z,t)$ is thus represented by

$$\Phi(x,y,z,\alpha,t) = < \Phi > (x,y,z,\alpha) + \phi(x,y,z,t) \qquad (4.2)$$

Table 4.1 Main Components of the Measurement System

Description	Specification
Argon-ion laser	Coherent Innova 90 Series(6 Watts)
Beam Splitters	DANTEC 55X Series
Bragg Cells	DANTEC 55X29
Optical fibers	DANTEC 60X Series
LDV Counters	DANTEC 55L96
Frequency Shifters	DANTEC 55N12
Encoder	EG&G 16-DM-1024-5-LD-A-S
Phase Counter	DANTEC 55L96
Traverse	VELMEX 8300 Series

Table 4.2 Parameters and settings used in the Measurement System in the Unsteady Flow Studies.

Parameters	Green Channel	Blue Channel	Purple Channel
Wave length(nm)	514.5	488	476.5
Size of Measuring volume (mm)	0.15 x 0.15 x 0.23	0.15 x 0.15 x 0.23	0.15 x 0.15 x 0.23
Focal length(mm)	600	600	600
Beam angle(degrees)	7.05	7.05	7.05
Fiber length (m)	10	10	10
Number of fringes	35	35	35
Beam diameter(mm)	1.35	1.35	1.35
Power after fibers (watt)	0.31	0.18	0.05
Typical data rate (Hz)	30	20	20
Typical validation(%)	50	30	30
Shift frequency	40 mega Hz	40 mega Hz	40 mega Hz
Downmix frequency	3 mega Hz	0.01 mega Hz	0.01 mega Hz
High-pass filter	1 mega Hz	1 mega Hz	1 mega Hz
Low-pass filter	4 mega Hz	2 mega Hz	2 mega Hz
Coincidence windows (μs)	100	100	200

where $< \Phi >$ is the ensemble-averaged or the phase-locked component and ϕ the random component of Φ. The phase-locked component is obtained by averaging the instantaneous values measured at the same angle of incidence during a number of different oscillation cycles. The instantaneous random component ϕ is then obtained from eq.(4.2). The mean square turbulent intensity $< \phi' > (x, y, z, \alpha)$ is obtained as $< \phi^2 >$, where the symbols <> denote ensemble averaging as defined above. Note also that by averaging the ensemble-averaged properties over a complete oscillation cycle, one can obtain the time averaged property, $\overline{\Phi}$.

In the experiments, the instantaneous velocities were subsequently ensemble averaged over a large number of oscillation cycles (ranging from 50 to 500) and samples (50 to 2000) to obtain phase-locked averages of the flow properties at various phase positions during the cycle. At each phase position, the data were averaged within an ensemble window of $\pm$ 0.3 degree. The data were obtained at downstream locations of $\bar{x}$ (measured from the trailing edge) = 10, 11, 20, 30, 40, 50, 60, 62, 80 and 100 cm (where x = $\bar{x}$ + 22.5 cm), corresponding to $\bar{x}/c \approx$0.33, 0.36, 0.66, 1.0, 1.31, 1.64, 2.0, 2.03, 2.62, 3.28. At each station, measurements were obtained across the vortex (in the $y-z$ plane) at about 500 points which formed a fine grid. The grid size and distribution were selected so as to span the region of significant vorticity during the entire oscillation cycle and provide a spatial resolution adequate for the evaluation of the vorticity vector. Figure 4.3 shows the grid used in the present measurements. Note that the grid spacing selected in the central part of the vortex is half of that in the outer part, this is because of the strong spatial gradients of velocity present near the vortex center. The data at the

each station presented in this paper were obtained from very long experiments, which ran in a fully automated mode, often for nearly a week.

The three phase-locked components of vorticity were derived from the three components of the phase-locked velocities by second-order central-difference numerical approximation. The vorticity components ω_y and ω_z have been obtained by assuming $\partial < U > /\partial x$ to be nearly zero. This approximation was verified by calculating $\partial < U > /\partial x$ by selecting some closed pairs of stations (viz, $\bar{x}$ = 10, 11; 60, 62). It was found that even at $\bar{x}$ = 10 cm (the nearest station to the trailing edge of the wing) the contribution to the magnitude of vorticity by $\partial < U > /\partial x$ was less than 7 percent of total vorticity in the vortex core region of a radius 0.012c, and 3 percent in the rest of the vortex area, so it was reasonable to neglect the velocity gradient of x direction in vorticity calculation.

During the experiments, the coincidence windows were set for the two stations, i.e, $\bar{x}$ = 30 cm and 100 cm, to obtain the turbulent properties accurately in the flow. The coincidence window was determined by the same method as used in the studies of the stationary wing, described in the Chapter 2. The window sizes used in this experiment are listed in the Table 4.2.

4.3 Uncertainty

For the experimental data obtained in this study, uncertainty estimates were performed taking into account the following parameters. The free stream velocity uncertainty, mainly due to the fluctuation of fan speed, and humidity in the room, was ± 3

% of U_∞, The temperature of the air was nearly constant inside the wind tunnel laboratory. Hence, for each test run the Reynolds number was constant within uncertainty of ± 3 %. The uncertainty in positioning of the measuring volume in the each direction (x, y and z) was 0.002 % c. The uncertainty in the mean, as well as instantaneous incident angle was $\pm$ 0.25 degree. Overall, the maximum uncertainty in the LDV measurements of the mean velocity and turbulent intensity were estimated to be 5 and 3 percent of freestream velocity respectively.

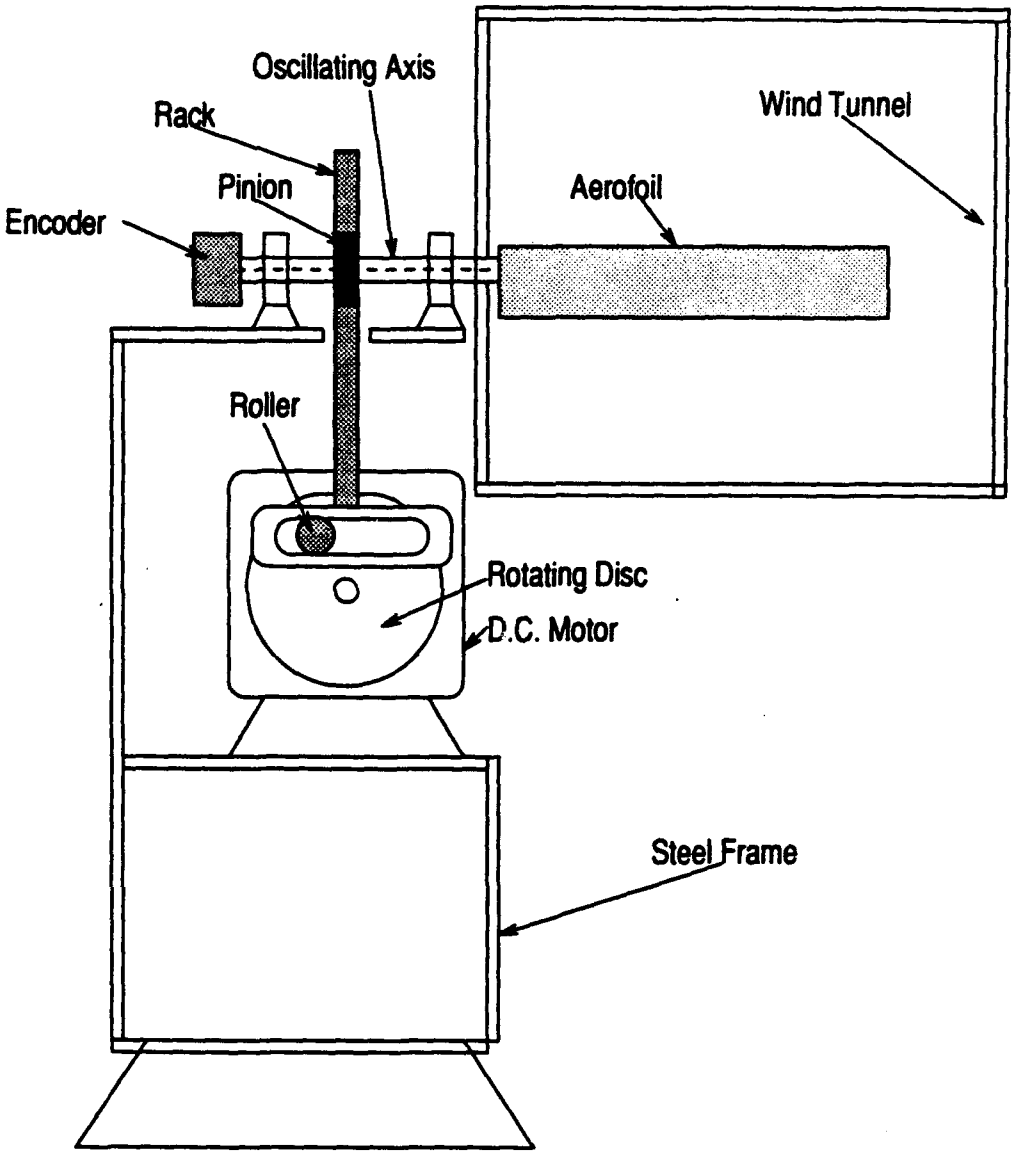

Figure 4.1 Schematic of the Scotch-Yoke Mechanism

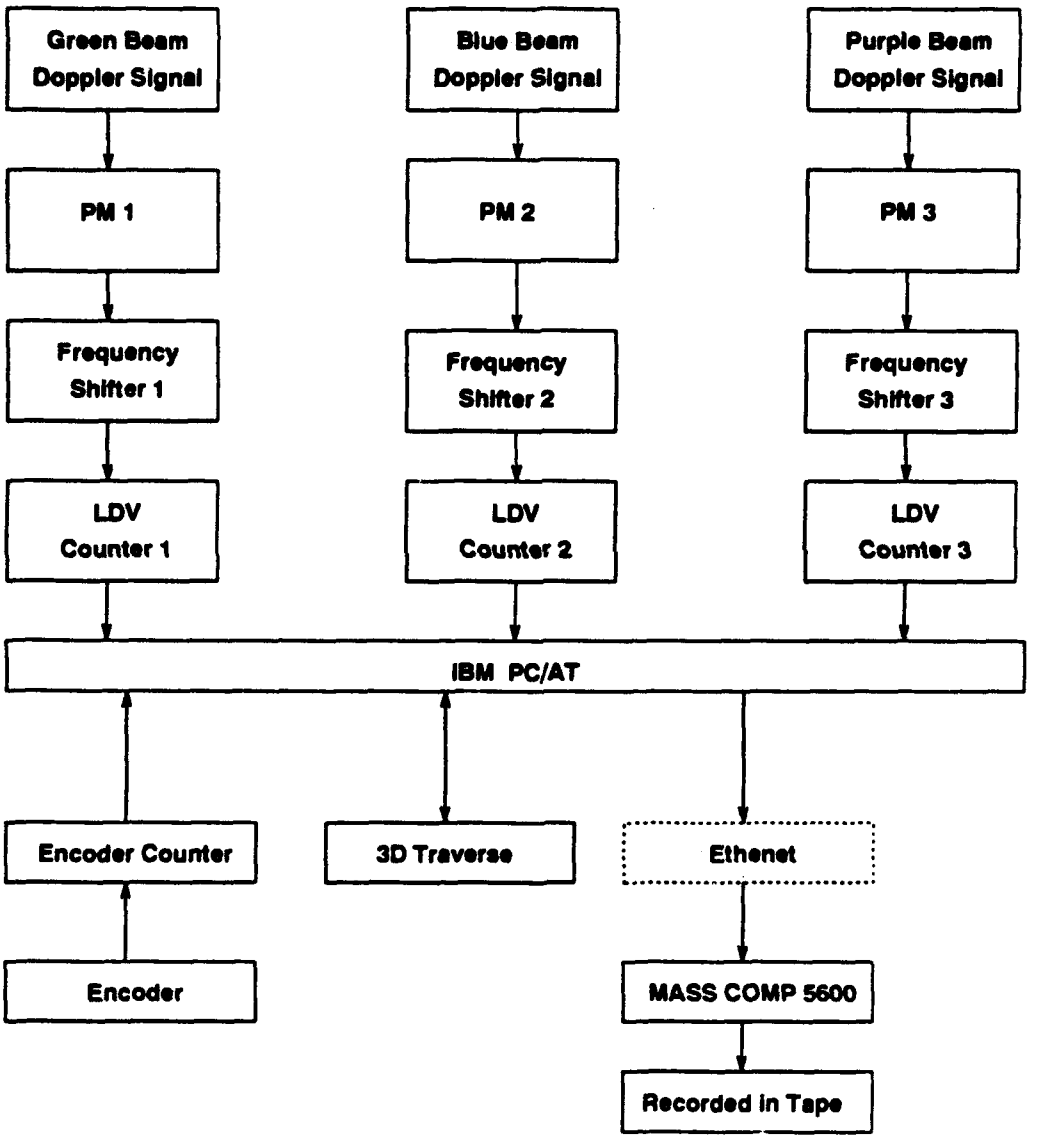

Figure 4.2 Instrumentation for the unsteady flow studies

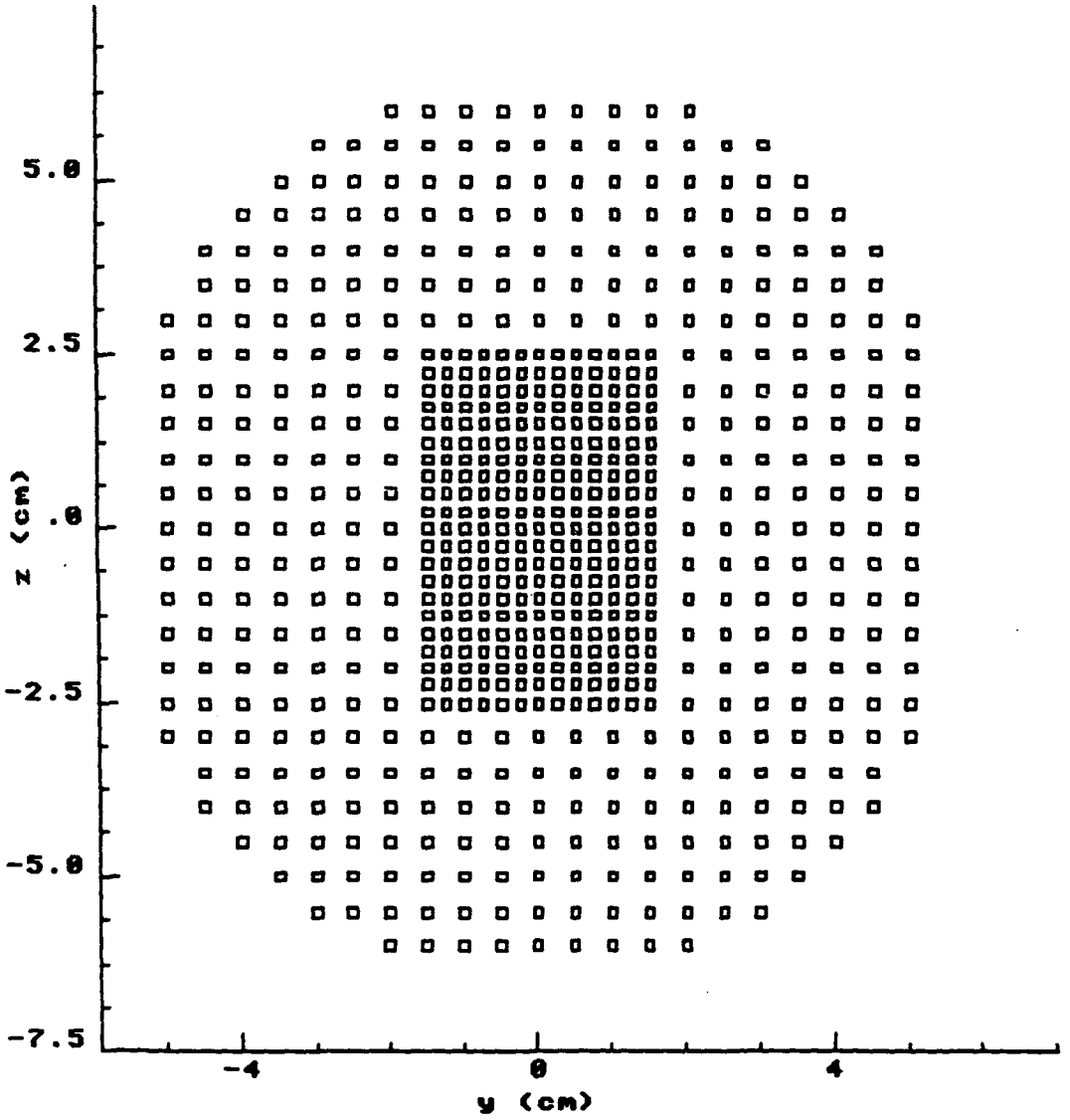

Figure 4.3 Measurement grid in the cross flow plane

CHAPTER 5

RESULTS AND DISCUSSIONS OF THE STUDIES OF THE UNSTEADY TIP-VORTEX

The extensive amount of detailed information obtained by processing the LDV data has been stored on tape. Typical results will be presented and discussed in this chapter. All experimental results presented in this paper are generally normalized by the freestream velocity U_∞ and wing chord c as the reference velocity and length scales respectively except in some cases, when r_1, the radius of the vortex at the maximum tangential velocity, and Γ_1, circulation at r_1, have been used as the normalizing scales. The origin of the coordinate system is located at the wing tip on the oscillating axis in the all figures presented. Also, for simplicity, the phase average symbol, <>, is dropped in the figures presented here. The measurement grid selected has been maximized for the LDV measurements. It was not possible to obtain more data beyond this region because of the lack of seed particles for the LDV, and also because of the range limitations of the LDV optics.

5.1 Velocity Distribution within the Vortex

Contours of the phase-locked longitudinal velocity $< U >$ across the tip-vortex at $\bar{x}/c = 1.32$ are shown in Figs. 5.1(a) and 5.1(b) for eleven instantaneous angles of incidence from 5 to 15 degrees, at increments of 1 degree. Figure 5.1(a) corresponds

to the "pitch-up" situation (increasing α), while Fig. 5.1(b) corresponds to the "pitch-down" situation (decreasing α). A significant feature that can be seen from these figures is the non-quasi-steady nature of the flow, namely, that the flow structure at any given angle of incidence is different for pitch-up and pitch-down situations. In other words, the instantaneous flow "remembers" the wing loading history it passed through. Other interesting features of the flow are also very strongly apparent. For example, it is clearly seen that in the early part of "pitching-down", (i.e., at high angle of incidence $\alpha = 15$ and 14 degrees), a spiral with lower velocity than in the free stream rolls up into the vortex. This spiral, which can be called the "low-spiral", is associated with the shear layer coming from the pressure side of the inboard regions of the wing, which is in a process of rolling up to form the axial tip vortex. As "pitching-down" continues and the angle of incidence decreases, another spiral can be distinguished to roll into the vortex with velocity lower than in the free stream. It is believed that this spiral, which can be called the "up-spiral", corresponds to the flow arriving into the vortex from the regions of the suction side of the inboard regions of the wing. These two spirals with the different axial velocities roll up into the tip vortex and interact with each other in the central region of the vortex. This results in a more turbulent and disorganized structure of the axial tip vortex as shown in the Fig. 5.1(b) for $\alpha = 7$, 8, 9, 10, 11 and 12 degrees. When the wing approaches its minimum angle of incidence in the pitch-down process the effect of the "up-spiral" is gradually reduced and the flow recovers to a better organized wake-like pattern (see $\alpha = 5$ and 6 degrees). During the pitch-up motion only the "low-spiral" dominates the vortex in the entire process of pitch-up of the wing. Hence the velocity decrease in the interior of the vortex is monotonic across the vortex from the

rim towards the center, and the flow is far more organized and nearly axisymmetric during most part of the pitch-up motion than during the pitch-down motion. In fact, the boundary layer development over the airfoil depends on the direction, velocity and acceleration of the wall motion. This dynamic effect , also referred to as the hysterisis effect, is well known from earlier studies of the pressure distribution on oscillating airfoil. Thus, during the pitch-up motion the boundary layer over the inboard regions of the wing tends to remain attached to the surface resulting in a wake that is less turbulent and better organized. This shear layer rolls up into the tip vortex. The flow over the wing during the pitch-down motion tends to detach itself from the surface, especially at the larger values of α. This also results in a more"disturbed" wake that rolls into the tip vortex. These changes cause the flow in the tip vortex to be non-quasi-steady. The effect, however, manifests neither immediately, nor without further distortion at the measuring station. The delay is introduced by the time required for the effects to be convected from the originating regions on the wings to the measurement location. This effect will be discussed in more detail later. The distortion of the vortex is due to the nonlinear interactions of the spirals and generation of the turbulence from these interaction. This non-quasi-steady behavior of the flow is an important feature that can be observed in all the flow properties studied. The same general behavior of the vortex can be observed in Fig. 5.2 at $\bar{x} = 10$ cm. However, the flow is strongly three-dimensional in this initial region of the near wake.

Figures 5.3(a) and 5.3(b)show the typical distributions of the phase-locked, cross-stream velocity vectors ($\vec{j} < V > + \vec{k} < W >$) across the vortex for the same downstream

distance and the angles of the incidence as Fig. 5.1. Figure 5.3(a) corresponds to the pitch-up motion of the wing and Fig. 5.3(b) to the pitch-down motion. The axis of oscillation of the wing is shown by the solid straight line, and the trailing edge position is represented by a dashed line in each figure. The magnitudes of the cross-stream velocity vectors, which were found to be of the order of $0.5U_\infty$, are shown by the length of the arrows in these figures. It is seen that velocity vectors are distributed quite smoothly over the entire vortex, except for the few located near the rim of the vortex. This scatter is due to the poor data rate, caused by insufficient seed particles. If one looks at the cross stream flow at any angle of incidence, the general properties of the flow in the cross-stream plane appear to be quite similar to the steady case (stationary wing). For example, the tangential velocities are seen to increase rapidly from almost zero at the center of the vortex to a maximum at some distance r_1 from the center, beyond which they decrease gradually. Also, just as in the case of the stationary wing, near the trailing edge the velocities in the upper left region of the vortex (outboard of the tip) are seen to be generally larger than those on lower right region (inboard of the tip) due to the three-dimensional effects of the wing tip. Furthermore, comparison of Fig. 5.3(a) with 5.3(b), shows that, as in the case of axial velocities, the cross stream velocities are higher during the pitch-down than during the pitch-up at all angles of incidence. In fact, the departure from quasi-steady behavior is clearly seen, both not only with respect to the magnitude of the cross-stream velocities but also with respect to the locations of the vortex center, at different angles of incidence.

In fact, from plots like Figs. 5.3(a) and 5.3(b), one can locate the center (zero cross-stream velocity) of the tip vortex with very good accuracy for stations $\bar{x}/c \geq 1.0$, by linear interpolation/extrapolation. It was found that the spanwise coordinate of the vortex center essentially remained constant during the entire oscillation cycle at approximately $0.12c$ in board of the wing tip. The vortex center, however, moved up and down during the cycle. Figure 5.4 shows the z_0 coordinate of the vortex center as a function of time during the oscillation cycle at the downstream locations $\bar{x}/c =$ 1.0, 1.32, 2.0 and 2.62. It is seen that the vertical movements of the vortex center are not purely harmonic during the cycle of the wing motion. A sinusoidal curve such as shown by the solid line in Fig. 5.4 can be considered to be an approximate fit to these data. While the up and down motion of the vortex center corresponding to a similar motion of the wing tip is expected, it is interesting to note that there is a phase difference between the two motions, and that phase difference varies in the downstream direction. The time delay t_0 of the vertical motions of the vortex center with respect to the motion of the wing, vs downstream distance $\bar{x}$ is plotted in Fig. 5.5. The linear plot suggests that the vortex is convected at a constant velocity given by the slope of the line

$$t_0 U_\infty / c = 1.07(\frac{\bar{x}}{c}) + 1.25 \tag{5.1}$$

Thus the convective velocity U_c can be evaluated as:

$$\frac{U_c}{U_\infty} = \frac{1}{U_\infty}\frac{d\bar{x}}{dt_0} \approx 1/1.07 = 0.935$$

This convective velocity is very close to the freestream velocity U_∞. Also, the value of $\bar{x}_0/c$ for $t_0 = 0$ is -1.17. This $\bar{x}_0/c = -1.17$ can be considered to be the virtual origin for the evolution of the vortex.

One can thus estimate the phase delay of the flow properties at the any downstream position in the near wake, relative to the instantaneous wing incidence. For example, at the station, i.e., $\bar{x} = 0.4$ m, the time delay due to convection is from eq. (5.1), about 0.1 second, which corresponds to about 2 degrees of angular motion of the oscillating wing.

5.2 Vorticity Distributions within the Vortex

The high density of data points obtained in these experiments made it possible for one to estimate the components of the phase-locked vorticity in the flow within the vortex. Some typical results for the evolution of the non-dimensional axial vorticity component $\omega_x c$ during the pitch-up and pitch-down positions of the oscillating cycle are shown in the contour plots in Figs. 5.6(a) and 5.6(b) for the same downstream distance and angle of incidence as Fig. 5.1. Figure 5.6(a) corresponds to the pitch-up case and Fig. 5.6(b) to the pitch-down case. It was observed that nearly 85% of the axial vorticity is concentrated within a radius of the order of 0.15c. It is, however, seen that there is a significant distribution of axial vorticity over this radius. This distribution is due to viscous and/or turbulent diffusion. The maximum (negative) vorticity is observed near the center of the vortex. The magnitude of this vorticity is generally higher, and the vorticity distribution more nonaxisymmetric during the pitch-down motion. This

is consistent with the observed behavior of the cross-stream velocity vectors. The non-quasi-steady nature of the flow is thus once again apparent even after the phase delay is taken into account. The same behavior of ω_z can be seen in Fig. 5.7 at $x/c = 0.33$ except for the much stronger three dimensionality.

As the shear layer rolls up, the spanwise vorticity carried by it rotates into the axial direction and augments the axial vorticity of the tip-vortex. This is clearly seen from Figs. 5.8(a) and 5.8(b), which show typical plots of the non-dimensional cross-stream vorticity vector ($\vec{j} < \omega_y > + \vec{k} < \omega_z >$) across the vortex, for α from 5 to 15 degrees at increments of 1 degree, during pitch-up and pitch-down portions of the cycle. The dashed and solid horizontal lines once again indicate the oscillation axis and trailing edge respectively as in Fig. 5.3. The maximum magnitude of this vorticity vector is about 25% of the magnitude of the total vorticity (with the exception of a few irregular data points in the figure). The vortex core is dominated by the axial component of vorticity ω_z, specially at the higher angles of incidence. Once again, the roll-up process resulting in the transfer of the cross-stream vorticity to the longitudinal direction is well organized during the pitch-up process. Very little cross-stream vorticity is seen in the shear layer during the pitch-down motion, which indicates that this layer was 'detached' from the wing surface when it started moving towards the tip.

5.3 Circulation Distributions within the Vortex

Integration of the axial vorticity over the area of the vortex up to any radius r yields the circulation associated with this vorticity around a circle of that radius.

Figures 5.9(a) and 5.9(b) show typical distributions of the ensemble averaged circulation $< \Gamma > /U_{\infty}c$ as a function of the distance from the vortex center for several angles of incidence during pitch-up and pitch-down motions. Also shown for comparison in each figure are the distributions of the time-average circulation by a dashed line, and the circulation corresponding to the mean angle of incidence of 10 degrees in steady flow, by a solid line. There is no spectacular difference between these two distributions. However, the circulation during the pitch-down motion is substantially larger than during the pitch-up process, but it is noted that the phase delay between these two figures is equivalent to 2 degrees of angular motion of the wing. This means, for example, the actual circulation at 10 degrees during the pitch-up motion corresponds to that at about 12 degrees at the measurement station in Fig. 5.9(a), while circulation at the same incidence during the pitch-down motion is that at about 8 degrees in Fig. 5.9(b). It can be seen that the circulation at 12 degrees in Fig. 5.9(a) is above the solid line (the circulation at 10 degrees in the steady flow) and the circulation at 8 degrees in Fig. 5.9(b) is near the solid line. Thus it can be concluded that more circulation (or, vorticity) is associated with the tip vortex during pitch-up than during the pitch-down. Since the strength of the axial vortex is related to the spanwise distribution of lift over the wing, one can also conclude that more lift is generated during pitch-up than pitch-down. This result is consistent with the measurements of spanwise lift distribution on the surface of the wing. The circulation distribution varies considerably during the oscillation cycle and this variation is significantly non-quasi-steady and is not simply accounted for by a phase shift. The circulation in Figs. 5.9(a) and 5.9(b)has not reached a constant value in some of the distributions at the smaller angles of incidence. This is possibly due to

the fact that the roll-up of the shear layers at small values of α is slow and hence not complete at this downstream distance. The seed particles introduced near the outboard regions of the wing did not spread far enough to allow the measurements to be continued to more inboard locations in the wake (i.e., larger values of r).

Earlier steady flow studies (Hoffmann & Joubert 1963, and Phillips 1981) on fully-developed, axisymmetric, turbulent, line vortices have resulted in the identification of three regions within the vortex on the basis of phenomenological reasoning analogous to turbulent boundary layers. Thus, there exists a "core" region where the circulation is proportional to r^2, analogous to the laminar sublayer; an intermediate region where the circulation distribution is semi-logarithmic, analogous to the log layer; and an outer region where a "defect law" applies, analogous to the outer region of a turbulent boundary layer. It would be interesting to examine, in the above light, the behavior of $< \Gamma >$ in the inner two layers for the evolving three-dimensional unsteady vortex, even though the vortex studied is very different from the fully developed steady line vortex. Figure 5.10 shows a plot of $< \Gamma >$ vs r in semilogarithmic coordinates, for $\alpha = 5$, 10 and 15 degrees at $\bar{x}/c = 1.31$, and Fig. 5.11 for $\alpha = 10$ degrees at $\bar{x}/c = 0.66$, 1.31, and 2.62. Similar to the steady flow studies, a mean (averaged in circumferential direction) length scale of r_1, the vortex radius of maximum tangential velocity, and $< \Gamma_1 >$, circulation at r_1, were used to normalize all the results in the figures. The subscript '+' in the figures represents pitch-up and '-' represents pitch-down motion. It is seen that there is a small region ($r/r_1 \leq< 0.4$) near the vortex center where Γ can be described as:

$$\frac{< \Gamma >}{< \Gamma_1 >} = 1.6(\frac{r}{r_1})^2 \tag{5.2}$$

The coefficient 1.6 is slightly different from the value of 1.83 suggested by Hoffmann & Joubert (1963). Also, there is an other region between $0.6 < r/r_1 < 1.4$, where $< \Gamma >$ does seem to follow a semilogarithmic variation with r

$$\frac{< \Gamma >}{< \Gamma_1 >} = ln(\frac{r}{r_1}) + 1.0 \tag{5.3}$$

this is also consistent with the description of Hoffmann & Joubert for a turbulent line vortex. These aspects of behavior are exactly the same as in the case of the steady tip vortex. described in the Chapter 3. Unsteadiness only affects the length scale r_1, and the circulation scale Γ_1. It is interesting to see how these scales change with time. These are plotted in Fig. 5.12 and 5.13. First, it is seen that these variations with time are not quite harmonic, indicating nonlinear effects. Secondly, even if they are considered to be approximately harmonic, the variations exhibit some phase lag with respect to the wing motion. Thus the non-quasi-steady behavior of the flow is once again apparent. The length and velocity scales used in the above circulation distribution seem suitable for describing the unsteady vortex.

5.4 Turbulent Intensity Distribution within the Vortex

The rms turbulent intensities and turbulent shear stresses can be obtained from the instantaneous velocities. Typical results for the distribution of the phase-locked rms intensity of longitudinal velocity $< u' >$ across the vortex are shown in the contours of Figs. 5.14(a) and 5.14(b) for α = 5, 7, 10, 13 and 15 degrees at $\bar{x}/c = 1.31$. It is seen that this intensity is associated mostly with the spiralled shear layer during the pitch-up. The shear layer coming from the wake carries with it the wake turbulence, and rolls up

into the center of the vortex, resulting in the concentration of turbulence at the center of the vortex (Fig. 5.14(a)). This behavior is very similar to the steady tip vortex in the near wake. The maximum intensity is about 11%. The spiral is apparently broken in Fig. 5.14(b) during the pitch-down motion. Combined with the distribution of the velocity in Fig. 5.1, it can be deduced that the break down of the spiral is associated with the interaction of the double spirals during the pitch-down. Thus the turbulence level during this part of the cycle is very much higher (maximum value of 20% U_∞). These results are consistent with the observations made with regard to the velocity and vorticity data.

5.4 Downstream Development of the Vortex

The downstream development of the vortex at a fixed angle of incidence can be obtained by revising the phase of the flow due to the phase delay. The phase delay at a downstream station can be obtained by the time lag from eq.(5.1). Thus, the flow, for example, at 9 degrees and $\bar{x}$ = 0 cm, should correspond to that at 10 degrees if $\bar{x}$ = 40 cm, and 11 degrees if $\bar{x}$ = 80cm. By this manner, the phase-locked downstream development of the longitudinal velocity component U are.shown in Figs. 5.15(a) to 5.15(b) during the pitch-up and pitch-down motions. The initial station is selected at $\bar{x}/c = 0.33$. The angle are $\alpha = 9$ degrees for the pitch-up motion, and $\alpha = 11$ degrees for the pitch-down motion. The phase uncertainty in these stations is within a round off error of 0.5 degree. It shows that during the pitch-up motion, the shear layer, associated with the flow coming from the pressure side of the wing, rolls up into the spiral. The

spiral becomes tighter and tighter as the flow moves downstream. The vortex exhibits well organized structure after one chord distance from the trailing edge. These behaviors are quit similar to those in the case of the steady flow. It can be also observed that the velocity defect is gradually reduced due to viscous diffusion/dissipation. However, the structure of the vortex is not so well organized during the pitch-down motion due to the interaction between the double spirals in the center of the vortex. It seems that the interaction of the double spirals is gradually reduced as the flow moves downstream.

Figures 5.16(a) and 5.16(b) show the downstream development of the longitudinal vorticity component ω_x at the same angles of incidence and downstream locations as in Fig. 5.15. Basically, these distributions are similar to velocity U distribution. However, there are still some other features that can be distinguished. For example, during the pitch-down motion, the interaction of the double spirals only affects the central region of the vortex, thus the distributions of the vorticity are still nearly axisymmetric in the regions slightly beyond the vortex center after $\bar{x}/c > 1.0$. On the whole, the distributions of the vorticity are non-axisymmetric at all the stations, even for $\bar{x}/c > 2.5$. Once again, non-quasi-steady behavior is strongly exhibited in the both the velocity distributions and vorticity distributions during their downstream development.

5.5 Conclusions for the Unsteady Flow Experiments

The three-component LDV measurements in the tip vortex of an oscillating wing, obtained at several downstream distances from the trailing edge have shown that the flow is strongly three-dimensional. The data indicate, as in the case of the steady vortex,

that the shear layer from the trailing edge of the wing rolls up into a spiral in this region carrying with it, the wake turbulence and cross-stream vorticity. During the roll-up process, the cross-stream vorticity vector associated with the shear layer is rotated into a streamwise direction augmenting the vorticity in that direction at the center of the tip vortex. The vortex core is dominated by axial vorticity. The phase-locked circulation distribution across the inner part of the vortex is very similar to that observed in fully developed axisymmetric trailing vortices, namely, it varies as r^2 very near the center and follows a semilog law over a part of the region beyond. The convective velocity of the phase is nearly equal to the free stream velocity during the cycle. While the time-mean flow is not significantly different from steady flow at the mean angle of incidence, the periodic flow is not quasi-steady at the oscillation frequency studied. This is due to the non-quasi-steady effects of unsteadiness on the turbulent boundary layer in the inboard planes and the consequent effects on the spanwise lift distribution. It will therefore be necessary to use dynamic models to obtain correct predictions of the instantaneous flow. The data presented here are probably the first of their kind and will be useful as a database for the development and verification of numerical predictive models.

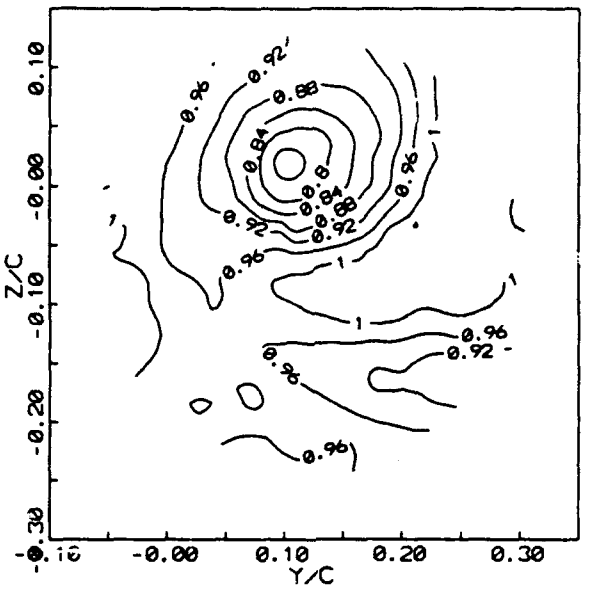

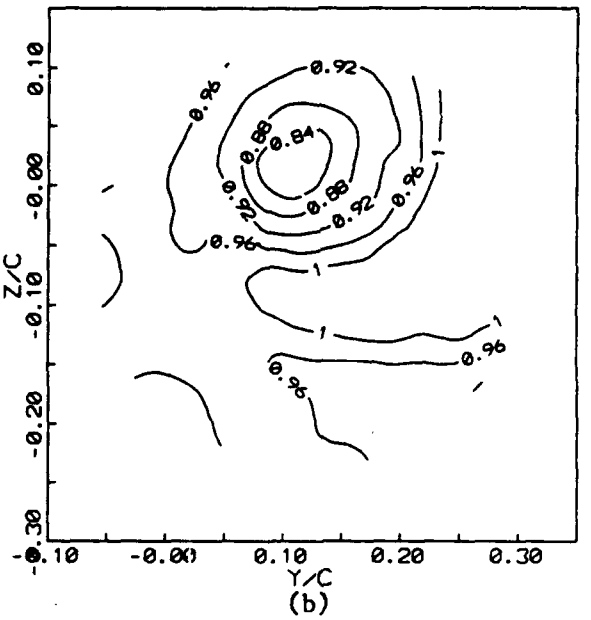

a = 5 degrees

Figure 5.1 Mean velocity $< U >$ contours at x = 40 cm, α = 5 to 15 degrees by increments of 1 degree. a)Pitch-up. b)Pitch-down

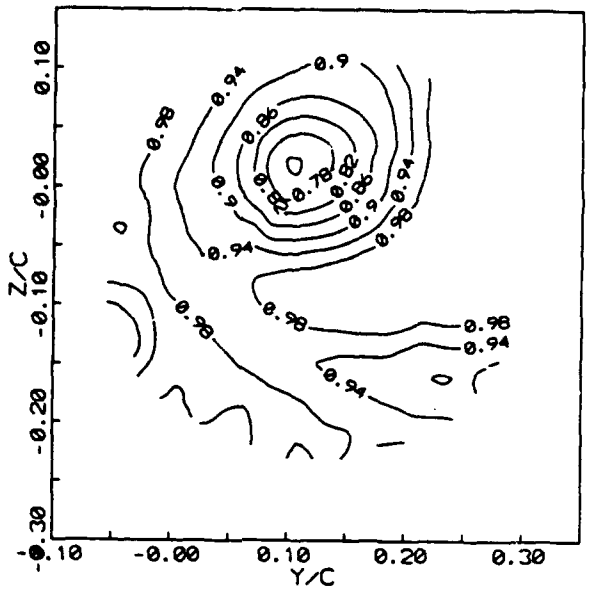

(a)

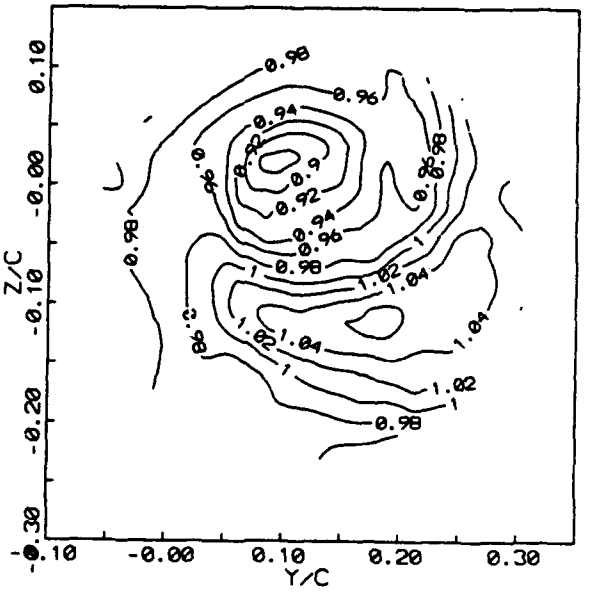

(b)

a = 6 degrees

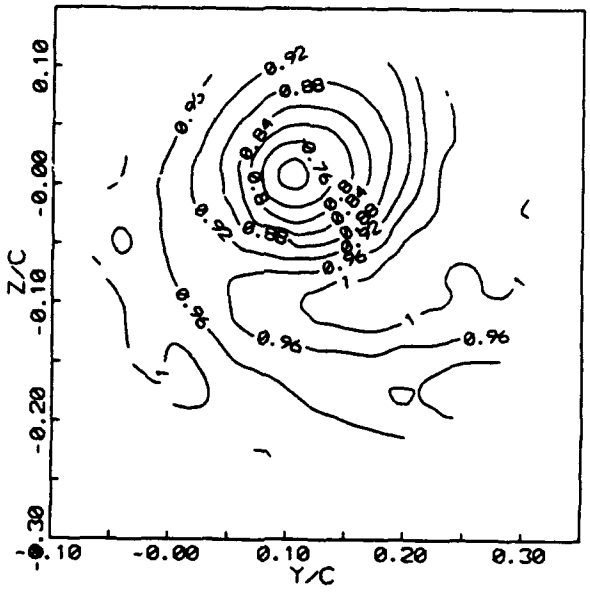

(a)

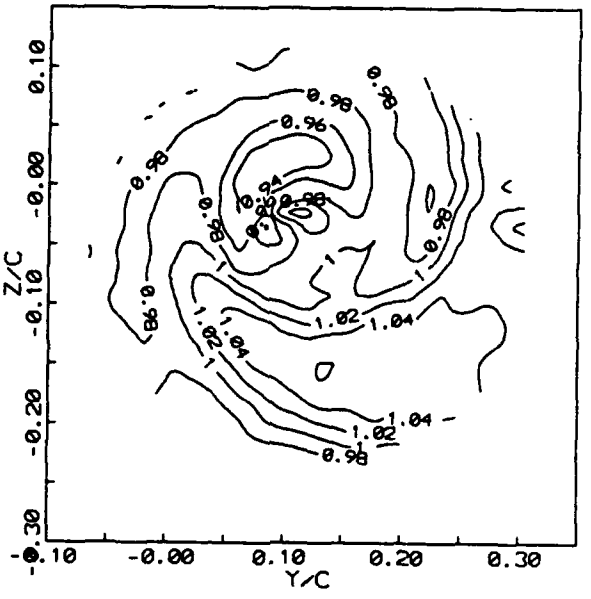

(b)

a = 7 degrees

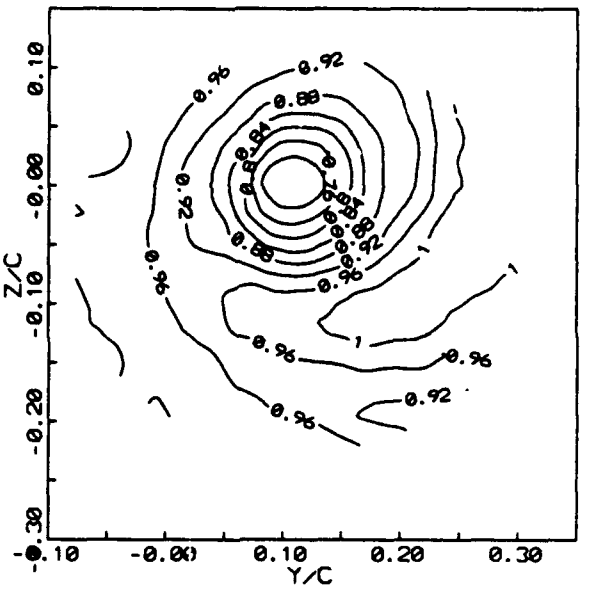

(a)

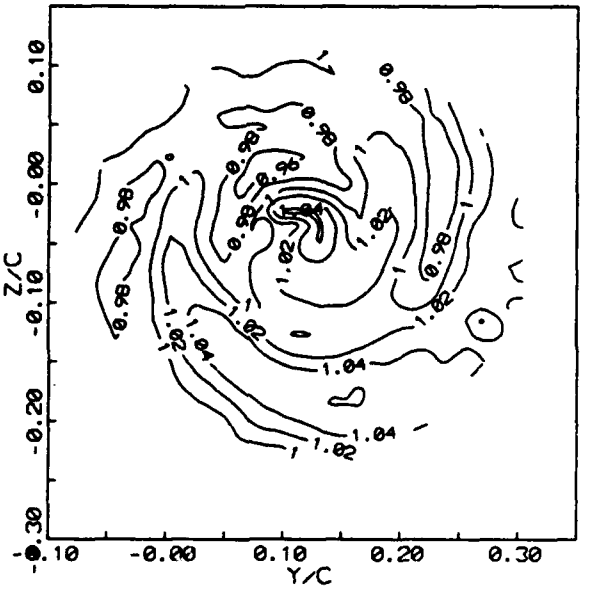

(b)

a = 8 degrees

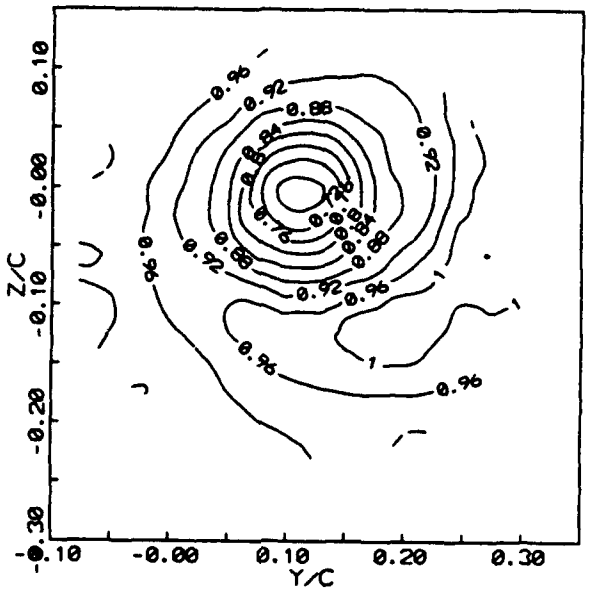

(a)

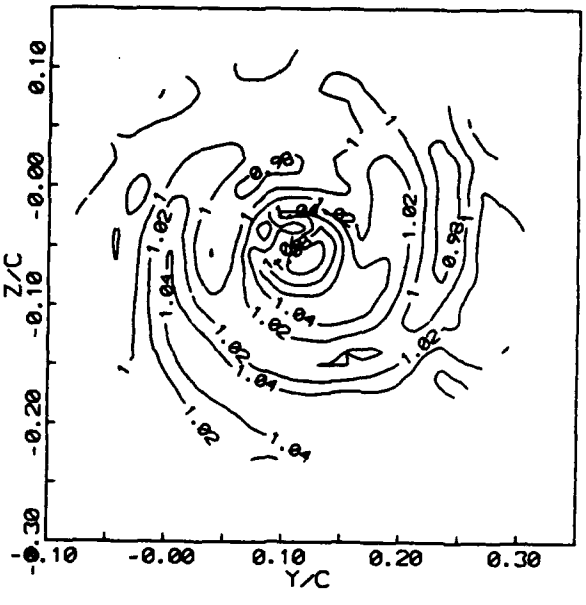

(b)

a = 0 degrees

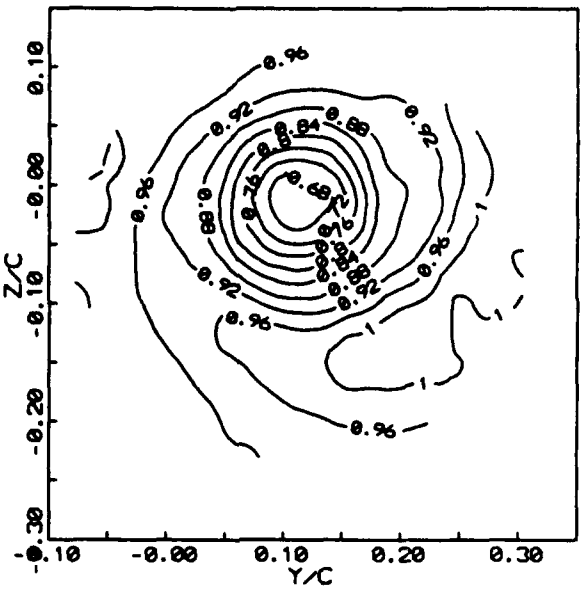

(a)

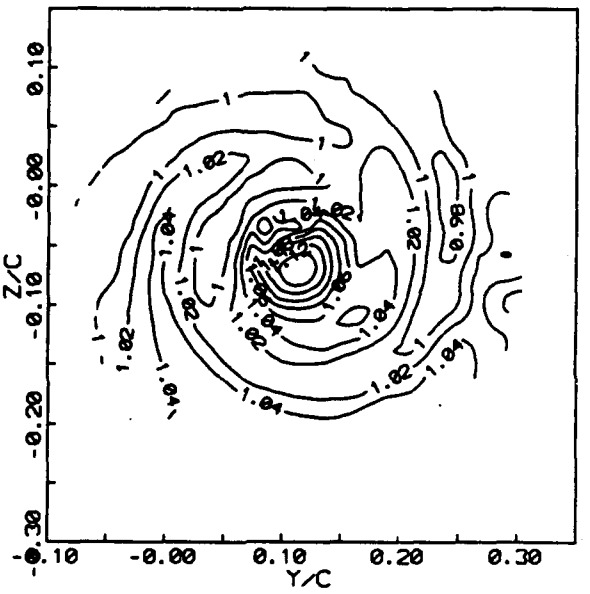

(b)

a = 10 degrees

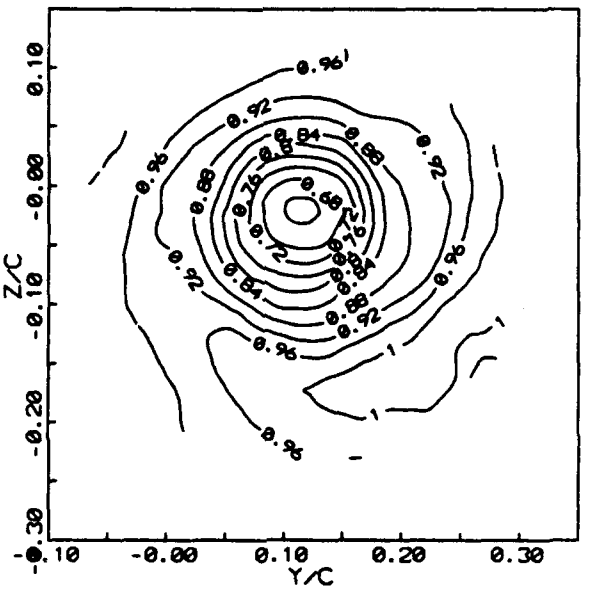

(a)

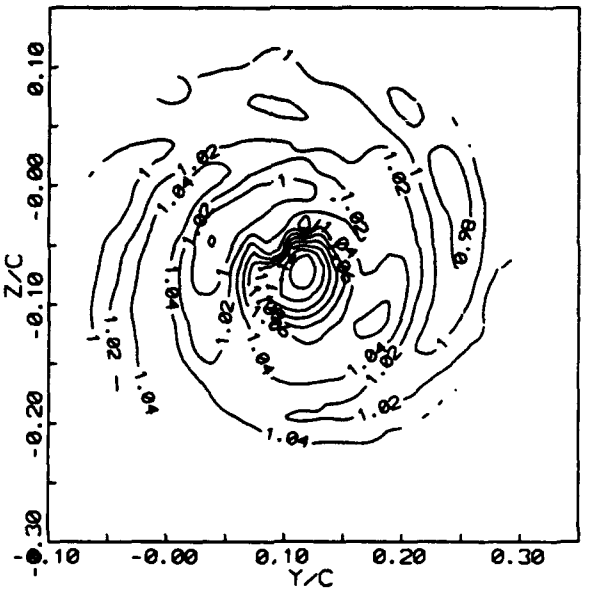

(b)

a = 11 degrees

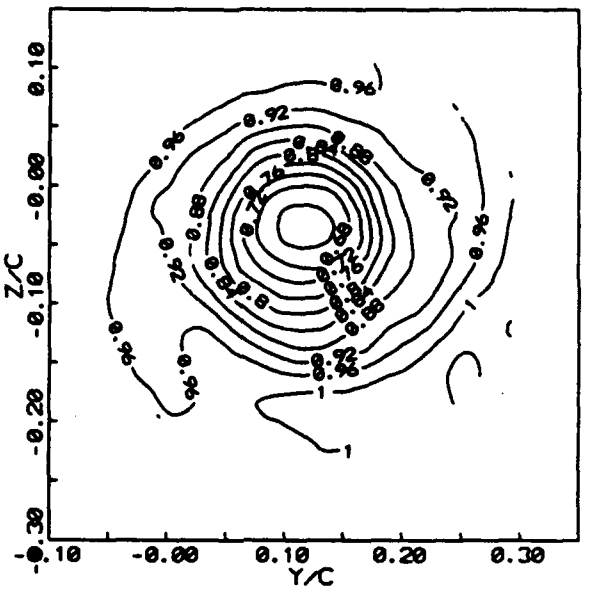

(a)

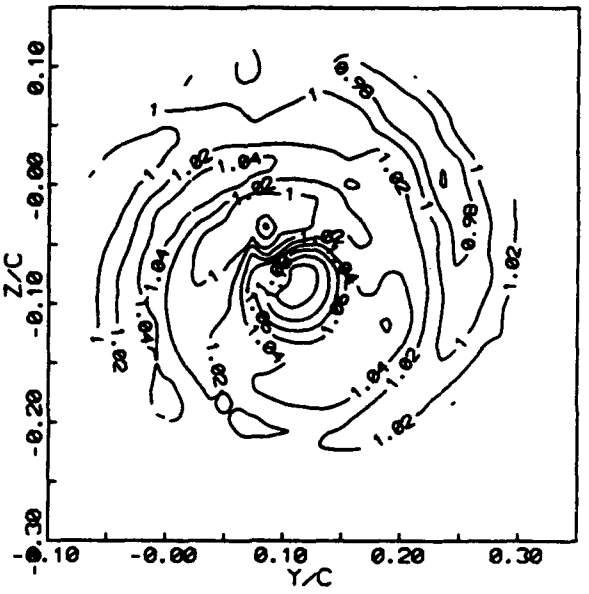

(b)

a = 12 degrees

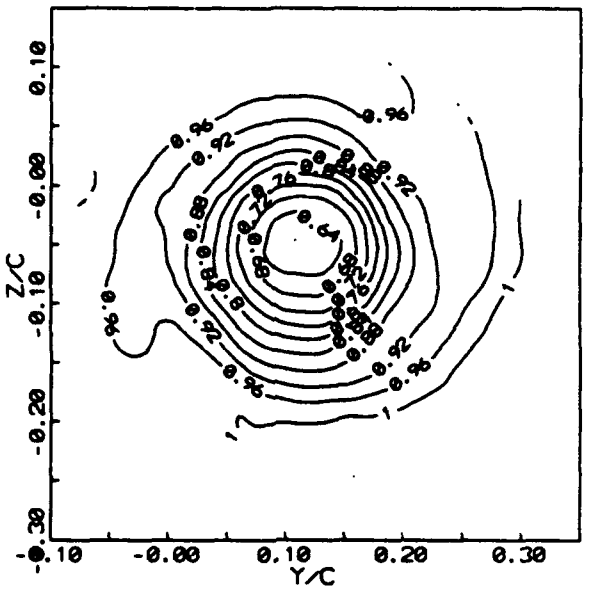

(a)

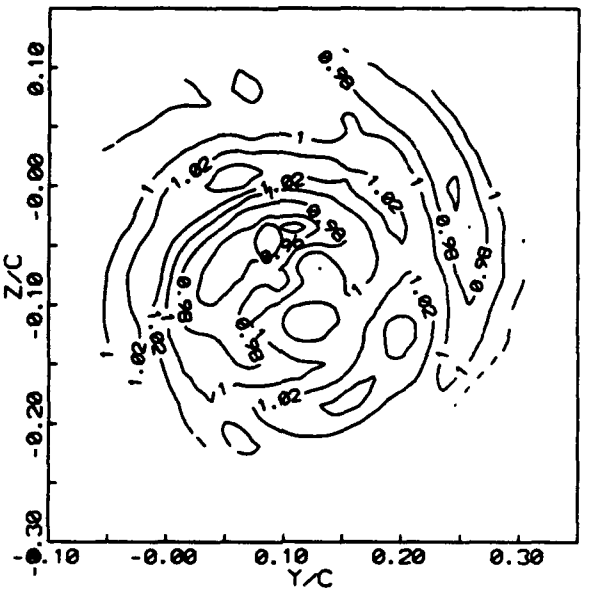

(b)

a = 13 degrees

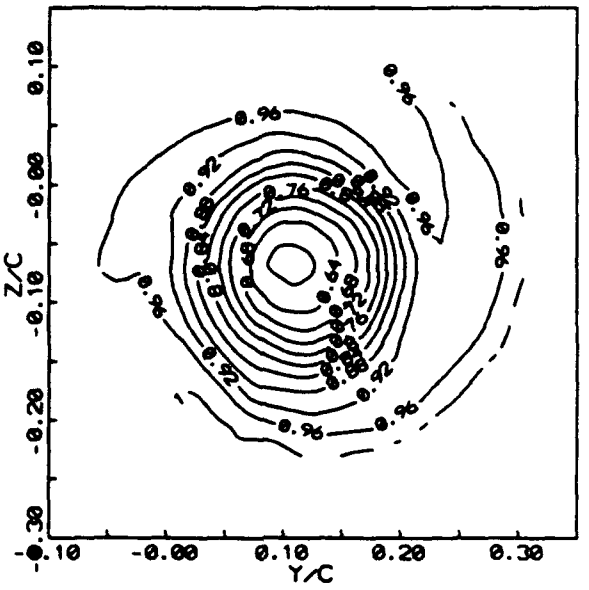

(a)

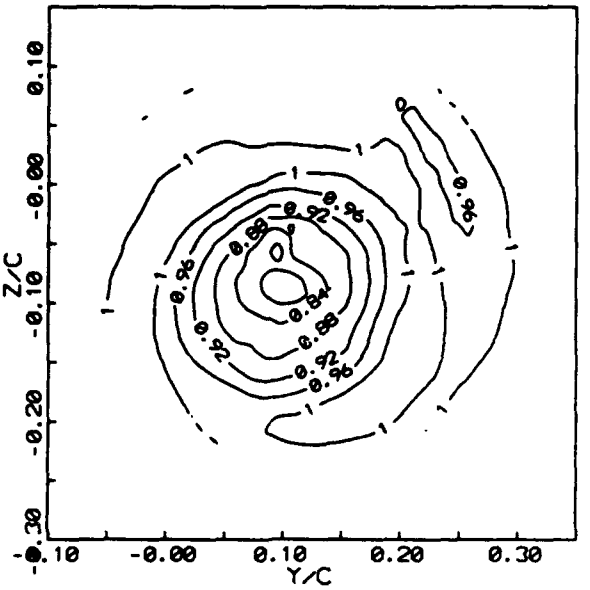

(b)

a = 14 degrees

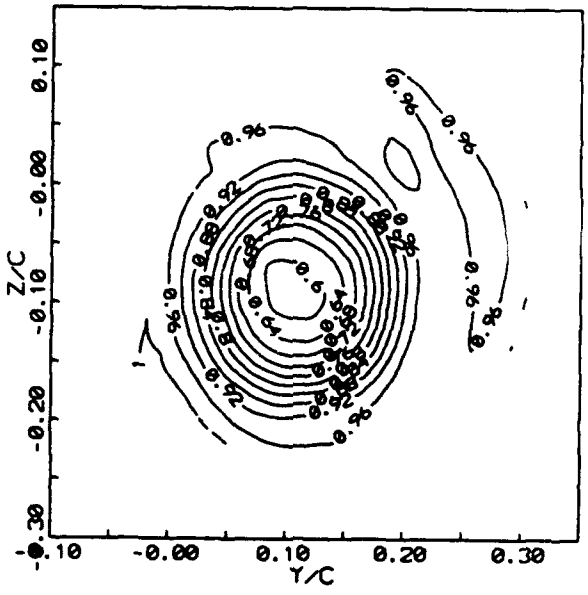

(a)

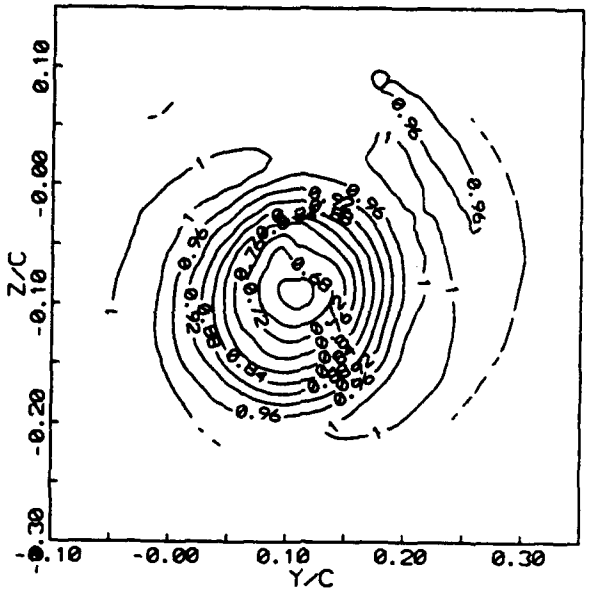

(b)

a = 15 degrees

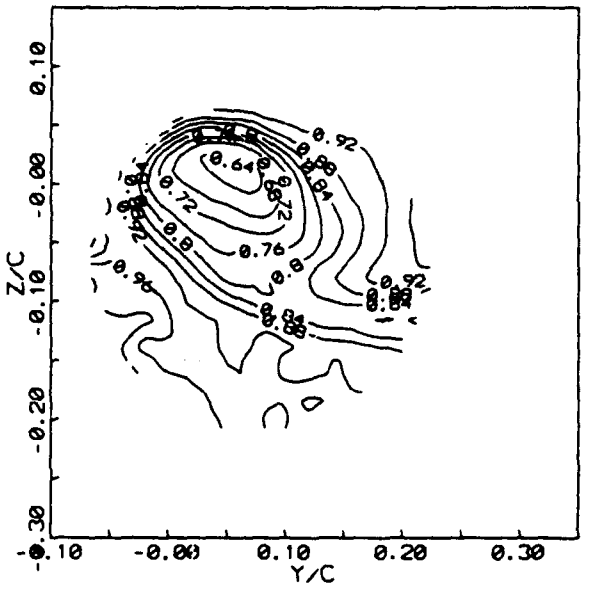

(a)

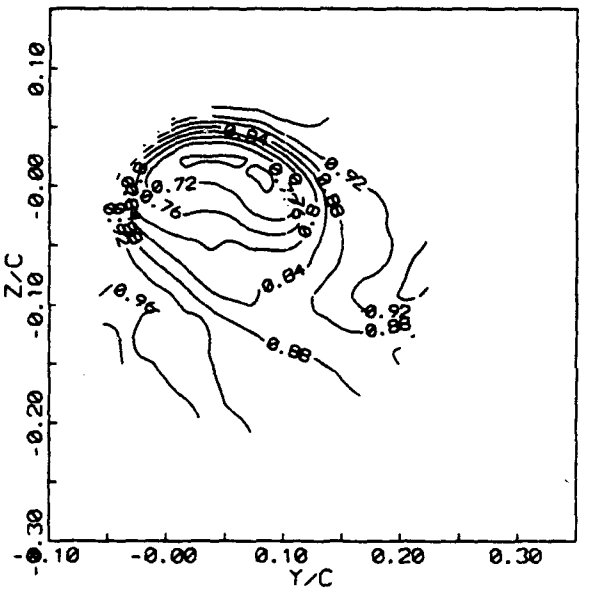

(b)

a = 6 degrees

Figure 5.2 Mean velocity $< U >$ contours at x = 10 cm, α = 6 to 14 degrees by increments of 2 degree. a)Pitch-up. b)Pitch-down

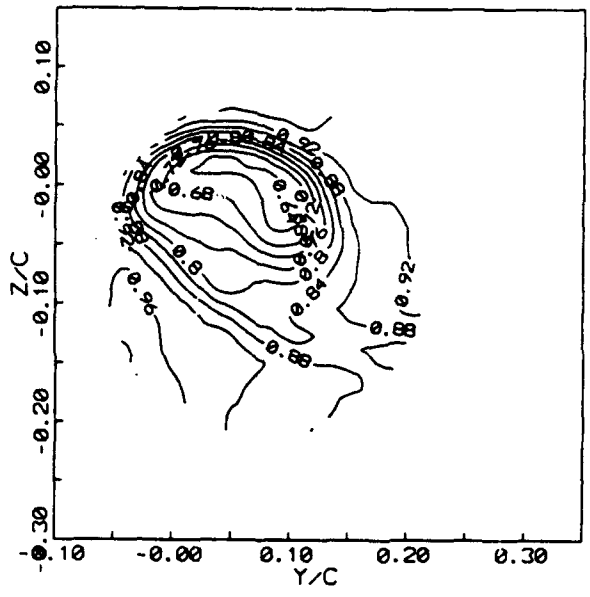

(a)

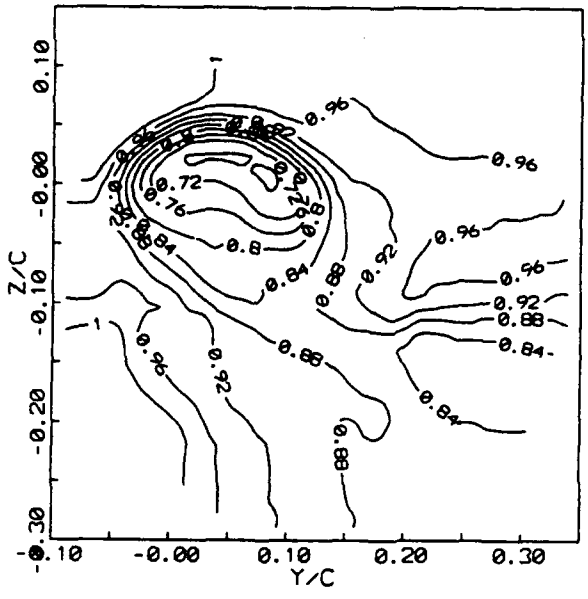

(b)

a = 8 degrees

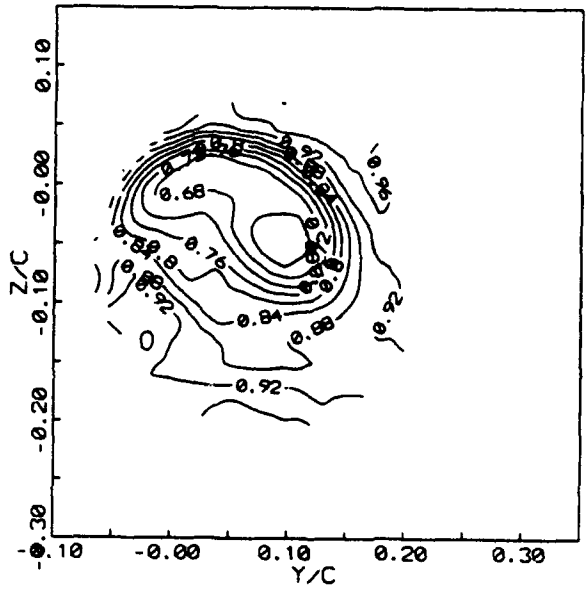

(a)

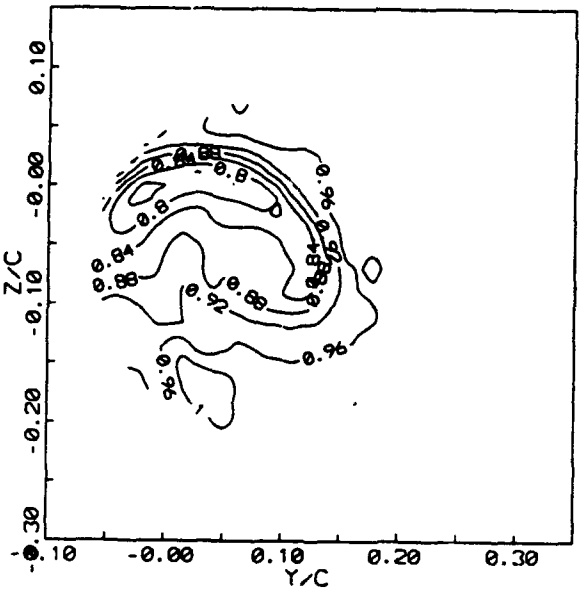

(b)

a = 10 degrees

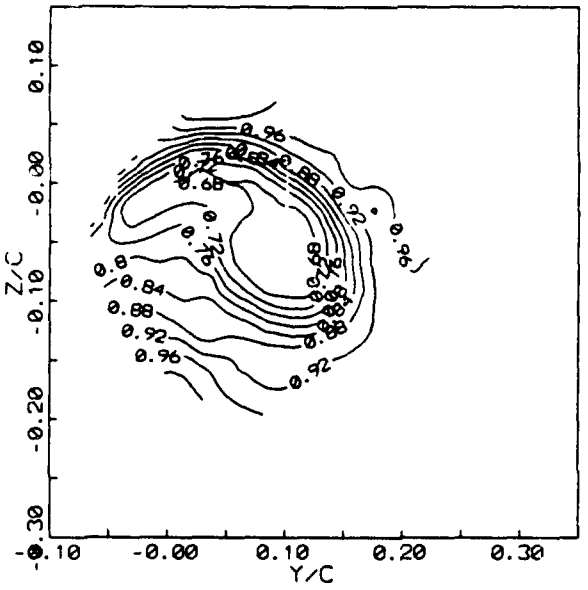

(a)

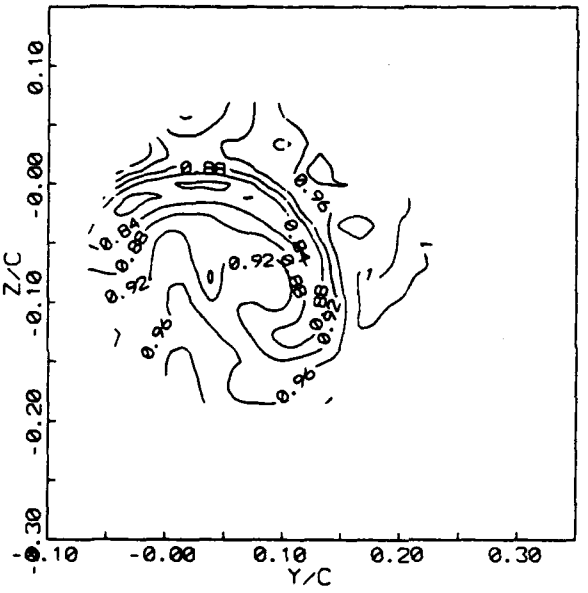

(b)

a = 12 degrees

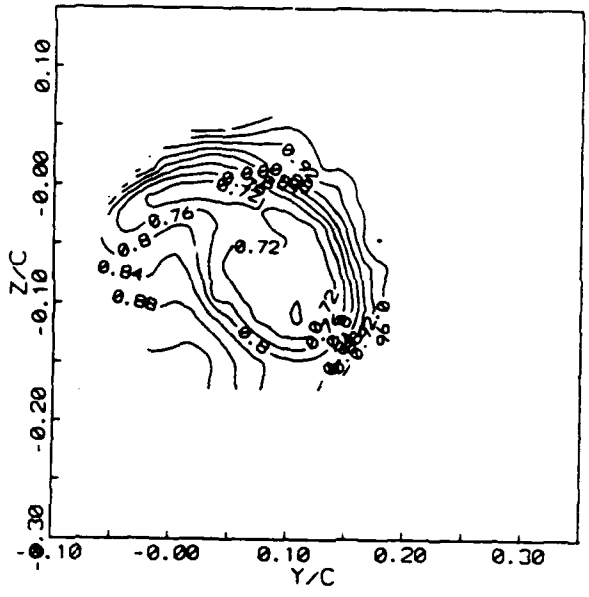

(a)

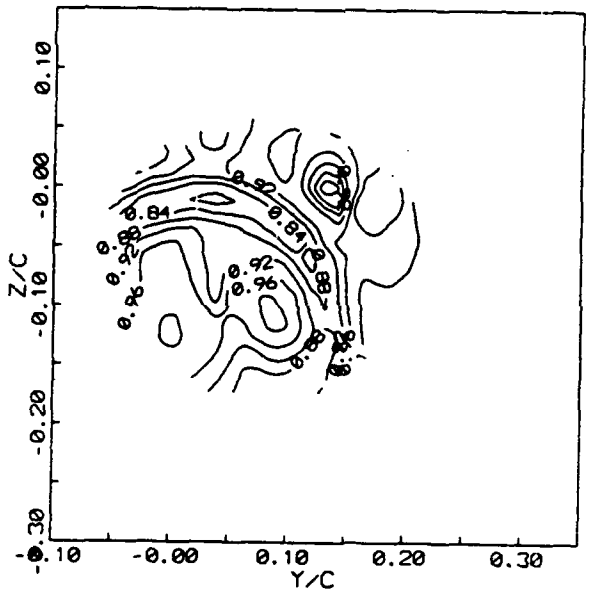

(b)

a = 14 degrees

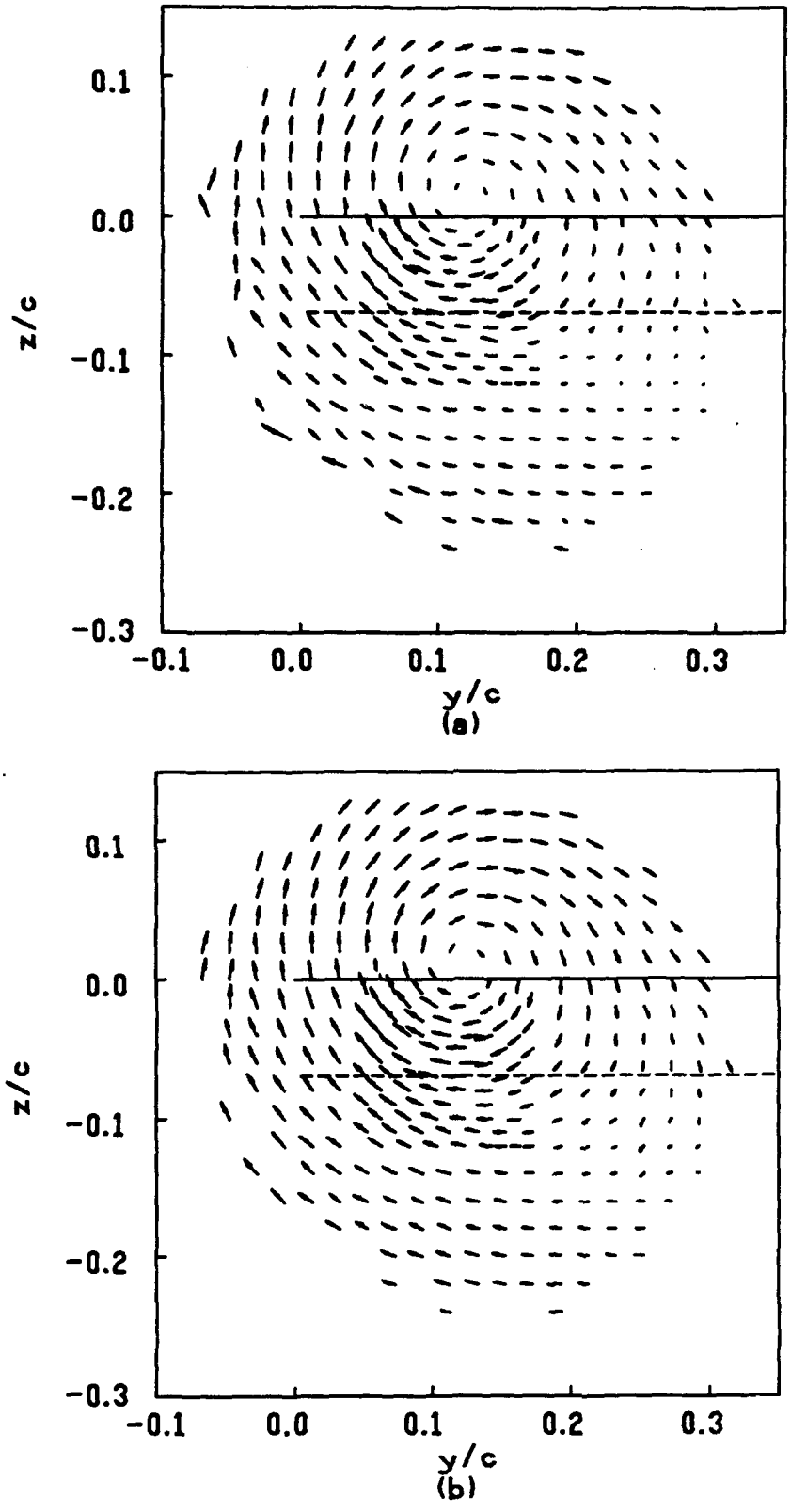

a = 5 degrees

Figure 5.3 Distribution of the mean velocity vector, ($\vec{j} < V > + \vec{k} < W >$) in the cross-stream plane at the same downstream distance and angles of incidence as Fig. 5.1. a)Pitch-up. b)Pitch-down. The magnitude of velocity is proportional to the length of the arrow.

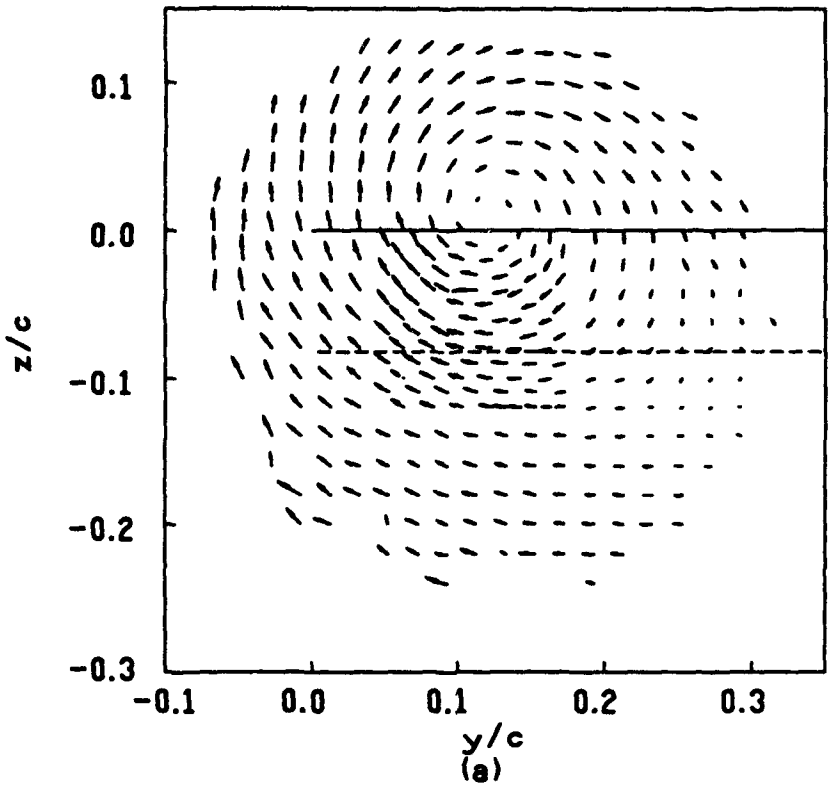
0.1
0.0
-0.1
-0.2
-0.3
z/c
-0.1
0.0
0.1
0.2
0.3
y/c
(a)

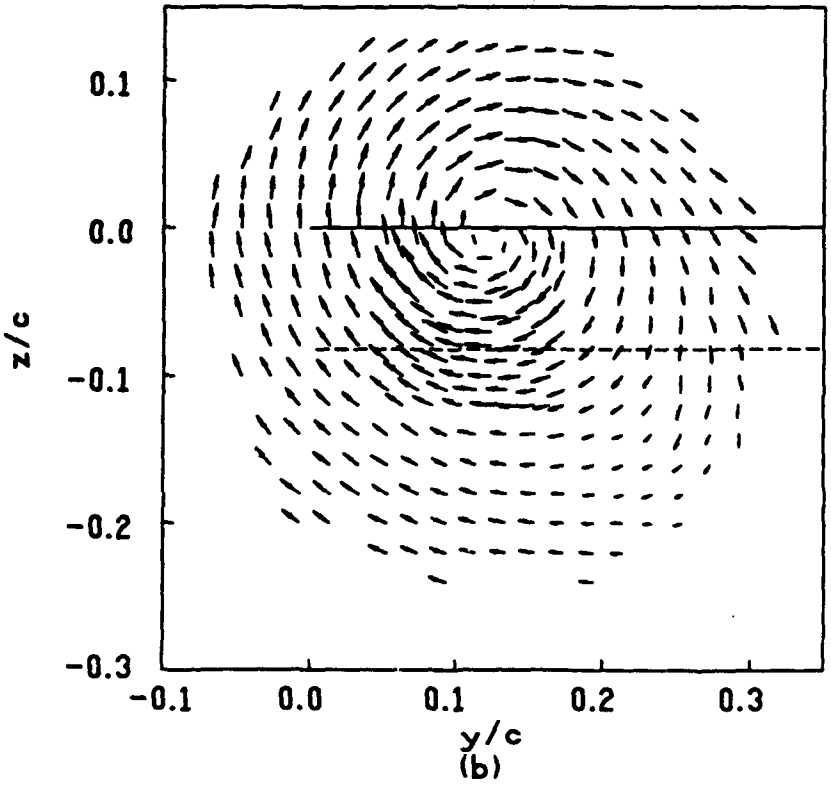
0.1
0.0
-0.1
-0.2
-0.3
z/c
-0.1
0.0
0.1
0.2
0.3
y/c
(b)

a = 6 degrees

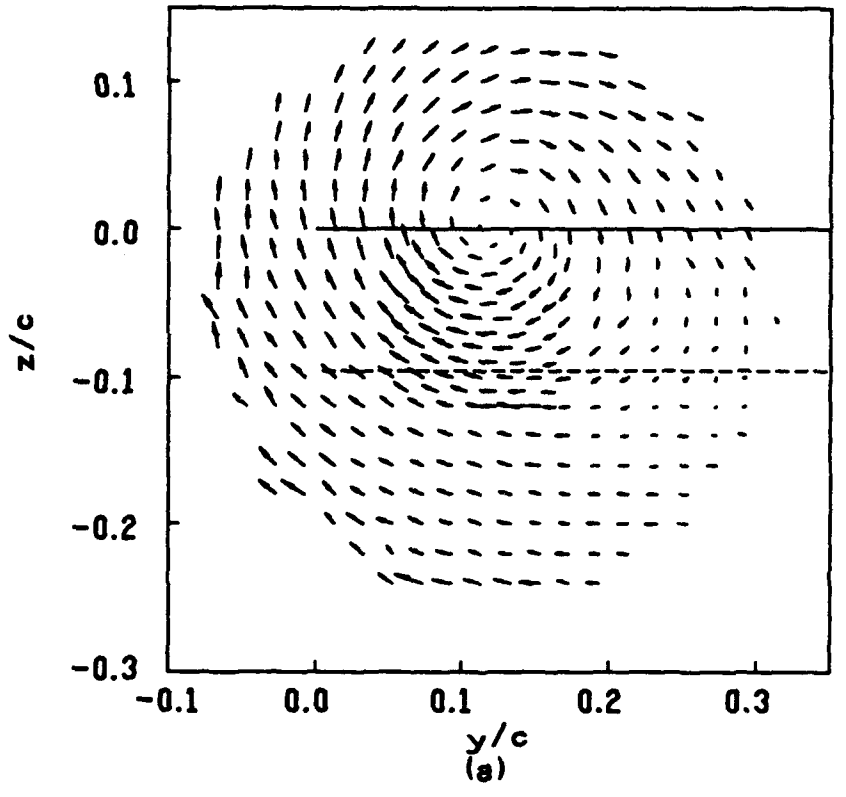
0.1
0.0
-0.1
-0.2
-0.3
z/c
-0.1
0.0
0.1
0.2
0.3
y/c
(a)

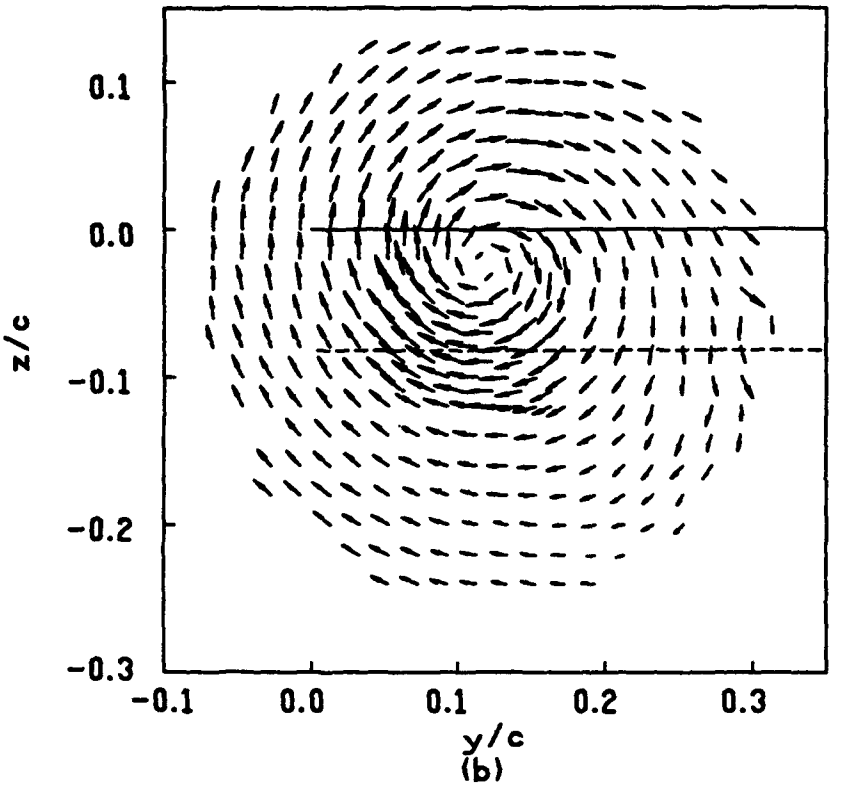
0.1
0.0
-0.1
-0.2
-0.3
z/c
-0.1
0.0
0.1
0.2
0.3
y/c
(b)

a = 7 degrees

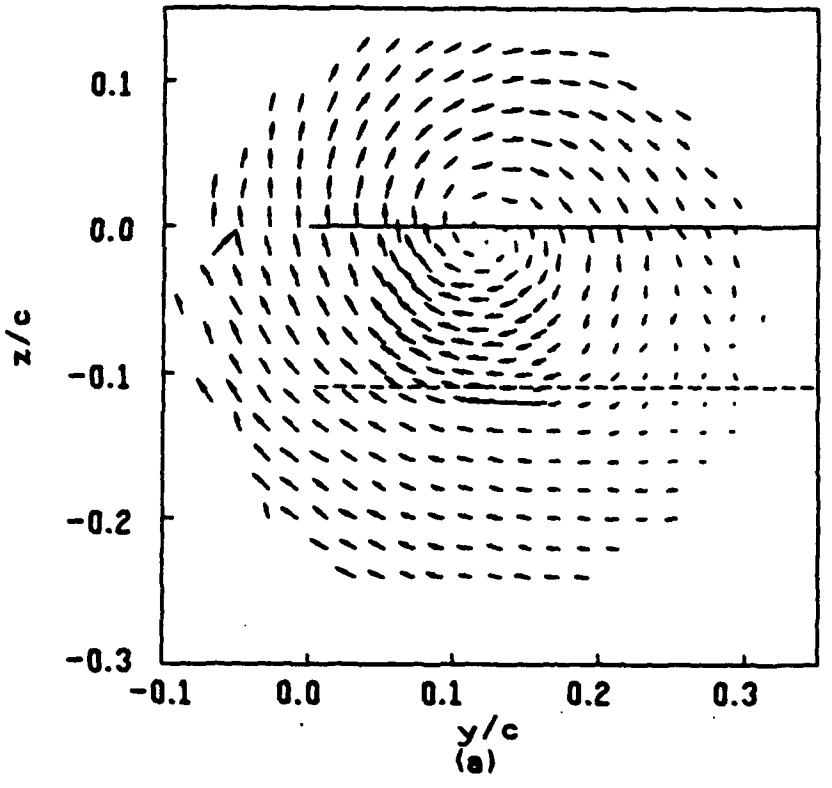
0.1
0.0
-0.1
-0.2
-0.3
z/c
-0.1
0.0
0.1
0.2
0.3
y/c
(a)

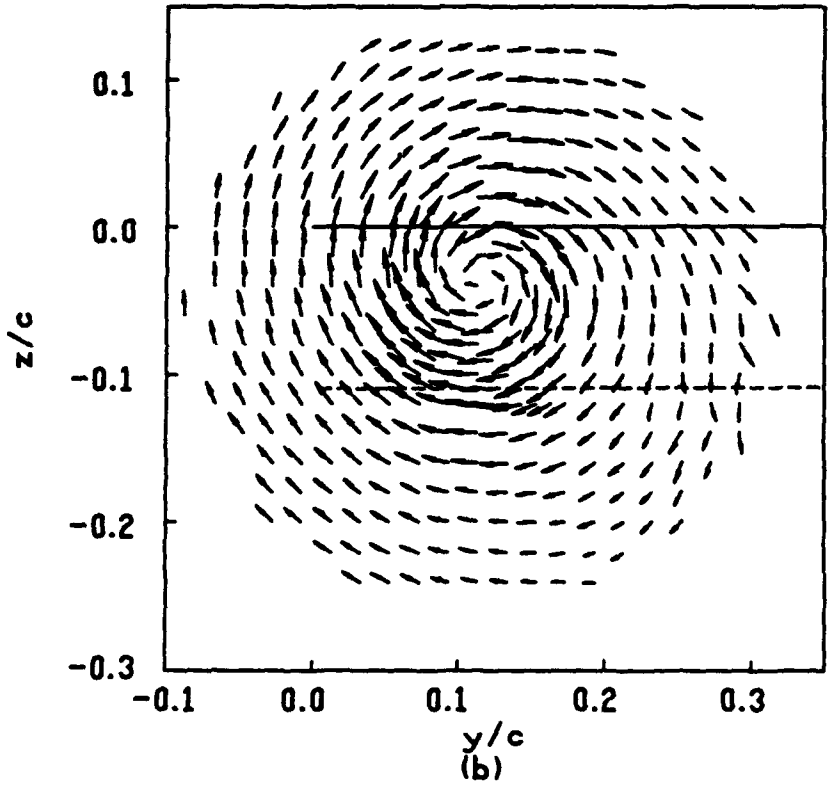
0.1
0.0
-0.1
-0.2
-0.3
z/c
-0.1
0.0
0.1
0.2
0.3
y/c
(b)

a = 8 degrees

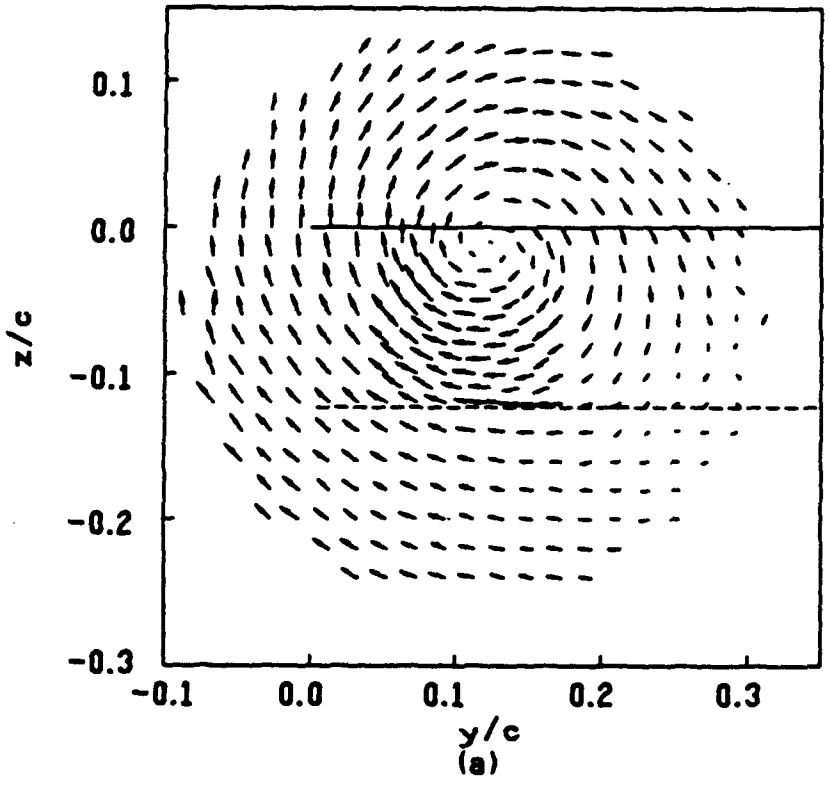
0.1
0.0
-0.1
-0.2
-0.3
z/c
-0.1
0.0
0.1
0.2
0.3
y/c
(a)

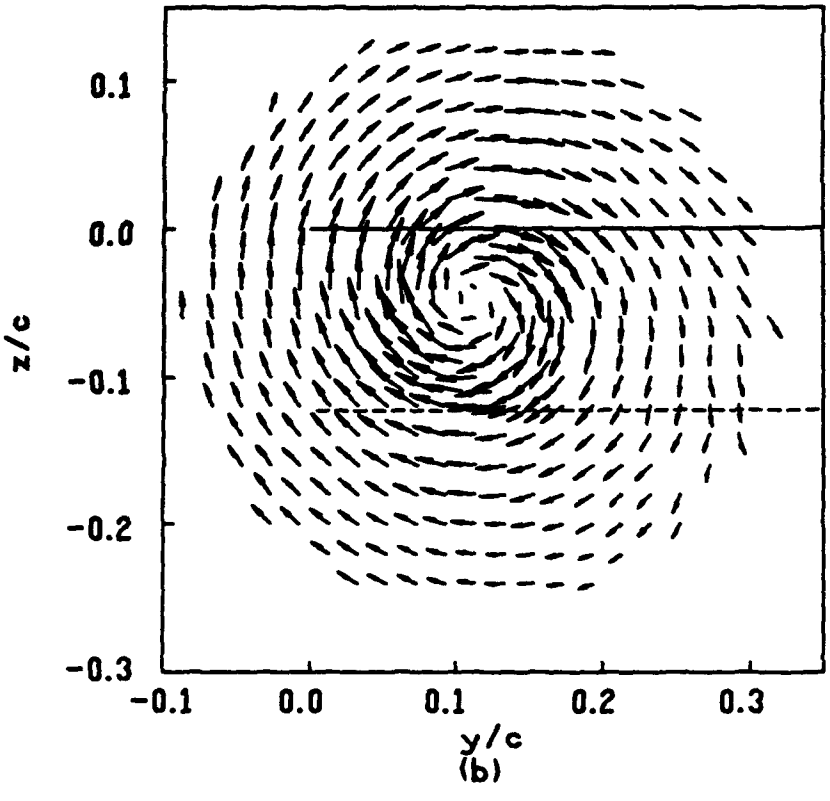
0.1
0.0
-0.1
-0.2
-0.3
z/c
-0.1
0.0
0.1
0.2
0.3
y/c
(b)

a = 9 degrees

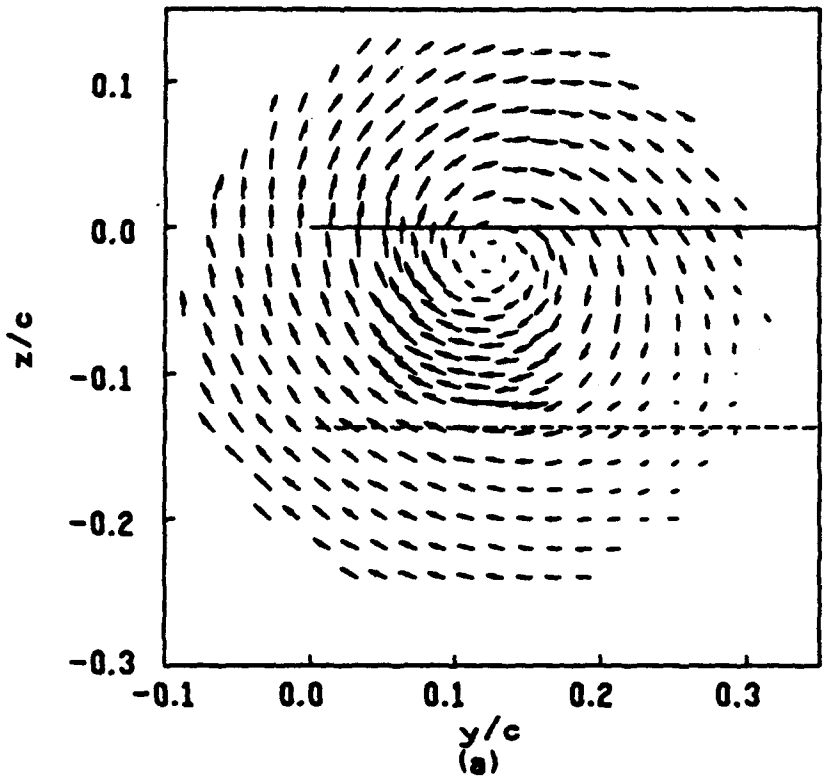
0.1
0.0
-0.1
-0.2
-0.3
z/c
-0.1
0.0
0.1
0.2
0.3
y/c
(a)

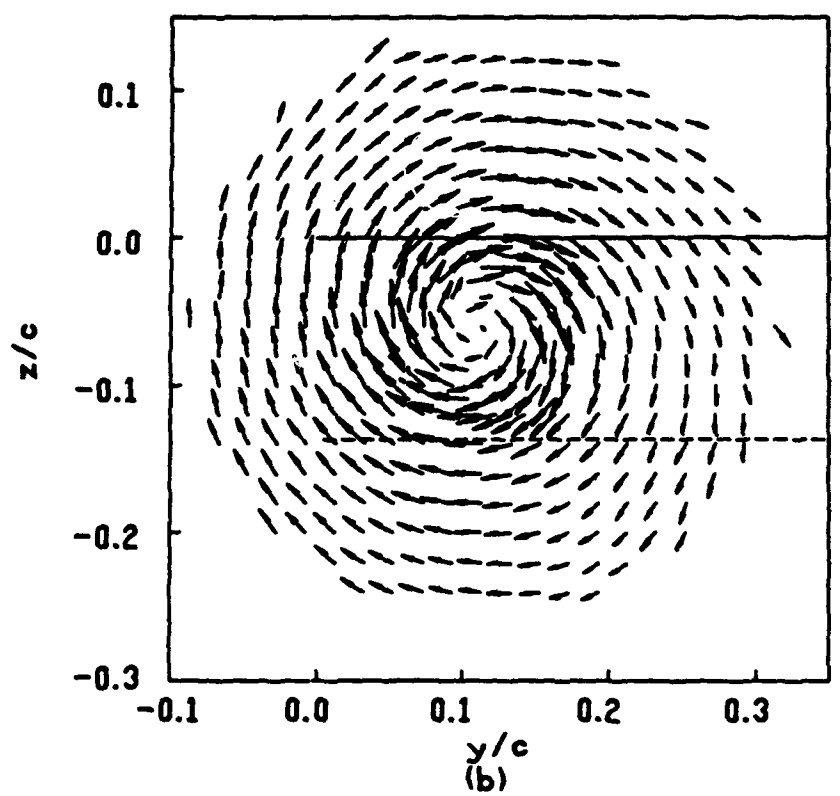
0.1
0.0
-0.1
-0.2
-0.3
z/c
-0.1
0.0
0.1
0.2
0.3
y/c
(b)

a = 10 degrees

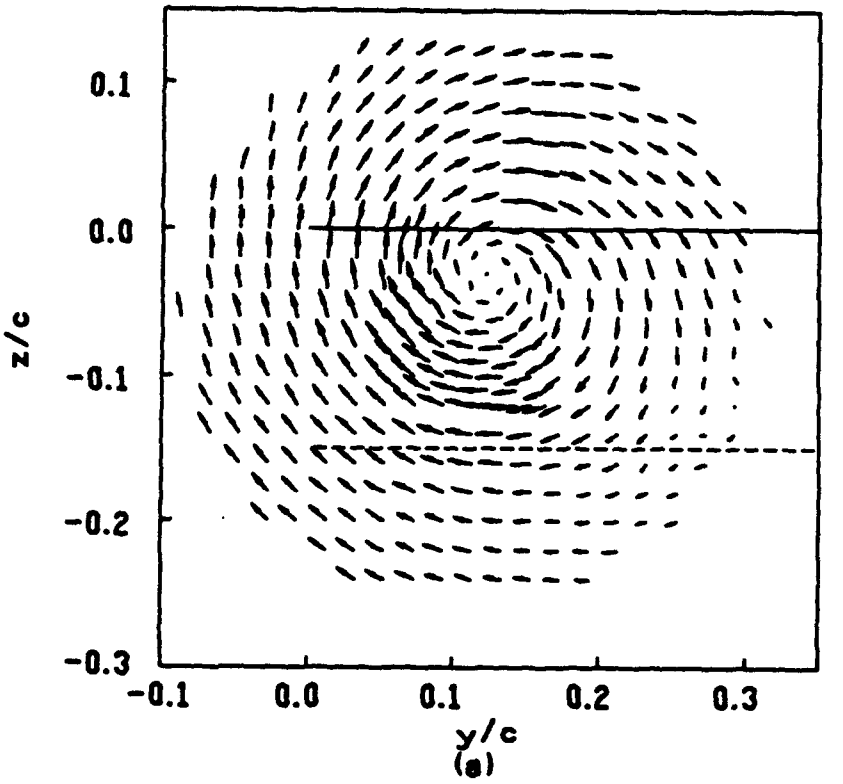
0.1
0.0
-0.1
-0.2
-0.3
z/c
-0.1
0.0
0.1
0.2
0.3
y/c
(a)

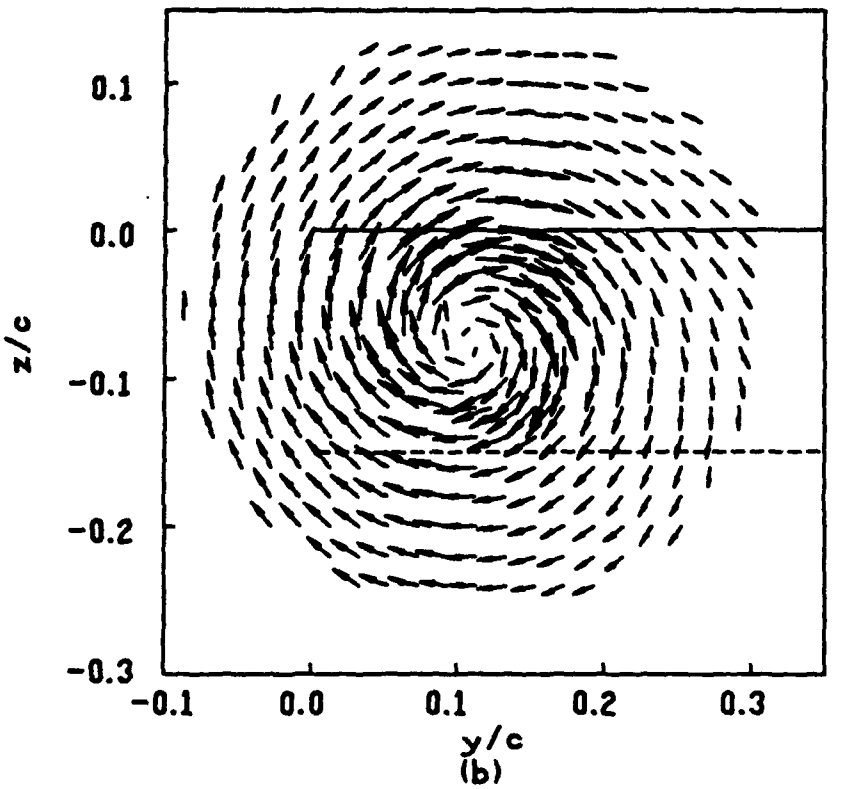
0.1
0.0
-0.1
-0.2
-0.3
z/c
-0.1
0.0
0.1
0.2
0.3
y/c
(b)

a = 11 degrees

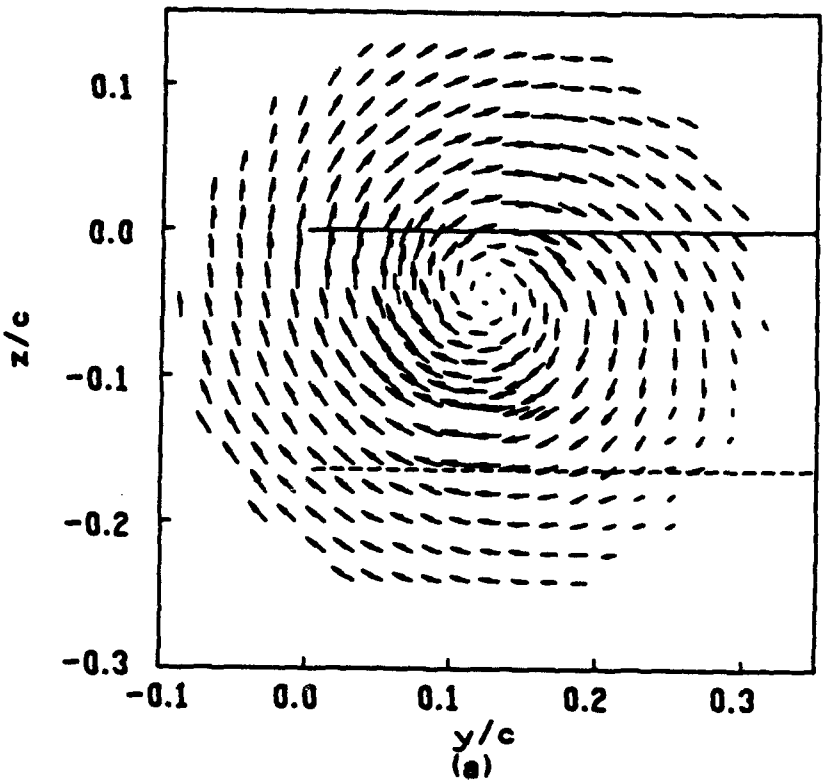
0.1
0.0
-0.1
-0.2
-0.3
z/c
-0.1
0.0
0.1
0.2
0.3
y/c
(a)

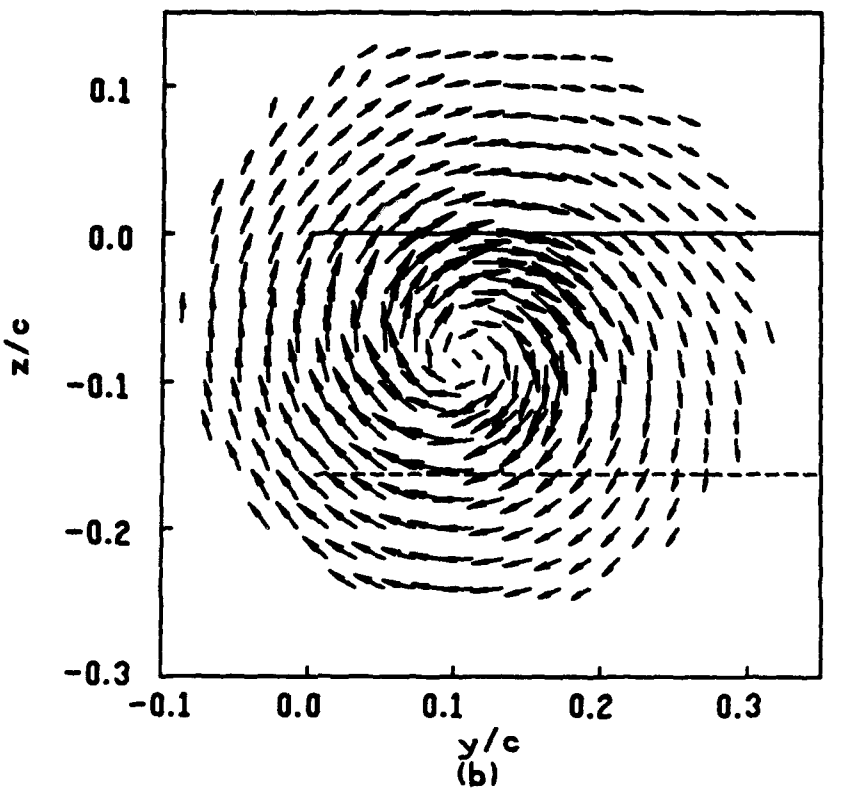
0.1
0.0
-0.1
-0.2
-0.3
z/c
-0.1
0.0
0.1
0.2
0.3
y/c
(b)

a = 12 degrees

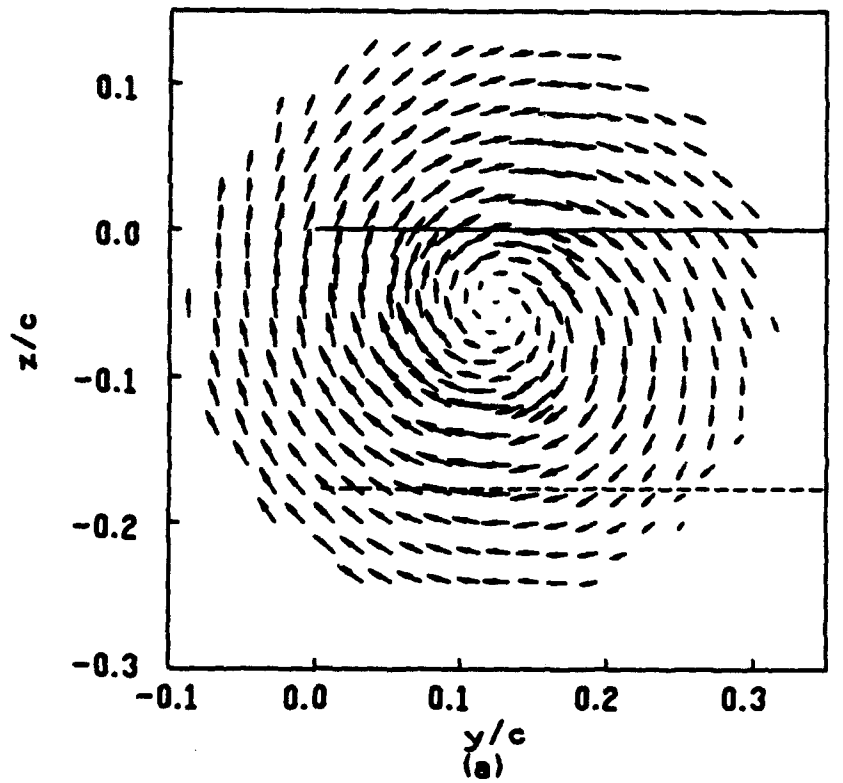
0.1
0.0
-0.1
-0.2
-0.3
z/c
-0.1
0.0
0.1
0.2
0.3
y/c
(a)

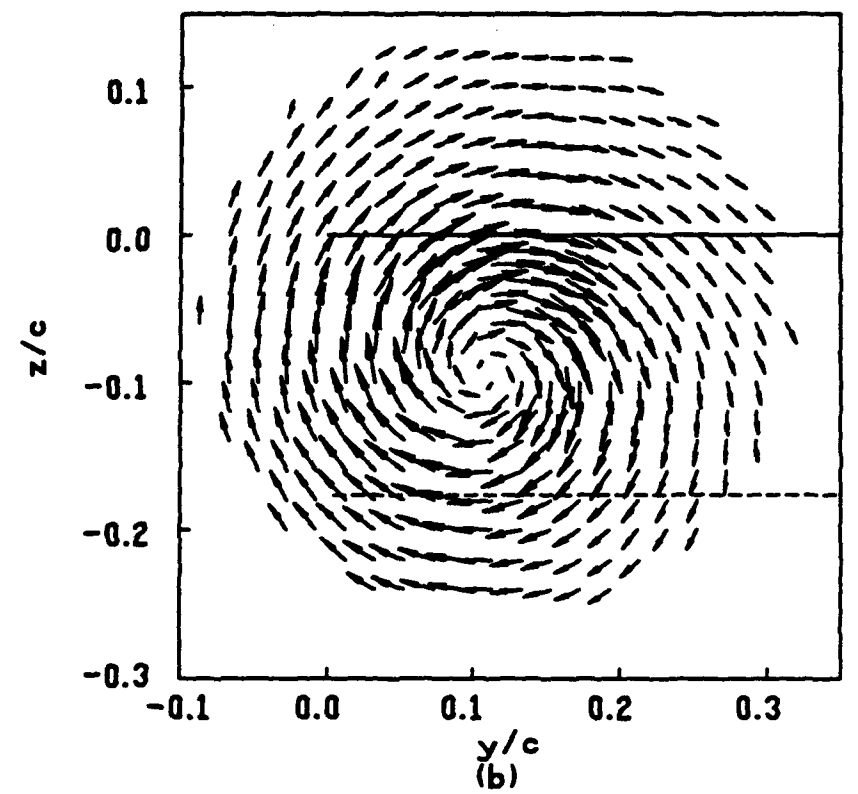
0.1
0.0
-0.1
-0.2
-0.3
z/c
-0.1
0.0
0.1
0.2
0.3
y/c
(b)

a = 13 degrees

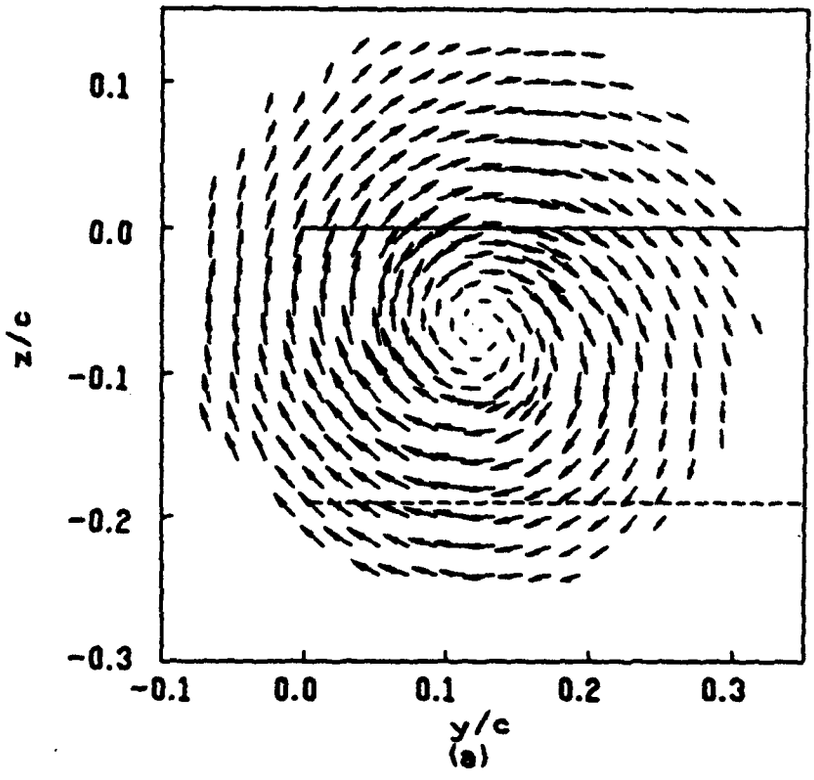
0.1
0.0
-0.1
-0.2
-0.3
z/c
-0.1
0.0
0.1
0.2
0.3
y/c
(a)

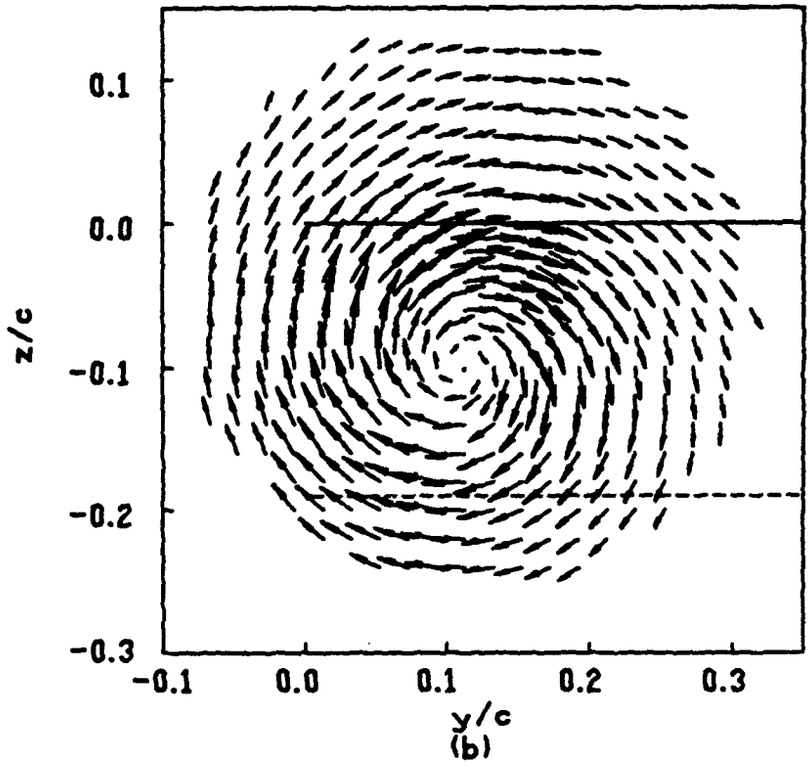
0.1
0.0
-0.1
-0.2
-0.3
z/c
-0.1
0.0
0.1
0.2
0.3
y/c
(b)

a = 14 degrees

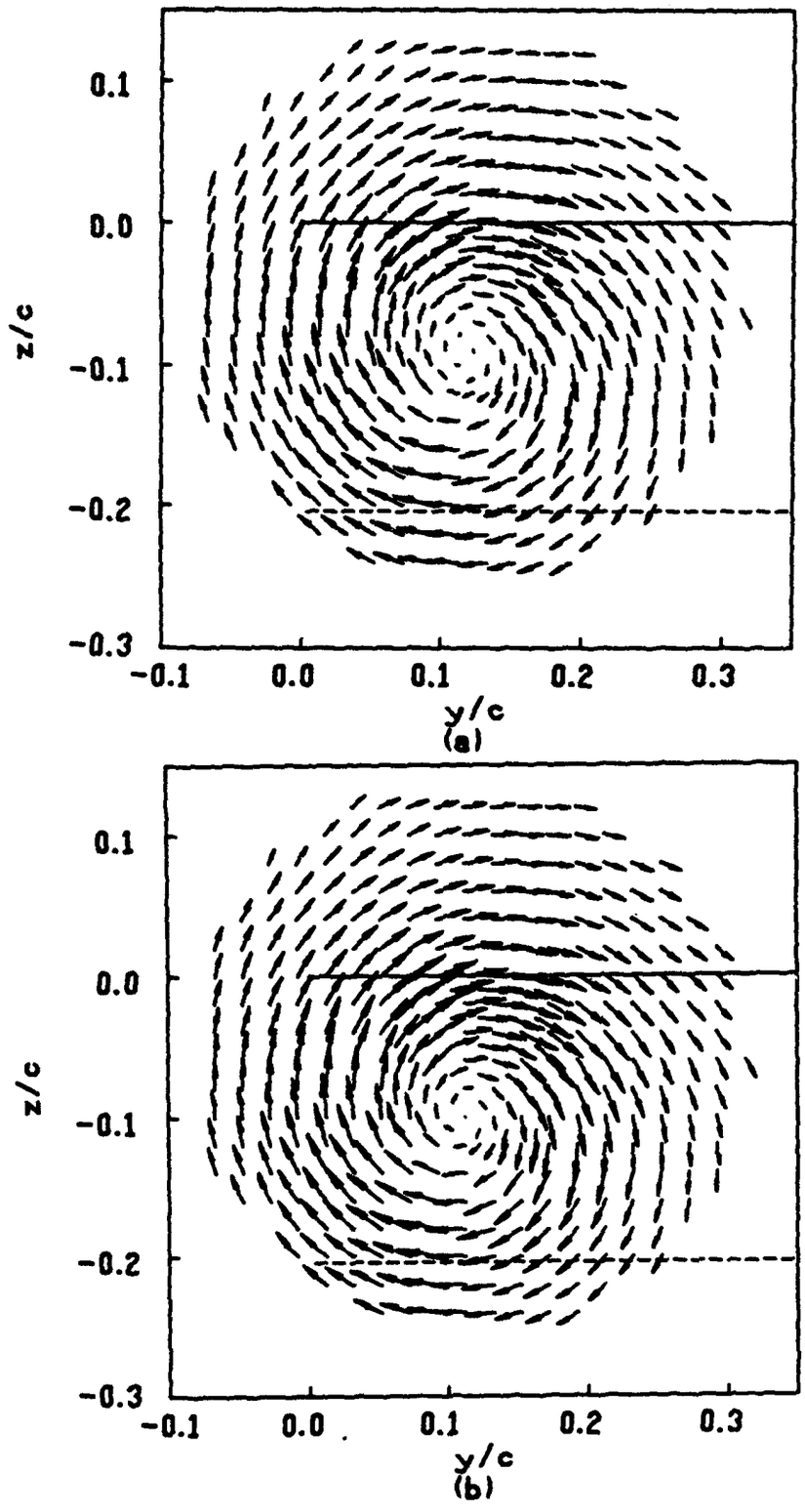
0.1
0.0
-0.1
-0.2
-0.3
z/c
-0.1
0.0
0.1
0.2
0.3
y/c
(a)
0.1
0.0
-0.1
-0.2
-0.3
z/c
-0.1
0.0
0.1
0.2
0.3
y/c
(b)

a = 15 degrees

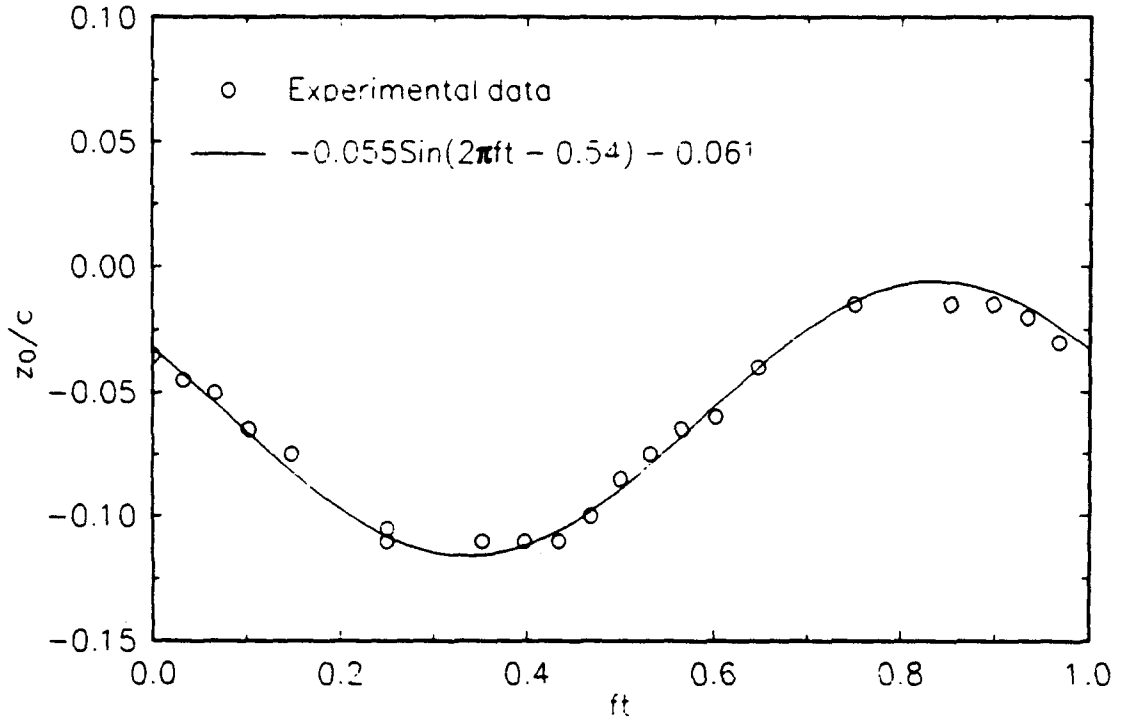

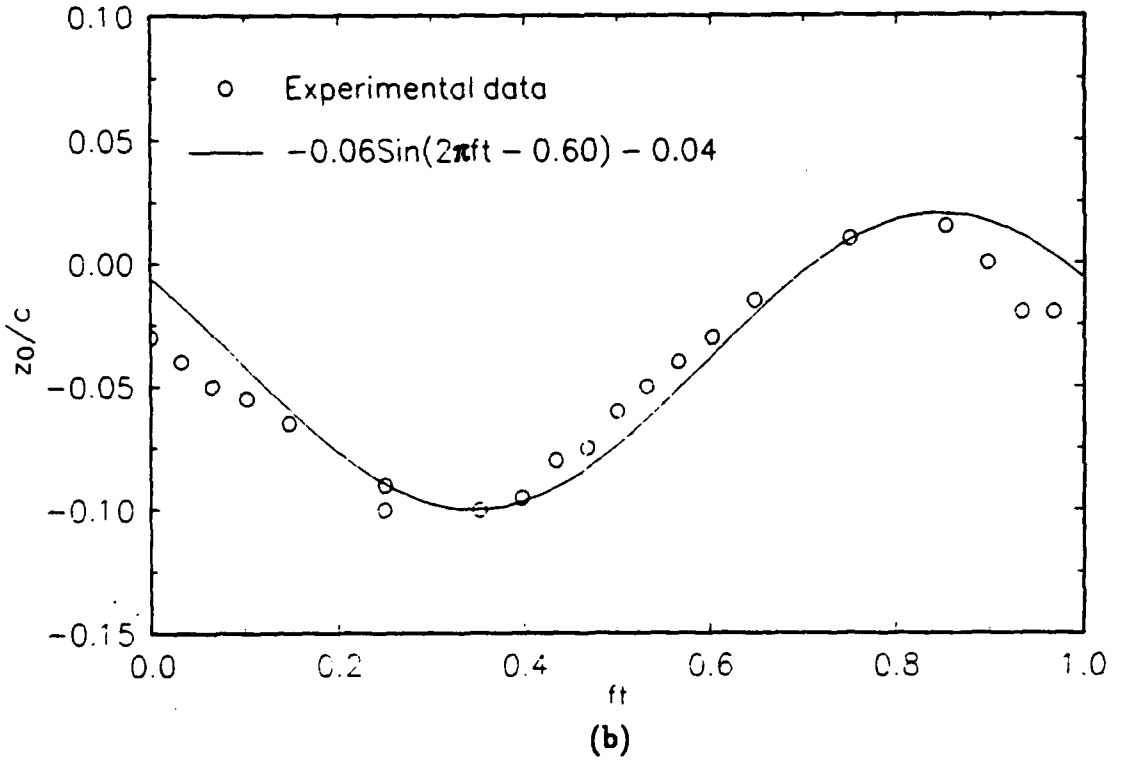

Figure 5.4 Vertical movement of the vortex center during the oscillating cycle at a) $z/c = 1.0$, b) $z/c = 1.33$, c) $z/c = 2.0$, d) $z/c = 2.62$.

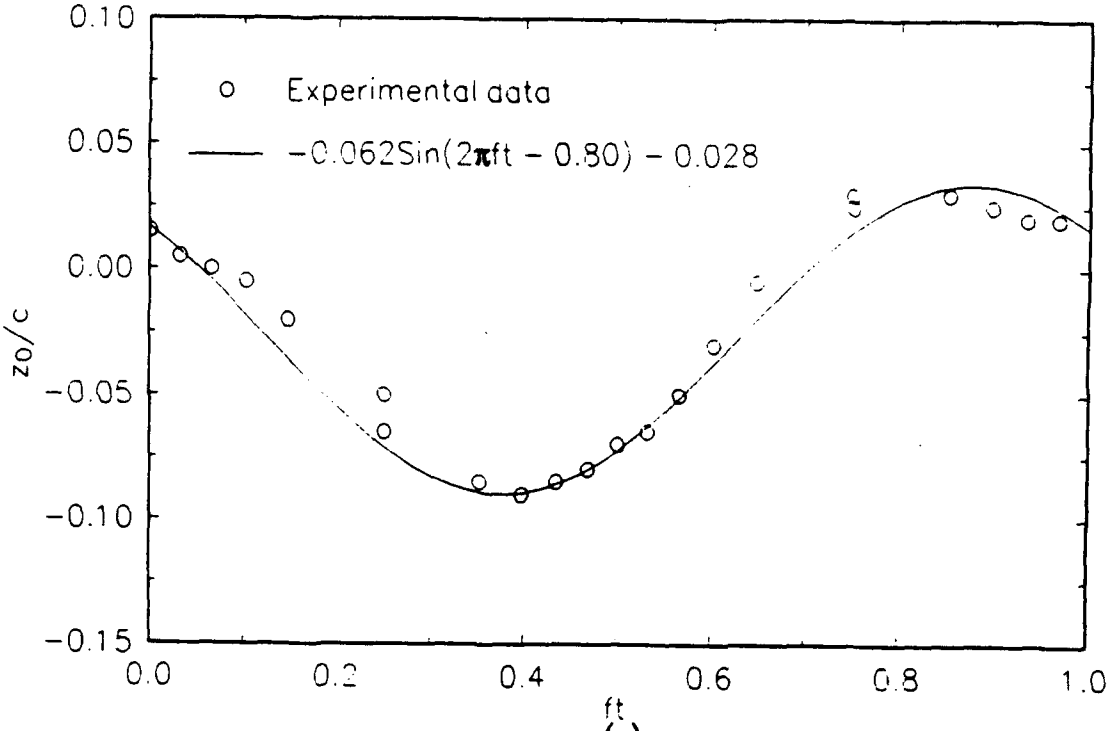
0.10
0.05
0.00
−0.05
−0.10
−0.15
0.0
0.2
0.4
0.6
0.8
1.0
z0/c
ft
Experimental data
−0.062Sin(2πft − 0.80) − 0.028

(c)

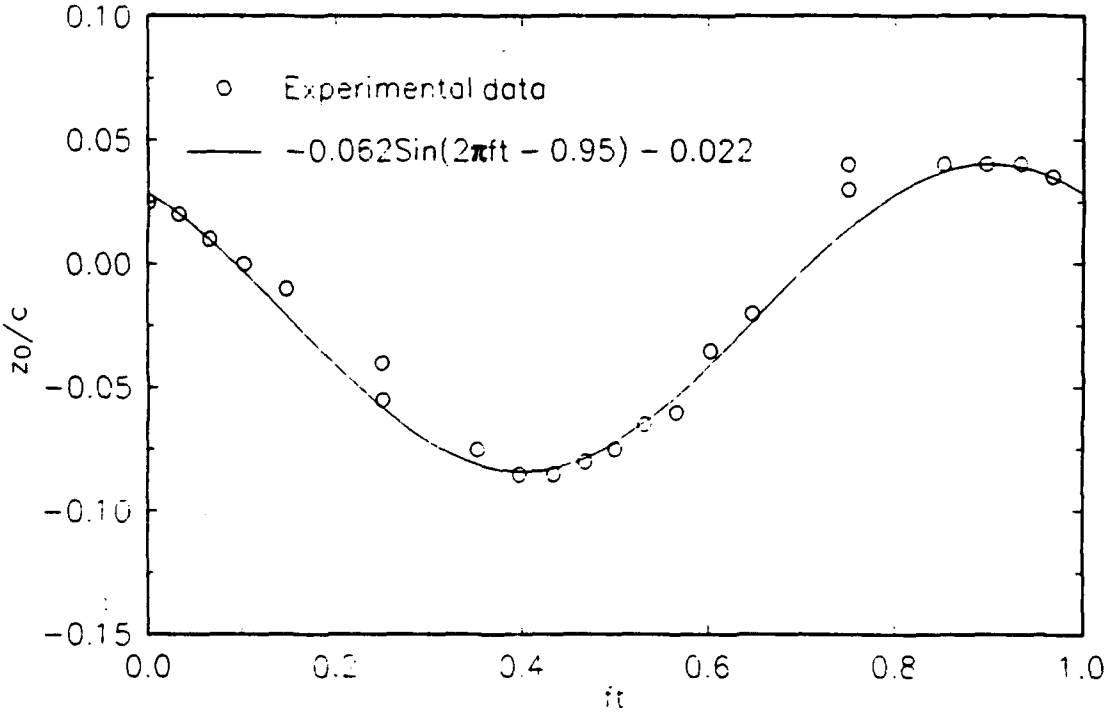
0.10
0.05
0.00
−0.05
−0.10
−0.15
0.0
0.2
0.4
0.6
0.8
1.0
z0/c
ft
Experimental data
−0.062Sin(2πft − 0.95) − 0.022

(d)

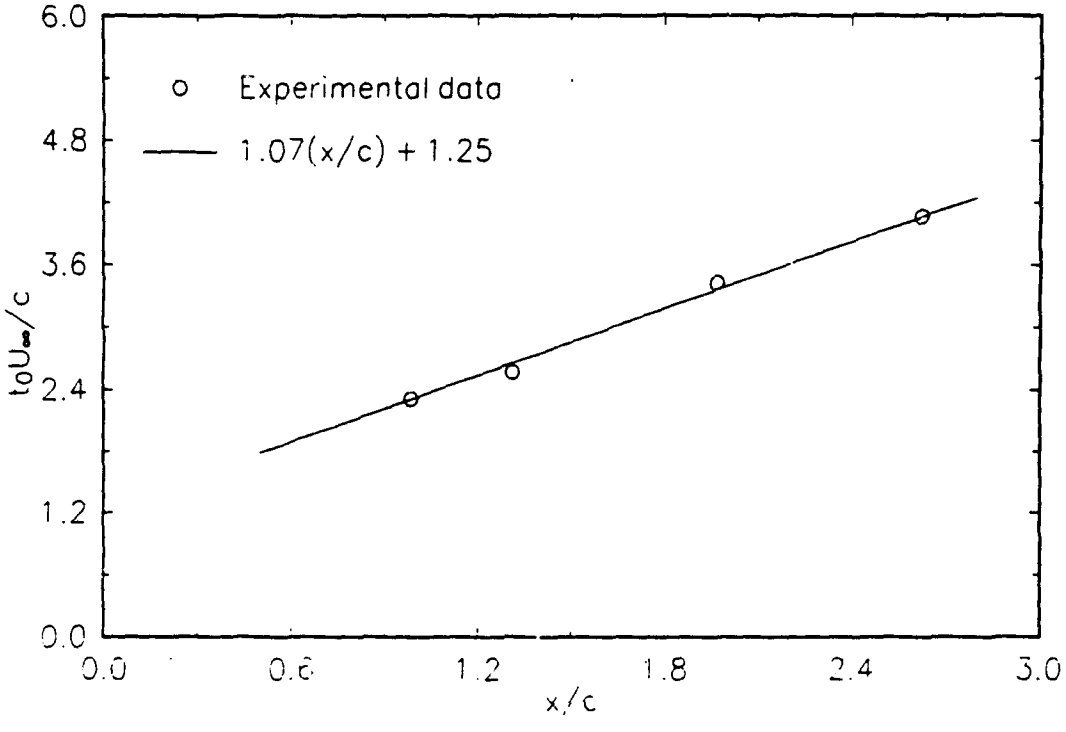

Figure 5.5 Plot of the phase delay t_0 *vs* the downstream distance x.

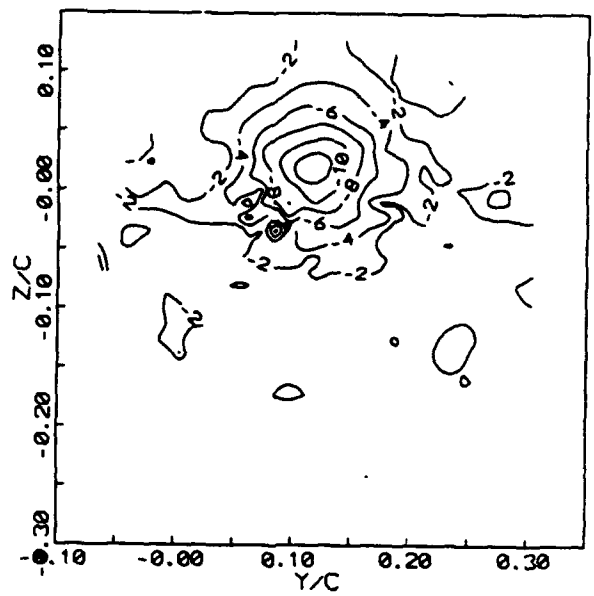

(a)

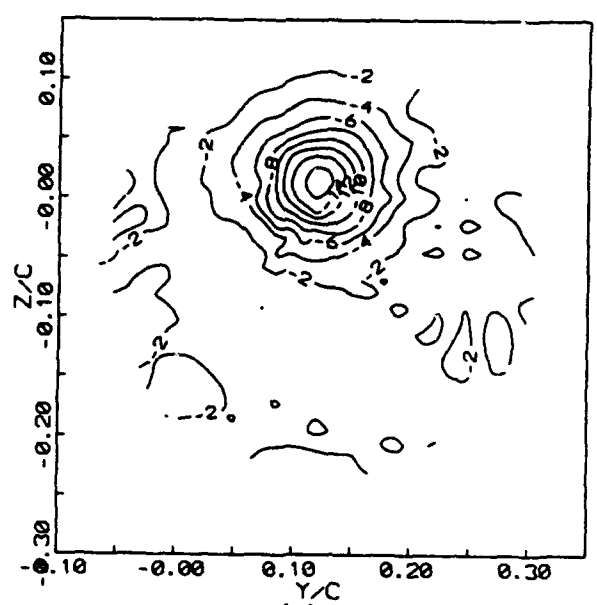

(b)

a = 5 degrees

Figure 5.6 Axial-vorticity $< \omega_x >$ contours at the same downstream distance and angles of incidence as Fig. 5.1. a)Pitch-up. b)Pitch-down.

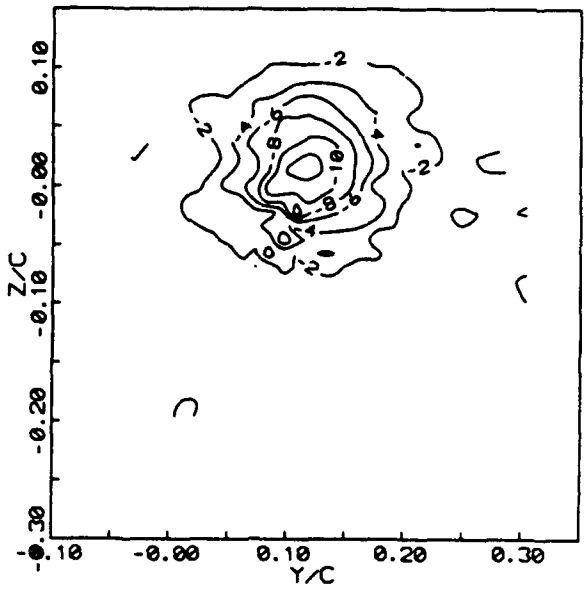

(a)

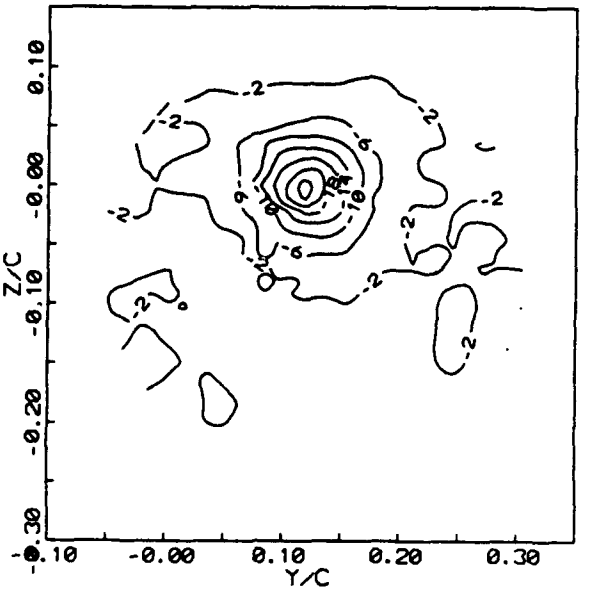

(b)

a = 6 degrees

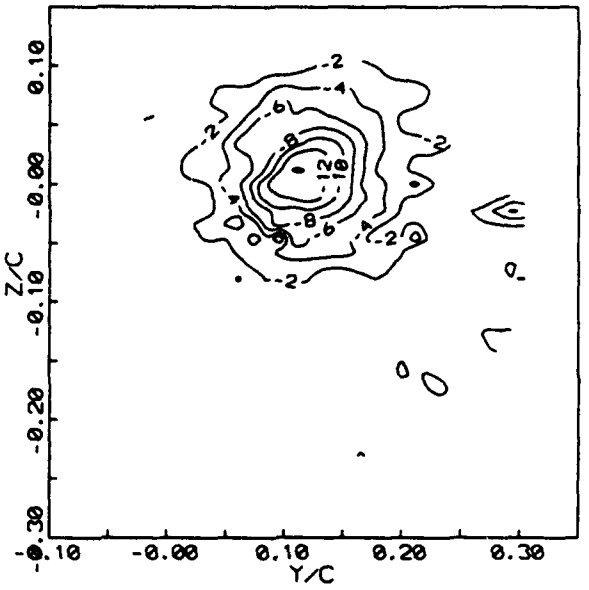

(a)

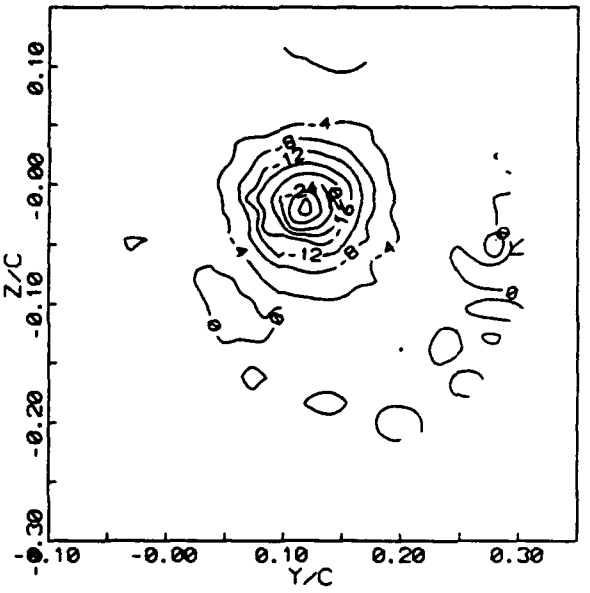

(b)

a = 7 degrees

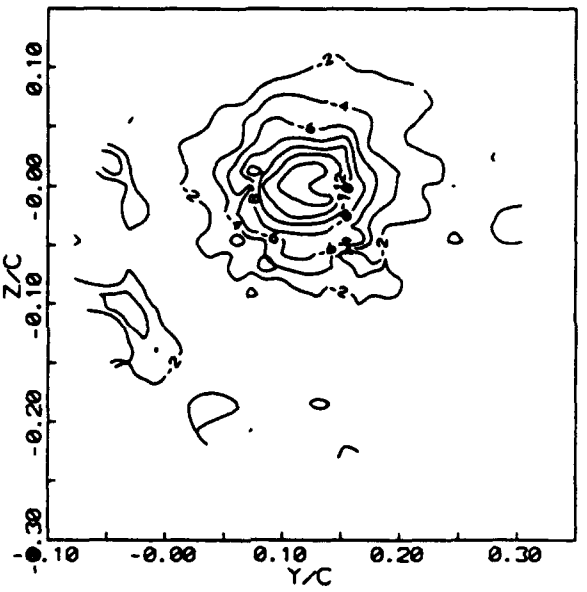

(a)

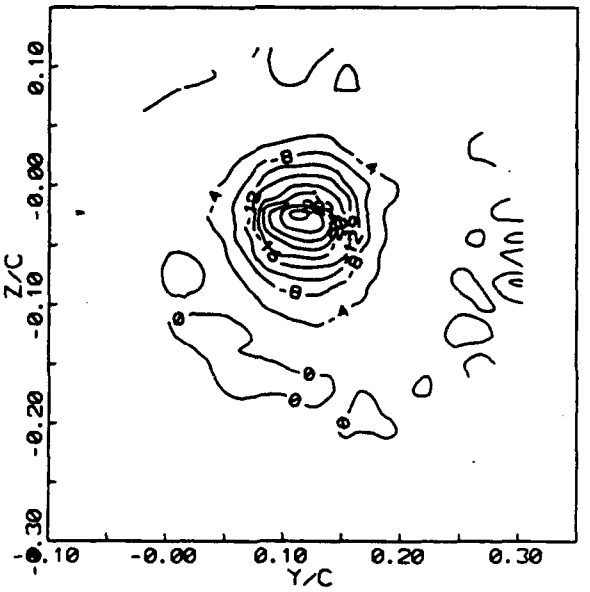

(b)

a = 8 degrees

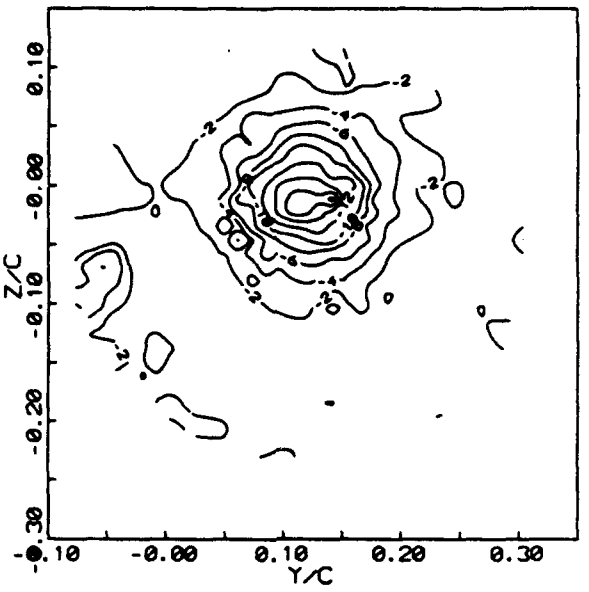

(a)

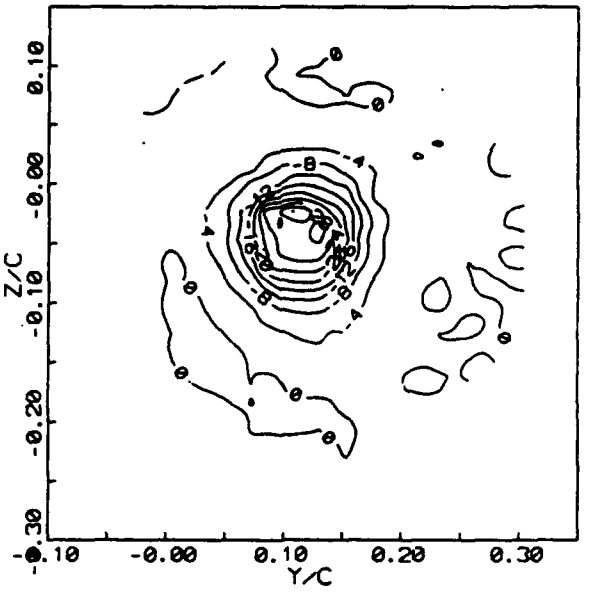

(b)

a = 9 degrees

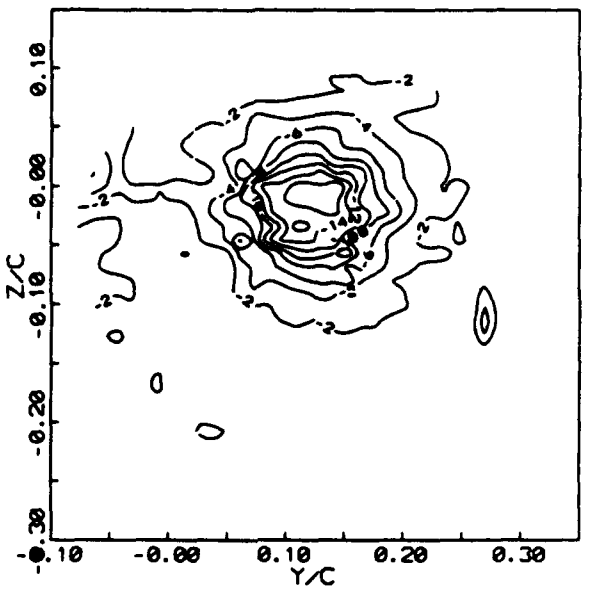

(a)

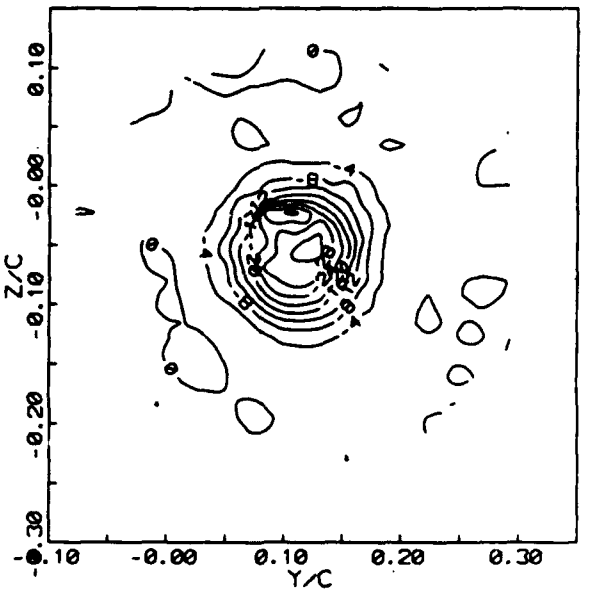

(b)

a = 10 degrees

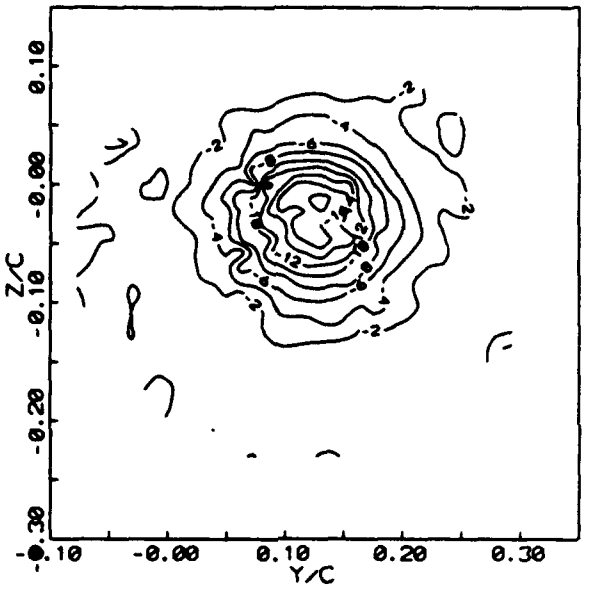

(a)

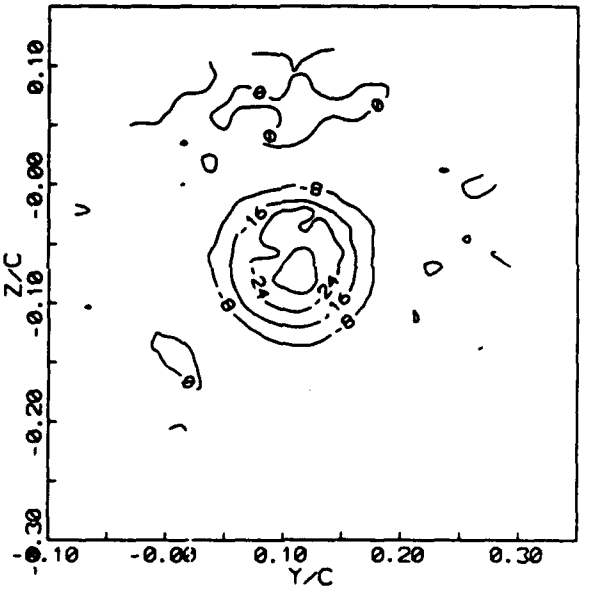

(b)

a = 11 degrees

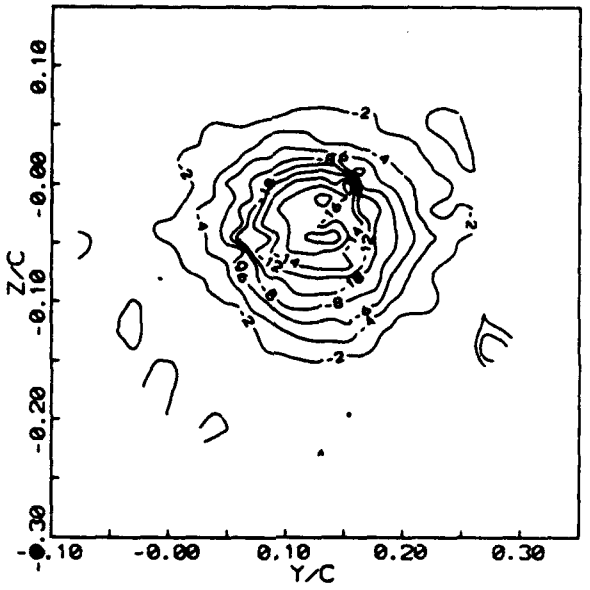

(a)

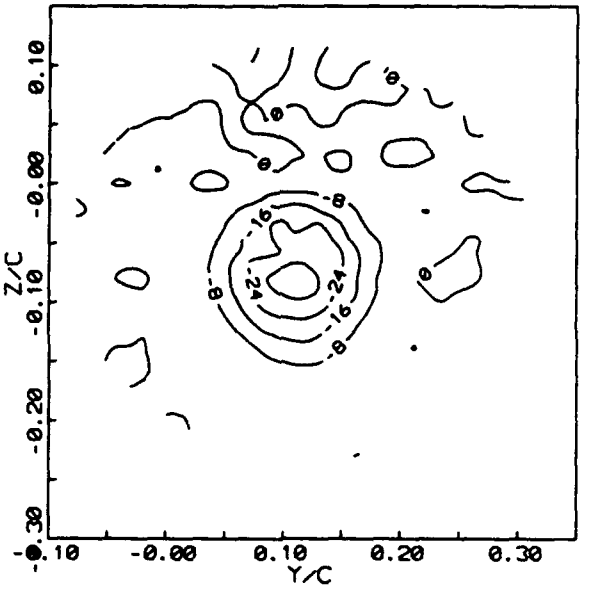

(b)

a = 12 degrees

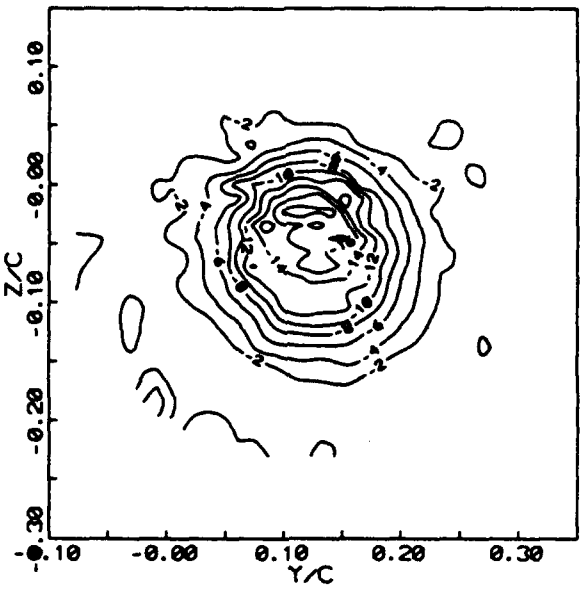

(a)

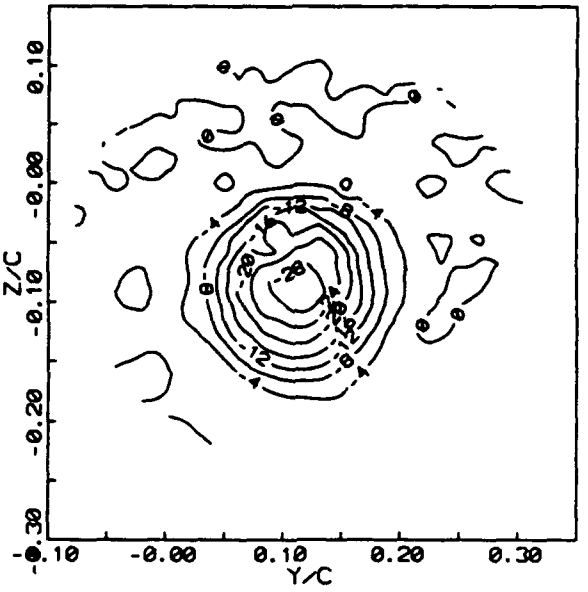

(b)

a = 13 degrees

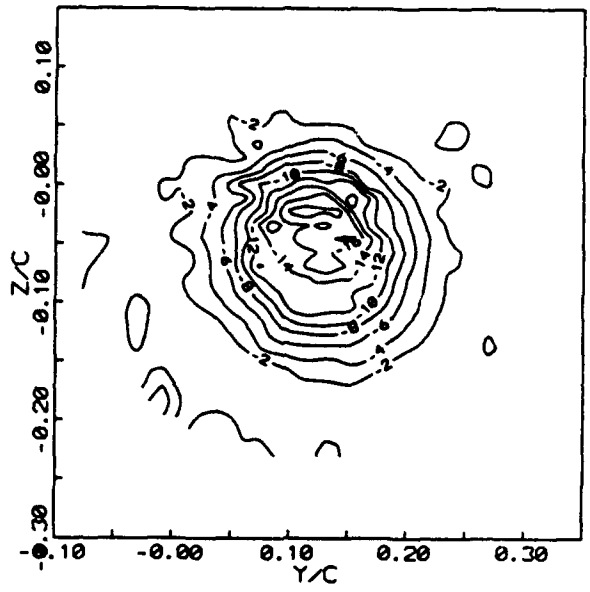

(a)

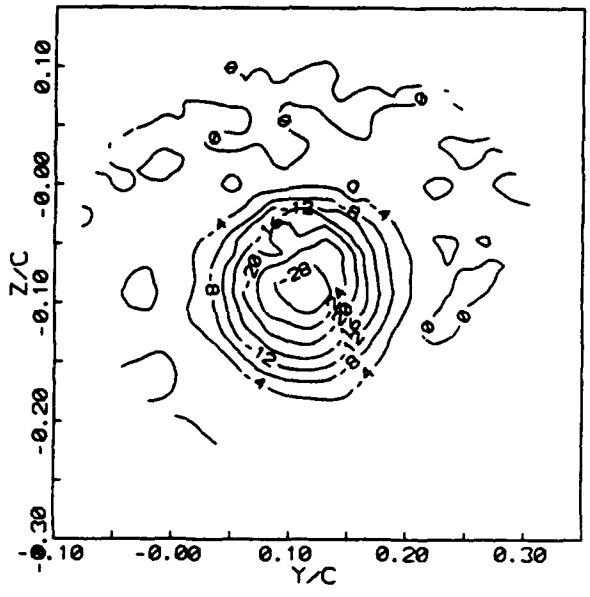

(b)

a = 14 degrees

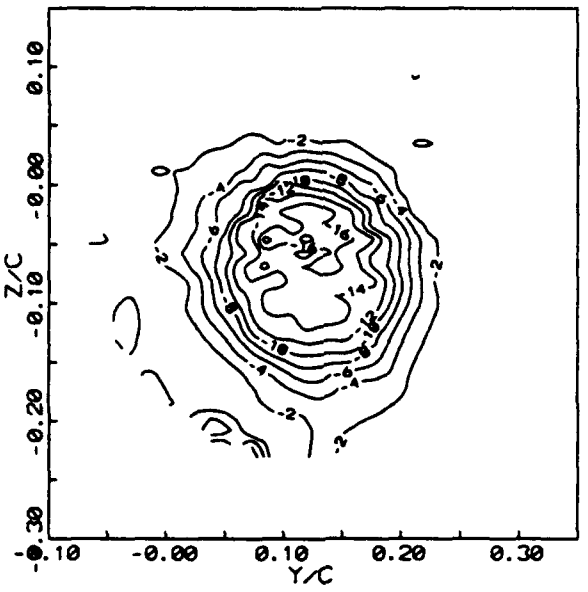

(a)

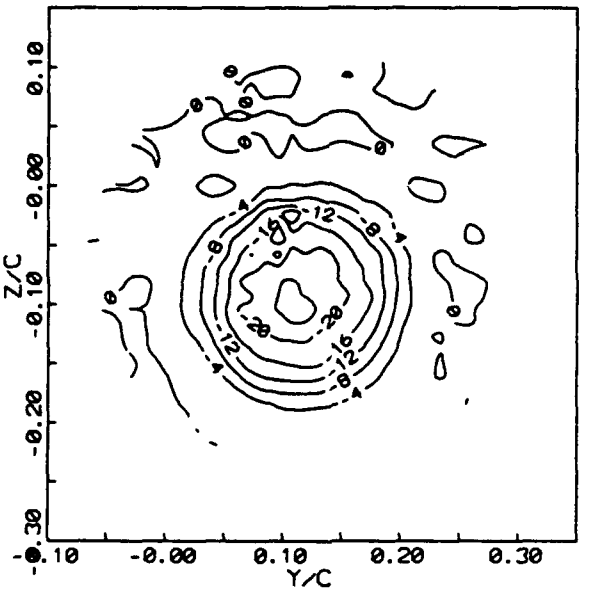

(b)

a = 15 degrees

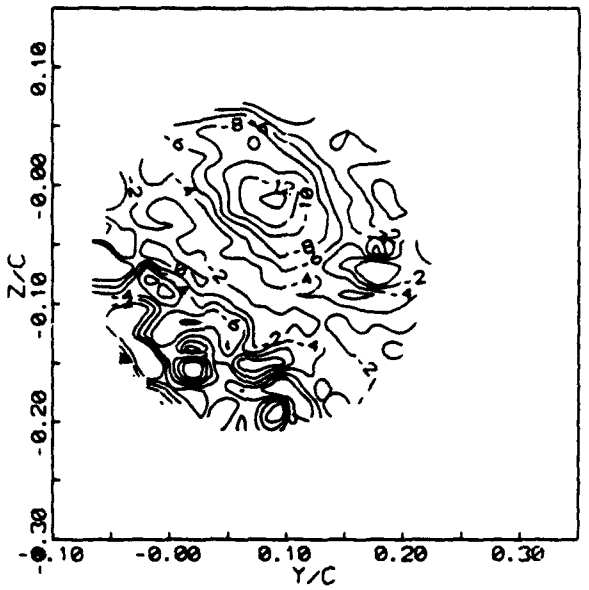

(a)

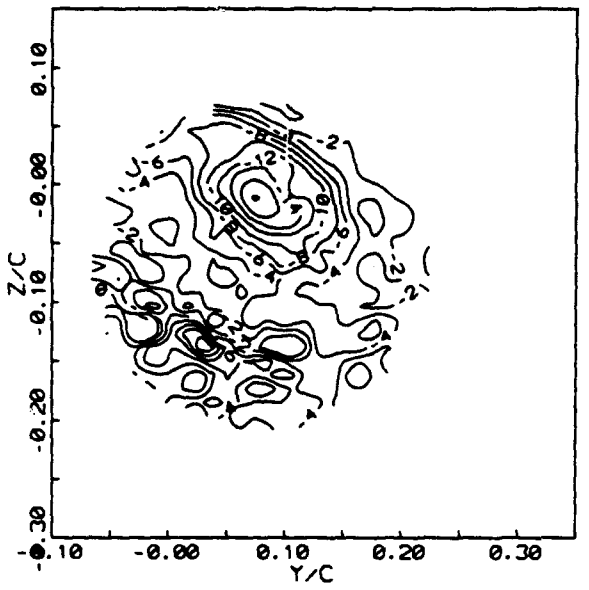

(b)

α = 6 degrees

Figure 5.7 Axial-vorticity $< \omega_x >$ contours at the same downstream distance and angles of incidence as Fig. 5.2. a)Pitch-up. b)Pitch-down.

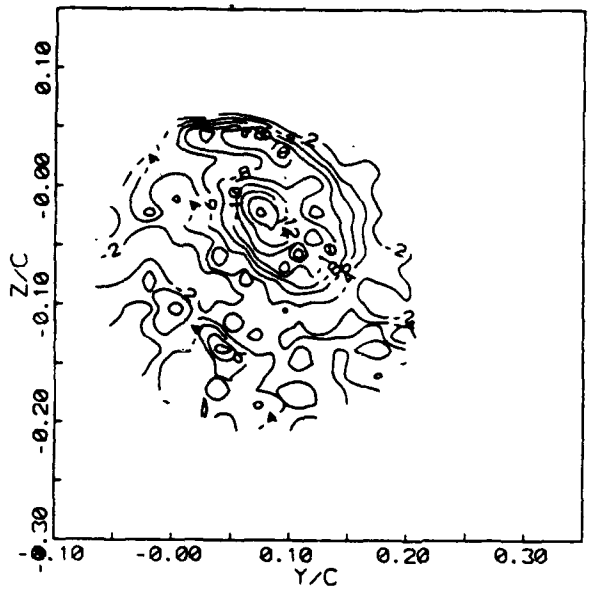

(a)

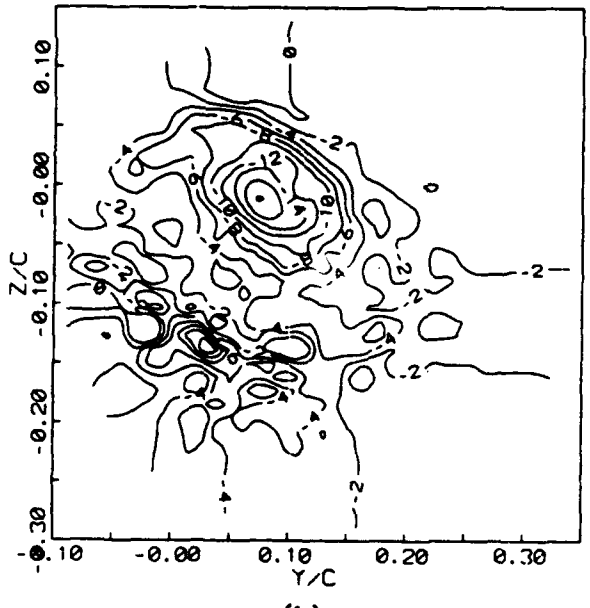

(b)

a = 8 degrees

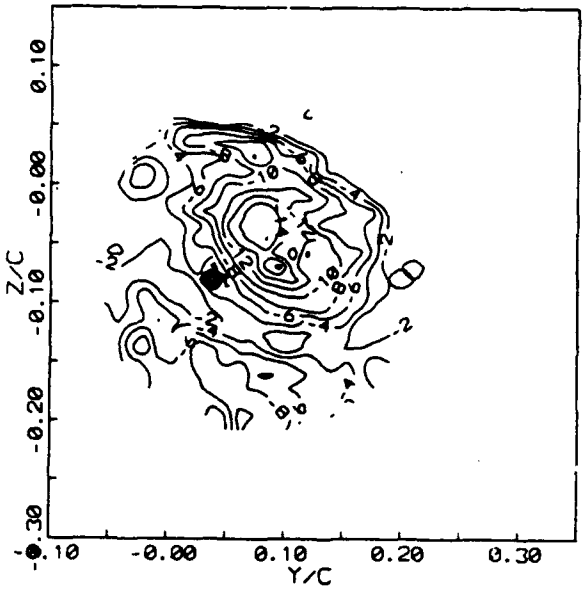

(a)

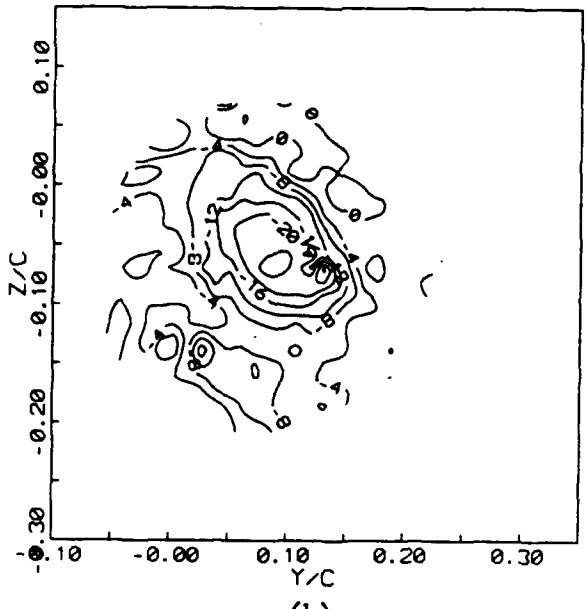

(b)

a = 10 degrees

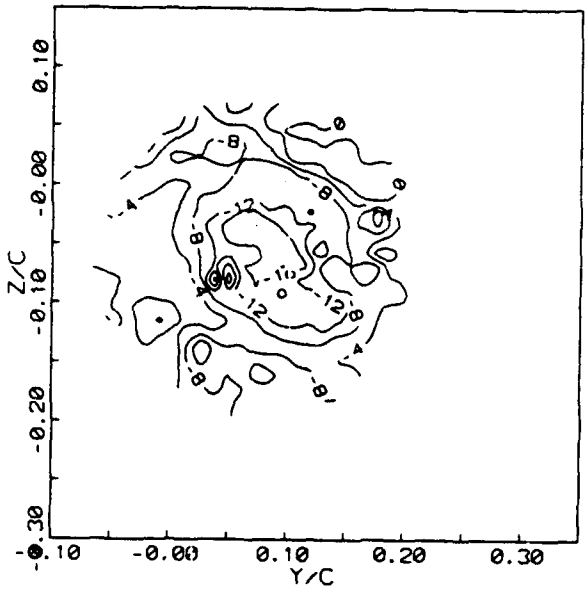

(a)

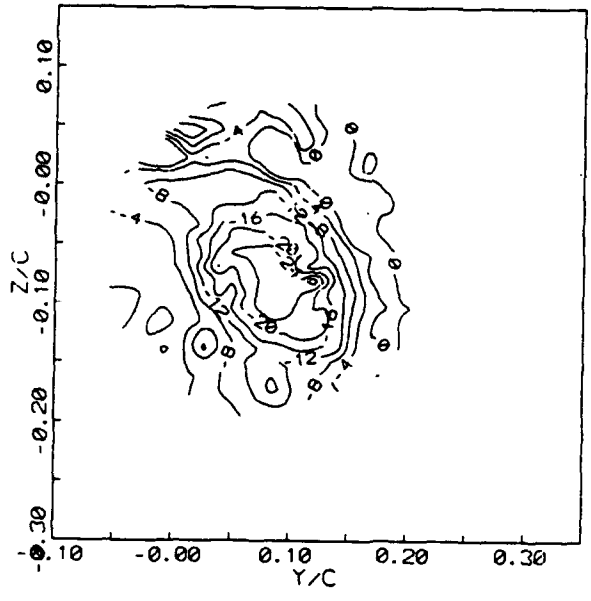

(b)

a = 12 degrees

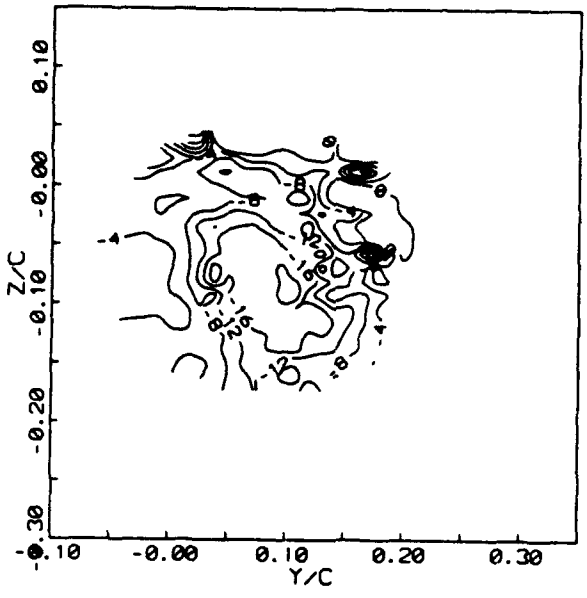

(a)

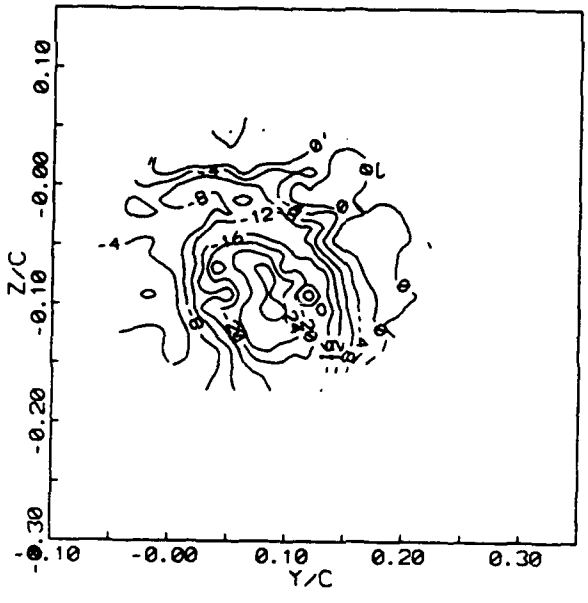

(b)

a = 14 degrees

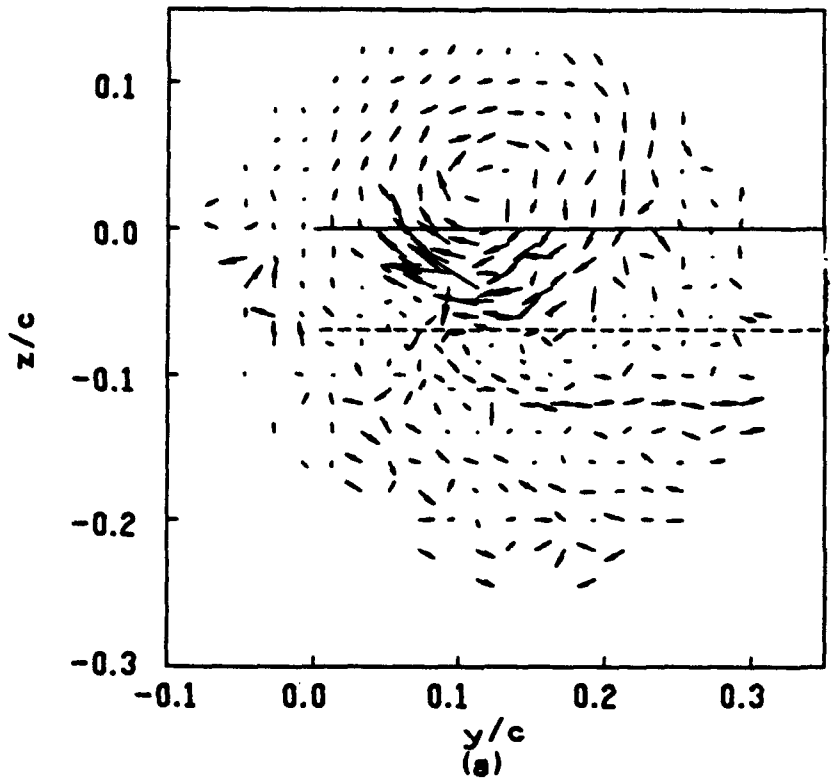

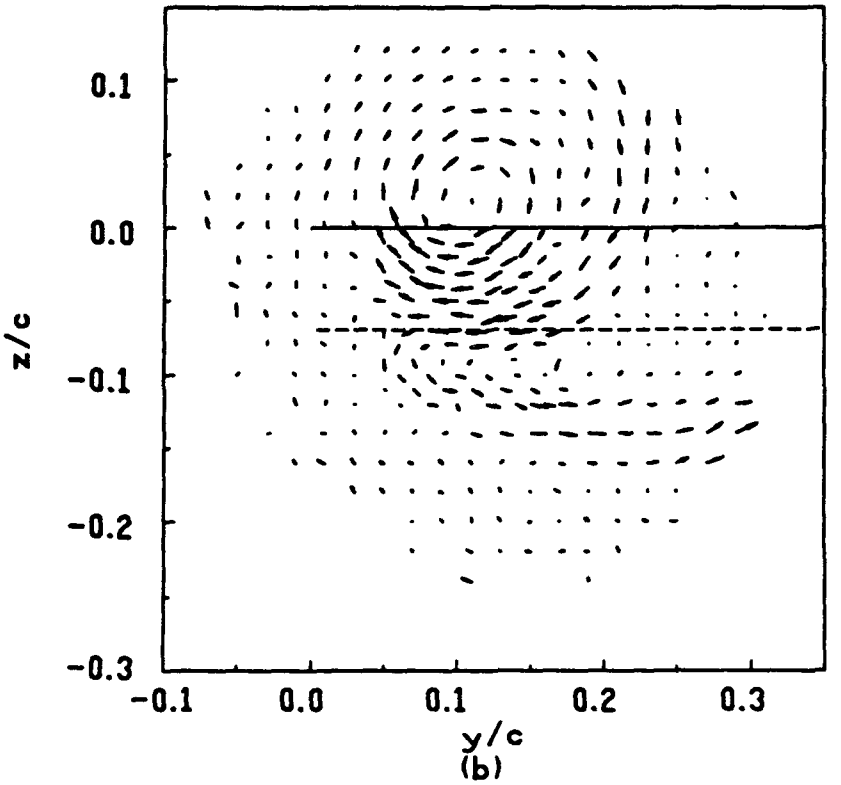

$\alpha = 5$ degrees

Figure 5.6 Distribution of the cross-stream vorticity vector ($\vec{j} < \omega_y > + \vec{k} < \omega_z >$) across the vortex at the same downstream distance and angles of incidence as Fig. 5.1. a)Pitch-up. b)Pitch-down. The magnitude of vorticity is proportional to the length of the arrow.

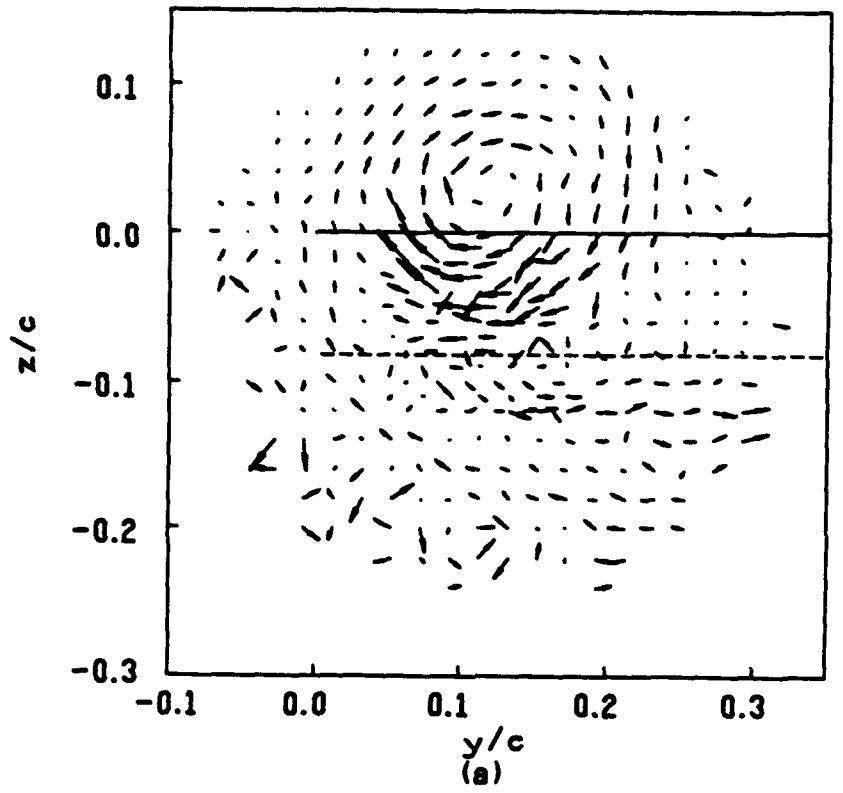
0.1
0.0
-0.1
-0.2
-0.3
z/c
-0.1
0.0
0.1
0.2
0.3
y/c
(a)

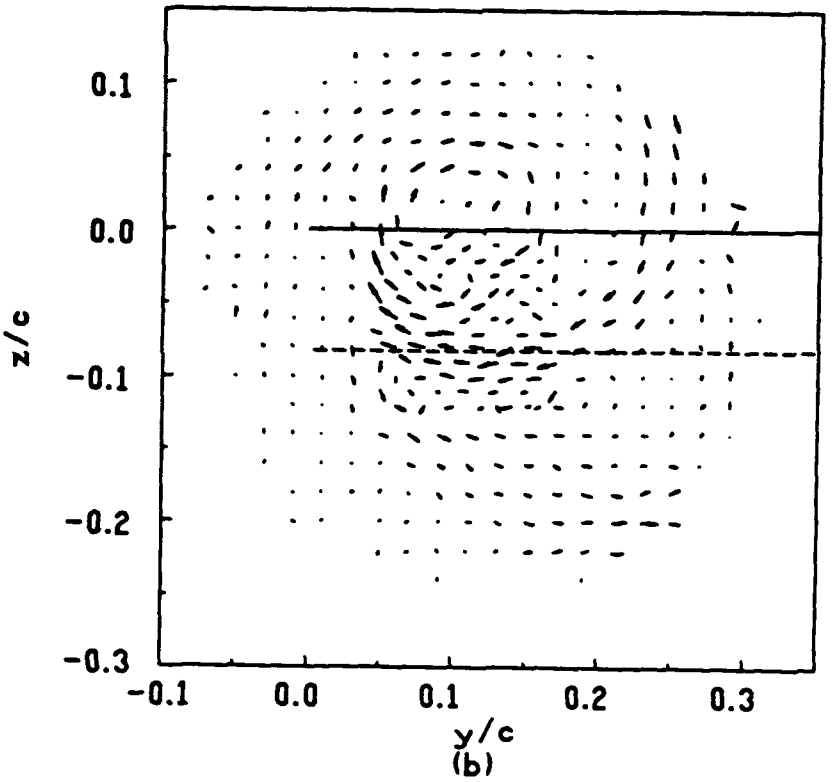
0.1
0.0
-0.1
-0.2
-0.3
z/c
-0.1
0.0
0.1
0.2
0.3
y/c
(b)

a = 6 degrees

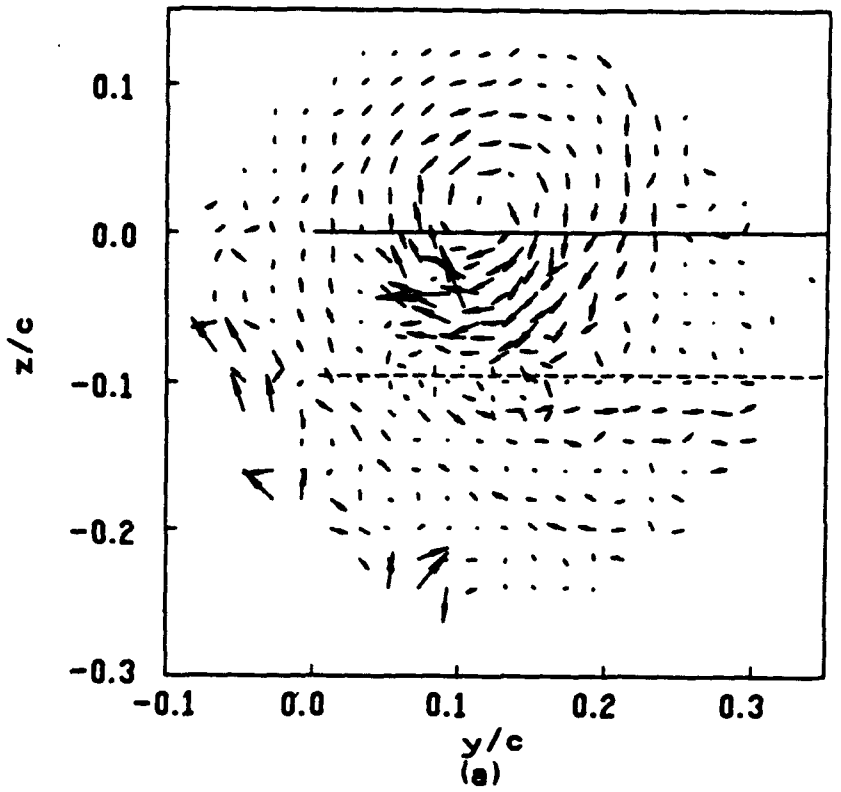
0.1
0.0
-0.1
-0.2
-0.3
z/c
-0.1
0.0
0.1
0.2
0.3
y/c
(a)

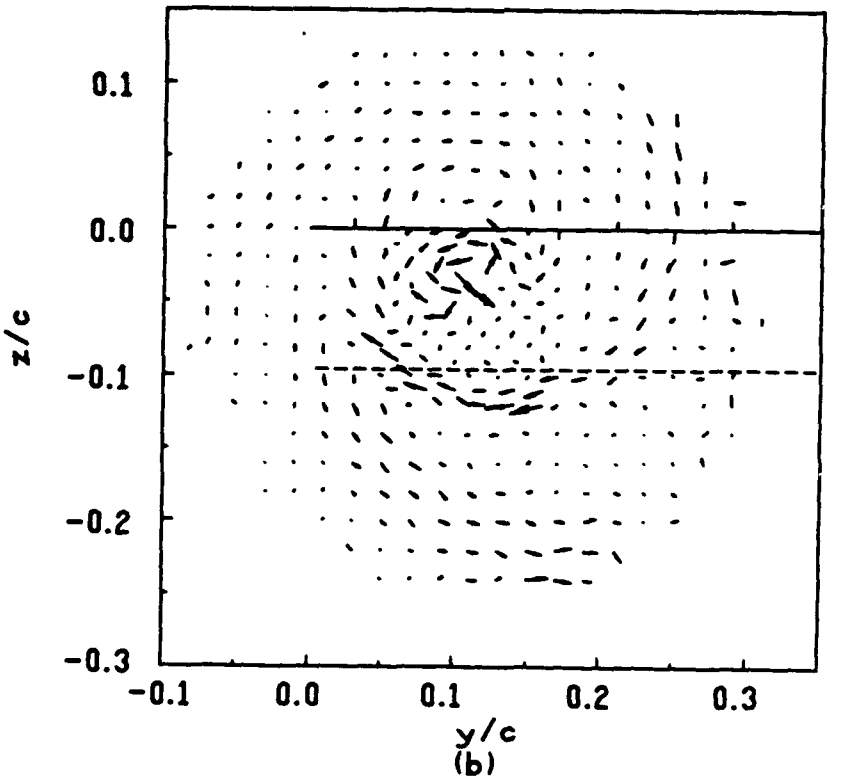
0.1
0.0
-0.1
-0.2
-0.3
z/c
-0.1
0.0
0.1
0.2
0.3
y/c
(b)

a = 7 degrees

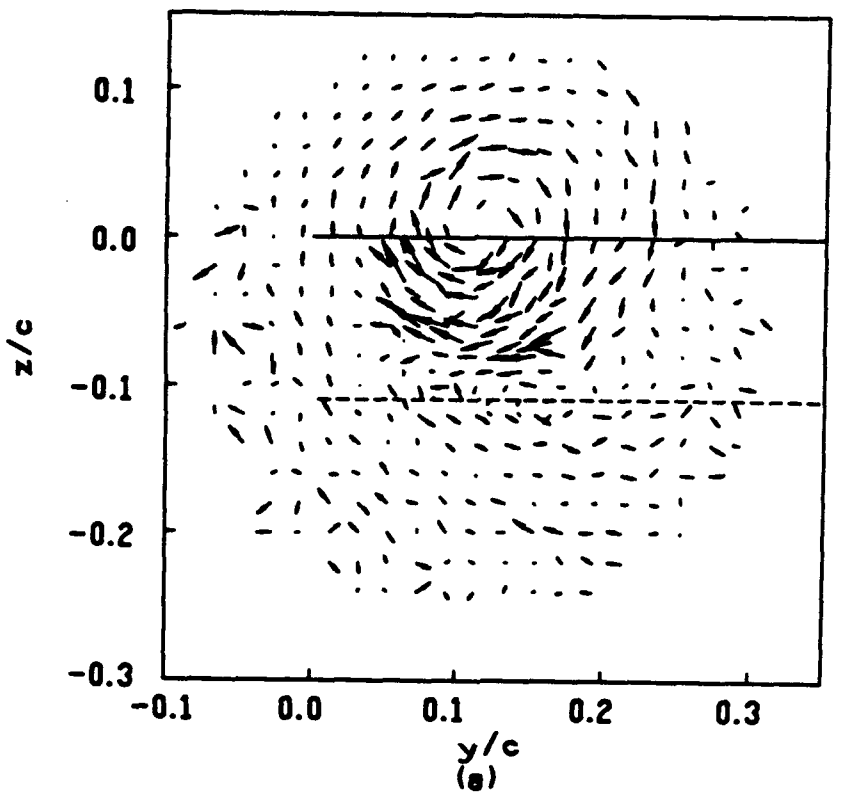
0.1
0.0
-0.1
-0.2
-0.3
z/c
-0.1
0.0
0.1
0.2
0.3
y/c
(a)

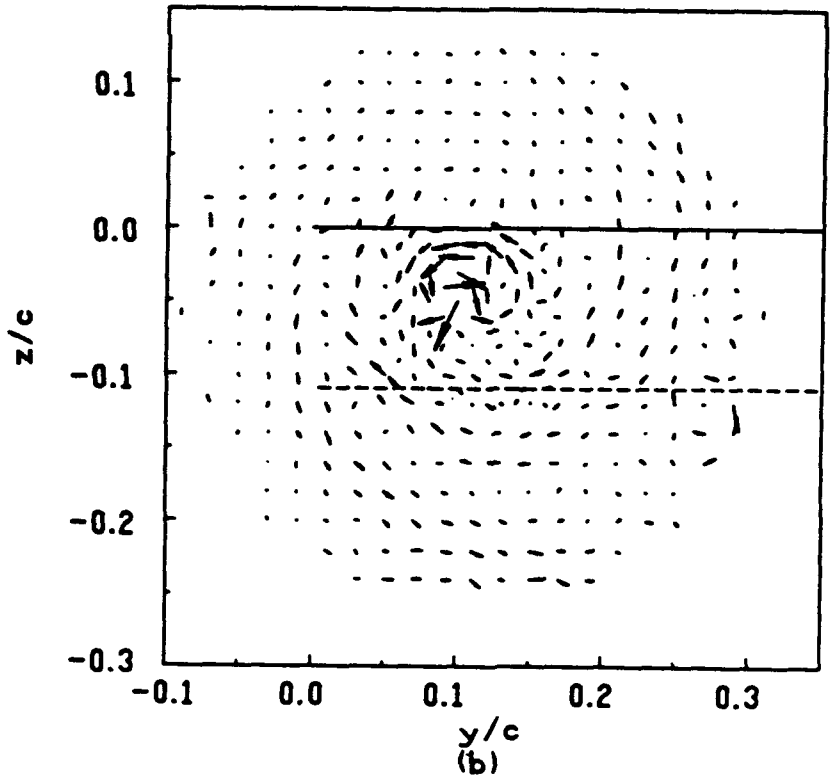
0.1
0.0
-0.1
-0.2
-0.3
z/c
-0.1
0.0
0.1
0.2
0.3
y/c
(b)

a = 8 degrees

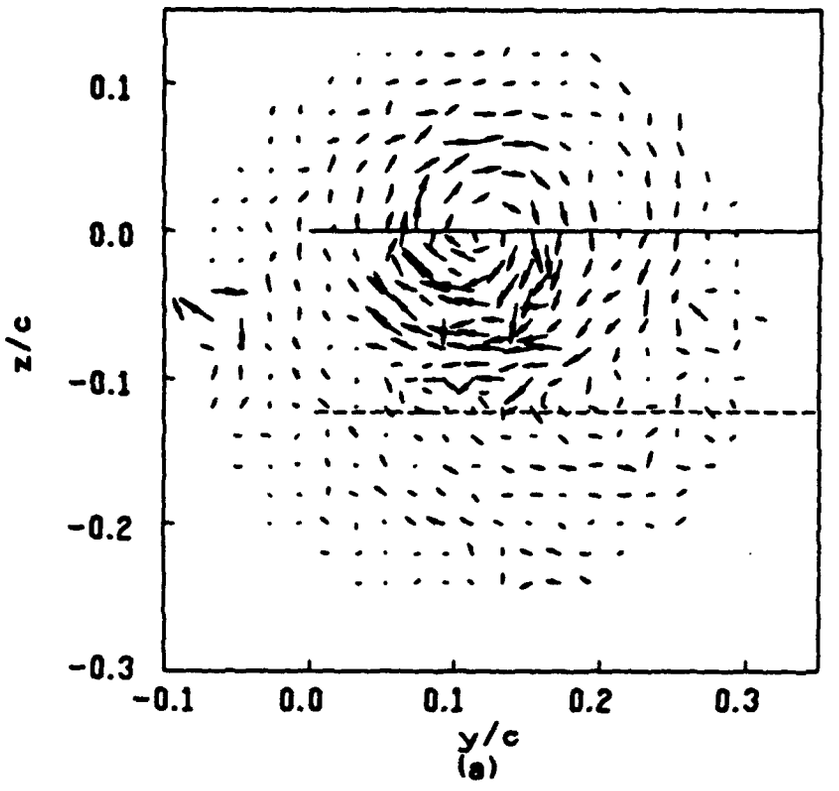
0.1
0.0
-0.1
-0.2
-0.3
z/c
-0.1
0.0
0.1
0.2
0.3
y/c
(a)

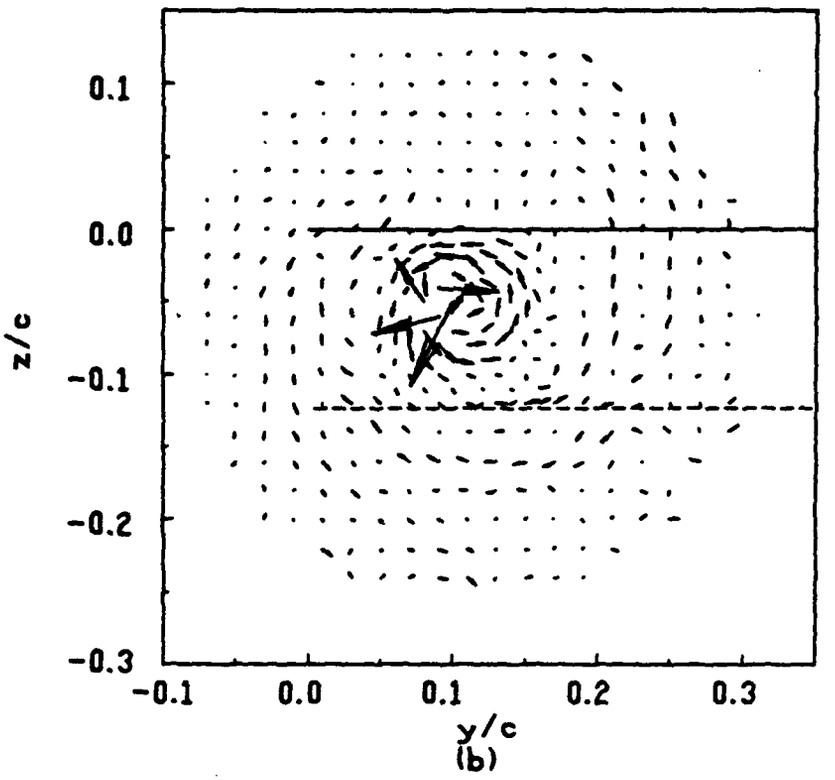
0.1
0.0
-0.1
-0.2
-0.3
z/c
-0.1
0.0
0.1
0.2
0.3
y/c
(b)

a = 9 degrees

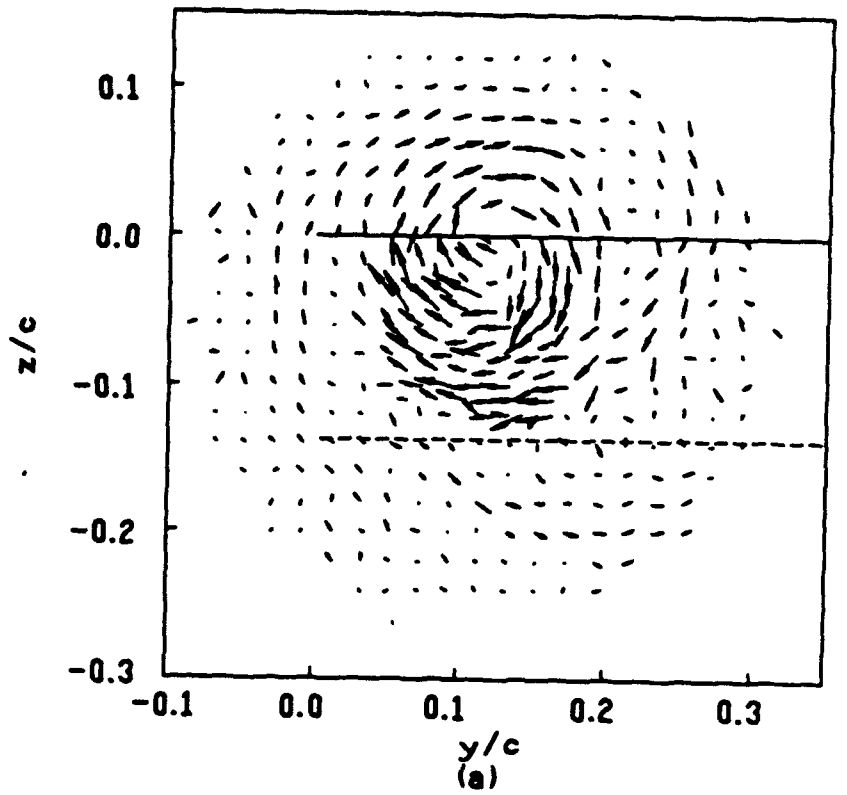
0.1
0.0
-0.1
-0.2
-0.3
z/c
-0.1
0.0
0.1
0.2
0.3
y/c
(a)

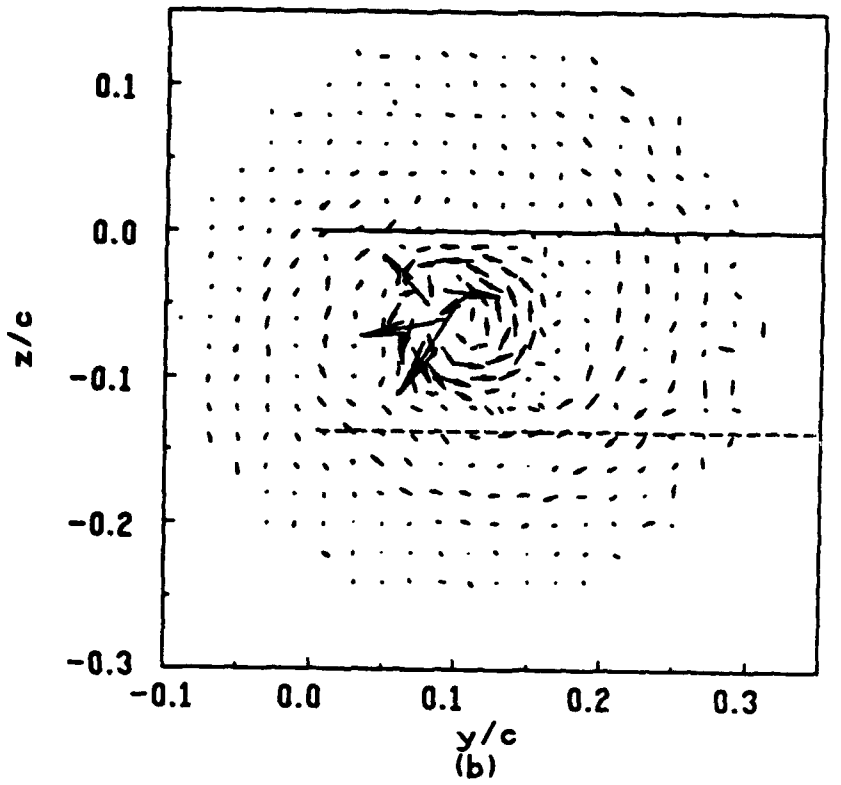
0.1
0.0
-0.1
-0.2
-0.3
z/c
-0.1
0.0
0.1
0.2
0.3
y/c
(b)

a = 10 degrees

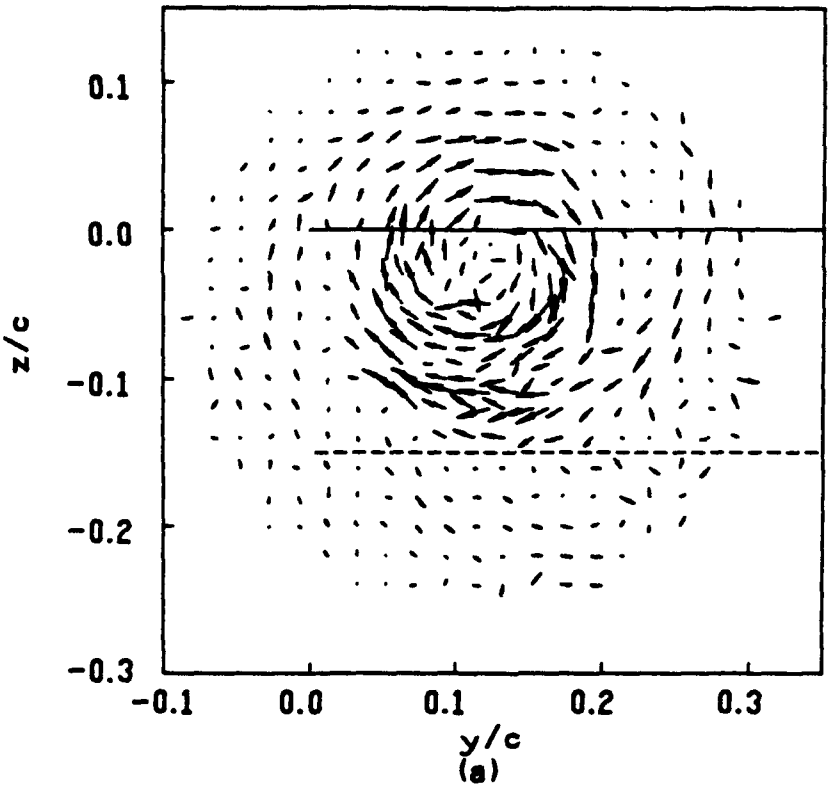
0.1
0.0
-0.1
-0.2
-0.3
z/c
-0.1
0.0
0.1
0.2
0.3
y/c
(a)

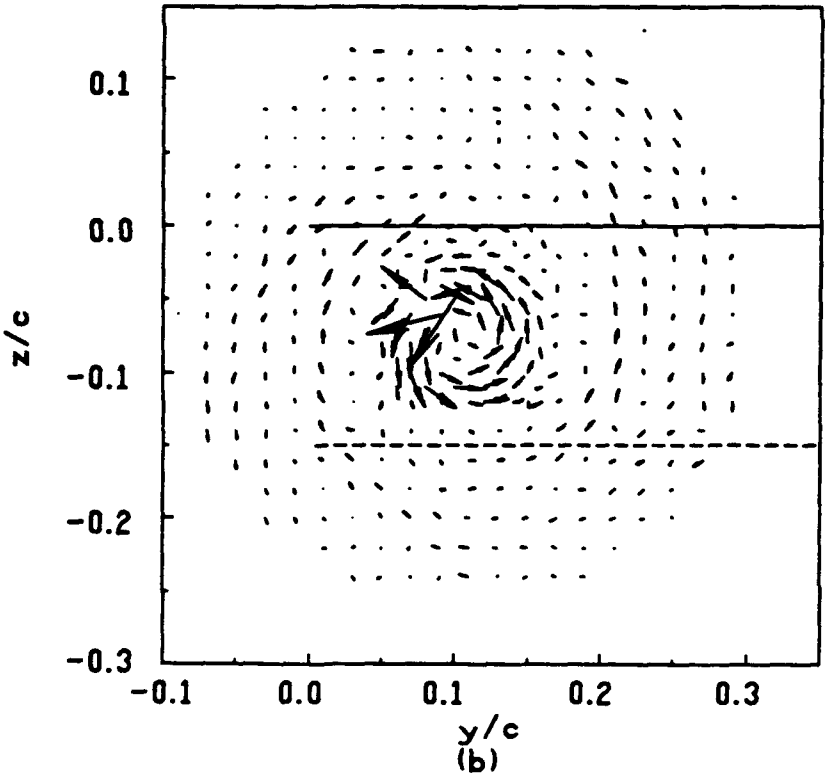
0.1
0.0
-0.1
-0.2
-0.3
z/c
-0.1
0.0
0.1
0.2
0.3
y/c
(b)

a = 11 degrees

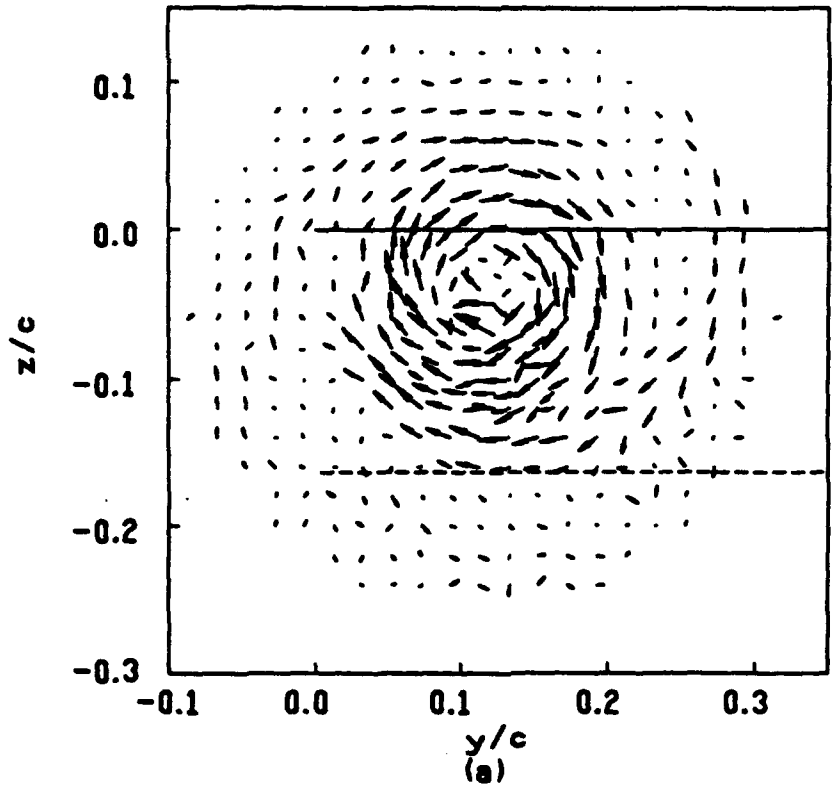

(a)

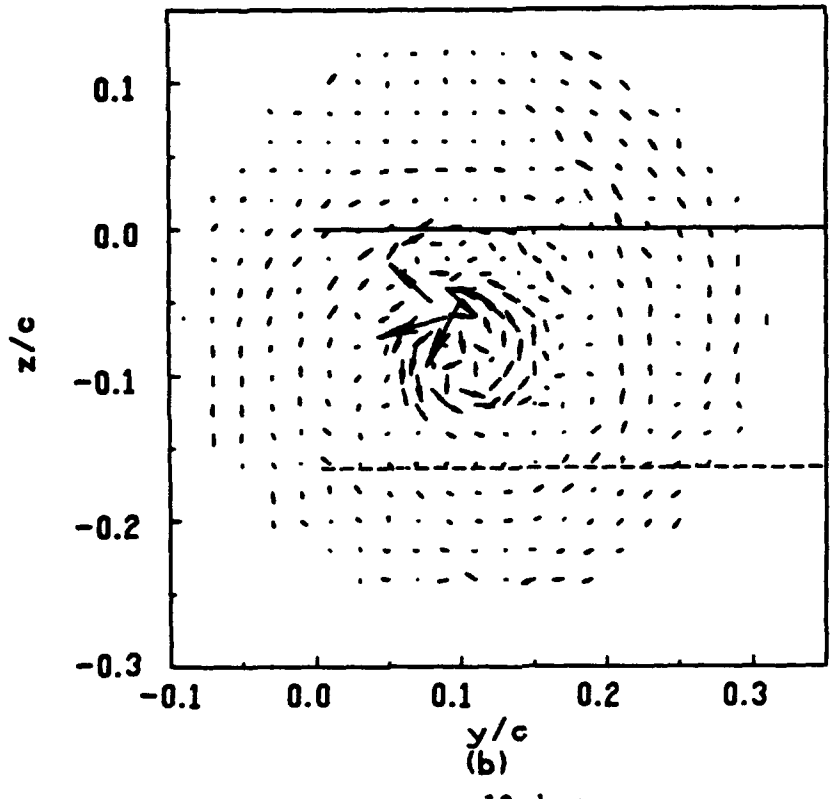

(b)

a = 12 degrees

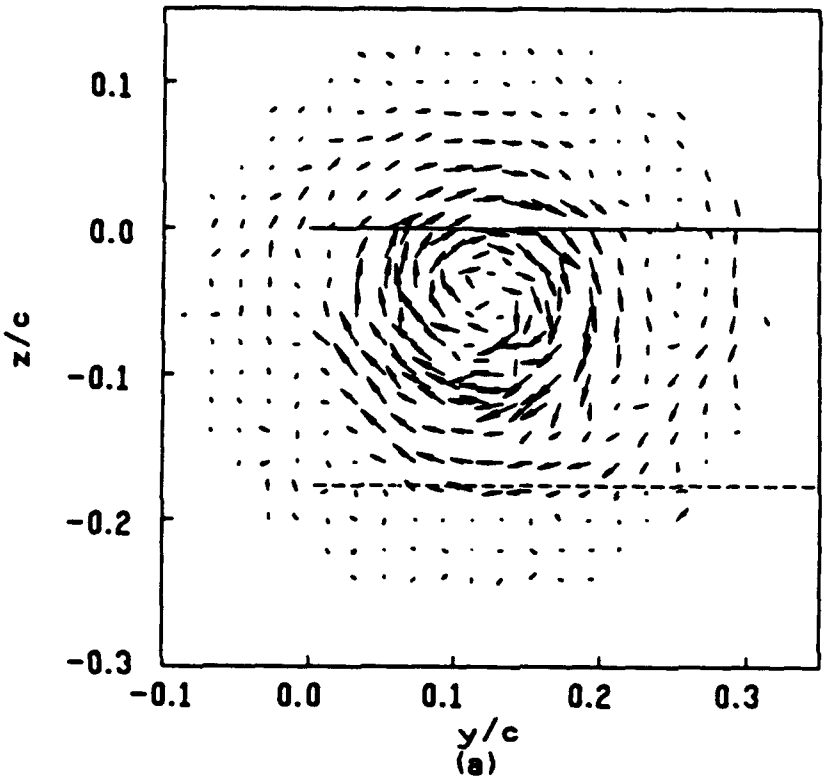

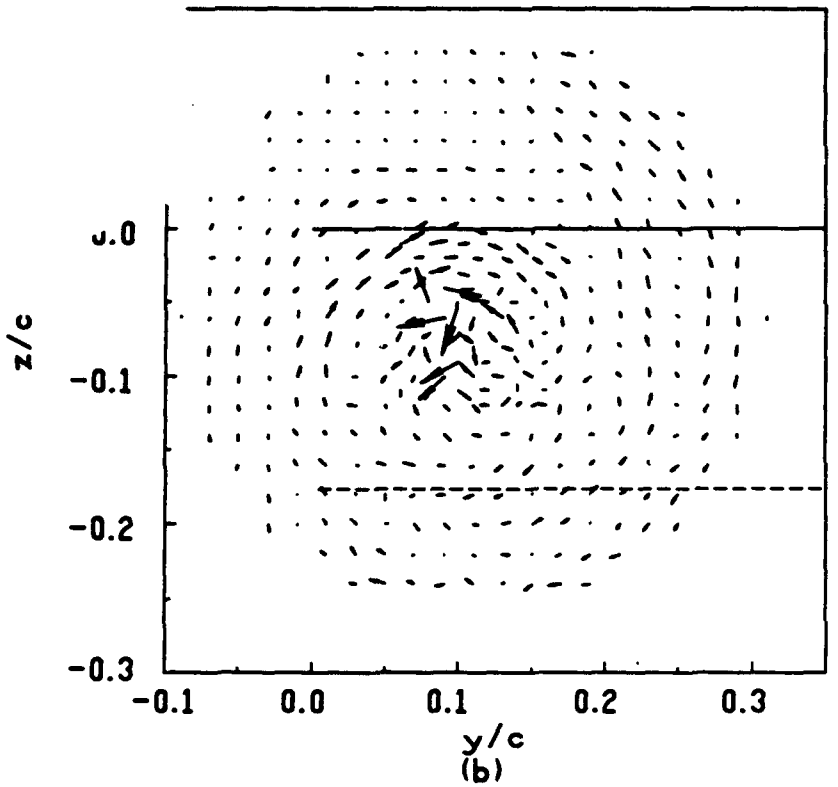

a = 13 degrees

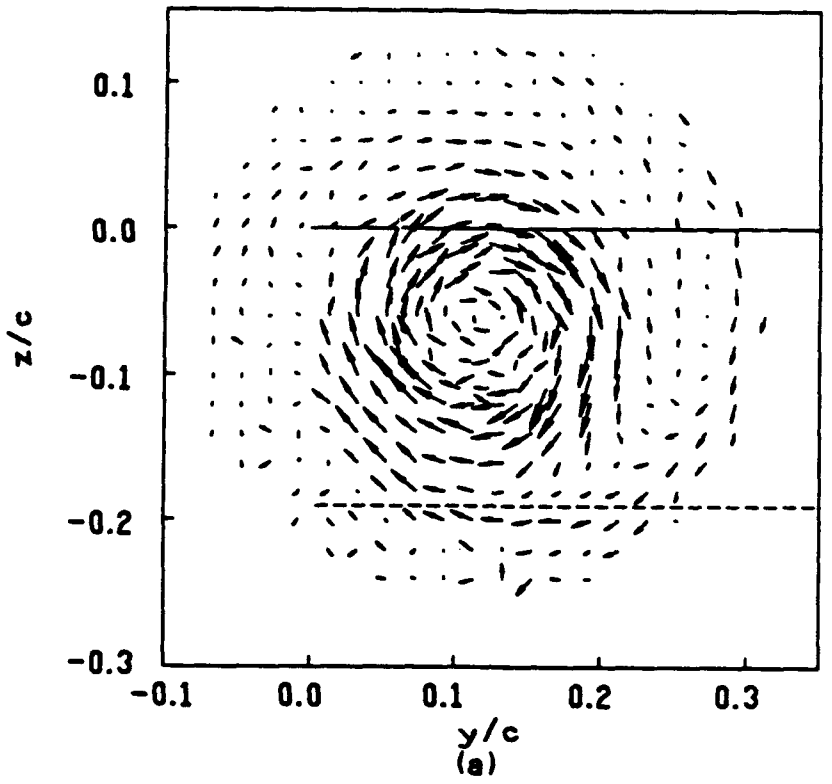
0.1
0.0
-0.1
-0.2
-0.3
z/c
-0.1
0.0
0.1
0.2
0.3
y/c
(a)

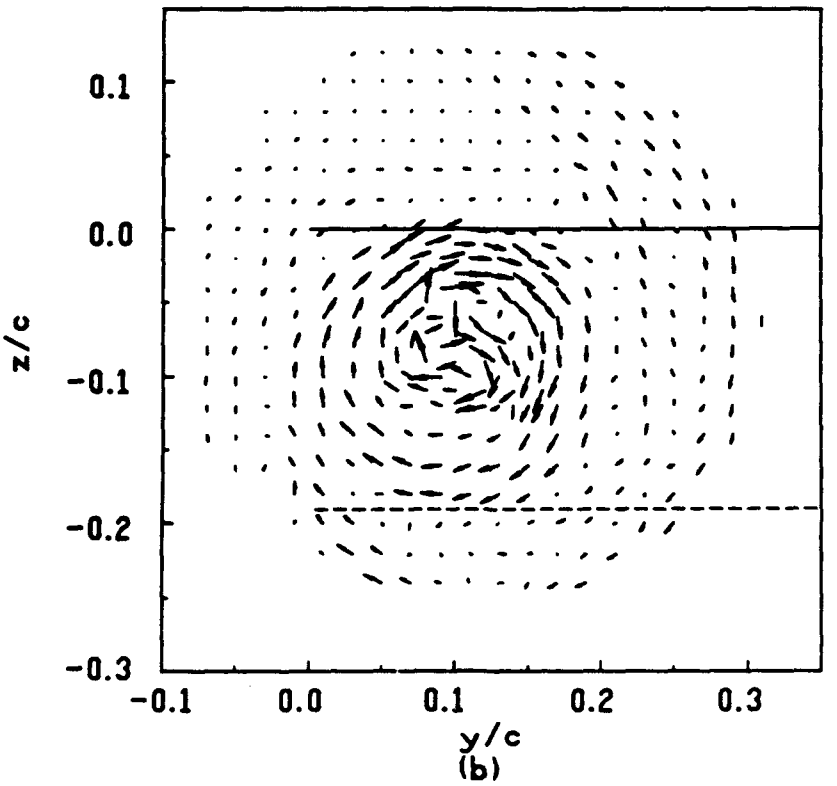
0.1
0.0
-0.1
-0.2
-0.3
z/c
-0.1
0.0
0.1
0.2
0.3
y/c
(b)

a = 14 degrees

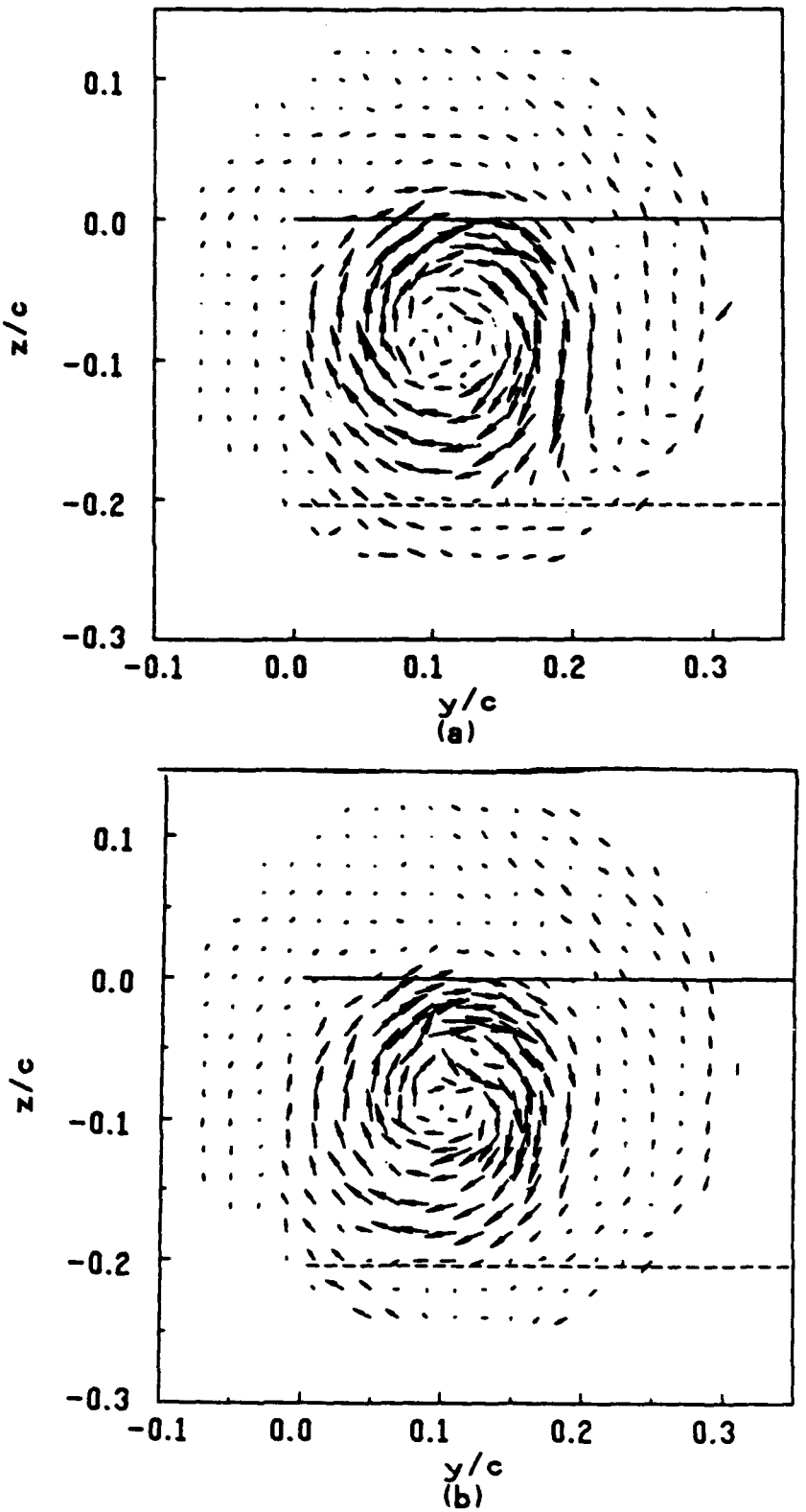
0.1
0.0
-0.1
-0.2
-0.3
z/c
-0.1
0.0
0.1
0.2
0.3
y/c
(a)
0.1
0.0
-0.1
-0.2
-0.3
z/c
-0.1
0.0
0.1
0.2
0.3
y/c
(b)

a = 15 degrees

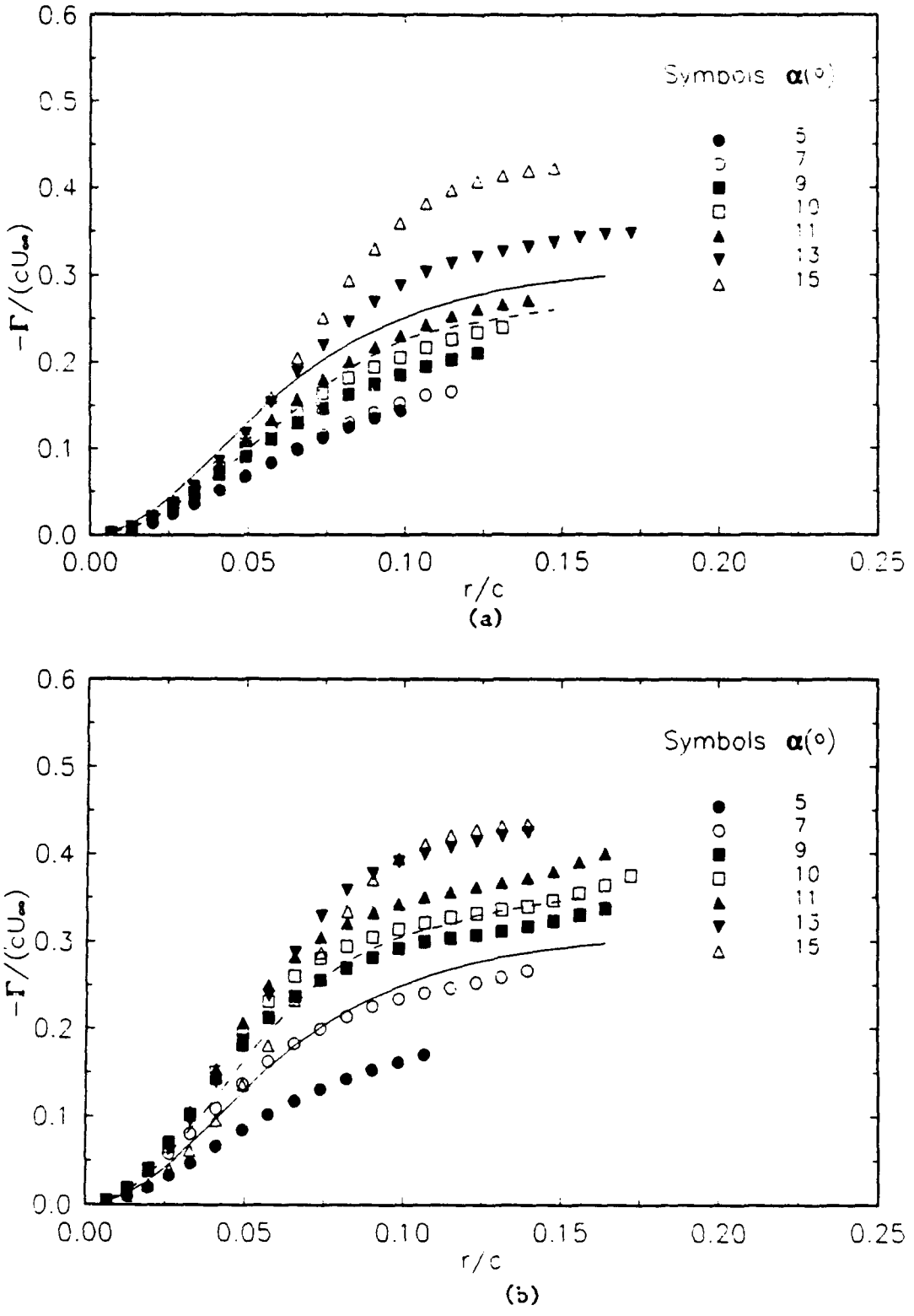

Figure 5.9 Variation of circulation $< \Gamma >$ with distance r from the vortex center. a)Pitch-up. b)Pitch-down.

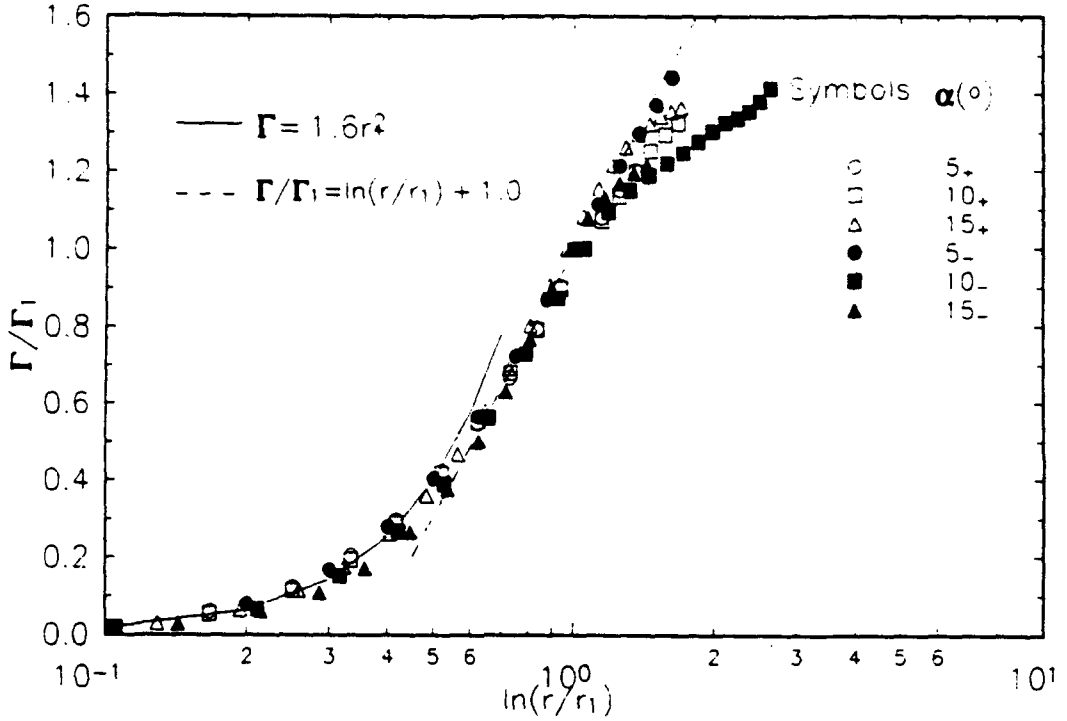

Figure 5.10 Semilogarithmic plot of Γ/Γ_1 vs r/r_1 for α = 5, 10 and 15 degrees at $\bar{x}/c$ = 1.31, '+' for pitch-up and '-' for pitch-down.

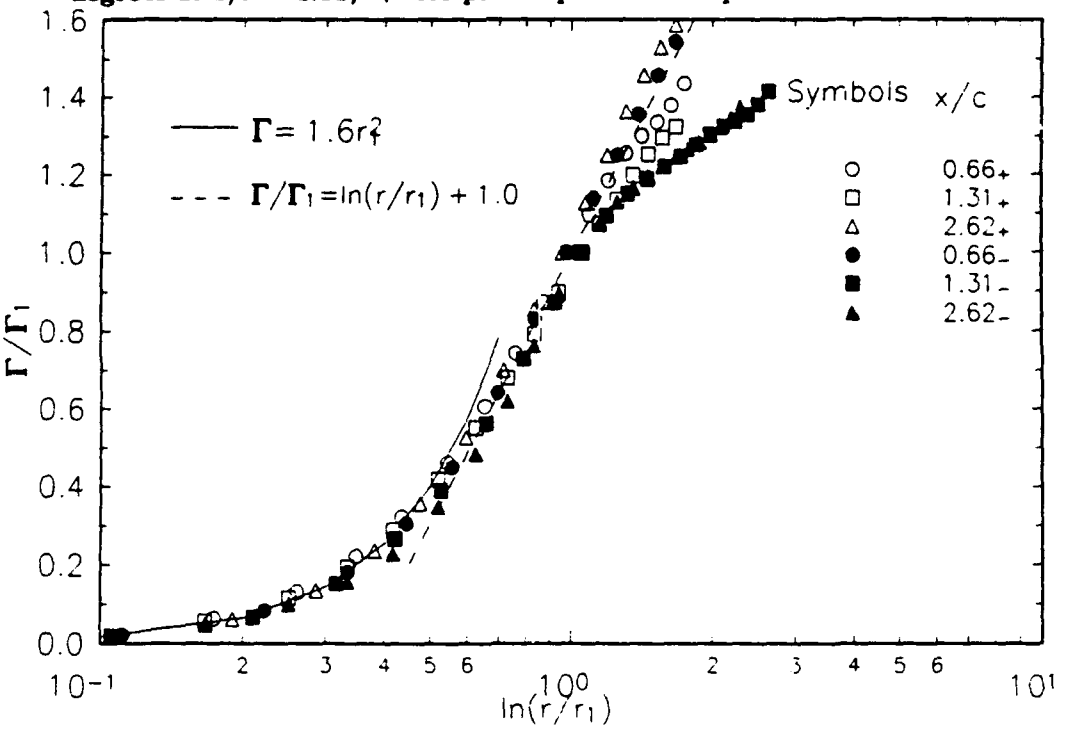

Figure 5.11 Semilogarithmic plot of Γ/Γ_1 vs r/r_1 for α = 10 degrees at $\bar{x}/c$ = 0.66, 1.31 and 2.62, '+' for pitch-up and '-' for pitch-down.

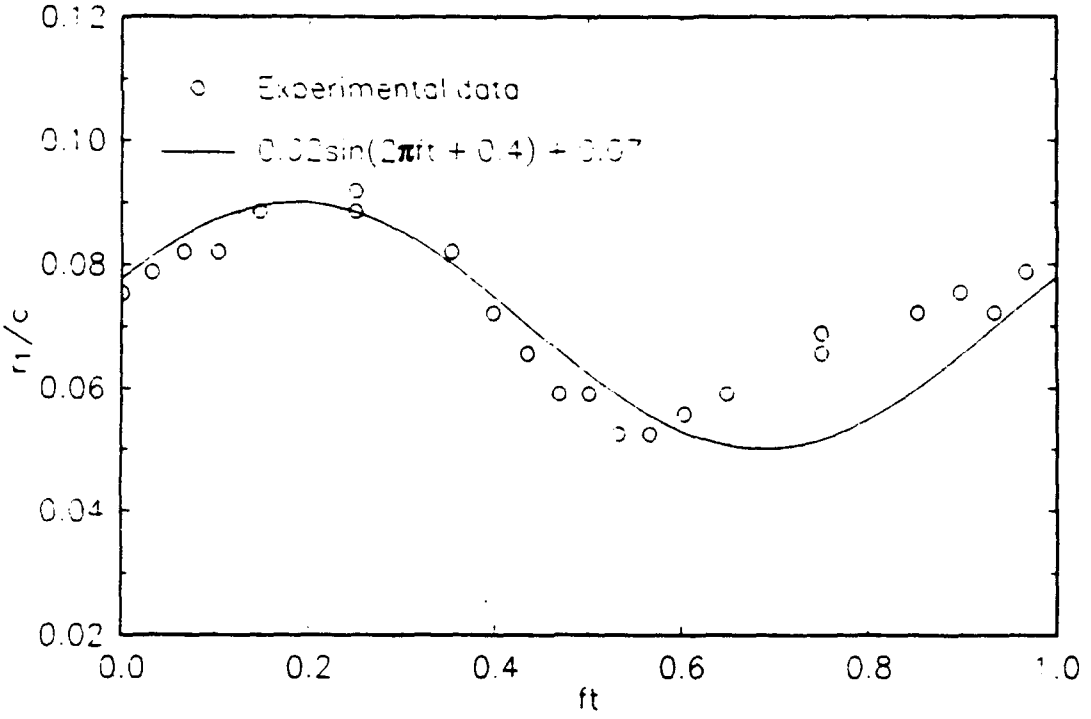

Figure 5.12 Changes of the length scale r_1 with time at $\bar{x}/c = 1.31$.

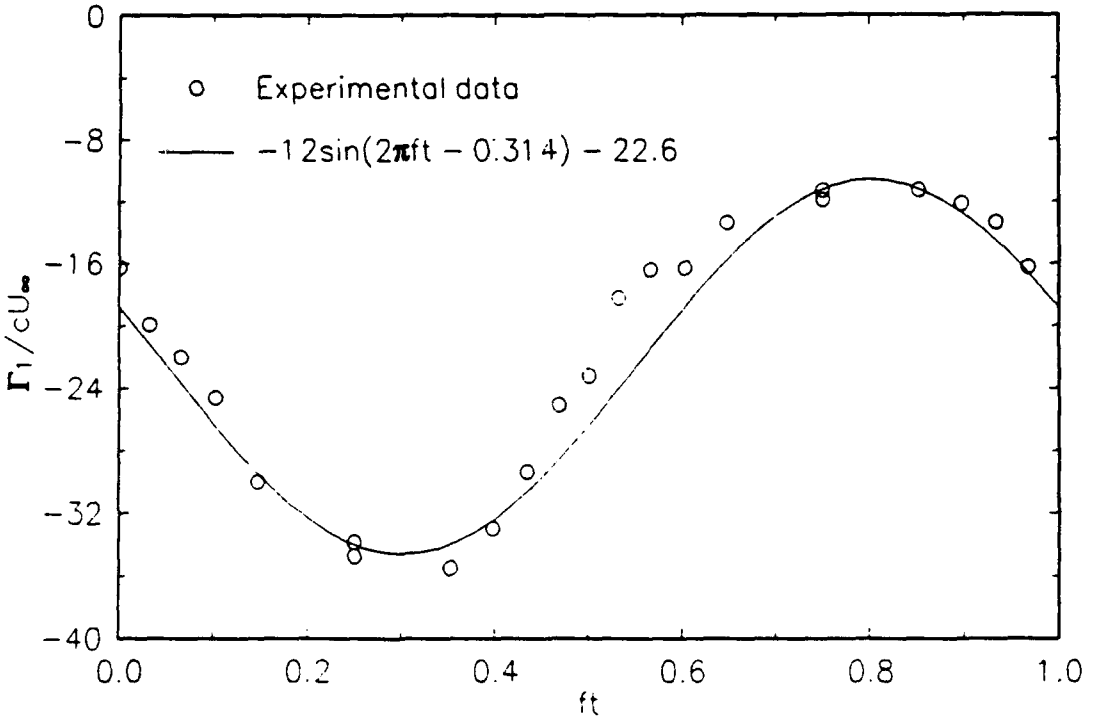

Figure 5.13 Changes of the circulation scale Γ_1 with time at $\bar{x}/c = 1.31$.

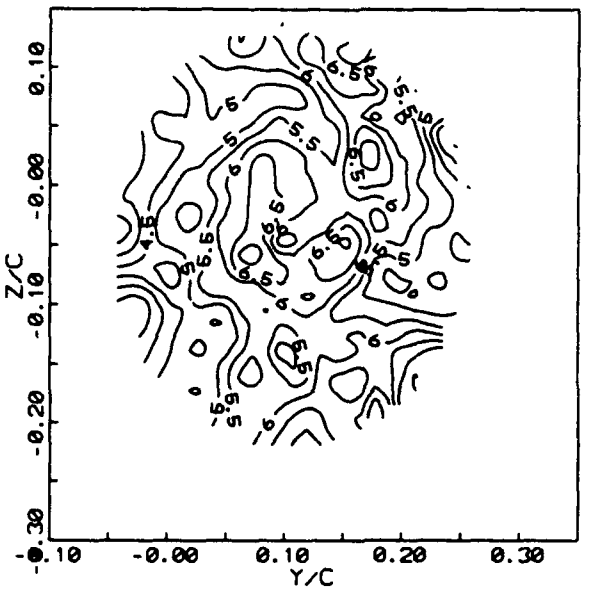

(a)

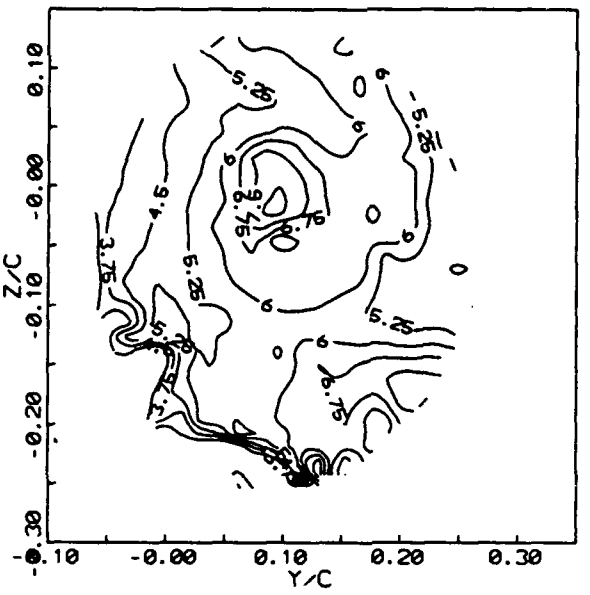

(b)

(i)

Figure 5.14 Distribution of the longitudinal component of the non-dimensional turbulent intensity u' across the vortex at (i) $\alpha = 5$, (ii) $\alpha = 7$, (iii) $\alpha = 9$, (iv) $\alpha = 11$, (v) $\alpha = 13$, (vi) $\alpha = 15$ degrees at $\bar{x}/c = 1.0$. (a) pitch-up, (b) pitch-down.

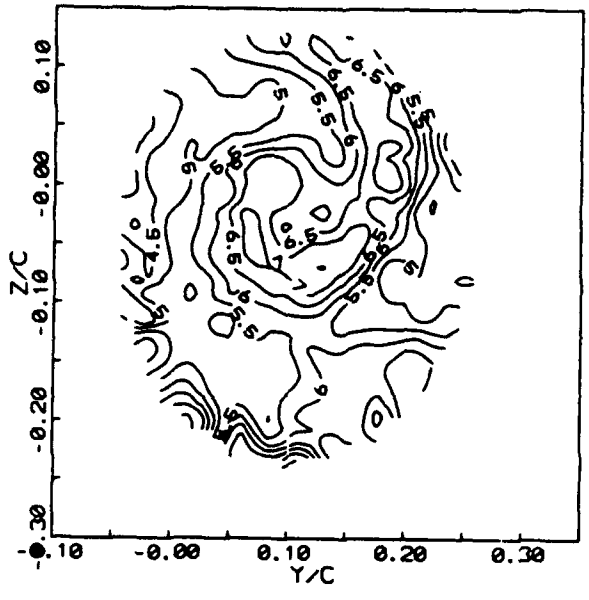
Z/C
0.10
-0.00
-0.10
-0.20
-0.30
-0.10
-0.00
0.10
0.20
0.30
Y/C

(a)

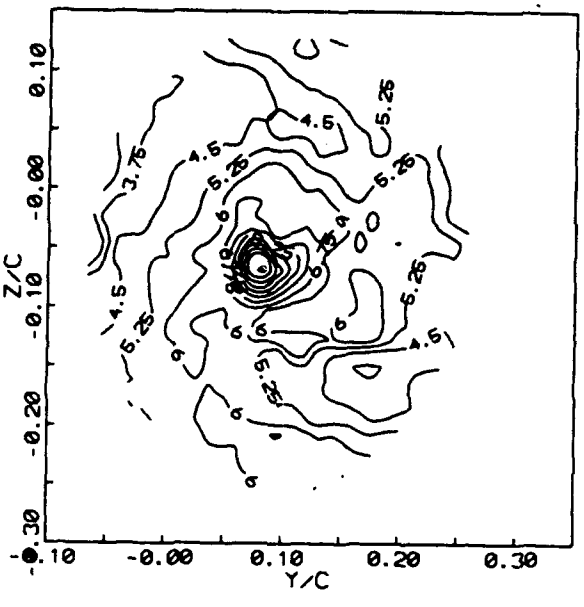
Z/C
0.10
-0.00
-0.10
-0.20
-0.30
-0.10
-0.00
0.10
0.20
0.30
Y/C

(b)

(ii)

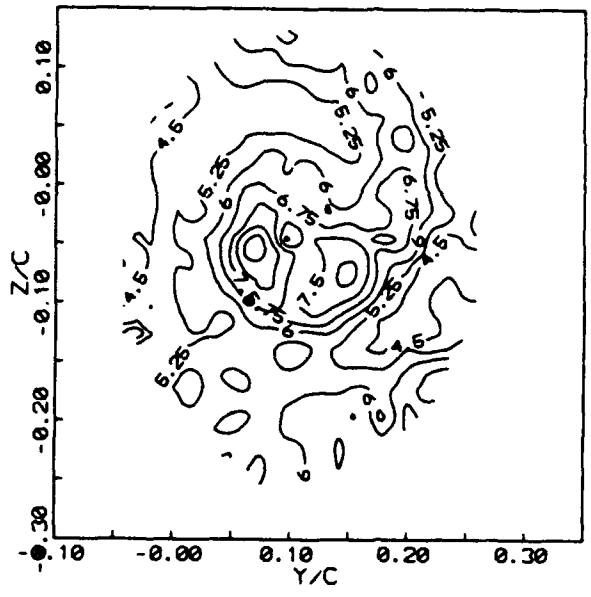
Z/C
0.10
-0.00
-0.10
-0.20
-0.30
-0.10
-0.00
0.10
0.20
0.30
Y/C

(a)

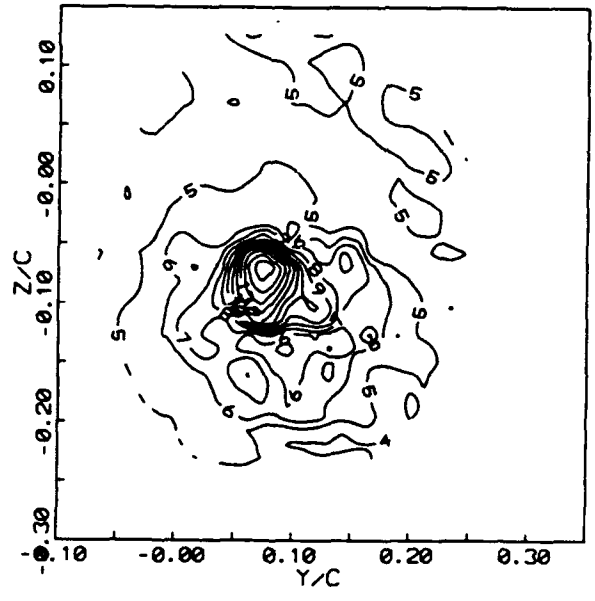
Z/C
0.10
-0.00
-0.10
-0.20
-0.30
-0.10
-0.00
0.10
0.20
0.30
Y/C

(b)

(iii)

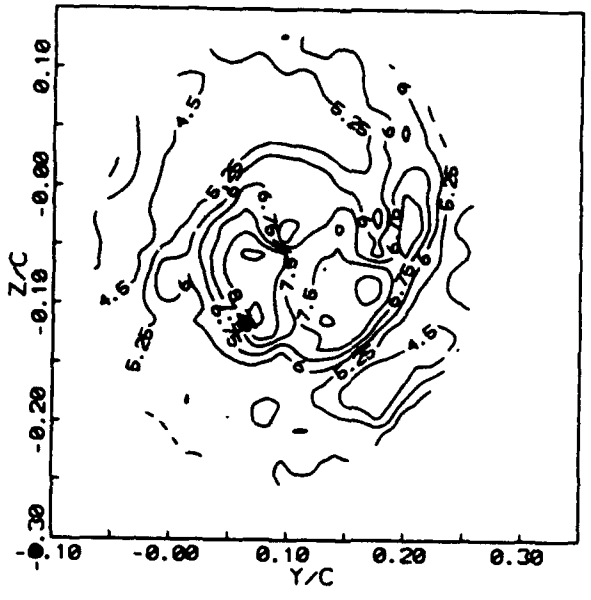
Z/C
0.10
-0.00
-0.10
-0.20
-0.30
-0.10
-0.00
0.10
0.20
0.30
Y/C

(a)

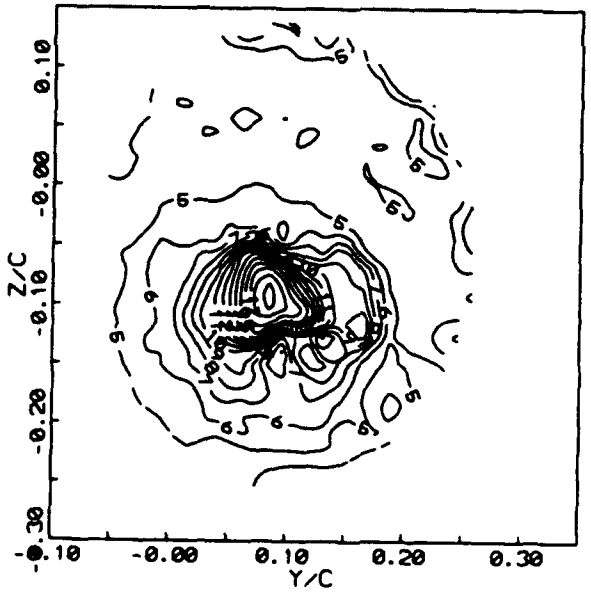
Z/C
0.10
-0.00
-0.10
-0.20
-0.30
-0.10
-0.00
0.10
0.20
0.30
Y/C

(b)

(iv)

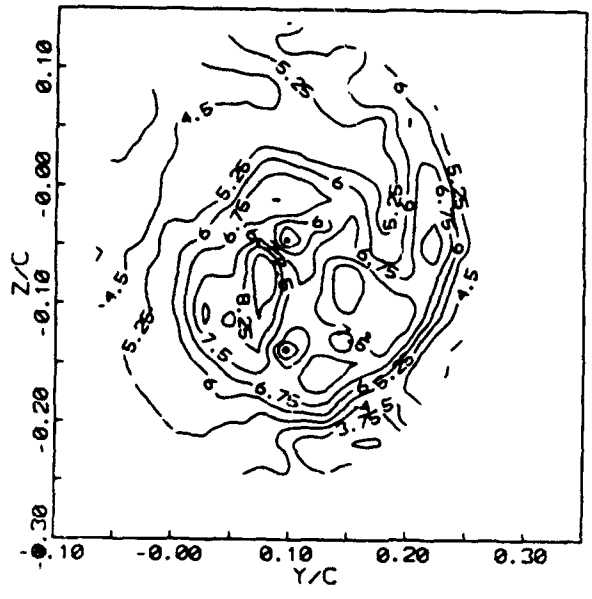
Z/C
0.10
-0.00
-0.10
-0.20
-0.30
-0.10
-0.00
0.10
0.20
0.30
Y/C

(a)

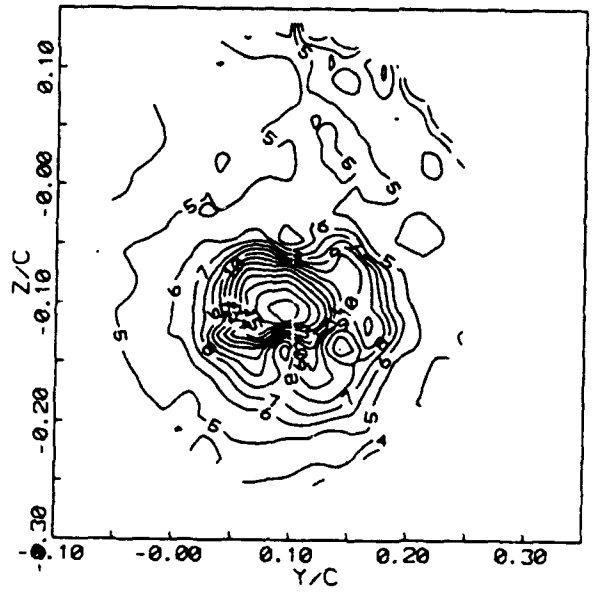
Z/C
0.10
-0.00
-0.10
-0.20
-0.30
-0.10
-0.00
0.10
0.20
0.30
Y/C

(b)

(v)

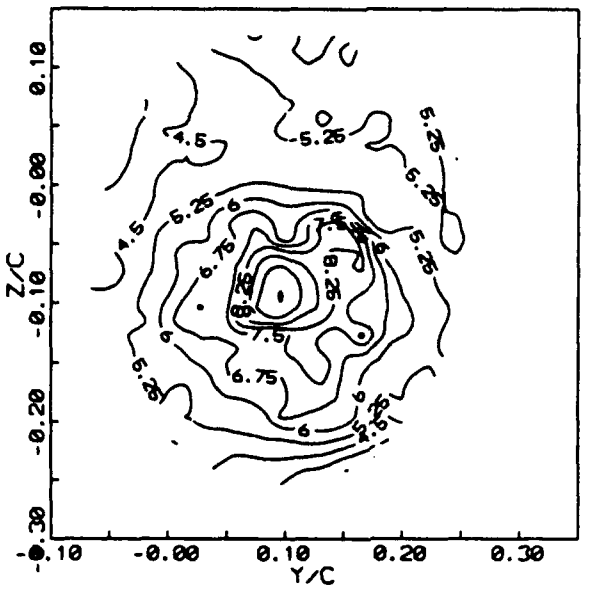
Z/C
Y/C
0.10
-0.00
-0.10
-0.20
-0.30
-0.10
-0.00
0.10
0.20
0.30
4.5
5.25
6
6.75
7.5
8.25

(a)

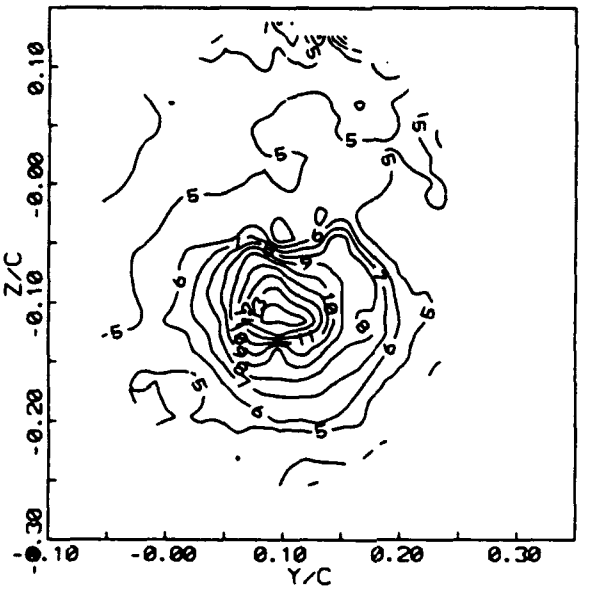
Z/C
Y/C
0.10
-0.00
-0.10
-0.20
-0.30
-0.10
-0.00
0.10
0.20
0.30
5
6
7
8
9
10
11
12

(b)

(vi)

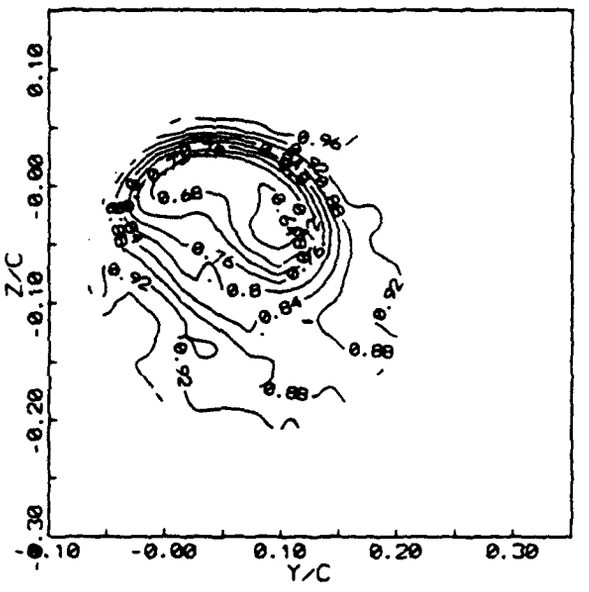

(a) $\alpha = 9$ degrees

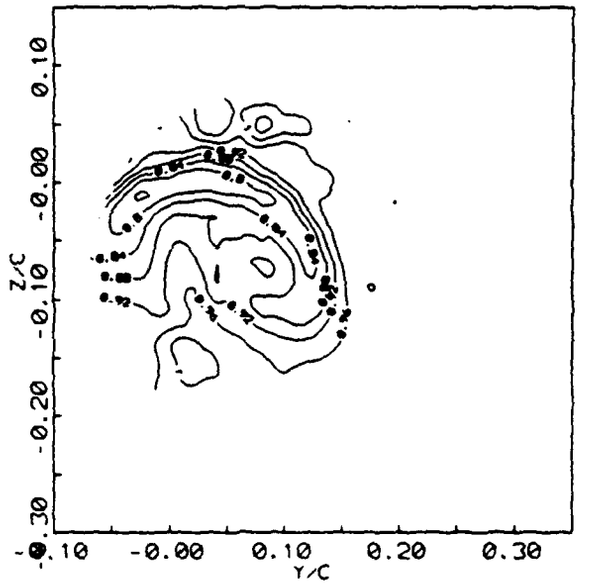

(b) $\alpha = 11$ degrees

(i)

Figure 5.15 Downstream development of the longitudinal component of the velocity U across the vortex. (a) pitch-up. (b) pitch-down. (i) $\bar{x}/c = 0.33$. (ii) $\bar{x}/c = 0.66$. (iii) $\bar{x}/c = 1.0$. (iv) $\bar{x}/c = 1.32$. (v) $\bar{x}/c = 1.64$. (vii) $\bar{x}/c = 2.62$.

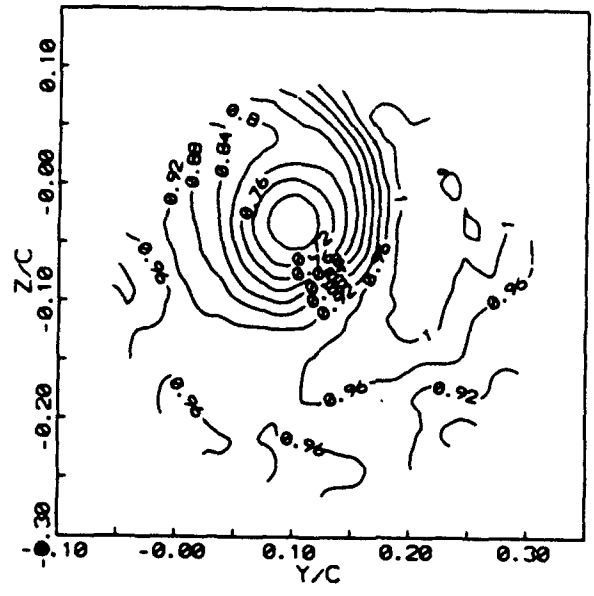

(a) $\alpha = 9$ degrees

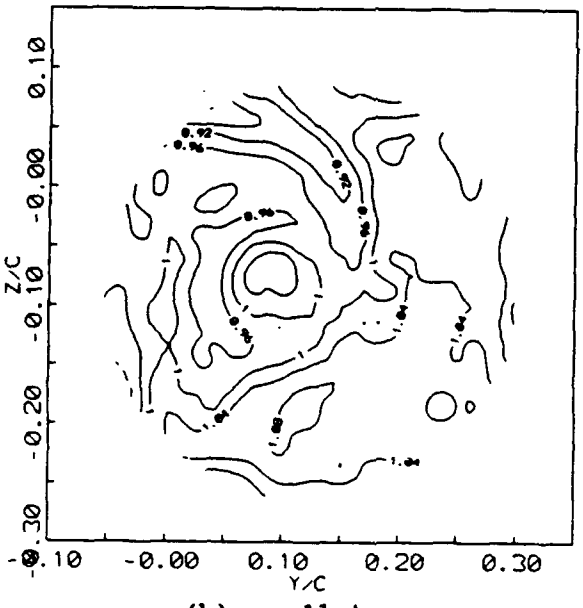

(b) $\alpha = 11$ degrees

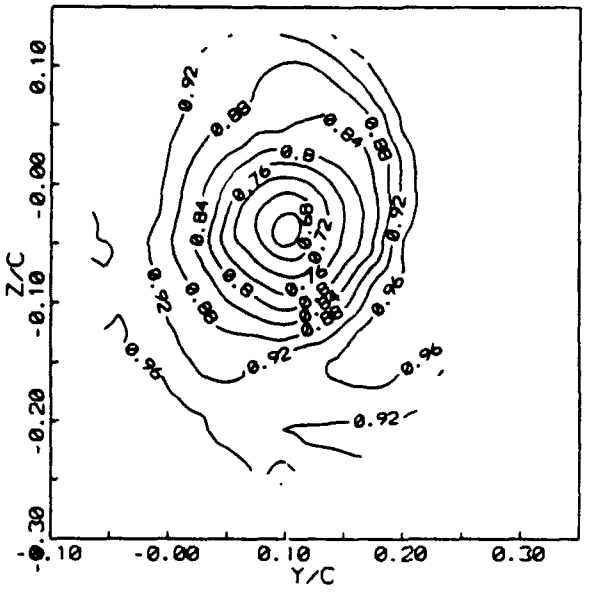

(a) $\alpha = 10$ degrees

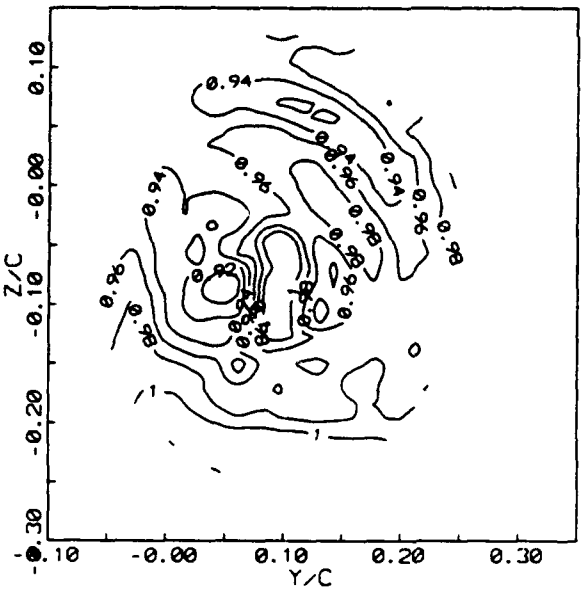

(b) $\alpha = 10$ degrees

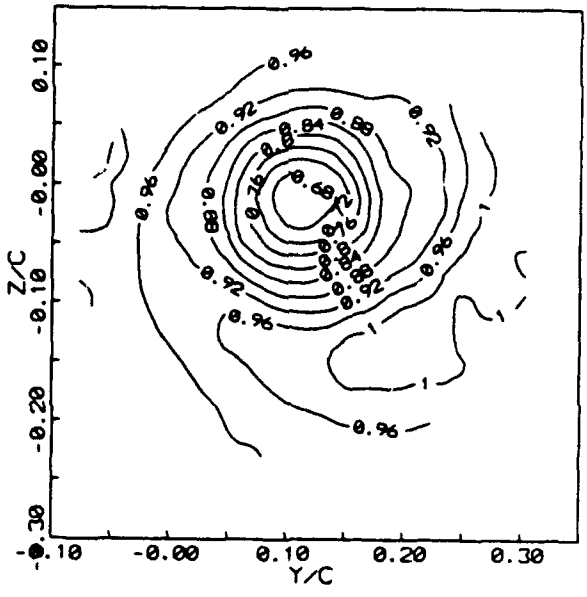

(a) $\alpha = 10$ degrees

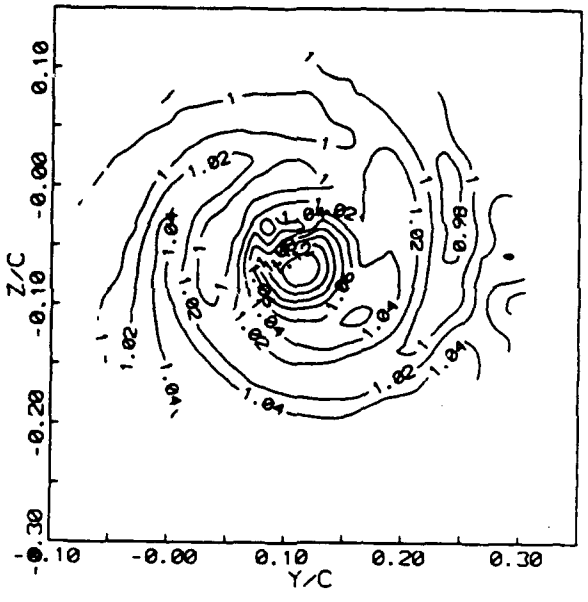

(b) $\alpha = 10$ degrees

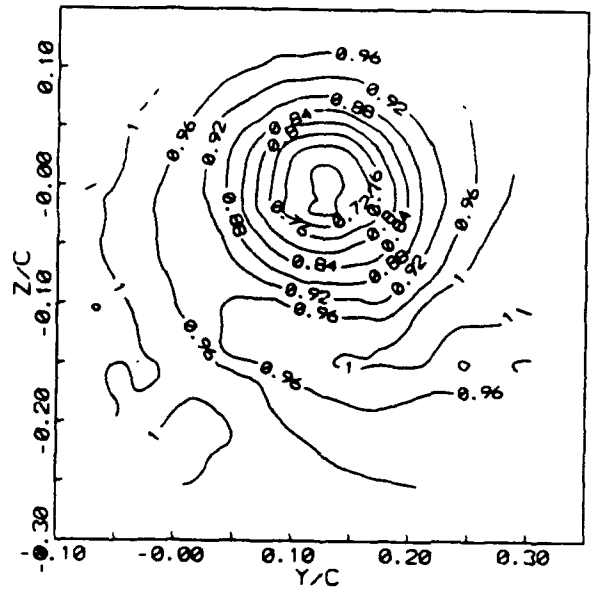

(a) $\alpha = 10$ degrees

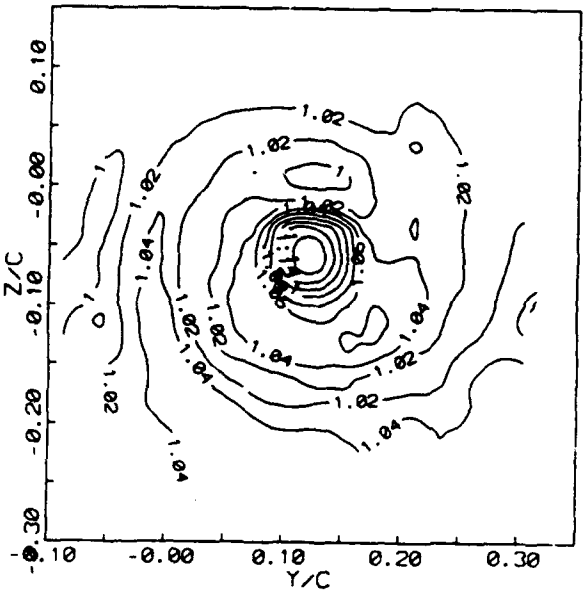

(b) $\alpha = 10$ degrees

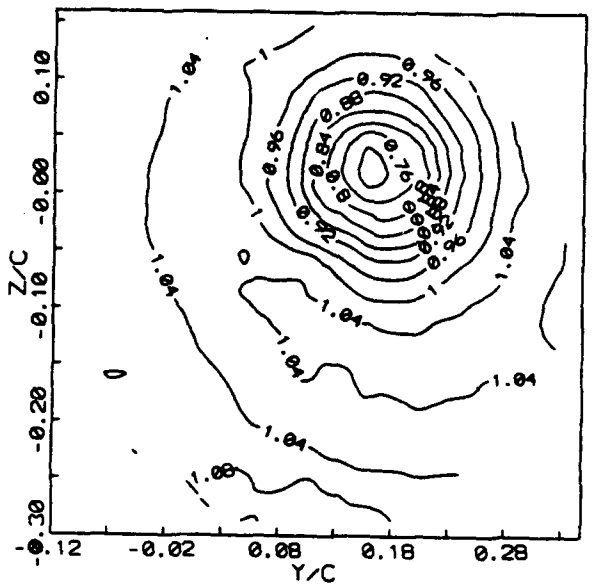

(a) $\alpha = 11$ degrees

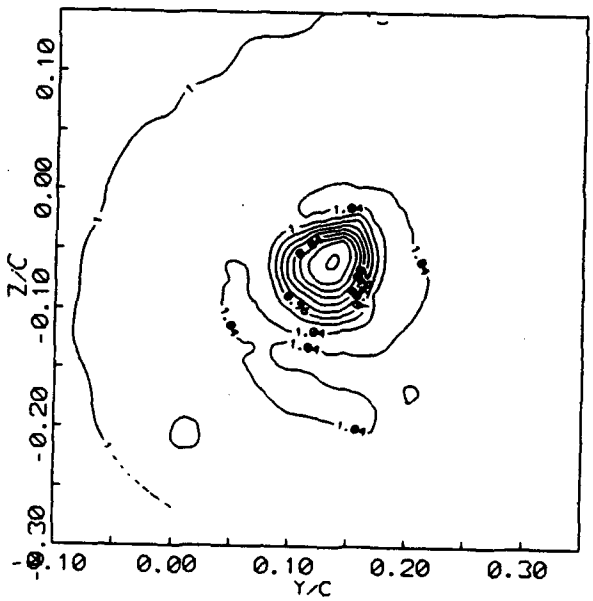

(b) $\alpha = 9$ degrees

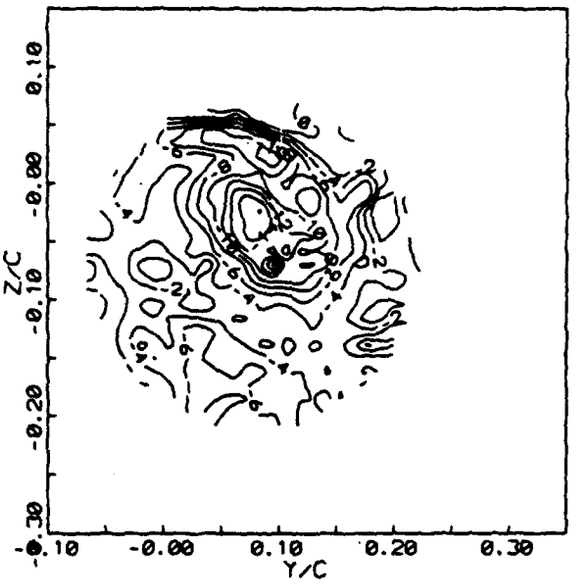

(a) $\alpha = 9$ degrees

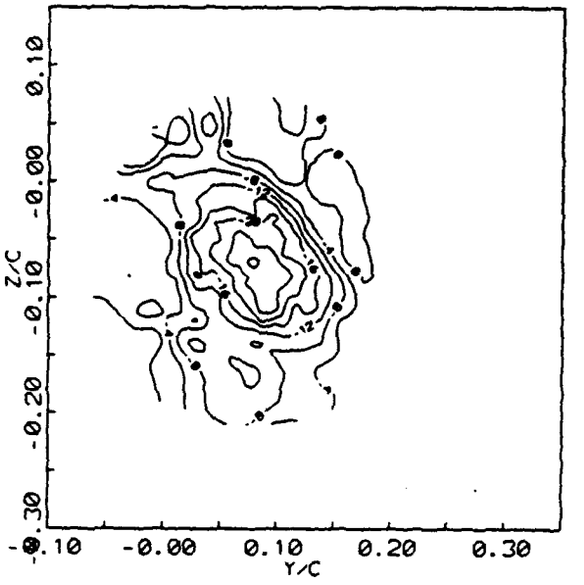

(b) $\alpha = 11$ degrees

(i)

Figure 5.16 Downstream development of the longitudinal component of the vorticity ω_x across the vortex at the same angles of incidence and downstream locations as in Fig. 15. (a) pitch-up. (b) pitch-down.

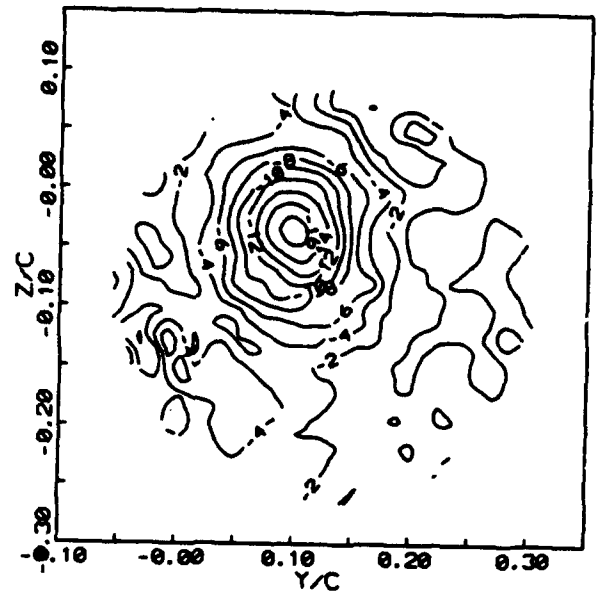

(a) $\alpha = 9$ degrees

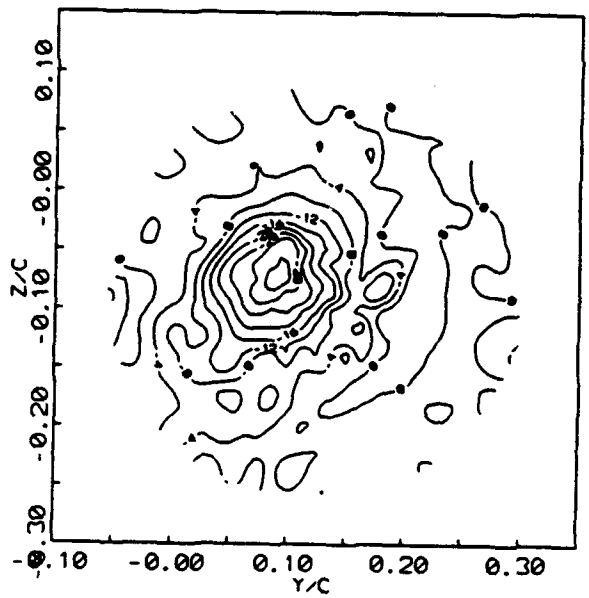

(b) $\alpha = 11$ degrees

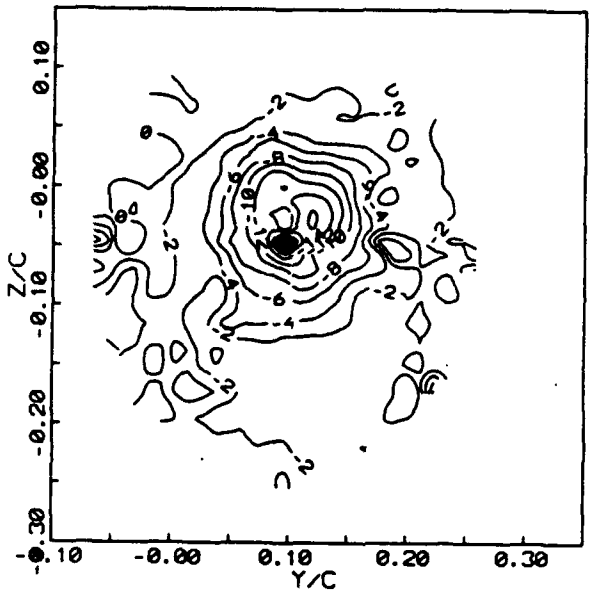

(a) $\alpha = 10$ degrees

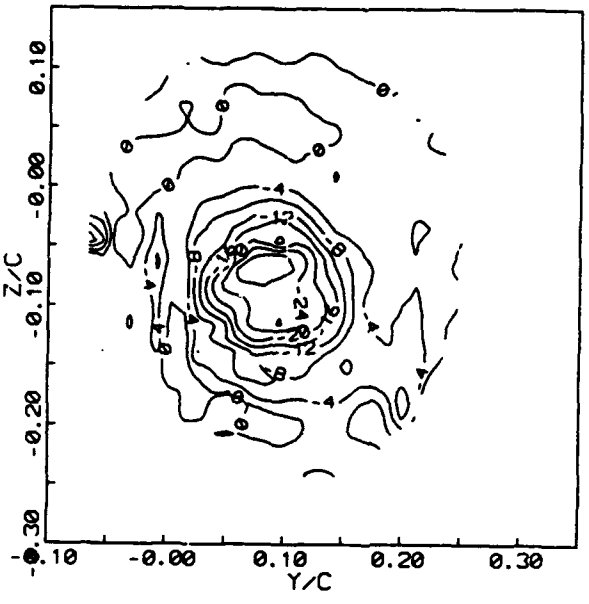

(b) $\alpha = 10$ degrees

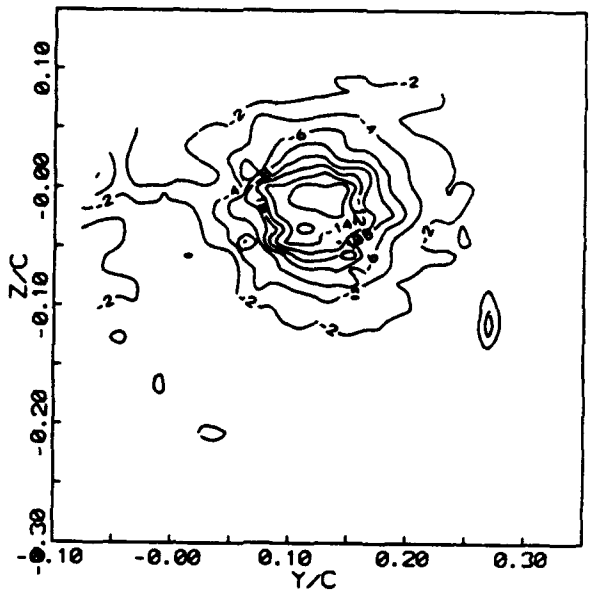

(a) $\alpha = 10$ degrees

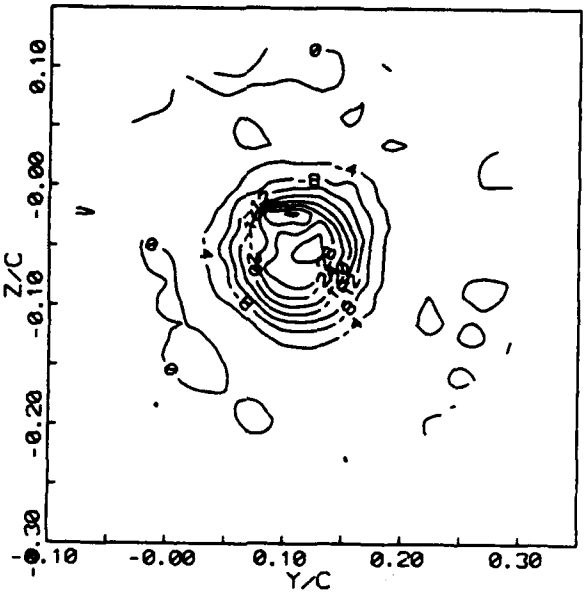

(b) $\alpha = 10$ degrees

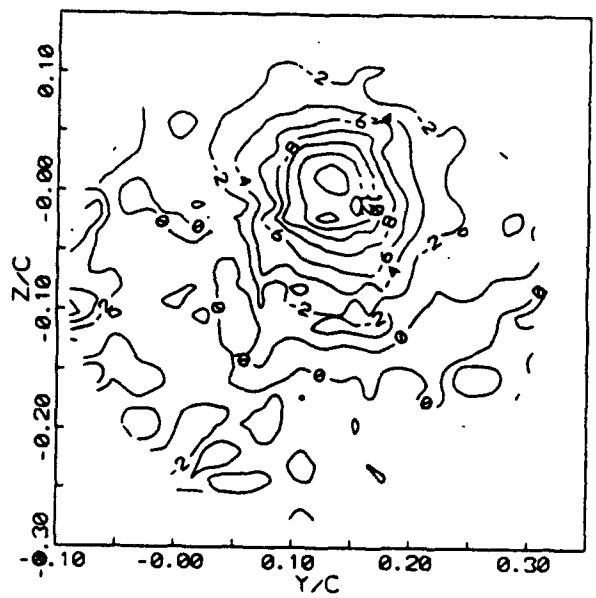

(a) $\alpha = 10$ degrees

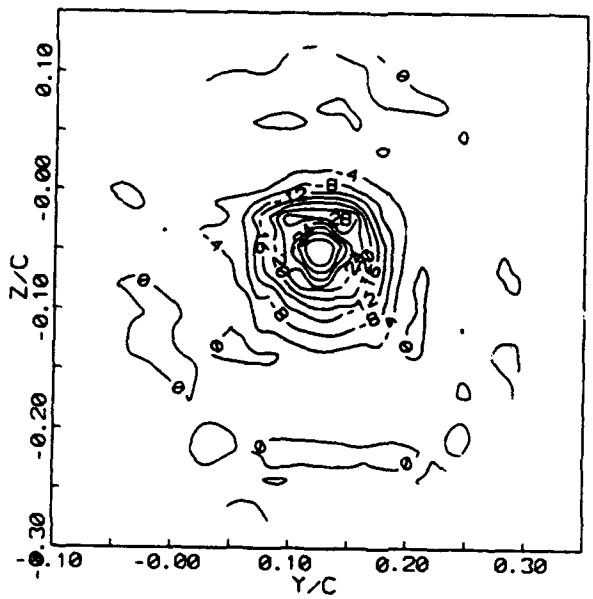

(b) $\alpha = 10$ degrees

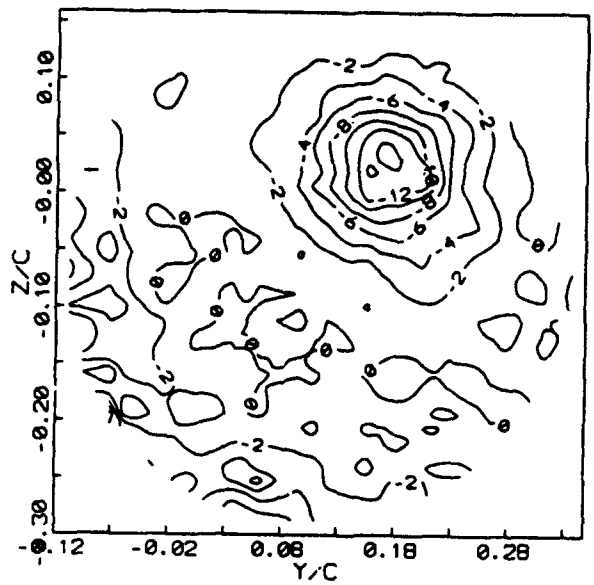

(a) $\alpha = 11$ degrees

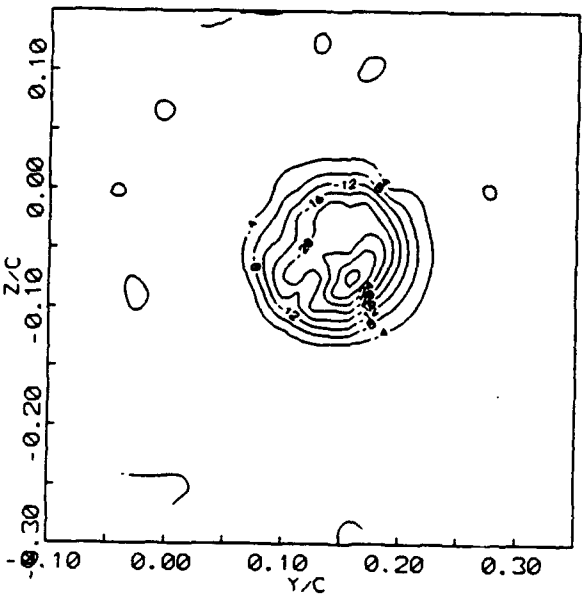

(b) $\alpha = 9$ degrees

CHAPTER 6

CONCLUSIONS AND RECOMMENDATIONS

The experimental studies of tip vortex in the near wake of a rectangular wing have resulted in following conclusions

Steady Flow Experiments

1. The shear layer from the trailing edge rolls up into a spiral in the vortex
2. Cross-stream vorticity is rotated into a streamwise direction in the core region of the vortex augmenting ω_z
3. The vortex core is dominated by ω_z
4. The turbulence in the vortex is associated with the spiralled shear layer
5. Circulation varies as r^2 in the core region and follows a semilog law in the outside region

Unsteady Flow Experiments

In addition to the same conclusions as in the case of the steady vortex, the following conclusions can be obtained in the unsteady flow experiments

1. The convective velocity of the phase is nearly equal to the free stream velocity

2. The periodic flow is not quasi-steady

For future study, it is recommended that the seeding method be improved to obtain the flow properties in more spanwise and longitudinal regions of the vortex so that the decay rates of the vortex, such as the size and circulation, can be obtained. The measurements should also be extended to the regions close to the tip, to study the interactions between the spanwise and longitudinal vorticities. Besides, numerical models need to be developed by using present experimental database for the prediction of the development of steady and unsteady wing tip vortices.

REFERENCES

Ahmed, S. and Chandrasekhara, M.S., (1991) "Reattachment Studies of an Oscillating Airfoil Dynamic Stall Flow Field", AIAA-91-3225.

Atler, J.N. and Luttges, M.W., (1985) "Three-dimensionality in Unsteady Flow about a Wing", AIAA-85-0132.

Baker, G.R., and Barker, S.J., and Bofah, K.K., and Saffman, P.G., (1974) "Laser anemometer measurements of trailing vortices in water", J. Fluid Mech., Vol. 65, part 2, pp. 325-336.

Bandyopadhyay, P.R., Stead, D.J. and Ash, R.L. (1991) " Organized nature of a turbulent trailing vortex", AIAA J., 29(10), pp. 1627-1633.

Brooks, Thomas F.; Marcolini, Michael A. (1986) "Airfoil Trailing-Edge Flow Measurements", AIAA J., 24(8), pp. 1245-1251.

Cad-el-Hak, Mohamed & Ho, C.Ming., (1986) "Unsteady vertical flow around three-dimensional lifting surface", AIAA J., Vol.24, No.5, pp. 713-721.

Carr, L.W., and Chandrasekhara, M.S., (1989) "Design and Development of a Compressible Dynamic Stall Facility", AIAA-89-0647.

Carr, L.W., Chandrasekhara, M.S., and Brock, N.J., (1991) "A Quantitative Study of Unsteady Compressible Flow on an Oscillating Airfoil", AIAA-91-1683.

Chandrasekhara, M.S., and Ahmed, S., (1991) "Laser Velocimetry Measurements of Oscillating Airfoil Dynamic Stall Flow Field", AIAA-91-1799.

Chandrasekhara, M.S.; Carr, L.W. (1989) "Flow Visualization Studies of the Mach Number Effects on the Dynamic Stall of an Oscillating Airfoil", AIAA-89-0023.

Chen, D.R. and Yue, R., (1989) "Numerical Solutions for Oscillatory Aerofoil at High Reduced Frequency", Comp. Methods in Appl. Mech., Vol.65, pp. 325-336.

Dagan, A. & Almosnino, D., (1991) "Vorticity equation solutions for slender wings at high incidence", AIAA J., Vol.29 No.4, pp. 497-504.

Francis, Michael S., and Kennedy, Donald A., (1979) "Formation of a Trailing Vortex", J. Aircraft, Vol.16, No.3, pp. 148-154.

Francis, T.B. & Katz, J., (1988) "Observations on the development of a tip vortex on a rectangular hydrofoil", J. Fluids Engrg., Vol.110, pp. 208-215.

Freymuth, P., (1989) "Visualizing the Connectivity of Vortex Systems for Pitching Wings", J. Fluids Engrg., Vol.111, pp. 217-220.

Freymuth, P., (1988) "Three-Dimensional Vortex Systems of Finite Wings", J. Aircraft, Vol.25, pp. 971-972.

Freymuth, P., (1991) "Vortex Topology for the Wings in Pictures, Sketches and Conjectures", AIAA-91-1824.

Freymuth, P., and Finaish, F., and Bank, W., (1986a) "Visualization of Wing Tip Vortices in Accelerating and Steady Flow", J. Aircraft, Vol.23 No.9, pp. 730

Freymuth, P., Finaish, F. and Bank, W., (1986b) "The Wing Tip Vortex System in a Starting Flow", Zeitschrift fur Flugwissenschaften und Weltraumforschung, Vol.10, pp. 116-118.

Gorsiglia, V.R., (1973) "Rapid scanning, three-dimensional hot-wire Anemometer surveys of wing-tip vortices", J. Aircraft, Vol.10, No.12, pp. 752-757.

Higuchi, H.; Quadrell, J.C. and Farell, C., (1986) "Vortex Roll-up for an Elliptically-Loaded Wing at Moderately Low Reynolds Number", AIAA Paper 86-0562, AIAA 24th Aerospace Science Meeting, 1986.

Hoffmann, E.R., and Joubert, P.N., (1963) "Turbulent line vortices", J. Fluid Mech., Vol.16, pp. 395-411.

Huyer, S.A., and Luttges, M.W., (1991) "The Vortex Kinetics Associated with an Oscillating Delta Wing", AIAA-91-1797.

Ikohagi, T.H. & Arndt, R.E.A., (1986) The Structure of Trailing Vorticies, Advancement in Aerodynamics, Fluid Mechanics and Hydraulics, AIAA/ASME Symposium, Univ. of Minnesota, 1986.

Kim, J. S. and Park, S.O., (1988) "Smoke Wire Visualization of Unsteady Separation over an Oscillating Airfoil", AIAA J., Vol.26, No.11, pp. 1408-1430.

Liang, X. & Ramaprian, B. R., (1991) "Visualization of the wing-tip vortex in temporal and spatial pressure gradient", J. Fluids Engrg., Vol.113, pp. 511-515.

Liou, S.G., (1990) "Measurement of the interaction between a rotor tip vortex and a cylinder", AIAA J., Vol.28, No.6, pp. 975-981.

Mason, W.H. and Marchman III, J.F., "Far-Field Structure of Aircraft Wake Turbulence", J. Aircraft, Vol. 10, 1973, pp. 86-92.

McAlister, K.M. and Takahashi, R.K., (1991) "Wing Pressure and Trailing Vortex Measurements", AVSCOM Technical Report 91-1-003, NASA Tech. Paper 3151.

Menedez A.N. and Ramaprian B.R., (1989) ' 'Experimental Study of a Periodic Turbulent Boundary Layer in Zero Mean Pressure Gradient", Aeronautical Journal of the Royal Aeronautical Society, June/July.

Ohmi, K., (1990) "Vortex formation around an oscillating and translating airfoil at large incidences", J. fluid Mech., Vol.211, pp. 37-60.

Park, S.O., (1990) Hot-wire measurements of near wakes behind an oscillating airfoil AIAA J., Vol.28,No.1, pp. 22-28.

Patel, M.H. & Hancock, G.J. (1974) Some experimental results of the effect of a streamwise vortex on a two-dimensional wing Aeronautical J., 1974(4), pp. 151-155.

Phillips, W.R.C., (1981) "The turbulent trailing vortex during roll-up", J. Fluid Mech., Vol. 105, pp. 451-467.

Phillips, W.R.C., and Graham, J.A.H., (1984) "Reynolds-stress measurements in a turbulent trailing vortex", J. Fluid Mech., Vol. 147, pp. 353-371.

Roberts, T.W., and Murman, E.M., (1984) "A Computational Method for Helicopter Vortex Wakes", AIAA-84-1554.

Ronald, L.P., William, L., and Soskic, N., (1980) "Flight Measurements of a Wing Tip Vortex", J. Aircraft, Vol.17 No.4, pp. 250-259.

Saffman, P.G., (1973) "Structure of turbulent line vortices", The Physics of Fluids, Vol.16 No.8, pp. 1181-1188.

Sarpkaya, T., (1989) "Computational Methods with Vortices–the 1988 freeman scnolar lecture", J. Fluids Engrg., Vol.111, pp. 5-52.

Spivey, R.F. (1968) " Blade tip aerodynamics - profile and planeform effects", 24th Annual National Forum Proceedings of the American Helicopter Society, Washington D.C., 1986.

Spreiter, J.R. and Sacks, A.H., (1951) "The Rolling Up of the Trailing Vortex Sheet and its Effect on the Downwash Behind Wings", J. Aeronautical Science, vol. 18, no.3, pp. 260-267.

Tung, C., and Pucci, S.L., and Caradonna, F.X., and Morse, H.A., (1981) "The Structure of Trailing Vortices Generated by Model RotorBlades", NASA Technical Memorandum 81316.; Vertica, Vol.7, pp. 33-43.

Yeh,D.J. & Plotkin, A. (1986) "Vortex panel calculation of wake roll-up behind a large aspect ratio wing", AIAA J., Vol.24, No.9, pp. 1417-1423.

Yin,X.Y.& Deng, G. (1989) "Numerical simulation of rolling up of leading/trailing-edge vortex sheets for slender wings", AIAA J., 27(10), pp. 1313-1318

Zheng Y. and Ramaprian B.R., (1991) "LDV Measurements in the Roll-up Region of the Tip Vortex from a Rectangular Wing", AIAA Paper 91-1685, 1991

Zheng Y. and Ramaprian B.R., (1991) "LDV Measurements in the Unsteady Tip-Vortex behind an oscillatting Rectangular Wing", Proc. of 8th Symposium on Turbulent Shear Flow, 1991.

Appendix A

DESCRIPTION OF DATA FILES

The processed data consisting of the distributions of the mean or phase-locked velocity, vorticity and Reynolds stresses across the vortex at different downstream locations are archived on a set of 9 IBM compatible, $5\frac{1}{4}^{"}$ floppy disks (MME-TF-93-1/1-9). The data are normalized using freestream velocity U_∞ and wing cord c as the velocity and length scales respectively. There are a total of 43 data files for the steady flow experiments. These cover the data from x = 4-100 cm and angle of incidence α = 2-15 degrees. There are a total of 220 data files for the unsteady flow experiments. These cover 10 streamwise locations in the range x =5-100 cm and provide the phase-locked results at intervals of 1 degree in incidence from 5-15 degrees, separately for the pitch-up and pitch-down phases of the oscillation cycle(i.e. 22 data files per each $x-$ location).

The typical data file name for the steady flow experiments is as follows:

UYY.XX for velocity data

UUYY.XX for turbulent stress data

where

YY: Angle of incidence of the wing in degrees

XX: Downstream distance from the trailing edge in centimeters

The data format of these files is:

Velocity data:

y	z	U	V	W	ω_x	ω_y	ω_z
0.0754	0.0885	0.6971	0.1046	0.0770	-21.2384	-0.0074	0.2529
0.0836	0.0885	0.7031	0.1262	-0.0030	-20.3197	0.3496	-0.7253

.....

Turbulent stress data:

y	z	100 u'	100 v'	100 w'	100 uv	100 uw	100 vw
.1098	.1098	6.9012	7.7110	6.9829	-.0613	-.0260	-.0546
.1098	.1016	7.4293	8.2085	8.1256	-.0593	-.0396	-.1211
.1098	.0934	7.4476	7.8415	7.5768	.0492	-.0500	-.0465

.....

For the unsteady flow experiments, the typical data file name is:

UYY_ D.XX for velocity data

UUYY_ D.XX for turbulent stress data

where

YY: Instantaneous angle of incidence of the wing in degrees

D: 0 or 1, direction of the wing motion

(0 for pitch-up and 1 for pitch-down)

XX: Downstream distance from the trailing edge in centimeters

The format of these date files is the same as those in the steady flow experiments.